CENTRO DE INVESTIGACIÓN Y DE ESTUDIOS
AVANZADOS DEL INSTITUTO POLITÉCNICO NACIONAL

UNIDAD ZACATENCO

DEPARTAMENTO DE QUÍMICA

“Understanding the solvation process of imidazole and pyrazole derivatives in some protic and aprotic solvents through thermochemical measurements, ^{1}H NMR spectroscopy and crystal structure analysis”

T E S I S

Que presenta

I.Q. Filiberto Herrera Castro

Para obtener el grado de

DOCTOR EN CIENCIAS

En la especialidad de

CIENCIAS QUÍMICAS

Director de la Tesis:

Dr. Luis Alfonso Torres Gómez

Ciudad de México Septiembre, 2019

El presente trabajo se realizó en el Departamento de Química del Centro de Investigación y de Estudios Avanzados del Instituto Politécnico Nacional (CINVESTAV), bajo la dirección del Dr. Luis Alfonso Torres Gómez y con el apoyo económico otorgado por el Consejo Nacional de Ciencia y Tecnología (CONACYT) a través de la beca con número 556996.

Dedico esta tesis a mis padres, Rosa y Filiberto y a mis hermanos, Sergio Alberto y Rosalyn.

Gracias por acompañarme en este camino. Los amo.

Agradecimientos

Al Dr. Luis Alfonso Torres por su confianza y apoyo a lo largo de esta etapa de formación.

A la auxiliar de investigación Myriam Campos Ruiz de la Peña por su apoyo incondicional.

Al técnico Javier Cesáreo López Crisanto por su apoyo y disponibilidad.

A todo el personal del Departamento de Química que apoya en diferentes aspectos de ésta etapa académica.

A mis compañeros estudiantes. La convivencia entre nosotros enriquece el camino que transitamos en esta etapa de nuestras vidas.

A los profesores que formaron parte del jurado evaluador por sus valiosos comentarios:

Dra. María de los Ángeles Paz Sandoval
Dr. Aarón Rojas Aguilar
Dr. Jorge Tiburcio Báez
Dr. José Miguel Méndez Alcaráz
Dr. Miguel Antonio Costas Basín

Content

Resumen

Se realizó un estudio termodinámico que incluye la determinación de la temperatura y la entalpía de fusión, la entalpía de sublimación y la entalpía de solución en agua, metanol y acetonitrilo para algunos derivados del imidazol y pirazol; específicamente: imidazol, 2-metil-, 2-etil-, 2-isopropilimidazol, pirazol, 3,5-dimetil- y 3,4,5-trimetilpirazol. Con los valores de las dos últimas propiedades descritas, se determinó la entalpía de solvatación para todos los compuestos estudiados en los tres disolventes utilizados.

El uso de la ecuación de Pierotti, que incorpora la entalpía de formación de cavidad y la reorganización del solvente para cada soluto en cada solvente, en conjunto con los valores de entalpía de solvatación, permiten la determinación de la entalpía de interacción entre cada soluto y solvente.

Se analizó la estructura cristalina de los compuestos estudiados con el uso de un programa cristalográfico, con el fin de identificar las interacciones intermoleculares presentes en la fase sólida. De este análisis, se racionalizó la magnitud de las entalpías de fusión y sublimación en términos de la estructura molecular y del cristal también en términos de las interacciones no covalentes presentes en la fase sólida.

La magnitud de la entalpía de solución y solvatación también se explica en términos de las interacciones moleculares entre solute y solvente, los cuales presentan diferente comportamiento prótico y aprótico, así como diferente naturaleza química. Este estudio muestra la importancia de la entalpía de interacción, la cual reúne la magnitud de todas las interacciones soluto-solvente, lo que permite comprender con mejor detalle el proceso de solvatación.

La discusión del proceso de solvatación y la magnitud de las entalpías de interacción se basa en las interacciones específicas, como el enlace de hidrógeno, $H \cdots \pi$ y/o interacciones no específicas (llamadas también fuerzas de dispersión de London). Ésta discusión se apoya en las características de los espectros de RMN de ^{1}H de cada soluto en cada solvente deuterado. También se discute la correlación de las entalpías de interacción con el volumen molecular, estimado a partir de la densidad electrónica, misma que se atribuye principalmente a las fuerzas de dispersión promovidas por los substituyentes del anillo aromático.

Abstract

The thermodynamic research, that includes the experimental determination of the melting temperature, the enthalpy of fusion, the enthalpy of sublimation and the enthalpy of solution in water, methanol and acetonitrile, for imidazole and pyrazole derivatives, was performed; specifically: imidazole, 2-methyl-, 2-ethyl- and 2-isopropylimidazole, pyrazole 3,5-dimethyl- and 3,4,5-trimethylpyrazole. With the values for the two last enounced properties, the enthalpy of solvation values for all the studied compounds were determined in the three used solvents.

The Pierotti equation, which incorporates the enthalpy of cavity formation and the solvent reorganization for each solute in each solvent, together with the enthalpy of solvation values, allow the determination of the corresponding enthalpies of interaction between each solute and solvent.

The crystal structures of the studied compounds were investigated, using a crystallographic software, in order to identify the sites for the intermolecular interactions, present in the solid phase. From this analysis, the magnitude and trend of the enthalpies of fusion and sublimation were rationalized and explained in terms of the corresponding molecular and crystal structure and also in terms of the non-covalent interactions in the solid state.

The magnitude and trend for the enthalpy of solution and solvation are also explained in terms of the intermolecular interactions between solute and solvent in the three solvents, with different protic and aprotic behavior as well as chemical nature. This study shows the relevance of the enthalpy of interaction, that gathers all the involved energies of interaction, allowing to understand the process of solvation.

The discussion of the solvation process and enthalpies of interaction of the studied compounds is based on the specific intermolecular interactions, like hydrogen bonds, $H \cdots \pi$ and non-specific interactions from London forces nature, supported by the features of the ^{1}H NMR spectra of each solute in each deuterated solvent. A correlation of the enthalpies of interaction with the molecular volume based on the electronic density is explained, mainly in terms of the dispersion forces promoted by the substituents in the aromatic rings.

Introduction

Intra- and intermolecular interactions are essential in the comprehension of the features and behavior of many chemical systems. The magnitude of these interactions is responsible of the exhibited properties of chemical compounds and materials. Ionic, covalent and coordinated bonds are the most evident interactions that build molecules with different stabilities.

Other kinds of chemical interactions, currently known as weak interactions, such as the hydrogen bond or dispersion interactions, among other ones by a cumulative effect, are responsible of the stability of condensed phases and the amount of energy involved in the processes of phase changes, solution and solvation. In particular, the thermodynamic properties are related to the molecular structure and chemical nature of molecules and systems, even if a precise relationship between them might not be clearly apparent.

The molecular interactions play also a central role in chemical reactions, which most of them occur in solution phase. A feasible example of their importance is the development of frontier research areas, like supramolecular chemistry, in the last thirty years[1]. The study of a specific chemical reaction that occurs in a liquid phase, involves the study of the solvent effect on the reactants; this are the molecular interactions established between the solute and the solvents[2], like in the case of the solvatochromism phenomena[3].

The study of the solvent interactions with a specific solute, leads to a deeper comprehension of the energy terms involved in the solution process and how the chemical structure affects the magnitude of these interactions and the related thermodynamic properties. In chemistry, there are two important examples where the study of molecular interactions plays a main role to understand the stability of the studied phases at the established experimental conditions.

In the first example, the interactions between molecules responsible to keep stable a crystal structure. The molecules are arranged in such a way that the possible interactions between neighbor molecules lead to reduce the entropy of the ordered phase[4]. As a consequence, in the last thirty years, the study of the crystal structures from the molecular interactions has derived in the born of the crystal engineering discipline[5].

In the second example, the energy of interaction between solute and solvent mediates the solution process and the stability of the final solution. If this energy term relative to solute-solvent interaction is higher than the summation of the separated energy terms of solute-solute and solvent-solvent interactions, a solution is formed.

To connect these two cases from a thermodynamic or macroscopic point of view, we can consider that, when a solid compound sublimates or is dissolved at infinite dilution

in a liquid solvent, both processes have in common that the initial state corresponds to a pure solid phase and the final state corresponds to an ideal phase.

In the first case, the pure gas phase is considered as an ideal gas and in the second case the solute is completely surrounded by solvent molecules, and the solution has an ideal solution behavior. In terms of a molecular approach, in both final states, the ideal gas and solution, the molecular interactions occurring in the solid phase no longer prevail.

The enthalpy value for a hypothetical process that consist of the transfer of a mole of molecules in the ideal gas phase, to an excess of solvent to produce an infinitely diluted solution is derived from the enthalpy values for sublimation and solution process. This is better known as the solvation process.

When the concentration of the solute is small enough, a solution reaches a limit called "infinite dilution", where solute-solute interactions no longer prevail[6, 7].

In order to study the magnitude of these remained interactions, the use of thermochemical techniques become important to determine the enthalpy of each process and to relate their values with the molecular structure. The magnitude of the total of interactions in the solid phase is accounted in the enthalpy of sublimation of a compound and the enthalpy change for breaking solute-solute and solvent-solvent interactions and the formation of new solute-solvent interactions are gathered in the enthalpy of solution. In order to have a more accurate approach to the study of these interactions, the enthalpy of solvation can be derived from pure thermochemical measurements; the enthalpies of sublimation and solution.

The solvation process has been also widely studied and reviewed in the literature and it has been shown that is a suitable way to study the intermolecular interactions in the formation of a stable solution[8-18]. The hypothetical solvation process also includes the formation of a cavity inside the solvent, with the suitable form and size to receive a solute molecule.

A more precise comprehension of the solute-solvent interactions and evaluation of their magnitude, can be achieved by the combination of the enthalpy of solvation, determined from experimental measurements, and the enthalpy of cavity formation, derived from statistical thermodynamics calculations, as proposed by the used of Scaled Particle Theory[19]. This new magnitude is named the "enthalpy of interaction". Moreover, the enthalpy of solvation is a thermodynamic property that is not completely able to fully describe the interactions established between solute and solvent. Thus, it is combined with terms concerning the enthalpy of cavity formation and solvent reorganization to lead to the enthalpy of interaction between solute and solvent.

From a pure chemical point of view, the molecular interactions between solute and solvent change the chemical environment of a nucleus that is active in Nuclear Magnetic Resonance (NMR) and this can be detected by a change in the chemical shift associated with the establishment of new interactions in solution, being these

interactions electrostatic in nature[4]. The analysis of the changes of the chemical shifts of the relevant hydrogen atoms of the studied solutes in different solvents would provide an insight about the nature of different interactions that are established in solution. This would be an evidence that how the magnitude of the thermodynamic properties of solvation accounts all the intermolecular interactions in solution.

The purpose of this work underlines the importance of molecular interactions in the formation of stable solid and solution phases and the relationship of thermodynamic properties with the chemical structure. The relationship between the magnitude of thermodynamic properties with the chemical nature of solute and solvent, the molecular and crystal structure, molecular volumes and NMR spectroscopy data for the compounds selected for the present study. In this way, it would be revealed how the magnitude of the thermodynamic properties contains the energetic information about the interaction between molecules other than ionic, covalent or coordinated bonds. This purpose can be more schematically summarized as to:

1.- Identify the intermolecular interactions that maintain stable the solid phase, through the study the crystal structures of some selected imidazole and pyrazole derivatives as solute

2.- Take the enthalpy values of phase change, fusion and sublimation, and the enthalpy of solution values of a solid in different solvents, as the properties that gather the energy related to all the molecular interactions that maintain stable the solid phase of selected solid compounds.

3.- Give an explanation of the magnitude of sublimation and fusion enthalpy values in terms of the crystal structure of the studied compounds.

4.- Take the enthalpy of solvation and interaction values as the properties that gather all the energy of molecular interactions between solute and solvent that remains at infinite dilution, in the solvents water, methanol and acetonitrile.

5.- Give a molecular explanation for the magnitude of these properties in terms of the chemical nature of the involved solute and solvent interactions.

6.- Explore the possible support or correlation of the NMR chemical shifts for the magnitude and trend of the enthalpy of solvation and interaction values, for the different chemical compounds in the corresponding solvent.

The molecules included in this work have been selected on the basis of a relative small size, the versatility to form different types of intermolecular interactions (i.e. hydrogen bonds, dipole-dipole, etc.), as well as the aromatic feature of the five membered imidazole rings and the possibility to study the aliphatic substituent effect on the solvation process. The solvents were selected on the basis of their behavior as proton donors and acceptors and their aprotic features.

In this work are presented the experimental results of the values of the enthalpy of fusion and sublimation for the studied compounds, the enthalpy of solution and solvation in three different solvents and the calculation of the enthalpies of cavity formation and interaction of every solute with every solvent. Also, the experimental procedures and results for the thermochemical and spectroscopic measurements are given in the corresponding sections and a discussion and conclusions are given in the above proposed terms.

I. Background

I.1 Non-covalent interactions

The existence of intermolecular forces can be deduced from two important macroscopic observations[20]: 1) All substances form condensed phases at sufficiently low temperatures; this indicates the existence of intermolecular attractions that are strong enough to hold together molecules with low kinetic energy. 2) All condensed phases strongly resist further compression; this indicates the existence of short-range repulsive forces that keep the molecules from coalescing once they are in "contact". At long range (a distance greater than the overlap of electron distributions is neglected) the interaction of two species can be treated largely in terms of classical electrostatics.

These interactions, existing at long-range, are called "non-covalent interactions" because they do not involve the overlap of atomic electron densities as in chemical bonds. Any atom, molecule or ion can be considered as a spatial distribution of electric charge.

The study of non-covalent interactions encompasses a wide variety of chemical systems and is central in the understanding of phenomena like self-assembly and the solvation process[2].

The study of molecular interactions had one of the first and important works with the proposal of van der Waals, who recognized them as responsible of the non-ideal behavior of gases. With his proposal of a new equation of state for a gas[4], equation (1) was described:

$$\left(P + \frac{a}{\bar{V}^2}\right)(\bar{V} - b) = RT \qquad (1)$$

In this equation, P is the pressure, $\bar{V}$ is the molar volume, T is the temperature and R is the gas constant. The comparison of this equation with the one for the ideal gas, $PV = nRT$, reveal that two new terms, a and b, were incorporated. The parameter a accounts for the intermolecular forces and the parameter b is the volume occupied by the incompressible gas molecules. Thus, a volume $(\bar{V} - b)$ remains for the free movement of the molecules[21]. The van der Waals equation reproduces the phase transition gas-liquid, because it takes into account the intermolecular interactions, while the ideal gas equation does not[4].

Non-covalent interactions are central in the field of supramolecular chemistry, which is defined as "the study of systems involving aggregates of molecules or ions, held together by non-covalent interactions such as electrostatic interactions, hydrogen bonding, dispersion interactions and solvophobic effects"[22].

Supramolecular chemistry is a recent research field[1], concerned with the study of the applications of non-covalent interactions and in the last twenty years has had an

enormous growth as a relevant field in chemistry. This discipline involves the study of the aggregation of molecules, molecular movements and solvation and is sometimes described as “host-guest” chemistry, an important term in molecular recognition, and can be classified in three categories, according to Ariga[23]: the chemistry associated with a molecule recognizing a partner molecule (molecular recognition chemistry); the chemistry of molecules built to specific shapes and the chemistry of molecular assembly from numerous molecules.
This recognition is driven by the “lock-key” principle[24], based in the idea that a host has molecular sites where interactions can be established with a guest. The sites in the host are “divergent” and in the guest “convergent”. In the literature, there are many graphical representations of this principle[25, 26].

Whitesides[27] defines self-assembly as “the autonomous organization of components into patterns or structures without human intervention”. This phenomenon is common in nature and has been widely used in nanotechnology. Intermolecular interactions are crucial and central in the study of self-assembly of supramolecular and nanotechnology systems[28].

I.1.1 Molecular interactions

These interactions are of various types and magnitude and can be classified as follows. All the interaction potentials are shown to illustrate the main factors that affect the magnitude of each interaction, such as distance, orientation or properties like dipole moment or polarizability.

I.1.1.1 Ion-dipole interactions

The electric charge of an ion can couple with the uneven electronic density distribution of an electrically neutral molecule, characterized by a dipole moment μ.

The potential of interaction between an ion and an electric dipole is given by equation (2).

$$u_{ion-dipole}(r) = -\frac{1}{4\pi\epsilon_0}\frac{ze\mu cos\theta}{r^2} \quad (2)$$

In this equation, $z \cdot e$ is the ion charge, θ is the dipole angle relative to the line r joining the ion and the center of the dipole and ϵ_0 is the vacuum relative permittivity[2].

Ion-dipole interactions are important in the process of solution of ionic compounds, where the coupling of these species with solvents has been extensively studied, principally with water[29].

I.1.1.2 Dipole-dipole interactions

The electric dipole moment is defined as $\vec{\mu} = \sum_i q_i \vec{r}_i$, where q_i is the electric charge of the particle i and $\vec{r}_i$ is the distance to a reference point. In a molecule, the electronic distribution creates an electric dipole moment around it when this distribution is uneven. That is, the sum of the partial charges times the distances to a reference point in the molecule is non-zero. A permanent dipole moment exists in all molecules in which the centers of positive and negative charge do not coincide[20]. The dipole-dipole interaction arises from the coupling of the dipole moments of two or more entities. The corresponding interaction potential is described by equation (3).

$$u_{dipole-dipole}(r) = -\frac{2\mu_1^2\mu_2^2}{(4\pi\epsilon_0)^2(3k_BT)}\frac{1}{r^6} \quad (3)$$

The dipole-dipole interaction is highly geometric dependent. If two molecules are correctly orientated, the dipole-dipole interaction would be the highest possible. In Figure 1 are illustrated two possibilities of interaction between two molecular models.

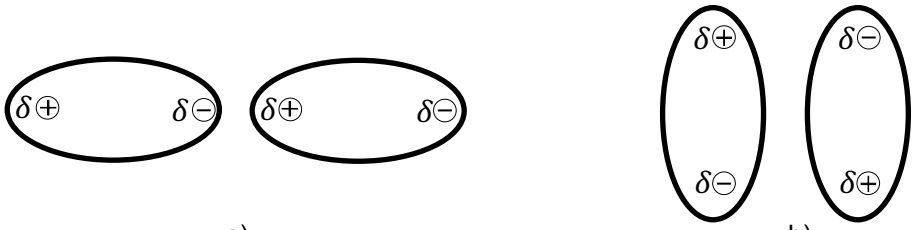

Figure 1. Illustration of the dipole-dipole interaction between two model molecules. The symbols δ indicate the partial charge in the molecule. The orientation of both molecules affects directly the magnitude of the interaction. In a) is shown the "head-to-tail" interaction and in b) is shown the antiparallel interaction. Figure was inspired from figure 2-3 in reference[2].

The dipole-dipole interaction is responsible of the self-aggregation of some aprotic solvents, like dimethyl sulfoxide[30] and is important in the study of the design and synthesis of new dye materials, which are important in non-linear optics[31].

I.1.1.3 Dipole-Induced dipole interactions

A molecule that has a permanent dipole moment can influence the electronic density of a neutral molecule and polarize it, when both molecules approached. This creates a temporal dipole moment in the neutral molecule that couples with the permanent dipole moment of the other molecule[1].

The corresponding interaction potential is shown in equation (4).

$$u_{dipole-induced\ dipole}(r) = -\frac{\mu_1^2\alpha_2+\mu_2^2\alpha_1}{(4\pi\epsilon_0)^2 r^6} \quad (4)$$

Where μ_1 is the dipole moment of the first molecule, α_2 is the polarizability of the neutral molecule. When the induced dipole moment μ_2 is created, this influences also the first molecule. Consequently, its polarizability α_1 is also affected. The dipole-induced dipole interactions are the reason why neutrally charged molecules, like hydrocarbons, can be, at least partially, dissolved in high polar solvents, like water[32].

I.1.1.4 Ion - π interactions

The electrical charge of an ion can interact with the delocalized electron density over an aromatic ring. The cation- π was extensively studied by Dougherty[33] in systems involving the bonding of organic cations such as tetraalkylammoniums and alkylpyridiniums to cyclophane receptors in water and has been recognized important in the phenomena of molecular recognition, macromolecular structure and drug receptor interactions[34]. According to these works, the binding energies of Li^+ and NH_4^+ with benzene are 160 and 90 kJ·mol^{-1}. The cation- π interaction is driven fundamentally by electrostatic forces[33]. The negative part of the quadrupole moment of an aromatic system can couple with the positive charge of a cation in order to solvate it. In Figure 2 is displayed an illustration of the cation- π interaction.

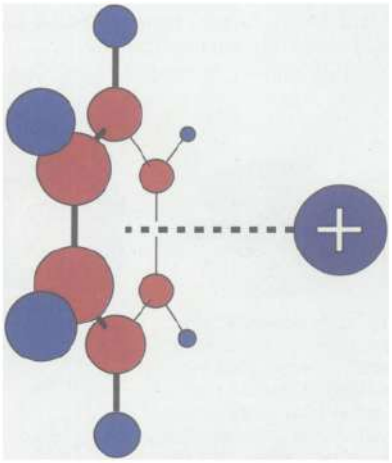

Figure 2. Illustration of the cation- π interaction. In this case, the π density of the benzene ring interacts with the positive charge of a generic ion. Figure taken from reference[35].

It is important to note that the cation- π interaction is not exclusive to the interaction of cations and aromatic systems. This interaction can be established between a cation and the π density of unsaturated hydrocarbons, like alkenes and alkynes[36, 37].

The anion-π interaction was not considered viable until recently[38]. This interaction is present between an anion and the delocalized π density over an aromatic ring that has electron withdrawing groups or N-heterocyclic rings. It can be considered as an "inverse" cation-π interaction.

The main energetic contributions to this interaction are electrostatic forces and the anion-induced polarization[39].

I.1.1.5 π − π interactions

The resonance effect and the delocalization of electron density over an aromatic ring create a quadrupolar moment, which promotes the establishment of interactions with other aromatic rings. This is caused by a polarization in the aromatic system where a positively σ-framework is between two negatively charged π-frameworks, as shown in Figure 3. These interactions are called $\pi - \pi$ interactions or also π-stacking interactions. The molecules can interact in several ways: edge-to-face or T-shaped, stacked and offset stacked[40, 41]. These are shown in Figure 4.

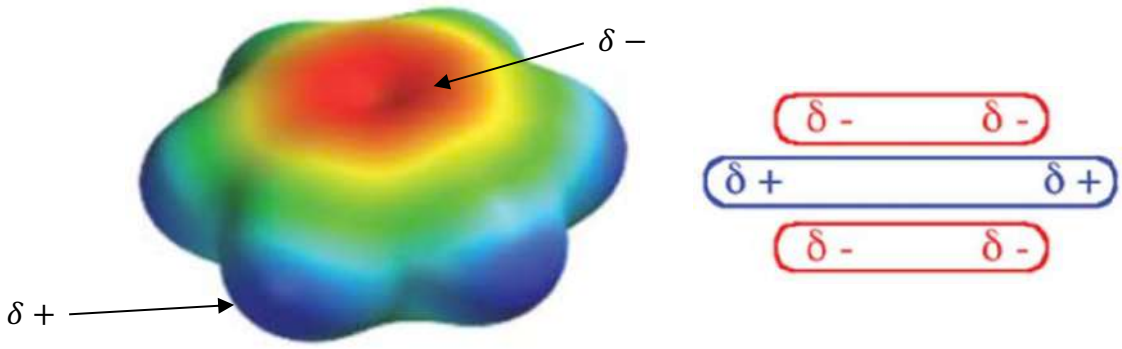

Figure 3. The electrostatic potential surface of benzene. This image reveals the polarization of the electron density in positively charged in the hydrogen atoms and negatively charged face of the aromatic ring, due to the quadrupolar moment of benzene. Figures taken from reference[42].

a) b) c)

Figure 4. Types of $\pi - \pi$ interactions between aromatic molecules. In image a) is represented the face-to-face or stacked geometry, in b) the edge-to-face or T-shape geometry and in c) the offset-stacked geometry. Figures taken from reference[44].

Hunter and Sanders[42] proposed three rules that drive the π-stacking: $\pi - \pi$ repulsion dominates in a face-to-face or stacked geometry, $\pi - \sigma$ attraction dominates in an edge-to-face or T-shaped geometry and $\pi - \sigma$ attraction dominates in an offset stacked geometry.

A good example of the influence of $\pi - \pi$ interactions in the crystal packing are the cases of the compounds benzene, pyrene and coronene[43]. The difference in the crystal packing reveals two ways of interaction through $\pi - \pi$ interactions, edge-to-face and offset-stacking, as shown in Figure 5.

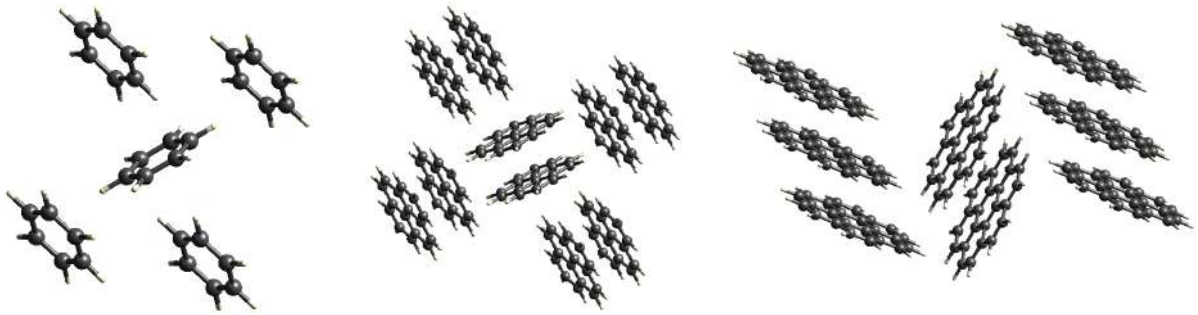

a) Benzene b) Pyrene c) Coronene

Figure 5. The crystal packing of benzene, pyrene and coronene. In benzene, a) the interaction edge-to-face is the only present in the crystal structure, while in coronene, figure c), the offset-stacking is the only one. In pyrene, figure b), both ways of arrangement are present in the crystal phase. The figures were taken from the CrystalExplorer software using the crystallographic files for benzene, pyrene and coronene taken from the Cambridge Crystallographic Data Base, with deposit names BENZEN, PYRENE and CORONE respectively. This figure was inspired in figure 2.3 of reference[43].

The difference in the melting points of this series of polycyclic aromatic hydrocarbons can be explained from $\pi - \pi$ interactions present in the crystal phase. $\pi - \pi$ interactions are also important in the understanding of the packing of aromatic molecules in crystals[43] and in stabilization of the DNA structure[44].

I.1.1.6 Hydrogen bond

The hydrogen bond is a strong, single point interaction with a very well-defined geometry and its magnitude is determined by the electrostatic forces between the donated hydrogen atoms and the acceptor atoms[45]. Hydrogen bond is a type of dipole-dipole interaction that can be represented, in general, as $A - H \cdots B$, where the atom A is called "hydrogen bond donor", the atom H is a hydrogen atom and the atom B is called "hydrogen bond acceptor". In this interaction, the hydrogen atom is attracted by a strong electrostatic force to both A and B atoms, so is considered as acting as a bond between them. The electronegativity of both atoms A and B plays an important role in the magnitude of a hydrogen atom. Only the most electronegative atoms should form hydrogen bonds and the strength of the bond increases with increase in the electronegativity of the two bonded atoms[46]. This bond can be characterized by the distance d between H and B atoms and the bond angle θ[47].

Due to its low electronegativity, hydrogen atoms bonded to O, N and C are partially positive charged. Therefore, organic molecules and macromolecules containing hydrogen atoms all have the possibility of forming hydrogen bonds.

Because hydrogen bonds are long-range interactions, one hydrogen atom can interact with more than one donor, or an acceptor atom can accept more than one hydrogen atom. These are called "bifurcated" hydrogen bonds[47]. In Figure 6 are illustrated several types of hydrogen bond interactions.

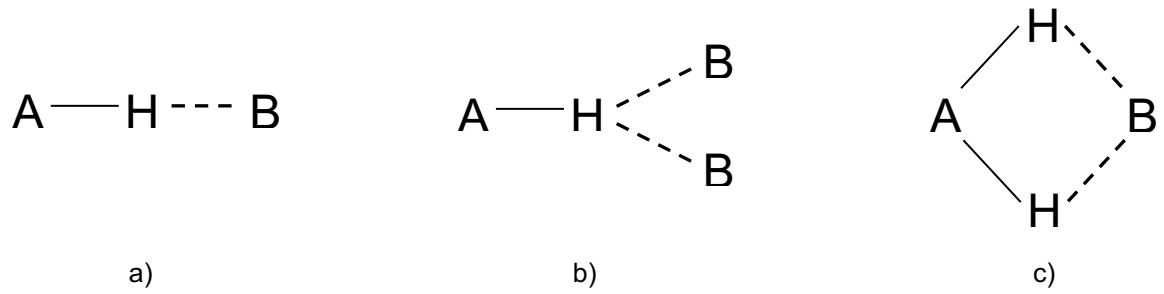

a) b) c)

Figure 6. Types of hydrogen bonds. A) Simple hydrogen bond, b) Bifurcated hydrogen bond where the hydrogen atom establishes interaction with two different acceptor atoms, c) Bifurcated hydrogen bond where two different hydrogen atoms establish interaction with one acceptor atom.

Depending on its magnitude, a hydrogen bond can be classified as very strong (60-170 kJ·mol^{-1}), strong (20-60 kJ·mol^{-1}) and weak (< 20 kJ·mol^{-1})[47].

Also, the delocalized electron density over an aromatic ring can polarize a hydrogen atom from a neighbor molecule and the interaction $H \cdots \pi$ can be established[43]. This can be considered as a weak hydrogen bond interaction.
Hydrogen bond interaction is important in understanding many of the crystal packing phenomena[48-50], macrocyclic chemistry[51], self-assembly phenomena[52, 53] and in the study of DNA structure[54]. Hydrogen bond is, arguably, the most important and the most studied noncovalent interaction.

In a later work, Desiraju[55] has proposed that the term “hydrogen bridge” is more adequate to describe this interaction. The justification is that the hydrogen bond interaction spans in many versatile ways, with an interaction magnitude wider than other non-covalent interactions. Even though, the general characteristics of each type of hydrogen bond are maintained.

I.1.1.7 Dispersion forces

Dispersion forces are effective electromagnetic forces acting between well-separated neutral, unpolarized and unmagnetized atoms or bodies in the absence of any applied electromagnetic field[56].

According to Salam[57], dispersion forces are ever present between all interacting atomic and molecular systems. Quantum mechanics explain successfully their in origin and arise from the coupling of the fluctuations in charge distribution at each atomic center due to motion of electrons. For the interaction of two neutral nonpolar molecules, the dispersion force is the only force in effect. The dispersion energy shift is also known as the induced multipole-induced multipole interaction, as the coupling is mediated by the temporary distortions in the electronic charge distribution in one species inducing a similar change in the charge density of the second molecule, leading to a transient moment being induced there, with coupling occurring between these induced moments. For a pair of molecules in the ground electronic state, the dispersion energy shift is always attractive. The interaction potential for the dispersion forces is shown in equation (5)[58].

$$u_{disp}(r) = -\frac{3}{2}\frac{\alpha_1\alpha_2}{(4\pi\epsilon_0)^2 r^6}\left(\frac{I_1 I_2}{I_1+I_2}\right) \quad (5)$$

Where α_i is the polarizability of the species i and I_i is the ionization potential of species i. It is worth to notice that in this equation, there are no dipole terms and the polarizability of any substance is always non-zero.

The dispersion forces are universal for all atoms and molecules; they are responsible of the aggregation of molecules which possess neither free charges nor electric dipole moments. A good example of this aggregation is the liquefaction of noble gasses[59].

One evidence of the influence of dispersion interaction in macroscopic properties is the change of the enthalpy of vaporization of alkanes[60]. The increment of size is proportional to the increasing in the magnitude of the dispersion forces established between hydrocarbon molecules. As this size increases, so the enthalpy of vaporization.

I.2 Crystal structure and crystal engineering. Solid state energetics.

One of the aims of the thermochemical studies of organic compounds is to relate the magnitude of the experimentally determined thermodynamic quantities, such as enthalpies of phase change, with the molecular structure of chemical compounds. Therefore, the molecular knowledge of the aggregate state of matter in which each of the compounds exists, is of great importance.

The crystal structures adopted by the chemical compounds are the result of intermolecular interactions[55] and given any particular crystal structure, it is generally possible to rationalize it in terms of the interactions within it. However, the reverse operation, namely, given the molecular structure of a compound, the deduction a crystal structure is decidedly nontrivial. This is so because a crystal structure is often not the result of hierarchic interaction preferences that follow from the molecular functionality.

A crystal can be defined as a supermolecule[61], an entity held together by molecular interactions, the same ones that are responsible of molecular recognition and complexation. These interactions play an important role not only in the formation and stability of the crystal structure, but also in the design and characterization of new crystal entities. The intermolecular interactions present in molecules mediate how they self-arrange to form a thermodynamic stable phase[5]. The design and preparation of crystalline material must be based on a knowledge of steric, electronic, topological and intermolecular binding capabilities of the constituent building blocks[1, 62, 63]. These building blocks are called synthons. Following the definition of Desiraju[64], supramolecular synthons are “units within supermolecules (crystals) which can be formed and/or assembled by known or conceivable synthetic operations involving intermolecular interactions”.

The goal of crystal engineering is the recognition and design of synthons that are enough to be exchanged from one network structure to another, which ensures generality and predictability, with the main objective, according to Desiraju[64], of “the understanding on intermolecular interactions in the context of crystal packing and in the utilization of such understanding in the design of new solids with the desired physical and chemical properties”. In order to achieve the goal of the optimal design of new solid materials, crystal engineering makes use of supramolecular synthons, also called “tectons”.

The energetics involved in this phase can be characterized by the enthalpy of fusion and enthalpy of sublimation and studied by calorimetric techniques, such as differential scanning calorimetry and Knudsen effusion. There have been works done[65-67] that relate the properties of the crystal packing with the enthalpy of sublimation. This thermodynamic property is a direct measurement of energy involved by all the molecular interactions in the crystal phase.

I.2.1 The Knudsen effusion methodology.

The enthalpy of sublimation is the enthalpy change associated to the transition of a mole of molecules from the solid state to the ideal gas phase. This thermodynamic property can be experimentally determined by two methodologies. The first one is a direct calorimetric measurement and the second is the determination of the equilibrium vapor pressure values at several temperatures.

One of the most used experimental methodologies to determine the enthalpy of sublimation, is the use of the Clausius-Clapeyron equation, equation (6). A thorough derivation of this equation from phase equilibria conditions is presented in reference[68].

$$lnP = -\frac{\Delta_{sub}H_m}{RT} + c \tag{6}$$

From the experimental determination of vapor pressure values at several temperatures, the graphic representation of lnP vs $1/T$ is a straight line and the enthalpy of sublimation can be determined from the corresponding slope.

One drawback about the experimental determination of vapor pressures of a solid is that these values are generally too low. Thus, the precise determination of the very low vapor pressure for a solid-gas equilibrium, represents a real experimental challenge[69]. Fortunately, exists a theoretical model, based on the kinetic theory of gases, that can be used to approximate the vapor pressure of a gas. This theory was proposed by James Clerk Maxwell[70] to describe the macroscopic behavior of a gas and provides a microscopic interpretation of the variables. The kinetic theory of gases assumes various basic suppositions of the structure of gases: the gas particles are identical, are rigid spheres, they do not interact with each other unless they collide and the collisions between them are “elastic”, which means that the momentum is conserved during the collision process.

In practice, a gas is considered as an ensemble of a huge number of molecules (10^{23}). Thus, the individual kinetic description of each of these molecules becomes impractical. Instead, the main objective of the kinetic theory of gases is to develop a function called the “distribution function”, which describes the statistical rate distribution of all the molecules. In this case, the average values for the mechanical properties can be calculated by the use of the rate distribution function, the variable of interest and the integration over the appropriate space.

The particles of a gas confined in a closed vessel exert a force perpendicular to the vessel wall when they collide with it. This microscopic behavior is translated to a macroscopic property, the gas pressure. The most important result of the kinetic theory of gases is the establishment of the relationship between the pressure and the statistical average of the total velocity of the gas molecules, given by equation (7).

$$PV = \frac{1}{3}Nm\langle u^2\rangle \tag{7}$$

This expression is the fundamental result of the kinetic theory of gases. In this equation, a macroscopic quantity, PV, is related with a molecular property, the total gas momentum $m\langle u^2\rangle$, where $u = \sum_j u_j /N$ is the sum of the velocities of all the number of molecules, N.

The merit of the kinetic theory is that the average values of microscopic mechanical variables can be identified with the thermodynamic macroscopic variables, like pressure, temperature or energy.

Martin Knudsen[71] studied thoroughly the phenomenon of effusion to derive an approximation for the calculation of the pressure of a gas. This process has been extensively used to determine vapor pressures of liquids and gases and also in the experimental test of the Maxwell-Boltzmann distribution law[20].

Consider a closed vessel that contains a gas at low pressure. This vessel has a small hole, with a diameter smaller than the mean free pathway of the gas molecules. Also, this vessel is contained in a vacuum chamber. With the aid of the kinetic theory of gases, an expression that relates the number of molecules that cross the hole per unit of area per unit of time, that also represents the mass loss in the vessel, with the pressure of the gas is given by $\Gamma_n = p/(2\pi m k_B T)^{1/2}$. This fact is expressed in equation (8).

$$\frac{dm}{dt} = \frac{(P - P_{ext})A}{\sqrt{2\pi RT/M}} \tag{8}$$

In this equation, P is the gas pressure in the vessel, which is the vapor pressure of the solid, P_{ext} is the exterior pressure and A is the hole area. This vapor pressure value is correct if, in the effusion process, the molecule that escapes from the vessel is immediately replaced by another molecule that comes from the solid to the gas phase to ensure the reestablishment of the thermodynamic equilibrium.

When the exterior pressure is small enough, it can be neglected, and the vapor pressure can be determined rearranging equation (8), leading to equation (9).

$$P = \frac{1}{A}\frac{dm}{dt}\sqrt{\frac{2\pi RT}{M}} \tag{9}$$

This equation represents a good approximation to the vapor pressure and can be used in the Clausius-Clapeyron equation, equation (6), in order to determine the enthalpy of sublimation.

I.3 Solvation process

The solvation process can be visualized in four principal steps[2]:

1. The cavity formation inside the solvent with a suitable size to accept a solute molecule.
2. The solvent molecules reorganization due to the perturbation of the introduction of solute molecules.
3. The establishment of anisotropic or specific interactions between solute and solvent, like hydrogen bonds or dipole-dipole interaction.
4. The total covering of a solute molecule by an excess of solvent molecules through isotropic or non-specific interactions, like dispersion forces.

The enthalpy associated with this process, the enthalpy of solvation, cannot be directly experimentally measured, with the exception of the study of the solubility of a gas in a liquid at high pressure conditions. Nevertheless, from the experimental determination of the enthalpy of sublimation and the enthalpy of solution of a solute in one solvent, the enthalpy of solvation can be indirectly determined, as it is shown in Figure 7 and equation (10).

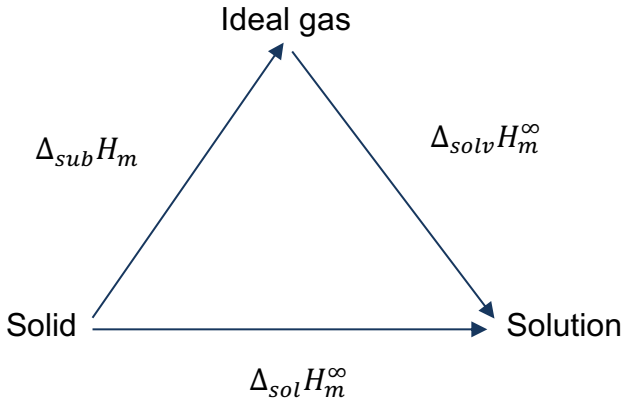

Figure 7. Scheme showing how the enthalpy of solvation can be determined from the enthalpies of sublimation and solution.

$$\Delta_{solv}H_m^{\infty} = \Delta_{sol}H_m^{\infty} - \Delta_{sub}H_m \quad (10)$$

The phenomenon of chemical reaction is, in the great majority of cases, performed in a solution phase. Then, the study of the solvation process involves the study of how the intermolecular interactions between solute and solvent create new structure in the bulk of the solution and the transformation of incoherent to coherent energy in solution at diminishing the degrees of freedom of the system[72, 73]; this favors the formation of a stable solution.

From the reported works in solvation thermodynamics, it can be noted that the study of the solvation process has been approached from a theoretical and an experimental point of view.

These previous works done in solvation show that there have been several efforts to obtain statistical mechanical expressions for the solvation chemical potential and the isolation of the solute-solvent interaction and solvent-solvent interaction and

reorganization terms. Also, the enthalpy of solvation has been used to correlate solvatochromic parameters and other solute and solvent properties in solution using acidity and basicity scales.

Nevertheless, the solvation process and the solute-solvent interactions are rarely correlated directly with the chemical structure of solute and solvent and the magnitude of these interactions are not often precisely quantified.

I.3.1 Theoretical approach to solvation thermodynamics

In the theoretical description of the process of solvation, a molecular study of solutions is necessary to model solute-solvent interactions. A statistical mechanical approach is applied in order to describe the potential energy between solute and solvent molecules and to obtain macroscopic expressions for the chemical potential from microscopic approaches.

Yan and Karplus[74] showed that "only averages over the solute-solvent interaction energy contribute to the free energy and that the solvent-solvent interaction term, which contributes the so-called cavity (solvent reorganization) term to the energy, is cancelled exactly by a corresponding term in the entropy". In this work, the site-site Ornstein-Zernike integral equations are used to determine the derivatives of the distribution functions with respect to the density. The procedure makes possible the calculation of the energetic and entropic contributions to the solvation free energy in the infinite dilution limit.

In his work[8], Ben-Naim set the correct definitions of solvation thermodynamics and proposed the introduction of the "pseudo" chemical potential, which was used to derive solvation thermodynamic functions that do not depend on a concentration scale. Also, Ben-Naim defines the solvation process as the transfer of a molecule from a fixed position in the gas phase to a fixed position in the solution phase[9]. The main contribution of this work is the definition of a quantity called "pseudo" chemical potential, shown in equation (11).

$$\mu_A^* = G(T, P, N_A + 1, N_B; \boldsymbol{R_0}) - G(T, P, N_A, N_B) \tag{11}$$

In this expression becomes evident the parametric dependence in the fixed position $\boldsymbol{R_0}$. This dependence is the difference between the ordinary chemical potential and the pseudo chemical potential.

Ben-Amotz[10] recalls previous work in solvation thermodynamics and derives a new expression for the chemical potential and solvation thermodynamics function using the Widom potential distribution theorem[75] and the Kirkwood coupled-parameter integration[76]. These statistical mechanical tools lead to the analytical expression of the solvation chemical potential and the derived thermodynamic properties of solvation.

The solvation chemical potential may be resolved into non-compensating energetic $\epsilon_\mu^x = \langle\Psi\rangle^{(1)}$ and entropic $-Ts_\mu^x = \frac{1}{\beta} ln\langle e^{\beta\delta\Psi}\rangle^{(1)}$ and this expression can be further extended to obtain a Gaussian fluctuation approximation, $(\beta/2)\langle(\delta\Psi)^2\rangle^{(1)} = (\beta/2)K_2(1)$, where $K_2(1)$ is the second-order cumulant over the solute-solvent interaction energy between solute and all solvent molecules, Ψ.

From the derivation of the expressions for ϵ_μ^x or s_μ^x, it is concluded that the chemical potential is not affected by solute-induced changes in the solvent-solvent interaction energy, at least not explicitly. This work relates the theoretical work with experimental solvation measurement in order to extract numerical values for the solute-solvent energy of interaction and the associated fluctuation entropy.

In a recent work[11], Ben-Amotz, *et. al.*, it is found that the first order coupling parameter methodology can be extended to a second order coupling methodology and with that, it is possible to obtain statistical fluctuations of the solute-solvent and solvent-solvent interaction energies. It is worth to note the efforts to obtain explicit statistical mechanical expression for the solvent-solvent energies and the analytical expression of the solvation chemical potential.

Lazaridis[12, 13] proposes an approximation using an inhomogeneous fluid model, where the solute is considered fixed at the origin and generates an external field that creates solvent density fluctuations around it, to obtain the energy and entropy of solvation. This approximation allows a model of the solvent-solvent reorganization energy and entropy with “correlation” and “liberation” terms, depending on the structural changes that the solute imposes on the solvent. The work proposes that the contribution is a connection between interfacial phenomena and microscopic solvation.

In order to start the statistical mechanical analysis of the thermodynamics of solutions, it is worth to mention the work of McMillan and Mayer[77] in dilute solutions; they showed that the activity coefficients are analogous to the coefficients in the virial state equation of a gas. This is useful because the density of the solute in a solution can be expressed with an analogous state equation that involves virial coefficients.

An important issue in the study of the thermodynamics of solvation is the formation of a suitable cavity inside the solvent, in order to receive a solute molecule. The scaled particle theory developed by Reiss *et. al.*[78] to determine the equation of state of a bulk rigid-sphere fluid, has been a useful contribution in the statistical mechanics study of the solution process. Scaled particle theory is a statistical mechanics tool that proposes an expression to the reversible work required to introduce a spherical particle into a fluid of spherical particles. The essence is that an amount of work is required to exclude the centers of the molecules from any specified region of space in a fluid. The probability to open a cavity inside the solvent with a suitable radius r is given by $p_0(r,\rho) = \exp[-(W(r,\rho)/kt)]$, where $W(r,\rho)$ is the work required to open the cavity and ρ is the number density of the fluid.

Pierotti[19] suggests an equation that proposes a decomposition of the enthalpy of solvation in contributions of various terms, as shown in equation (12).

$$\Delta_{solv}H_m^{\infty} = \Delta_{cav}H + \Delta_{int}H_m^{\infty} - RT(1 - \alpha_P T) \quad (12)$$

In this equation, the term $\Delta_{cav}H$ is the enthalpy necessary to open a cavity inside the solvent or the enthalpy of cavity formation; $\Delta_{int}H_m^{\infty}$ is the solute-solvent enthalpy of interaction at infinite dilution; α_P is the thermal expansion of the solvent; R is the gas constant and T is the temperature. The term $\Delta_{int}H_m^{\infty}$ accounts the whole set of interactions established between solute and solvent, specific and dispersion interactions.

The Scaled Particle Theory was applied by Pierotti to chemical systems[19], in order to propose an equation that calculates the enthalpy of cavity formation, equation (13).

$$\Delta_{cav}H = \alpha_P RT^2 \frac{y}{(1-y)^3}\left[(1-y)^2 + 3(1-y)\frac{\sigma_2}{\sigma_1} + 3(1+2y)\left(\frac{\sigma_2}{\sigma_1}\right)^2\right] + pV_1^*\left(\frac{\sigma_2}{\sigma_1}\right)^3 \quad (13)$$

Where σ_1 and σ_2 are the solvent and solute molecular diameters, respectively, V_1^* is the molar volume of the solvent, T is the temperature p is the pressure and R is the gas constant. This equation is valid for a cavity whose radius is equal to $r = (\sigma_1 + \sigma_2)/2$. The quantity y is the volume fraction occupied by the solute molecules and is defined as $y = N_A\pi\sigma_1^3/6V_1^*$, where N_A is the Avogadro number.

The enthalpy of interaction is calculated from combination of equation (12) and equation (13).

I.3.2 Experimental approach of solvation thermodynamics

One of the most used experimental approaches in chemistry to understand the solvation of a solute is the Abraham[79, 80] solvation model. The vision of relating solvatochromic parameters to thermodynamic properties, like the enthalpy or free energy of solvation, was proposed by of Kamlet and Taft[81-83] with their acidity, basicity and polarity scales and the Linear Free Energy Relations.

From this work, Abraham proposed the Linear Solvation Energy Relations (LSER)[79, 80], in order to correlate partition coefficients, free energies of transfer and other thermodynamic properties through a multilinear fit of these properties with solvatochromic parameters. The Abraham solvation model argues that each of the parameters that are involved in a LSER is related with some kind of solute-solvent interaction. This model has been employed to obtain relationships between thermodynamics and solubility parameters. A discussion about the validity of these relations is given by reference[84]. In this work, it is argued that LSER are not fundamental relations of nature and are just empirical models.

In general, it is not clear if the experimental conditions where the solubility and spectroscopic experiments are the same as the ones required to describe the solvation process, the exact quantity or parameters that must be related with the thermodynamic properties of solvation or which is the correct thermodynamic quantity that should be related to solvatochromic parameters.

Following with the designed works to determine the hydrogen bond magnitudes, Fuchs[85] used the results of the "pure base" (PB) methodology of Arnett[86] and compared it with the "enthalpy of solvation" (SE) method in the calculation of enthalpies of formation of hydrogen bond in 1-octanol.

The pure base method (PB)[86] is based in the assumption that the enthalpy of formation of a hydrogen bond (ΔH_h) can be calculated from differences in the enthalpies of solution between model compounds in order to cancel all the enthalpy terms that belong to non-hydrogen bond interactions. The methodology is as follows: the enthalpy of solution of an alcohol A, which is a good hydrogen bond donor and a probe compound M, which is not a hydrogen bond donor, are determined in a solvent S, which acts as a hydrogen bond acceptor and this enthalpies are also determined in an inert, reference solvent. The enthalpy of formation of hydrogen bond can be calculated from the equation (14).

$$\Delta H_h(PB) = (\Delta_{sol}H_S^A - \Delta_{sol}H_S^M)_B - (\Delta_{sol}H_S^A - \Delta_{sol}H_S^M)_{ref} \quad (14)$$

By other hand, the methodology of enthalpy of solvation (SE) makes the assumption that the enthalpy of formation of hydrogen bond is just the difference in the enthalpies of solvation (gas-solution transfer) of compounds A and M into the solvent S, as shown in equation (15). No reference solvent is needed.

$$\Delta H_h(SE) = \Delta\Delta H(g \rightarrow S) = \Delta H(g \rightarrow S)^A - \Delta H(g \rightarrow S)^M \quad (15)$$

From equation (14) and equation (15), equation (16) is obtained.

$$\Delta H_h(PB) = \Delta H_h(SE) - \Delta\Delta H(g \rightarrow ref) \quad (16)$$

Both methodologies assume that the difference in the enthalpies of solution and/or solvation cancels the enthalpy terms that belong to other interactions and the enthalpy of hydrogen bond is obtained.

Another approach to hydrogen bond acidity and basicity scales was made by Laynez, *et. al.*[87, 88] who experimentally determined enthalpies of solvation and using probe molecules, developed a methodology to determine a solvent basicity scale based on the enthalpies of solvation and/or solution. The probe molecules were pyrrole (P), N-methylpyrrole (MP), benzene (B) and toluene (T). The differences of the enthalpies of solution are shown in equation (17).

$$\delta\Delta H_{solv}^o = (\Delta H_{solv}^o(P) + \Delta H_{solv}^o(T) - \Delta H_{solv}^o(MP) - \Delta H_{solv}^o(B))_{BASE} \quad (17)$$

The subindex BASE is a reference to the solvent under study. In this work, 35 different solvents were used. Laynez argument was that the value of $\delta\Delta H^o_{solv}$ is consistent with the β scale of Kamlet and Taft, and that is related to molecular properties of the solute in solution.

From these results, an acidity scale was proposed, following a similar methodology as above, using the probe molecules N-methylimidazole and N-methylpyrrole. The expression for the $\delta\Delta H^o_{solv}$ term is given in equation (18.1) and (18.2).

$$\Delta H^o_{solv} = (\Delta H^o_{solv}(P) + \Delta H^o_{solv}(T) - \Delta H^o_{solv}(MP) - \Delta H^o_{solv}(B))_{BASE} \quad (18.1)$$

$$\delta\Delta H^o_{solv} = \left(\Delta H^o_{sol}(P) + \Delta H^o_{sol}(T) - \Delta H^o_{sol}(MP) - \Delta H^o_{sol}(B)\right)_{BASE} + K$$

An acidity scale is proposed, following a similar methodology as above, using the probe molecules N-methylimidazole and N-methylpyrrole.

$$\delta\Delta H^o_{solv} = \left(\Delta H^o_{sol}(N-MeIm) - \Delta H^o_{sol}(N-MePirr)\right)_{BASE} + K \quad (18.2)$$

The term $\delta\Delta H^o_{solv}$ is related with the acidity scale of Kamlet and Taft and with the Onsager reaction field scheme, as shown in equation (19)

$$\delta\Delta H^o_{solv} = a\alpha_2^H + bf(\varepsilon) + c \quad (19)$$

where $f(\varepsilon) = (\varepsilon - 1)/(2\varepsilon + 1)$.

It is proposed that the value of α_2^H is proportional to the negative of the ΔH^{acid}, the enthalpy change of acidity of the solvent hydrogen bond.

Leitao[16, 17] determined the enthalpies of solvation of inositol compounds in different solvents and using the Pierotti equation (equation (13)), calculated the enthalpy of cavity formation values in order to correct the enthalpy of solvation values and to determine the enthalpy of interaction of each compound with each solvent and relate these values to OH functional groups present in the chemical structure of the studied compounds.

Matteoli[89], following similar objectives as Leitao, determined the enthalpies of solvation of some hydrocarbons in several solvents. The model used involves the contribution of each functional group to the enthalpy of solvation, according to Bondi's proposal[90] to explain the rising of molecular volume and van der Waals radii due to each functional group. It is proposed that the enthalpy of solvation can be expressed as $\Delta_{solv}H^0 = A + \sum_j n_j B_j$, where B_j is the contribution of an individual functional group to the standard enthalpy of solvation. The Pierotti equations were used to determine the enthalpies of cavity formation and interaction. However, their discussion was just

superficial and the molecular characteristic of the studied compounds, was not discussed.

Barannikov, *et. al.*[91] determined the enthalpies of solvation of ethylene oxide $CH_3O(CH_2CH_2O)_nCH_3$ with $n = 1$ to 4 oligomers in methanol, chloroform and water. A model is proposed to study polymer interactions in solution through the calculation of the pairwise interaction coefficient from the enthalpies of solution, as shown in equation (20).

$$\Delta_{\mathrm{sol}}H = \Delta_{\mathrm{sol}}H^0 + h_{22}m \tag{20}$$

In this expression, h_{22} is the enthalpic coefficient of solute-solute pairwise interaction and m is the molal concentration. In this work is reported an estimation of hydrogen bond enthalpies and the development of a group contribution model that permits the description of the enthalpies of solvation of monoethers and ethylene oxide oligomers in the used solvents.

It is also worth to mention the work of Solomonov[92, 93] where they correlated the enthalpy of solvation with molecular parameters. It is proposed that the enthalpy of solvation is linearly proportional of the molar refractivity. The main effort of research by Solomonov is to find the dependence of the enthalpy of solvation with a reduced number of molecular parameters than the Abraham solvation model, having these molecular parameters a more “definitive physical meaning”.

Solomonov uses two solvents as model, cyclohexane and carbon tetrachloride, with the argument that these solvents are not able to establish specific interactions. Nevertheless, the lack of a molecular insight in the analysis of solute-solvent molecular interactions and the use of “model” solvents makes this methodology a little impractical, with no clear arguments about which molecular parameters are the correct ones to be employed.

More recently, Baldwin[94] has employed the concept of solvation to understand peptide-water interactions[95] and to explain proteins hydrophobic effects and folding, using simulations and analogies of the solvation process of alkanes in water in order to correlate them with proteins.

II. Objectives

II.1 General objective

It is postulated that **the energetic information relative to non-covalent interactions in a crystal phase or between solute and solvent in a liquid solution, both weaker than the covalent chemical bonds, is contained in the macroscopic thermochemical properties. Then, the microscopic information provided by a molecular spectroscopic probe, must be consistent with the magnitude of those thermochemical properties experimentally obtained.**

From this, the objective of this research is to design and perform a thermochemical study to determine phase change thermodynamic properties whose magnitudes can be related to molecular properties and the intermolecular interactions between the involved compounds.

II.2 Specific objectives

To attain the general purpose of this research, it is necessary to perform an extended experimental work, involving different thermochemical and spectroscopic work. Also, an analysis of the imidazole and pyrazole derivatives crystal structures, through the use of specialized software, is previewed. The last could permit the comprehension of the relevant features to know the possible intermolecular interaction present in the solid phases and possible intermolecular interactions in solution with the proposed solvents.

Some concepts derived from statistical mechanics will be incorporated in order to understand, in more precise way, how the derived enthalpy of solvation or interaction values and trend, account all the non-covalent interactions between solutes and solvents included in this research. Also, the NMR spectroscopy as a molecular support and discussion element, for the experimental results, is expected.

Some of the involved tasks are by themselves experimental challenges or specific goals that can be highlighted as:

1.- Purification of the imidazole and pyrazole derivatives by the use of different methodologies (sublimation, crystallization, distillation, etc.).

2.- Determination of the purity, enthalpy and temperature of fusion by Differential Scanning Calorimetry.

3.- Experimental determination of the enthalpy of sublimation by the Knudsen Effusion Method.

4.- Experimental measurement of the enthalpies of solution of the proposed compounds in the solvents water, methanol and acetonitrile, by Isoperibolic Solution Calorimetry.

5.- Determination of the enthalpies of solution at infinite dilution for all the studied solutes in the three selected solvents.

6.- Determination of the enthalpies of solvation, through the enthalpy of sublimation and enthalpy of solution at infinite dilution values.

7.- Calculation of the enthalpy of the cavity formation for all solutes in all the solvents.

8.- Calculation of the enthalpy of interaction for all solutes, in the used solvents.

9.- Characterize all solutes by ^{1}H NMR spectroscopy in the deuterated solvents.

10.- Rationalization of the enthalpy of fusion and sublimation values in terms of the molecular and crystal structure features of solutes.

11.- Rationalization of the enthalpy of solvation or interaction values in terms of the nature of the molecular structure of the solutes and solvents and the intermolecular interactions.

III. Experimental section

III.1 Imidazole and pyrazole derivatives

The selected chemical compounds as solid solutes in this work were commercially obtained from Sigma-Aldrich Inc. and are classified in two groups on the base of the imidazole or pyrazole heterocycle ring included in their molecular structure. The solutes described as the imidazole derivatives are: Imidazole (CAS 288-32-4), 2-methylimidazole (CAS 693-98-1), 2-ethylimidazole (CAS 1072-62-4), 2-isopropylimidazole (CAS 36947-68-9). In the same way, the named pyrazole derivatives are: pyrazole (CAS 288-13-1), 3,5-dimethylpyrazole (CAS 67-51-6), 3,4,5-trimethylpyrazole (CAS 5519-42-6). The corresponding chemical structures are shown in Figure 8.

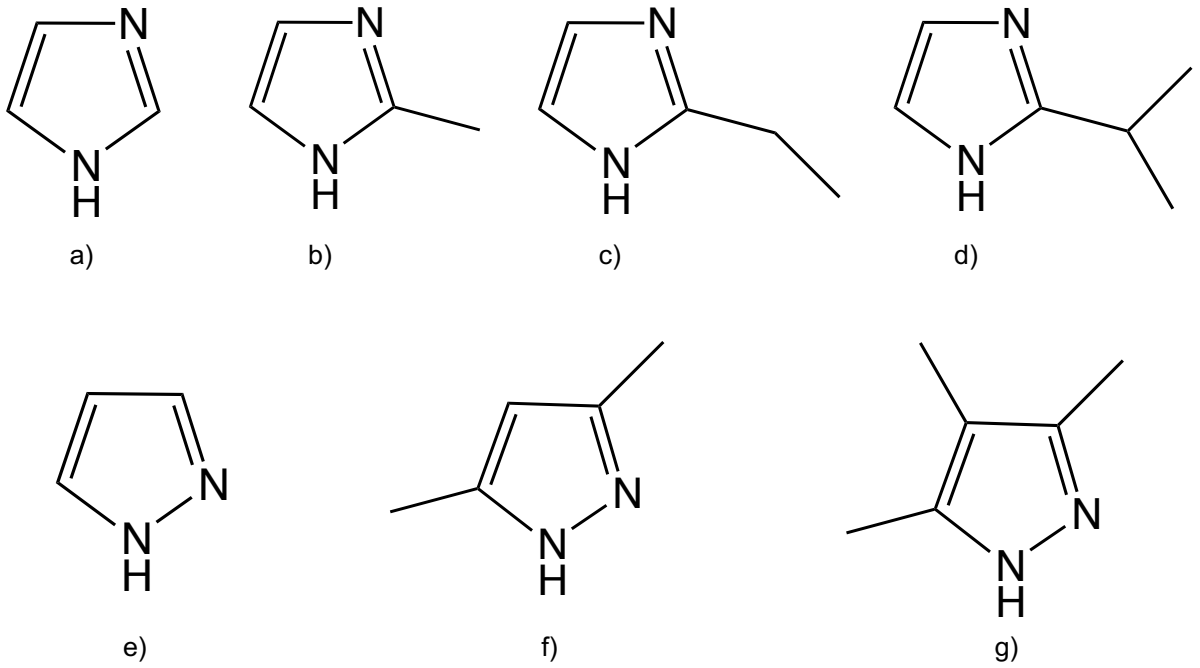

Figure 8. Studied compounds, a) imidazole, $C_3H_4N_2$, b) 2-methylimidazole, $C_4H_6N_2$, c) 2-ethylimidazole, $C_5H_8N_2$, d) 2-isopropylimidazole, $C_6H_{10}N_2$, e) pyrazole, $C_3H_4N_2$, f) 3,5-dimethylpyrazole, $C_5H_8N_2$, and g) 3,4,5-trimethylpyrazole, $C_6H_{10}N_2$.

III.1.1 Purification of imidazole derivatives

The solid compounds were purified by sublimation under reduced pressure (~7 Pa). The temperature of the silicone oil bath was adjusted at 398.15 K for 2-methylimidazole and at 403.15 K for 2-isopropylimidazole and the vacuum was kept for around 1200 to 1500 s, in order to discard as much impurities as possible. After this period, the finger

of the sublimation device was cooled by water recirculation at room temperature. In this way, the purified sample was collected for around 600 to 900 s.

The imidazole and 2-ethylimidazole were purified in a similar way but at 375.15 K for imidazole and at 383.15 K for 2-ethylimidazole. These temperatures are higher than the corresponding melting point temperatures. Actually, the process is a distillation process performed in a vacuum sublimation device. The liquid phase was evaporated and directly collected as a solid phase in a cold finger, maintained at room temperature. The described process leads to purities over 99.90 mole percent.

After purification, all the purified samples were grinded manually in an agate mortar. This procedure improves the thermal conductivity of the samples in the differential scanning calorimetry cell and does not lead to any phase transition, as verified by the technique itself under N_2 atmosphere.

III.1.2 Purification of pyrazole derivatives

In the case of the pyrazole, a sample from the commercial flask was taken and extended over a glass plane surface. This sample was dried under vacuum for two cycles of 300 seconds each, at a temperature of 328.15 K. With this procedure a purity over 99.90 mole percent was ensured.

The 3,5-dimethylpyrazole was purified using the sublimation methodology. When the bath temperature reached 348.15 K, the vacuum was immediately started and the sublimation process lasted 900 s. This procedure leads to a purity sample over 99.90 mole percent.

In the case of the 3,4,5-trimethylpyrazole, due to the lack of enough available mass, the compound was not further purified. Samples were taken from the commercial flask and directly used to perform the Knudsen effusion and solution calorimetry experiments.

III.1.3 Solvents

The solvents used in this work were water, methanol and acetonitrile. The deionized water was obtained through a Millipore® filter, with a resistivity of 18 MΩ. The organic solvents were always manipulated through a stainless-steel cannula, and under high purity nitrogen.

III.2 Differential scanning calorimetry experiments

As described by Höhne, *et. al.*[96], Differential Scanning Calorimetry (DSC) means the measurement of the change of the difference in the heat flow rate to the sample and to

a reference sample while they are subjected to a controlled temperature program. DSC measures the change of a property, namely of a heat flow rate difference, which normally is released due to an alteration of the temperature of the sample and allows to measure heat capacity, heat of transition, kinetic data, purity and glass transition.

The purity, the temperature and enthalpy of melting for the studied compounds were determined by differential scanning calorimetry (DSC) using a TA Instruments Q2000 calorimeter, shown in Figure 9.

Figure 9. Differential Scanning Calorimetry (DSC) Q2000 device used to perform the purity, temperature and enthalpy of fusion experiments.

The software associated to the instruments calculates the heat flow dH/dt, using equation (21).

$$\frac{dH}{dt} = C_p \frac{dT}{dt} + f(T,t) \tag{21}$$

Where H is the enthalpy, in J·mol^{-1}, C_p is the sample heat capacity, in J·mol^{-1}·K^{-1} and $f(T,t)$ is a kinetic response of the sample, in J·mol^{-1}·s^{-1}.

The purity of the compounds was determined with the basic model proposed by Van't Hoff. This model applies only when the impurity is not soluble in the solid phase, equation (22).

$$T = T_0 - x\left(\frac{RT_0^2}{\Delta_{fus}H}\right)\left(\frac{1}{f}\right) \tag{22}$$

In this equation, T is the experimental fusion temperature of the sample, T_0 is the fusion temperature of the pure sample, $\Delta_{fus}H$ is the enthalpy of fusion, x is the mole fraction of the impurity, f is the liquid fraction of the sample and R is the gas constant.

The equipment was frequently calibrated for temperature and energy using high purity standard reference material Indium NIST SRM 2232, with standard values of T_{fus} =(429.7485 ± 0.0003) K and $\Delta_{\mathrm{fus}}H$=(28.51 ± 0.19) J·g^{-1}. The heating rate used was 5 K·min^{-1} and all experiments were performed under a high purity N_2 atmosphere. All the samples were weighted in a Mettler-Toledo UMX2 micro balance.

III.3 Solution Calorimetry

The instrument used to determine the enthalpy of solution was an isoperibolic 2225 Precision Solution Calorimeter, incorporated into a Thermal Active Monitor TAM III, both systems provided by Thermometric. The stability of the bath was 10^{-6} K over 86400 s. The outer chamber of the system is in stainless steel and surrounds the calorimeter itself, that is a thin-walled Pyrex glass cell.

The glass cell acts as the reaction or solution calorimeter and incorporates a thermistor, for sensing temperature and a resistance heater for equilibration and calibration. The glass cell is attached to a cylindrical body that acts as thermal insulator and contains a Wheatstone bridge for precise resistance measurement.

A gold stirrer is attached to a small motor shaft and also acts as the ampoule holder. The ensemble is concentrically placed through the calorimeter body. The experimental device is shown in Figure 10.

a) b)

Figure 10. Solution calorimetry experimental device. In a) is shown the TAM III bath, in b) the solution-reaction calorimetric cell.

The data for the thermistor resistance as a function of temperature and all the necessary data for electrical calibration, are embedded in a ROM supplied with each particular calorimetric cell. Short time fluctuations into the calorimetric cell are within 10^{-5} K and the resolution attends 10^{-6} K that corresponds to (1-4)·10^{-3}J. Each calorimetric cell has its unique parameters that relate the electrical resistance of the thermistor with the temperature, as in equation (23).

$$R = Ae^{\frac{B}{T}+\frac{C}{T^2}} \tag{23}$$

In this equation, R is the electric resistance, A, B and C are parameters specific of the thermistor and T is the temperature of the cell.

The instrument works by comparison of the rise temperature produced in a solution or reaction experiment and that produced during an experiment in which a precise amount of electrical energy is performed during an elapsed time into the calorimetric cell. This time is adjusted to produce a rise temperature as near as possible to the corresponding solution experiment.

The temperature offset, during calibration before and after the main experiment, is continuously measured as a function of time. The time-temperature data are collected by a computational system using the SolCal software, that controls and analyzes the calorimetric experiment. The corrected rise temperature is calculated by the Regnault-Pfaundler method as for any typical experiment in isoperibolic calorimeters[97].

Freshly purified samples of each compound were used to perform the solution calorimetry experiments. The glass ampoules containing the samples were sealed with a silicon rubber stopper and with a fused beeswax droplet of over it. According to the expected concentration, samples of (3-15)·10^{-6} kg of the compound were charged in the ampoule. The ampoule was coupled to the stirrer and then introduced to the calorimeter for equilibration. The stirring speed was always fixed to 300 rpm. The same quantity of the solvent (25·10^{-6} m^3) for all the experiments was deposited in the calorimetric cell. The masses of the used solvent were determined from their corresponding density.

In order to calculate the heat of solution, an energy balance in the calorimetric cell is performed, equation (24).

$$-\frac{dQ}{dt}-\frac{dQ_F}{dt} = C\frac{dT}{dt} + k(T - T_S) \tag{24}$$

In this equation, k is the heat exchange coefficient in J·K^{-1}·s^{-1}, T_S is the temperature of the surroundings, in K, T is the reaction cell temperature, in K and C is the reaction cell heat capacity, in J·K^{-1}.

During the base line, dQ/dt is equal to zero, so equation (24) is reduced to equation (25).

$$-\frac{dQ_F}{dt} = C\frac{dT}{dt} + k(T - T_S) \quad (25)$$

In the base line, the temperature of the cell can reach an asymptotic value, the temperature of the surroundings at an infinite time $t = \infty$, so in this stage dT/dt is zero, and equation (25) reduces to equation (26).

$$-\frac{dQ_F}{dt} = k(T_\infty - T_S) \quad (26)$$

Where T_∞ is the constant steady-state temperature of the reaction cell.

Substituting equation (26) in equation (24), we get equation (27).

$$-\frac{dQ}{dt} = C\left(\frac{dT}{dt} + \frac{1}{\tau}(T - T_\infty)\right) \quad (27)$$

Where $\tau = \frac{C}{k}$, is the calorimeter time constant in s. The equation (27) is valid for the whole experiment sections, either the calibration or the solution section. Integrating equation (27), we obtain equation (28).

$$-Q = C\left(\Delta T_{obs} + \int_{t_{start}}^{t_{end}} \frac{1}{\tau}(T - T_\infty)dt\right) \quad (28)$$

Where $\Delta T_{obs} = T_{t_f} - T_{t_i}$. The equation (28) can be reduced to equation (29).

$$-Q = C\Delta T_{corr} \quad (29)$$

Where $\Delta T_{corr} = \Delta T_{obs} + \Delta T_{adj}$ and $\Delta T_{adj} = \int_{t_{start}}^{t_{end}} \frac{1}{\tau}(T - T_\infty)dt$. In order to obtain the values for τ and T_∞, the software uses the data from a base line and from the initial and the final temperatures in this period, considering that $-dQ/dt$ is zero, we obtain equation (30).

$$0 = C\left(\frac{dT}{dt} + \frac{1}{\tau}(T - T_\infty)\right) \quad (30)$$

This equation is a classic example of the Newton's cooling law, which has the solution shown in equation (31).

$$T - T_\infty = ce^{-t/\tau} \quad (31)$$

The software SolCal v1.2 fits the base line to this model. When the standard deviation of the fitting is $\sigma < 10\mu K$, the calorimetric cell reaches a pseudo-equilibrium state and a new experiment is suitable to be performed. From this adjustment, T_∞, τ and C can be calculated. With the T_∞ and τ, equation (30) can be integrated in order to obtain

ΔT_{adj} and then ΔT_{corr}. The heat of calibration Q_{cal} is known from the electric calibration and this value is used, together with ΔT_{corr} to obtain C, that is further used to obtain the heat of reaction Q_r. The enthalpy of solution is determined from the quotient of the heat of reaction and the number of moles of solute.

The enthalpy of solution of each compound in the three solvents was determined in a molal concentration range of 10^{-2} to 10^{-3}. In each experiment, the stirrer speed was maintained at 300 rpm and two different electric calibrations are performed before and after the breaking of the glass ampoule to determine de calorimetric coefficient of the cell. The total energy of the process was determined with the software provided with the instrument, which is based on the Regnault-Pfaundler method[97]. This value was corrected for each experiment with the thermal effect produced by the breaking of an empty ampoule. This last value is different in each of the studied solvent. The performance of the instrument was tested with the solution process of KCl (SRM 1655) from the NIST in water. The results meet correctly the established value of (17.584 $\pm$ 0.017) kJ·mol^{-1}.

III.4 Knudsen effusion experiments

The Knudsen method[98] is widely used to determine the vapor pressure of solids. If the procedure is applied to several temperatures, the dependence of the vapor pressure with temperature is obtained.

The method consists in the approach that a solid of interest with molar mass (M), is in equilibrium with its gas phase in a closed vessel, normally a cylinder, maintained at constant temperature T, and under high vacuum. The system consists in just one component and two phases in equilibrium. If under these conditions a small hole of area A is pierced in the top of the cylinder, the effusion of the gas phase begins. To maintain the equilibrium conditions, it is necessary that the hole area be so small to produce a molecular flow. In reality, the equilibrium conditions can be reached with the compromise of a small area hole and a large surface of the solid phase. The experimental variables during the experiment are the effusion area, the mass effusion (Δm) lost at each temperature, and the molecular mass of the compound under study. The relation between the pressure and the effusion rate dm/dt, is given by Knudsen equation, equation (9).

The use of the well-known Clausius-Clapeyron equation (equation (6)) provides the enthalpy of sublimation at the intermediate temperature of the measurement range.

The experimental device for these experiments consists in a cooper cylindrical block, over which five cylindrical cavities were machined in such a way to exactly match the geometrical form and size of the Knudsen cells, shown in Figure 11.

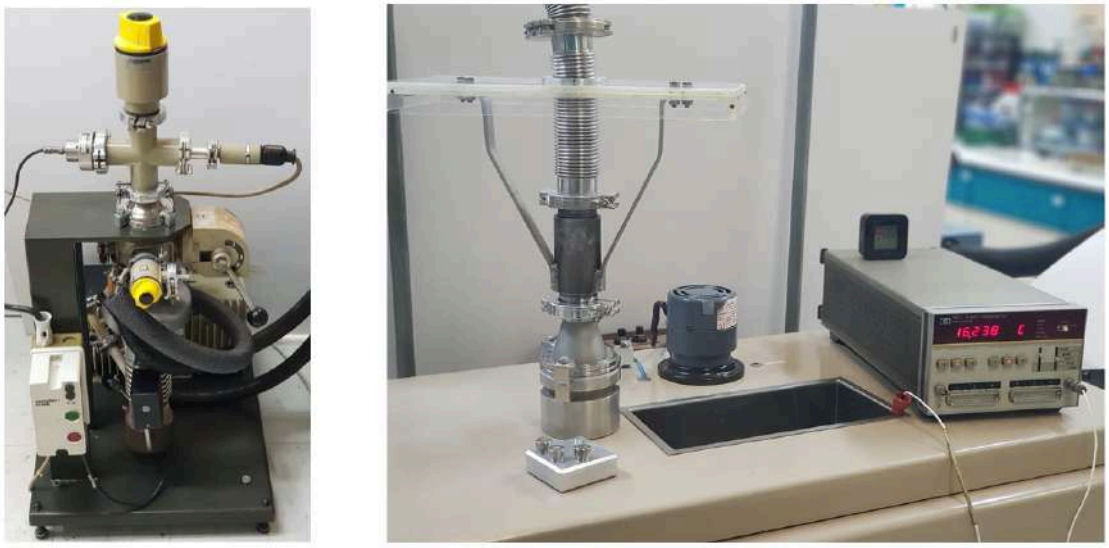

Figure 11. The Balzers vacuum diffusion pump coupled to the Knudsen effusion device, designed to determine the mass loss and then the vapor pressure at different temperatures.

Even the tightly mechanical contact between the cooper block and the effusion cells, the thermal contact can be easily improved by applying some amount of silicone grease. The cooper block is tightly adjusted to an aluminum block machined for an easy fitting to a commercial vacuum connector 63 ISO, obtained from any vacuum system components provider. The last piece is coupled to vacuum system composed by a flexible stainless-steel tube (40 KF), vacuum valves and manometers that are finally connected to a Balzers PVA 063 H diffusion pump.

The cylindrical body and lid of each Knudsen cells (Φ = 18 mm, h = 24.5 mm) were made in stainless steel. Over the lid a platinum foil collimator, currently used in electronic microscopy, was welded using a high content silver welding rod. Collimators with different hole diameter (100, 200, 250, 500, 1000, 1250 y 1375 μm) were welded over different lids in order to obtain several measurements of effusion rate at the same temperature in just one experiment. A flat Teflon joint was used to ensure a good seal between body and lid of the Knudsen cell. In order to ensure that effusion occurs just from the collimator hole, before the use, the cells were tested at the level of the welding and the Teflon seal, where no leakage was detected. The cells are shown in Figure 12.

Figure 12. The vacuum connector 63 ISO, on which is based the copper block that receive the Knudsen effusion cells used.

For an experiment, the mass used in the effusion experiments was the enough to cover the bottom of each cell. This is achieved by the use of around (200-400)·10^{-6} kg of a freshly purified sample. The closed and weighed cells were placed in the cavities of the copper block. A good thermal contact, between the block and cells is assured by applying some quantity of Apiezon M grease, in all the surface contact between them. The metallic block is attached to the vacuum system and is immersed in a water thermostatic bath (Tronac PTC-41), previously fixed at the desired temperature. When the thermal equilibrium is attained, the main valve is opened. Then, the residual pressure is immediately reduced until 10^{-6} bar and the sublimation process is promoted. Simultaneously the elapsed time starts to be counted. At the end of the experiment, the main valve was closed, the vacuum was stopped and the elapsed time registered. When the system is opened, the cells were extracted and immediately cleaned using n-hexane and toluene. Then, the solvent was evaporated, the cells were weighed at new and the mass lost by effusion was registered. Then, a new experiment at new temperature is started.

III.5 Solute and solvent diameters and enthalpy of cavity formation

The enthalpy of cavity formation is calculated from equation (13) proposed by Pierotti[19].

$$\Delta_{cav}H = \alpha RT^2 \frac{y}{(1-y)^3}\left\{(1-y)^2 + 3(1-y)\left(\frac{\sigma_2}{\sigma_1}\right) + 3(1+2y)\left(\frac{\sigma_2}{\sigma_1}\right)^2\right\} + pV_1^* y\left(\frac{\sigma_2}{\sigma_1}\right)^3 \quad (13)$$

Where the term α is the coefficient of thermal expansion of the solvent, R is the gas constant, T is the temperature (298.15 K), y is the fraction of solvent occupied by the solute, defined as $y = N_A\pi\sigma_1^3/(6V_1^*)$, where N_A is the Avogadro number, σ_1 and σ_2 are the solvent and solute diameters, respectively, p is the pressure (0.1 MPa) and V_1^* is the molar volume of the solvent, derived from the corresponding density values at 298.15 K. The solvent diameters and the coefficients of thermal expansion are the available literature values: σ_1 , in 10^{-6} m: Water[99] = 0.275, Methanol[100] = 0.380,

Acetonitrile[100] = 0.428 and $10^3\alpha_i$ values, in K^{-1}: Water[101] = 0.26, Methanol[102] = 1.20, Acetonitrile[101] = 1.37.

The solute molecular diameters were obtained from quantum mechanical calculations provided by the CrystalExplorer17 Software[103], used to analyze the crystal structure for the imidazole and pyrazole derivatives. The calculations where performed using a DFT methodology with the 6-31G(d) basis set and the B3LYP exchange/correlation functional, using the computational chemistry package "Tonto"[104], available from the library of CrystalExplorer17. The approximation used was that the volume of the molecular electronic density corresponds to the volume of a sphere.

III.6 ^{1}H NMR spectroscopy

The ^{1}H NMR spectra of the different imidazole compounds under study were taken in a Bruker 400 spectrometer. The samples were prepared directly in NMR tubes in which a solid sample of around $5 \cdot 10^{-6}$ kg was placed and the corresponding deuterated solvents were added (water, obtained from Sigma-Aldrich Co. with a deuterated percentage of 99.9%, methanol, obtained from ISOTEC Inc. with a deuterated percentage of 99.8% and acetonitrile, obtained from Cambridge Isotope Laboratories Inc. with a deuterated percentage of 99.8%). When the complete solution was achieved, the spectra were taken at room temperature.

III.7 Dipole moments of the studied compounds

The dipole moments of the solute molecules were obtained from quantum mechanical calculation using the computational package deMon2k[105]. The DFT optimized double-zeta valence polarization (DZVP) basis set in combination with automatically generated GEN-A2* auxiliary functions set was employed. The generalized gradient approximation in form of the PBE exchange-correlation functional was employed[106]. The deMon2k defaults settings were used in these calculations[107].

III.8 Crystal packing analysis

The crystal structures of 2-ethylimidazole and 2-isopropylimidazole obtained from X-ray monocrystal diffraction experiments and x-ray powder diffraction experiments, respectively, at Cinvestav, while crystallographic files for imidazole, 2-methylimidazol, pyrazole, 3,5-dimethylpyrazole and 3,4,5-trimethylpyrazole (with deposit names IMAZOL02, FULPIM, PYRZOL04, DASXEA and FITQEE respectively) were obtained from the Cambridge Structural Database[108].

III.8.1 Hirshfeld surface

The visualization and evaluation of bond lengths and angles is a common practice in chemistry, but it is interesting to analyze the possible interactions between molecules in a crystal phase. The electrostatic forces present in a crystal must be evaluated on the electronic densities of interacting molecules. For this purpose, a quantitative description of molecular charge distribution, Hirshfeld[109] proposed the dissection of a molecule in well-defined atomic fragments. As established by Hirshfeld himself, the procedure consists in the sharing of the charge density at each point among the several atoms in proportion to their free atomic densities at the corresponding distances from the nuclei. Algebraically, this is expressed by the definition of a weight function in the following equation (32).

$$w_a(r) = \rho_a^{at}(r) / \sum_{i \epsilon Molecule} \rho_i^{at}(r) \quad (32)$$

Where $w_a(r)$ is the atomic weight function and $\rho_a^{at}(r)$ is the individual spherically-averaged ground-state atomic density of an atom a in the molecule. The term in the denominator is the summation of all the densities of the individual atoms in the molecule. The weight function for atom a, $w_a(r)$ in equation (32), is a continuous scalar three-dimensional function, bounded by the values $0 \leq w_a(r) \leq 1.0$, where the value of 1.0 is because the proximity with a nucleus a, and zero at distances far from the nucleus. In this way the electron density of an atomic fragment is defined as in equation (33).

$$\rho_a(r) = w_a(r)\rho^{mol}(r) \quad (33)$$

Where $\rho^{mol}(r)$ is the molecular electron density. Because the denominator in equation (32) is the sum of spherically-averaged atomic electron densities for the molecule, the sum of all atomic weight functions at any point in space is necessarily the unity. Hence, the sum of the atomic fragments $\rho_a(r)$ in equation (33) is just $\rho^{mol}(r)$. The Hirshfeld's partitioning scheme leads to no empty regions into the crystal. These concepts allow the definition of a weight function for a molecule in a crystal, shown in equation (34).

$$w_a(r) = \sum_{i \epsilon molecule\ A} \rho_i^{at}(r) / \sum_{i \epsilon crystal} \rho_i^{at}(r) \quad (34)$$

$$w_a(r) = \rho_{promolecule}(r) / \rho_{procrystal}(r)$$

With this principle, it is possible the calculation of external electrostatic potentials and the interaction energy between molecules or between fragments of the same molecule.

Spackman and Byrom[110,111] described several forms of electron density partition, included the Hirshfeld's proposal. Based on the last one, they have defined a surface that guarantees maximum proximity of neighboring molecular volumes, but the volumes never overlap because of the nature of the weight function. This isosurface defined by $w_a(r) = 0.5$, is the Hirshfeld surface that envelops the molecule and defines the volume of space where the molecule electron density exceeds that from all neighboring

molecules. The Hirshfeld surface defines the space occupied by a molecule in a crystal for the purpose of partitioning the crystal electron density into molecular fragments. These surfaces are really useful in the exploration of intermolecular interactions in crystals.

The software package CrystalExplorer 17, developed by Spackman and co-workers[103], can provide an insight of the molecular interactions present in the crystal phase that uses the Hirshfeld surface. The reliability of the calculated Hirshfeld surface by CrystalExplorer17 is based in the fact that the volumes and surfaces areas calculated by this software are in good agreement with those obtained from an *ab initio* electron density calculation[112], the use of crystallographic values found in the used CIF files, such as the reflection parameters, and also, is supported by several works that use this tool to characterize and analyze the intermolecular contacts within a crystal structure, like "…present or missing intermolecular interactions as indicated in the Hirshfeld surface analysis are the most likely reason for the observed large discrepancies between the experimental and theoretical structure. Very short distances between hydrogen and carbon atoms strongly indicate $N-H\cdots\pi$ interactions"[113], "… mapping d_{norm} on the Hirshfeld surface provides a clear and thorough picture of the interactions occurring between the adjacent molecules or the molecular fragments that are shorter than the sum of the van der Waals radii (visualized as red spots on the Hirshfeld surface)"[114], "…The Hirshfeld surface not only describes the shape of a molecule, but its shape subject to the intermolecular interactions with its (typically crystalline) environment. Coupling this shape with surface properties such as electrostatic potential (ESP) or a short-contact descriptor called d_{norm} mapped on Hirshfeld surface seems a natural extension to enhance the description of the molecular environment" [115]. In other references[116-118] this tool is also used to analyze the interactions present in the solid phase.

There are various distance measurements that are significant in the study of the type of molecular interactions present in the crystal phase. The term d_i is the distance from a point on the surface to the nearest nucleus inside the surface, and the term d_e is the distance from a point in the surface to the nearest nucleus outside the surface. Both terms are used together with the van der Waals radii of atoms r_i^{vdW} and r_e^{vdW}, to define a normalized distance, d_{norm}, that represents a measurement of the contact between atoms. The definition of d_{norm}, in terms of the distances and the van der Waals radii, is given in equation (35).

$$d_{norm} = \frac{d_i - r_i^{vdW}}{r_i^{vdW}} + \frac{d_e - r_e^{vdW}}{r_e^{vdW}} \tag{35}$$

If the value of $d_{norm} < 0$, the distance of contact between the atoms is smaller than the sum of their van der Waals radii, if the value of $d_{norm} \approx 0$ the distance of contact between atoms has the value of the sum of van der Waals radii and when the value of $d_{norm} > 0$, the distance between atoms is bigger than the sum of van der Waals radii. In several works, the existence of molecular interactions is proposed from the d_{norm} values of the Hirshfeld surface.

As an example, the calculated Hirshfeld surface of the benzoic is shown in Figure 13. In this surface, it can be observed two red spots over the oxygen and hydrogen atoms of the carboxylic functional group. This indicates that the contact between these atoms and their neighbors is lower than the sum of their van der Waals radii. In the crystal structure of benzoic acid, the neighbor of the oxygen and hydrogen atoms is the carboxylic acid group of another molecule. The presence of these red spots is indicative of a high probability that a hydrogen bond interaction is established and consequently, the formation of dimers. The color of the Hirshfeld surface, which depends on the magnitude of d_{norm}, indicates possible intermolecular interactions in the crystal phase, based on the contact of neighboring atoms.

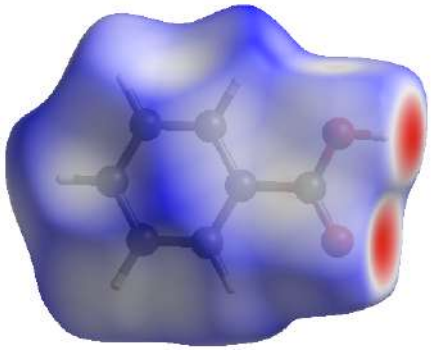

Figure 13. Calculated Hirshfeld surface for benzoic acid. The red spots over the oxygen and hydrogen atoms of the carboxylic group indicate the zone of an important interaction may occur.

III.8.2 Crystal packing analysis of imidazole and pyrazole derivatives

The imidazole and pyrazole derivatives showed several types of interactions in their crystalline structures. The types of interactions were characterized by Hirshfeld surfaces and these are related to the magnitude of the enthalpies of sublimation.

If a comparison between the crystal structures is made for the studied compounds it can be noticed that, other than the common hydrogen bond interaction, the remaining types of relevant interactions are quite different from one compound to another. In most of the cases, these interactions are characterized by dispersion interactions and occur between different groups of atoms depending on the chemical structure.

III.8.2.1 Imidazole derivatives

III.8.2.1.1 Imidazole

The Figure 14 shows the Hirshfeld surface for two successive molecules of imidazole in the crystal phase. It appears two red spots just above the nitrogen atoms. This indicates that these two atoms are able to participate in the hydrogen bond interaction.

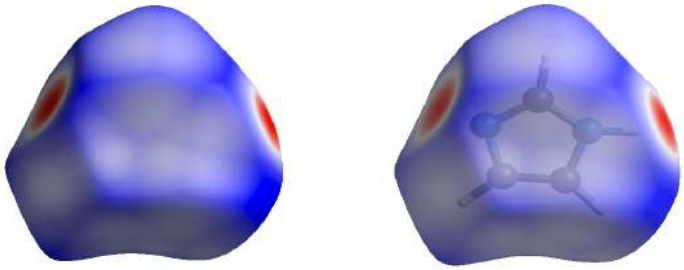

Figure 14. Hirshfeld surface for the imidazole molecule in the crystal phase.

Each imidazole molecule interacts directly with other two nearby molecules through the hydrogen bonds, as shown in Figure 15.

a)

b)

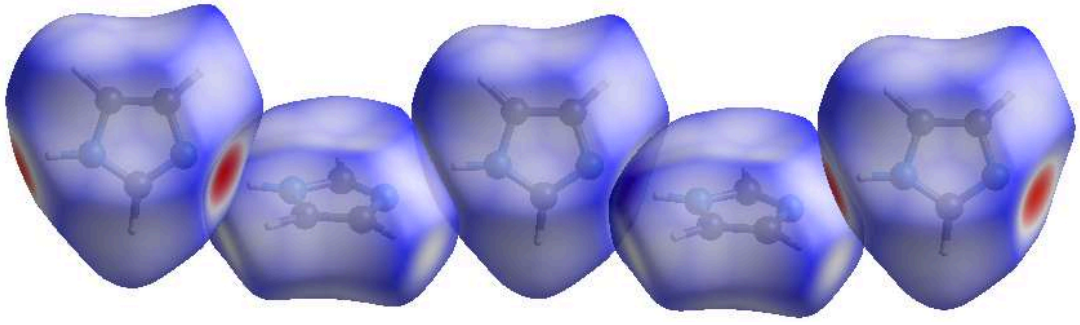

Figure 15. a) the molecular structure of five molecules involved in the formation of hydrogen bond molecular chain and b) the corresponding Hirshfeld surface of molecules in a hydrogen bond chain.

In the Figure 15 a) is clearly showed how the imidazole molecular structure promotes the hydrogen bond interactions. The Figure 15 b) displays the corresponding Hirshfeld surface to visualize the chain formation along the *c* axis within the crystal.

As represented in Figure 16, in the crystal package there are other six molecules that surround an individual imidazole molecule. The intermolecular interactions in this arrangement are the product of dispersion forces and are in the origin of the tridimensional growing of the crystal phase.

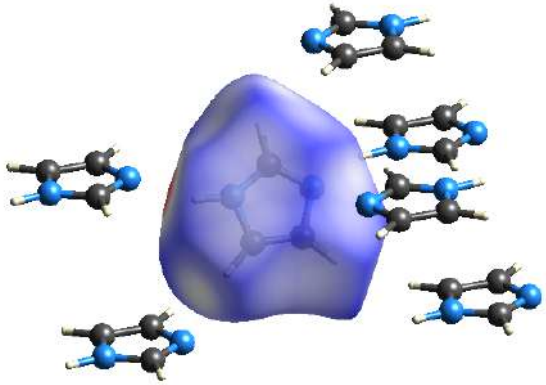

Figure 16. A central imidazole molecule interacts with other six adjacent molecules in the crystal.

In this central imidazole molecule, there are two possibilities to establish two dispersion interaction with two different adjacent molecules through the interaction represented as $C(4)-H\cdots H-C(5)$ and $C(5)-H\cdots H-C(4)$. The last notation indicates that the $C(4)$ atom from one imidazole molecule interacts only with $C(5)$ of an adjacent molecule, and that the $C(5)$ from the same molecule interacts with only the $C(4)$ of a third adjacent molecule. The values of d_{norm} over both hydrogen atoms are -0.009 and the associated distance between the hydrogen atoms in the interaction $C(4)-H\cdots H-C(5)$ (or $C(5)-H\cdots H-C(4)$) is $2.175\cdot10^{-10}$ m. This kind of interaction is shown in Figure 17.

a)

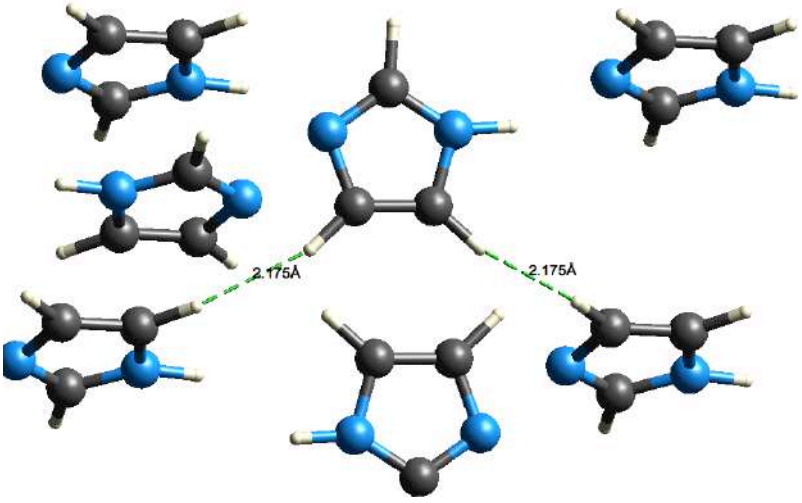

b)

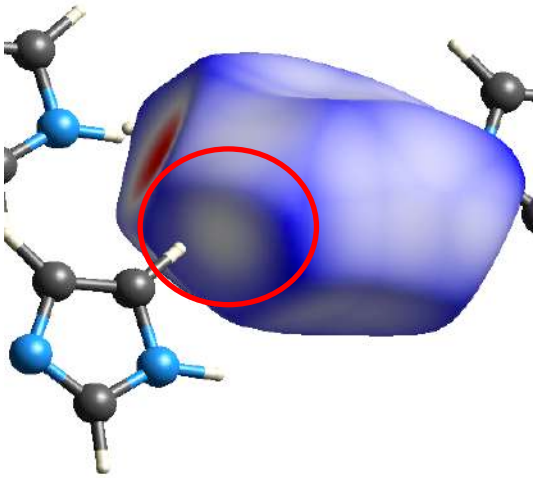

c)

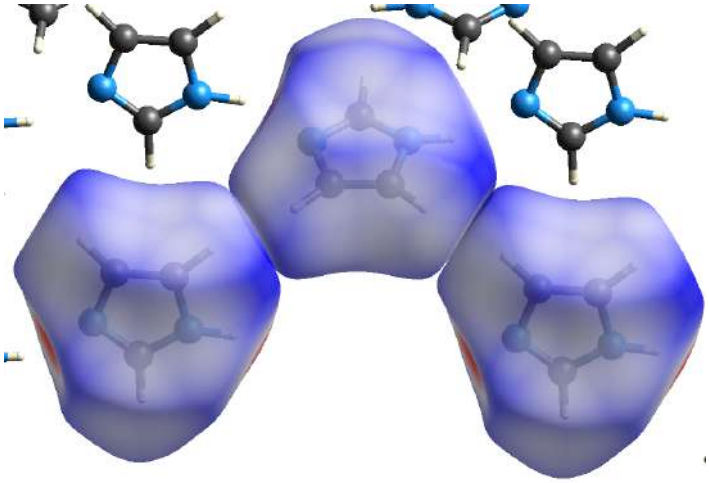

Figure 17. a) Ilustration of the dispersion interaction between imidazole molecules represented as $C(4) - H \cdots H - C(5)$ (or $C(5) - H \cdots H - C(4)$), b) the zone of the Hirshfeld surface where the interaction takes place is circled in red.

A second type of interaction is possible between the H atom bonded to $C(2)$ atom in the aromatic ring with the $N(3)$ atom from a neighboring molecule. This is described as a $C(2) - H \cdots N$ interaction and can be considered as a weak hydrogen bond with a distance $H \cdots N$ of $2.730 \cdot 10^{-10}$ m and an angle of 132.36º. From the Hirshfeld surfaces, the interacting molecules have a $d_{norm}\,(C(2) - H) \cdots N(3)) = 0.0825$; this value indicates that the distance between interacting atoms is nearly given by the addition of their van der Waals radii. This weak hydrogen bond interaction is a singular feature of this crystal structure and is responsible of the growing structure in a different direction of the hydrogen bond chain. This is illustrated in Figure 18. Also, each imidazole molecule acts simultaneously as a hydrogen bond donor and acceptor.

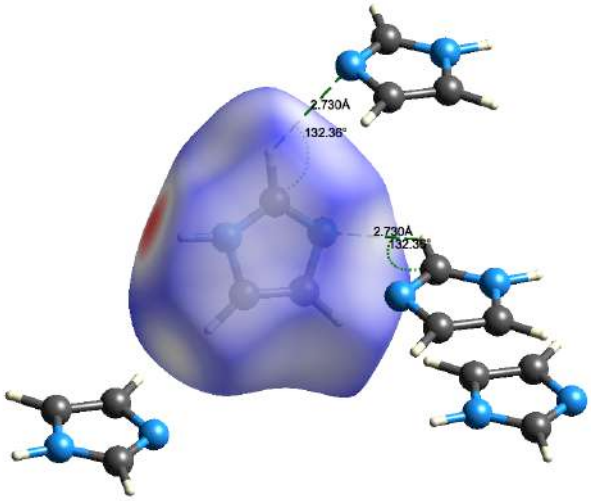

Figure 18. Illustration of the weak hydrogen bond interaction in the imidazole crystal phase.

III.8.2.2 2-methylimidazole

In the case of 2-methylimidazole, as described in Figure 19., the Hirshfeld surfaces, reveal other types of intermolecular interactions through the red spots over the aromatic ring and the $C(5)$ atom.

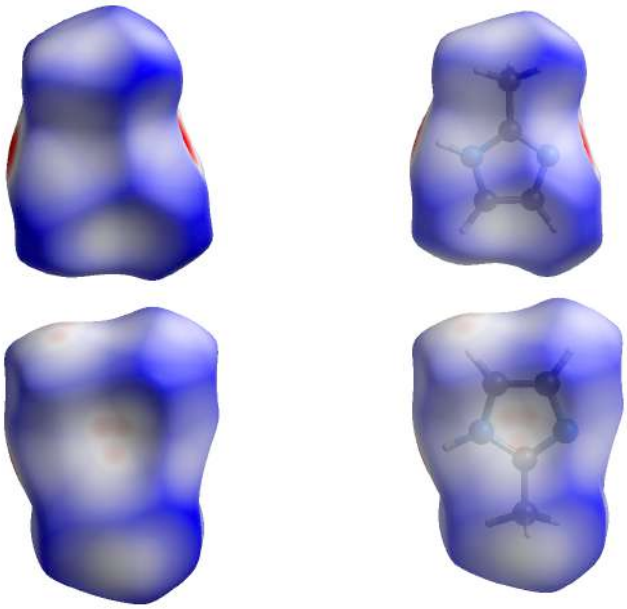

Figure 19. Hirshfeld surface images from the 2-methylimidazole crystal structures.

Each of the 2-methylimidazole molecules interacts with other six neighboring molecules via different kind of interactions as illustrated in Figure 20. An easy visualization of the hydrogen bond and $H \cdots \pi$ interaction is possible through the red spots in the image.

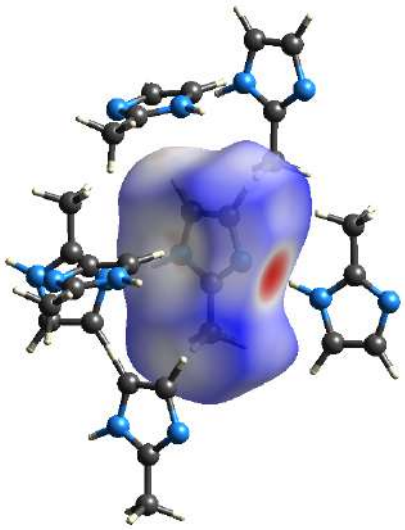

Figure 20. The 2-methylimidazole molecule and the corresponding Hirshfeld surface surrounded by six 2-methylimidazole molecules.

In Figure 21 it can be observed that successive molecules of 2-methylimidazole are arranged in such a way that along the hydrogen bond chain they are rotated, one respect to each other, at exactly 180º. This chain grows along the c axis. This is a singular feature for this crystal structure among the four studied imidazole derivatives.

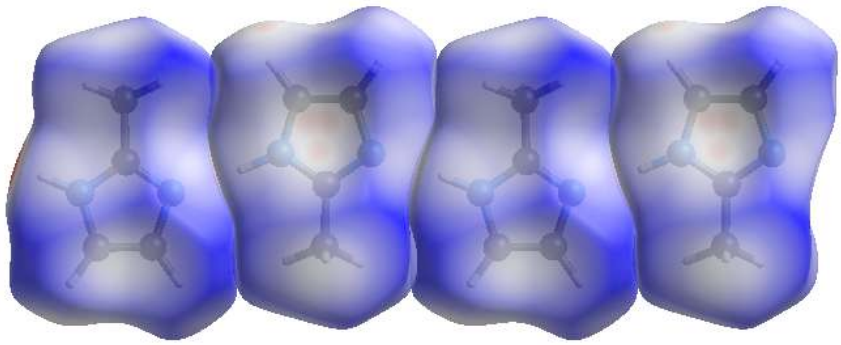

Figure 21. Illustration of the hydrogen bond chain formed in the crystal structure of 2-methylimidazole. It can be seen that adjacent molecules are successively rotated at 180º.

The second kind of interaction corresponds to the proton bonded to $C(5)$ with the delocalized π electron density of the aromatic ring, represented as $C(5) - H \cdots \pi$. The distance from the hydrogen atom to the red spot over the heterocycle to the Hirshfeld surface is $1.018 \cdot 10^{-10}$ m (Figure 22 a)). This type of interaction is present twice in the same molecule, as observed when the molecule is turned to give the image in Figure

22 b), the only difference between both interactions is that an individual molecule in the first case acts as an acceptor and in another as donor. The Hirshfeld surface values d_{norm} over the aromatic ring and over the hydrogen atom attached to the $C(5)$ atom -0.0746 and -0.0751 respectively. These values give insight of a little interpenetration of the van der Waals radii and give evidence of a closer contact between the hydrogen atom and the aromatic ring, enough to establish the described interaction. This is illustrated in Figure 22.

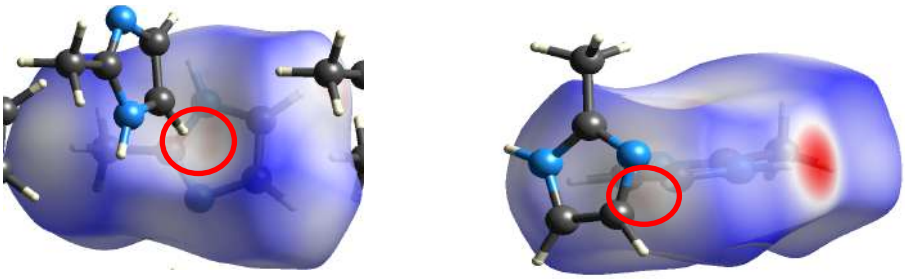

a) b)

Figure 22. Illustration of the interaction $C(5) - H \cdots \pi$. a) and b) correspond to the two possible interaction of this kind of interaction, over the two faces of the same molecule of the 2-methylimidazole.

The third kind of interaction corresponds to the dispersion forces occurring between the methyl group and the $C(4)$ and $C(5)$ atoms of an adjacent molecule. This interaction is circled in Figure 23. The related distances ($2.985 \cdot 10^{-10}$ m to $C(4)$ and $2.845 \cdot 10^{-10}$ m to $C(5)$) in this interaction does not permit to assign a preferred interaction with either $C(4)$ or $C(5)$ atoms. The site is circled in red, showing that each molecule interacts through the methyl group and the aliphatic carbons of the aromatic ring, stacking with adjacent molecules.

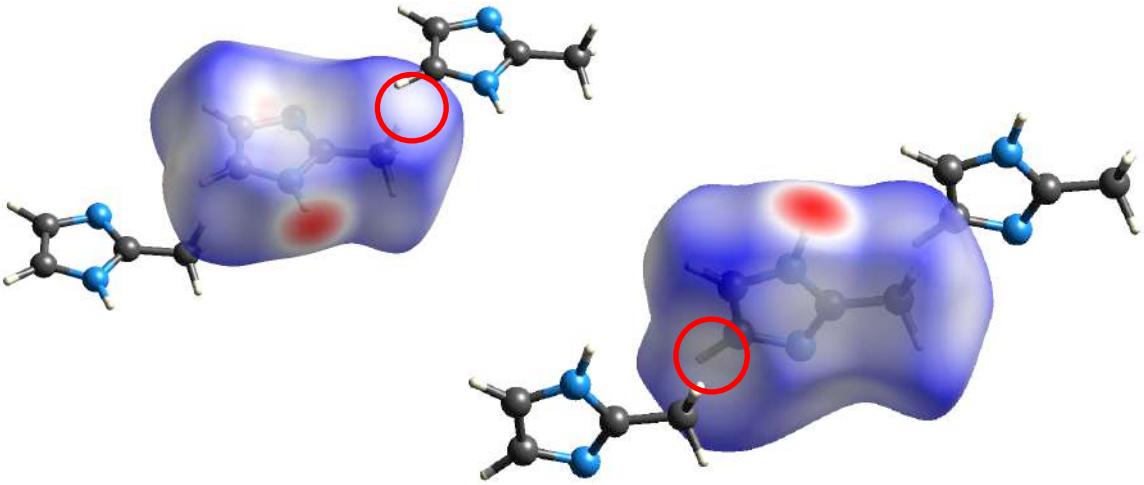

Figure 23. The illustrations show the possibility of a dispersion interaction between the methyl group and the $C(4)$ and $C(5)$ takes place in the 2-methylimidazole.

The crystal packing analysis clearly shows that the tridimensional crystal structure of 2-methylimidazole grows on the hydrogen bond interaction, the $C(5)-H\cdots\pi$ and the dispersion interactions between the methyl group and the $C(4), C(5)$ atoms of the aromatic ring.

III.8.2.3 2-ethylimidazole

The crystal phase of the 2-ethylimidazole shows two types of orientation of the ethyl group as is shown in Figure 24, together with their corresponding Hirshfeld surface images.

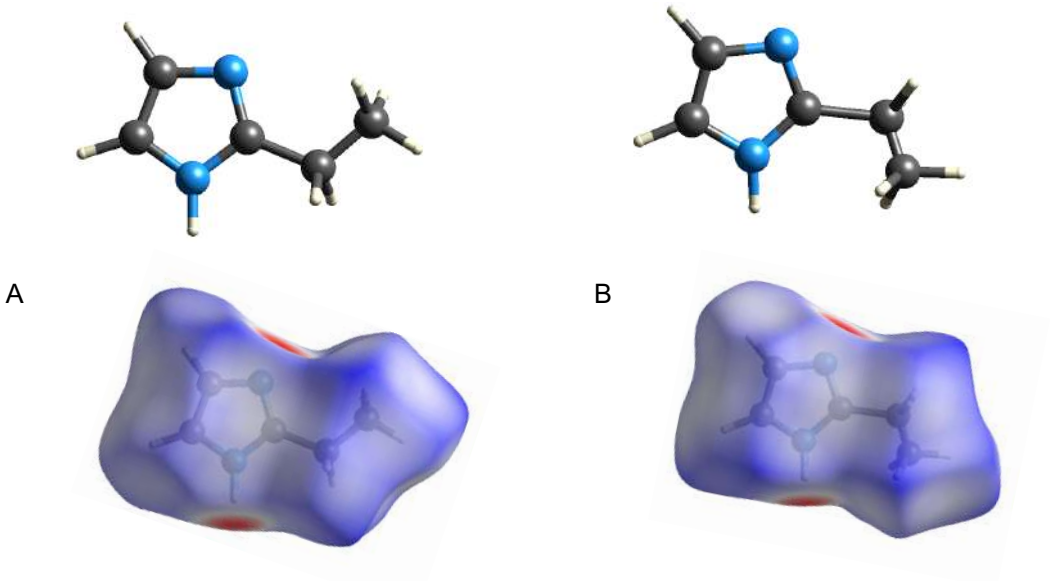

Figure 24. Molecular structure of 2-ethylimidazole with two possible A and B orientations and their corresponding images of Hirshfeld surface.

As a singularity among the studied imidazole derivatives, each molecule of 2-ethylimidazole has two possible orientations: A, which interacts with other 3 different molecules and B, which interacts with only two, as described in Figure 25.

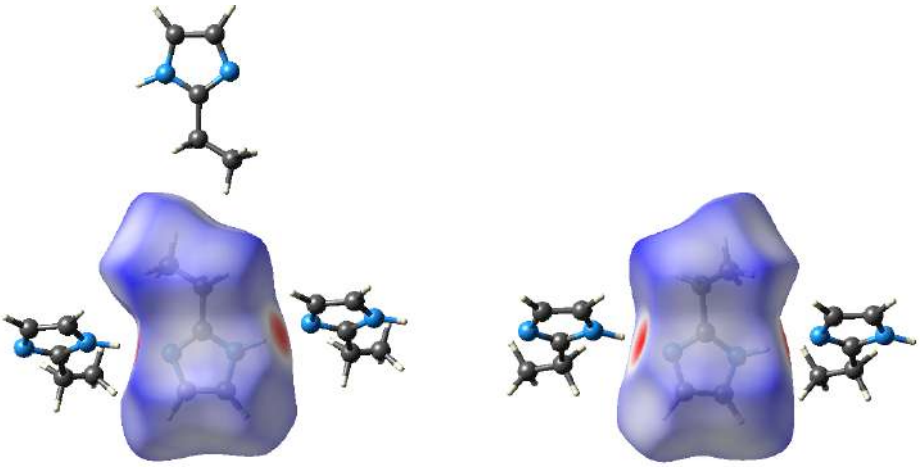

Figure 25. Illustration of the 2-ethylimidazole interacting with three or two other molecules by dispersion forces, depending on its orientation.

As we have pointed out, the hydrogen bond interaction is responsible of the formation of molecular chains in the crystal structure between 2-ethylimidazole successive molecules along the *b* axis; each of them comes from one of the two different asymmetric units. Thus, two of the five interactions correspond to this growing process, along an imaginary axis, as shown in Figure 26.

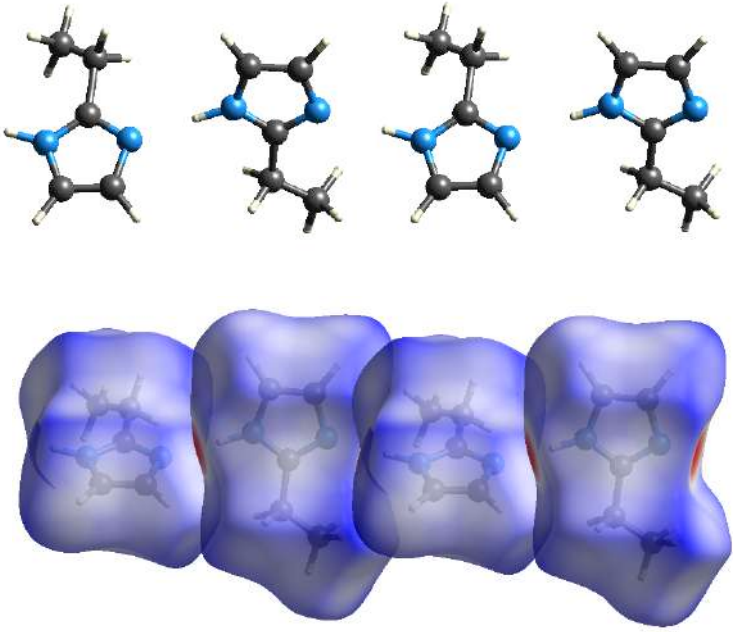

Figure 26. Molecular structure of 2-ethylimidazole and the corresponding images of Hirshfeld surface in the hydrogen bond chain promoted in the crystal structure.

The second kind of interaction in this crystal is of dispersion nature and is attributed to between the ethyl groups of different molecules. This is supported by the value of $d_{norm} = 0.0973$. This indicates that the contact corresponds to the close addition of van der Waals radii. The distance between ethyl groups $C - H \cdots C$ from nearby molecules is $3.286 \cdot 10^{-10}$ m. The interaction of molecules with orientation *A,* is shown in Figure 28.

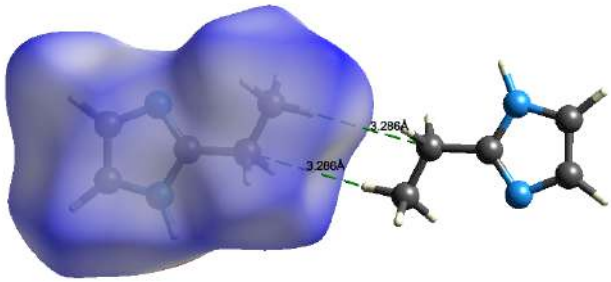

Figure 28. Illustration of the dispersion interaction established between the ethyl groups from molecules with orientation *A*.

III.8.2.4 2-isopropylimidazole

As expected by the three orientations of the isopropyl group in the imidazole ring, this molecule could show four different types of dispersion interaction, other than the hydrogen bond chain due to successive 2-isopropylimidazole moelcules. The three molecular structures and their respective Hirshfeld surfaces are shown in Figure 29.

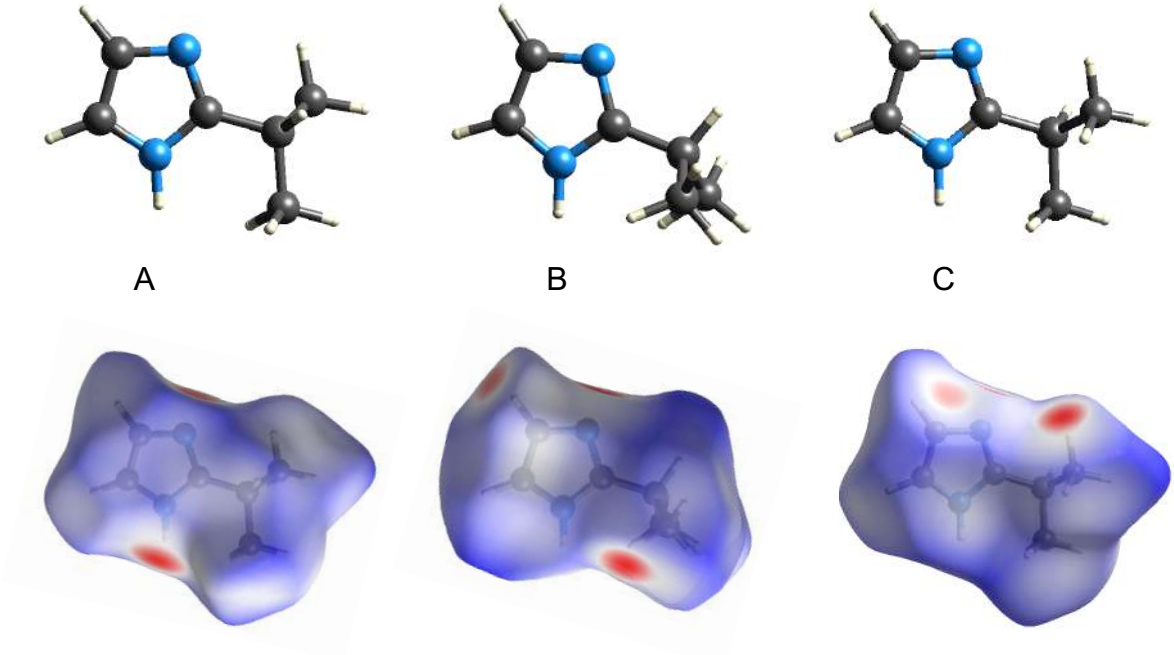

Figure 29. The molecular structure of the 2-isopropylimidazole with three possible orientations in the crystal phase. Also are shown the corresponding Hirshfeld surface images, labeled as A, B and C.

The molecules with orientations A and C, although the different rotation position of the isopropyl group, are capable of establish the same type of interactions in the crystal structure.

The isopropyl group from a 2-isopropylimidazole with the orientation B, interacts through its isopropyl group with the $C(4)$ atom of an adjacent molecule that has the orientation A, as shown in Figure 30 a) or with an adjacent molecule with orientation C, as shown in Figure 30 b).

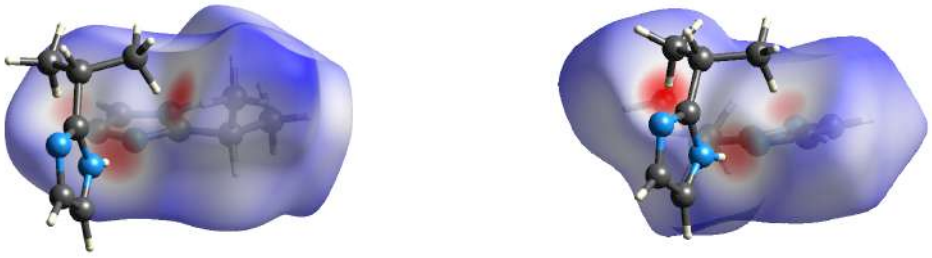

a) b)

Figure 30. Illustration of the interactions established between molecules of 2-isopropylimidazole with different orientations.

In addition to the hydrogen bond interaction, the molecules exhibit strong contact between the isopropyl groups and the isopropyl group of a molecule with orientation B, giving clue of the establishment of dispersion interactions between them.

The 2-isopropylimidazole has the singular characteristic of forming four types of molecular chains inside its crystal packing.

The first type of these chains is the well-established hydrogen bond interaction chain. This interaction is responsible of the crystal growth along one coordinate.

The second type is formed through dispersion interactions between the isopropyl group of one molecule and the $C(4) - H$ atoms of an adjacent molecule. In this case, the value $d_{norm} \approx -0.4420$ confirms that a close contact is present and is responsible for the crystal growing in a different direction than the hydrogen bond chain. These molecular chains only occur between molecules where the isopropyl group has the orientation B. The different kinds of molecular chains are shown in Figures 31, 32, 33, 34 and 35.

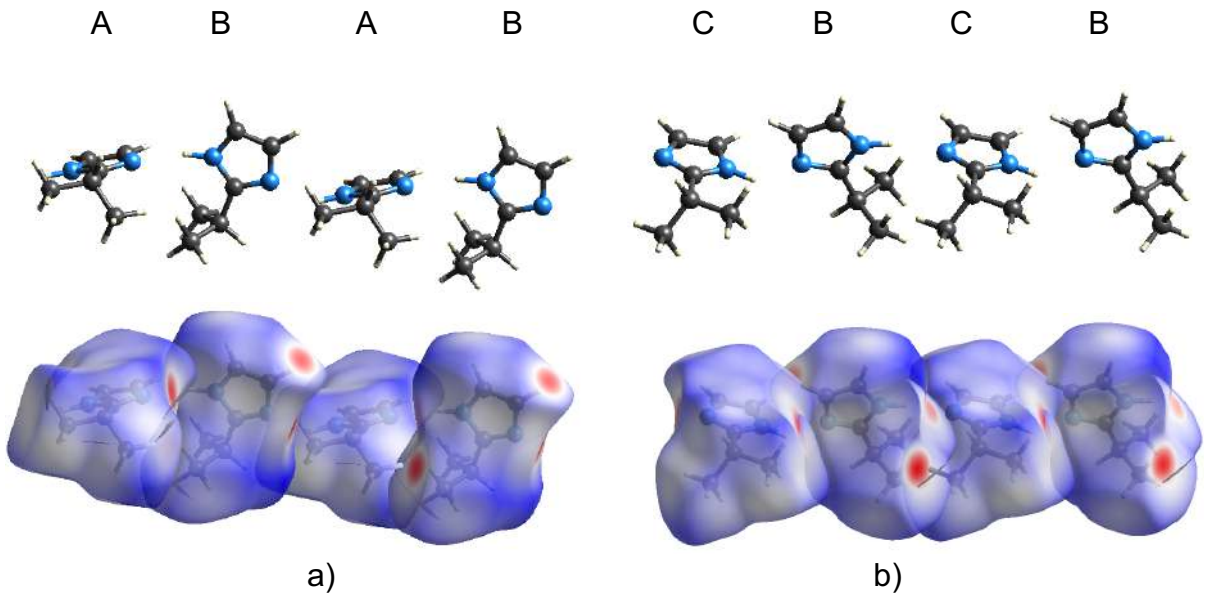

Figure 31. First type of molecular chain formed by the hydrogen bond. a) Hydrogen bond chain formed between molecules with orientation A and B. b) Hydrogen bond chain formed between molecules with orientation C and B.

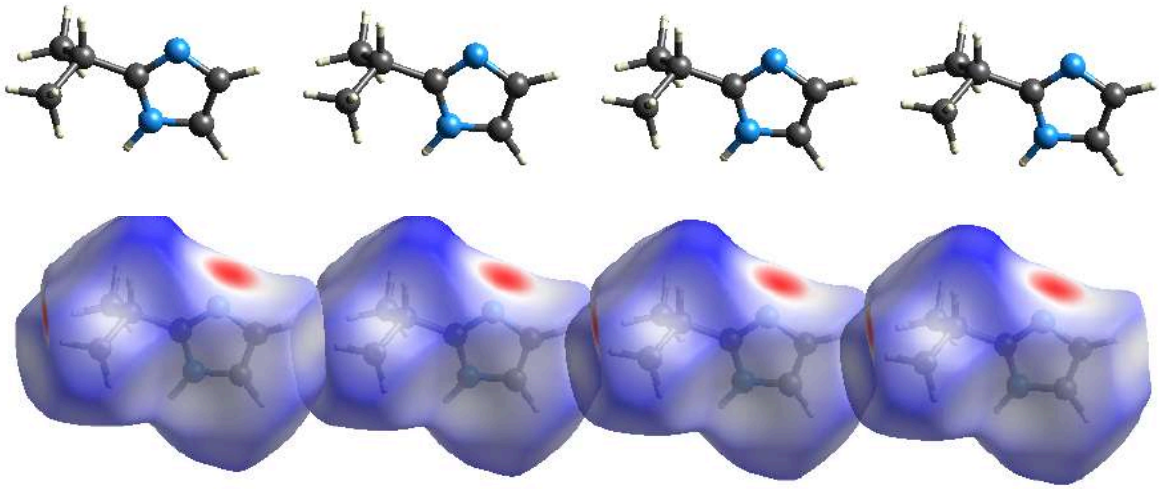

Figure 32. Second type of molecular chain from the compound 2-isopropylimidazole in the crystal structure. The isopropyl group of molecules with orientation b) interacts with the $C(4)-H$ atoms of and adjacent molecule, which at the same time interacts with its isopropyl group with another molecule. This creates “dispersion” molecular chains.

The molecular chain is formed when each isopropyl group interacts via dispersion interactions with the $C(4)-H$ atoms of an adjacent molecule as shown in Figure 35. The surface site where the interaction takes place is circled in red. This is evidenced by the d_{norm} value over the isopropyl group of -0.4420 and in the $C(4)-H$ bond of -0.4433.

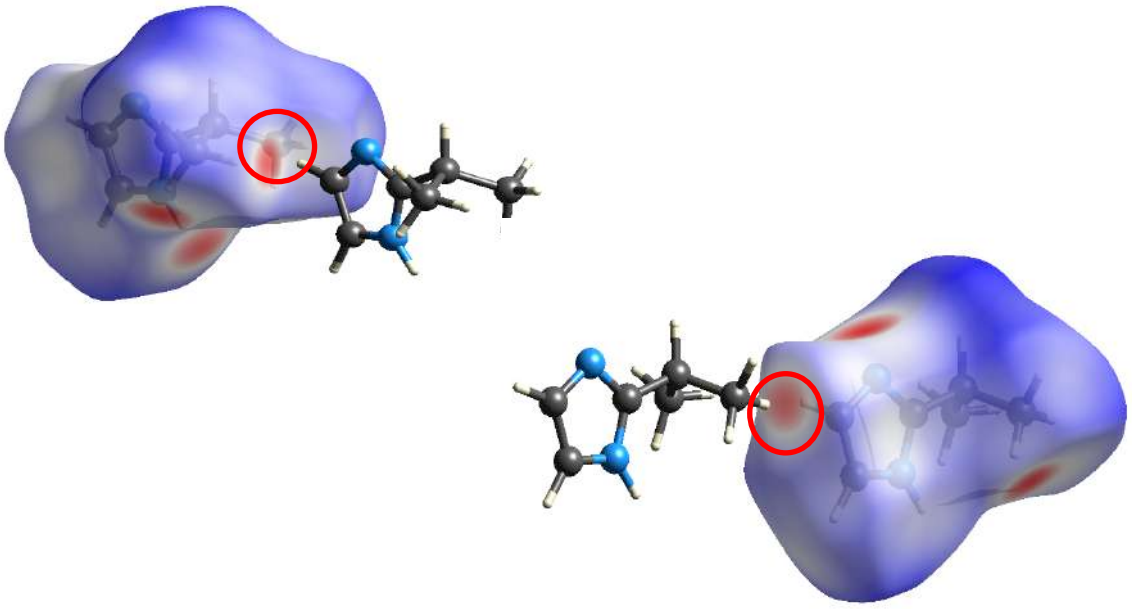

Figure 33. Illustration of the $C(4) - H \cdots isopropyl$ dispersion interaction between orientation B molecule. The interaction site is circled in red.

The third type of chain is formed by the interaction between the aromatic ring of a molecule with orientation B, with the isopropyl group and the $C(4) - C(5)$ atoms of a molecule with orientation A or C, through $H \cdots \pi$ interactions, along the c axis. Two molecules with orientation A (or C) interact with the π density of a molecule with orientation B in two different ways. One is established when a molecule donates a hydrogen atom from the isopropyl group to interact with the delocalized electron density and the second one is formed when a molecule donates a hydrogen from the $C(4)$ atom that interacts also with the electron density. This chain is illustrated in Figure 36.

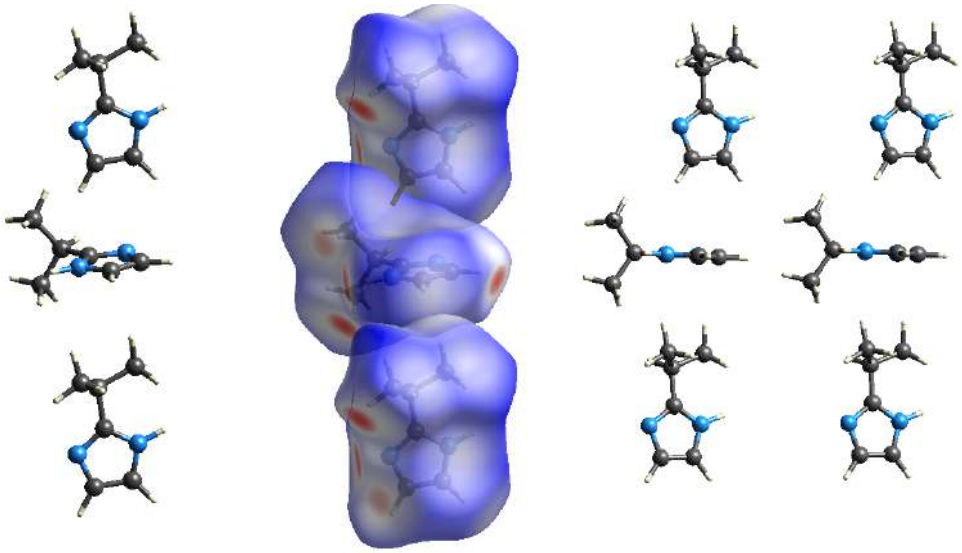

Figure 34. Third type of molecular chain in the crystal structure. The chain is formed by the interaction between the aromatic ring from a molecule with orientation B with the isopropyl group and the $C(4) - C(5)$ atoms from a molecule with orientation A or C, through $H - \pi$ interactions.

The fourth type of molecular chain is formed via the interaction of isopropyl groups from molecules with orientations A and C, illustrated in Figure 37.

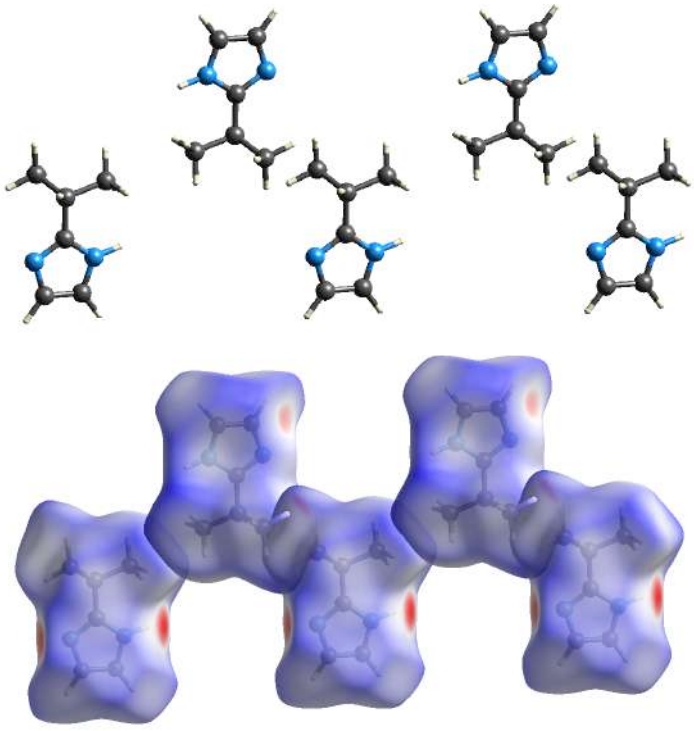

Figure 35. Illustration of the molecular chain of isopropyl groups from molecules with orientation A and C.

III.8.2.2 Pyrazole derivatives

III.8.2.2.1 Pyrazole

In Figure 36 are shown both faces of the Hirshfeld surface of pyrazole. Above the nitrogen atoms there are two red spots, which indicates that the pyrazole establishes hydrogen bonds with two different adjacent molecules. Also, above the aromatic ring, a slightly red spot indicates that an interaction with the π density is possible.

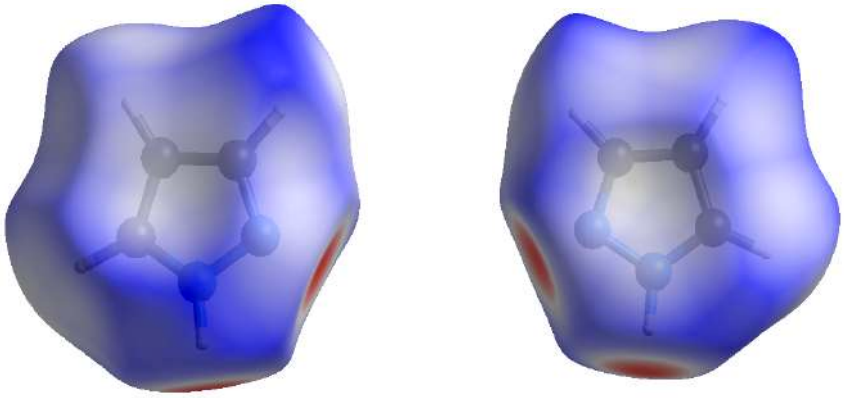

Figure 36. Hirshfeld surface of pyrazole. In the figure are shown both faces of the aromatic ring.

As shown in Figure 37, each pyrazole molecule interacts with other six different molecules in the crystal structure through two different types of interactions.

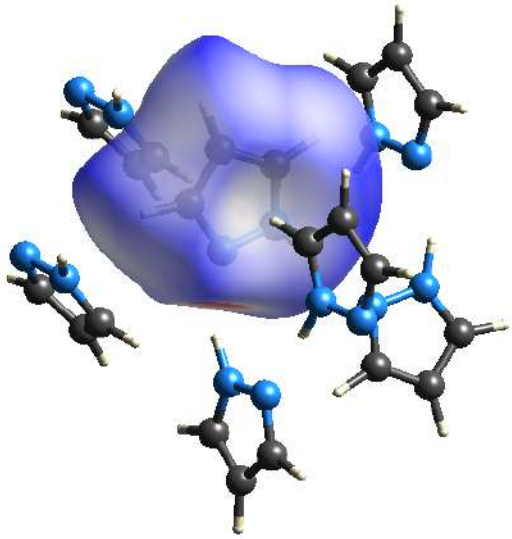

Figure 37. Ilustration of a pyrazole molecule surrounded by six different molecules.

The pyrazole molecules interact via the hydrogen bond interactions and form a chain along the *c* axis in the crystal. The hydrogen bond chain is not formed by successive molecules followed one to another, as in the imidazole derivatives. In pyrazole, the

chain is formed from a pair of interacting molecules. This couple of molecules is successively followed by another one, as shown in Figure 38.

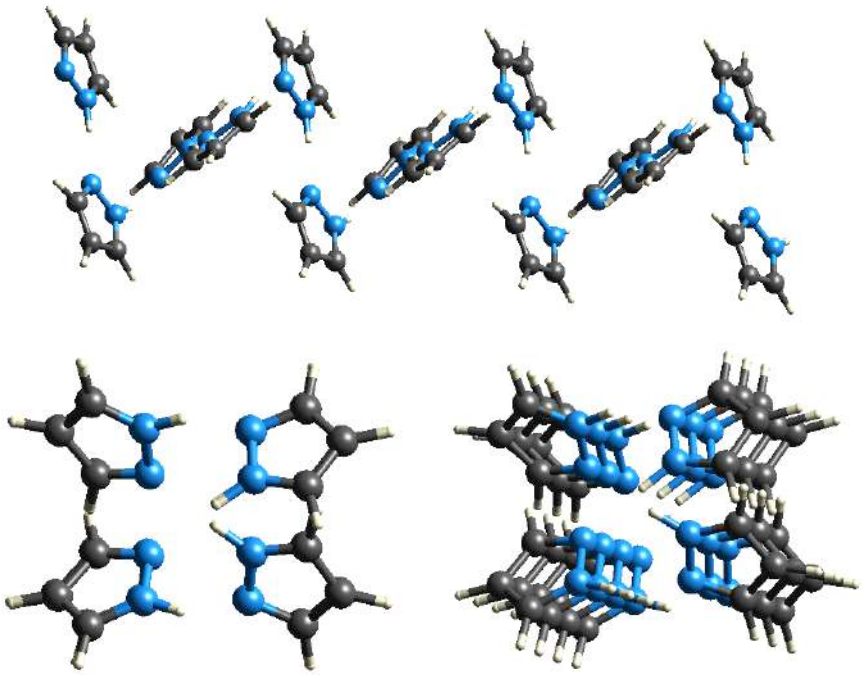

Figure 38. The molecular chain formed by the interaction of successive pyrazole molecules is not so linear and promotes the growth along the *c* axis.

Under the base of the d_{norm} values of around -0.0160 on the Hirshfeld surface over the aromatic ring and the $H-C(3)$ and $H-C(5)$ atoms, is inferred that intermolecular interactions are possible in these sites. From the crystal packing analysis, it is shown that the pyrazole molecules interact through the $H\cdots\pi$ interaction with nearby molecules. Each individual molecule acts as a $H\cdots\pi$ "donor" and "acceptor", simultaneously. One molecule donates the hydrogen atoms $H-C(3)$ and $H-C(5)$, to two different adjacent molecules and each individual molecule accepts two hydrogen atoms in both faces of the aromatic ring, as shown in Figure 39 a), b) and c).

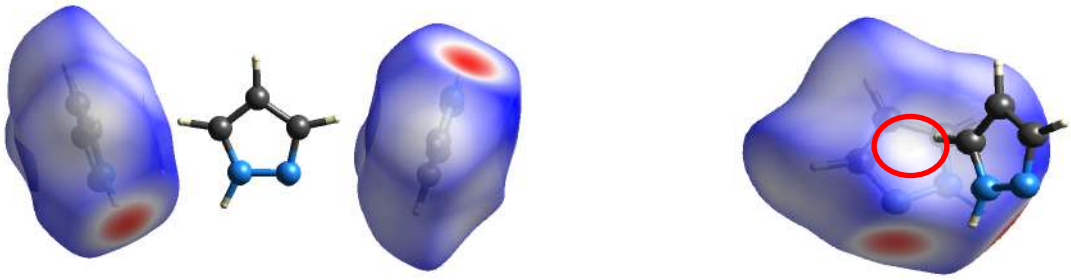

a) b)

c)

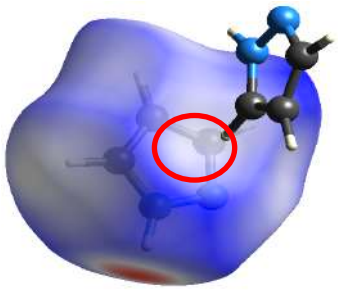

Figure 39. Representation of the $H \cdots \pi$ interaction present in the pyrazole crystal structure. In image a) is shown the donor capacity of an individual molecule. In images b) and c) is represented the acceptor feature of pyrazole, marked in red spots the site where the interaction occurs above the aromatic ring.

This interaction $H \cdots \pi$ is responsible for the growth of the crystal along two complementary axis, both perpendicular to each other. This feature is represented in Figure 40. The pyrazole molecules have the singular feature that an aromatic ring accepts hydrogen atoms of the same characteristics; the π density only interacts with two $H - C(3)$ or with two $H - C(5)$, but not with one $H - C(3)$ and one $H - C(5)$.

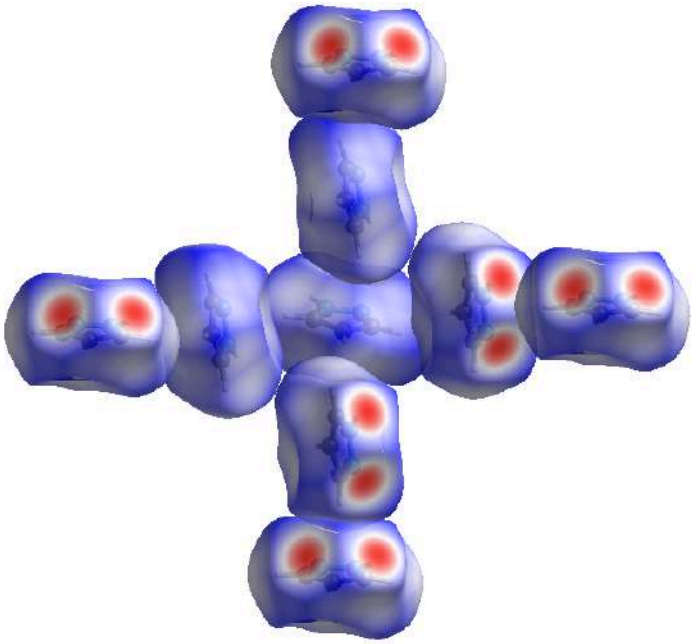

Figure 40. Illustration of the molecular chains inside the crystal structure of pyrazole. As can be seen, the molecules self-intercalate and the crystal grows over the red points, giving the possibility to establish hydrogen bond interactions to another plane of the crystal structure.

The $H \cdots \pi$ interaction, together with the hydrogen bond interaction, are responsible for the growth of the crystal structure in all directions.

III.8.2.2.2 3,5-dimethlypyrazole

The Hirshfeld surface for the 3,5-dimethylpyrazole is shown in Figure 41, where both faces of the aromatic ring are illustrated. This molecule presents four red spots, two different from the ones over the nitrogen atoms.

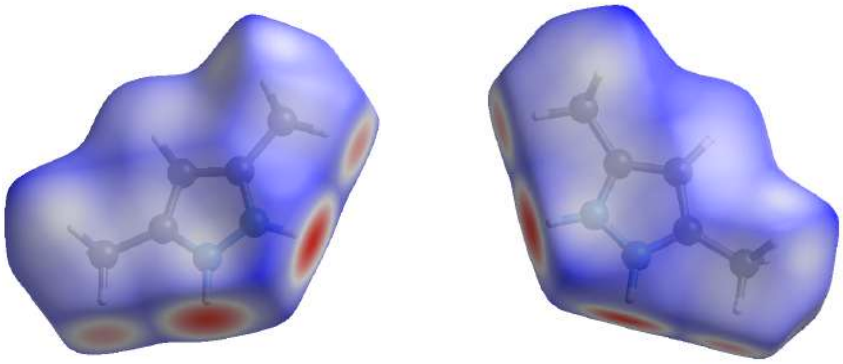

Figure 41. Hirshfeld surface of 3,5-dimethylpyrazole. Two red spots are present over the methyl groups, indicating a small contact with other methyl groups of an interacting neighbor molecule.

Each individual molecule interacts with other four different molecules. This is shown in Figure 42.

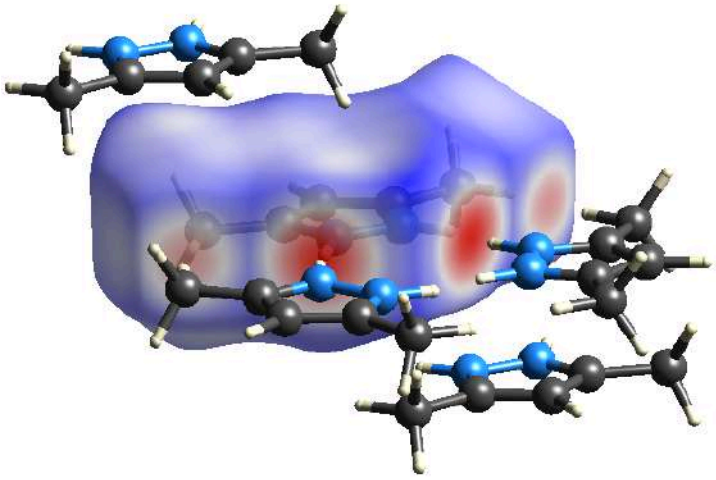

Figure 42. Illustration of the sites of interaction between two 3,5-dimethylpyrazole molecules.

The d_{norm} value on the methyl groups of -0.4147, see Table 24, along with the d_{norm} of the $N-H\cdots N$ and $N\cdots H-N$, described in Table 23, led to the formation of trimer of a planar and triangular form with three molecules of 3,5-dimethylpyrazole as shown in Figure 43.

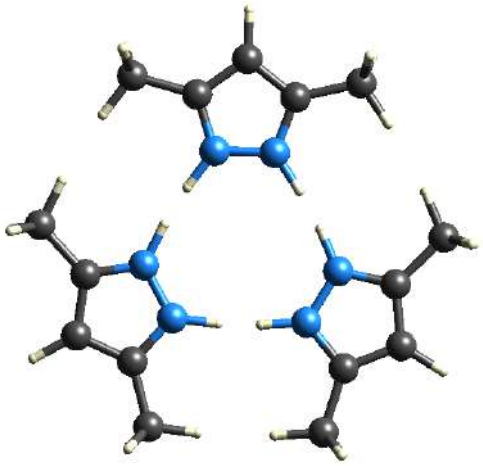

Figure 43. Trimer unit that is in the origin of the crystal structure growth of 3,5-dimethylpyrazole.

The crystal growth of the dimethyl substituted pyrazole allows a third kind of interaction present in the 3,5-dimethylpyrazole crystal structure. This is established between the $N(1)$ atom from a molecule and a hydrogen atom from a methyl group through a weak hydrogen bond interaction, represented as $H_2C - H \cdots N(1)$. These two molecules are located over two different but parallel planes. This feature is in the origin of formation of layers that include the described planar trimers. The distance between the nitrogen atom and the methyl group is $2.735 \cdot 10^{-10}$ m, the angle is 132.50º, allowing that trimers are not eclipsed. This is shown in the figures 44, 45 and 46.

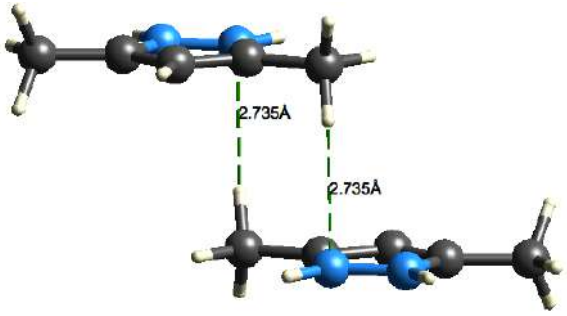

Figure 44. Illustration of the distance between the $N(1)$ and the methyl group. This shows that a weak hydrogen bond interaction can be established.

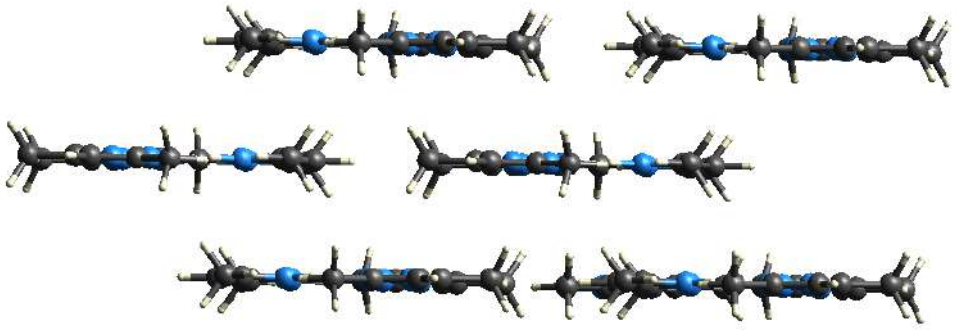

Figure 45. Illustration of the layer formation within the crystal structure of the 3,5-dimethylpyrazole.

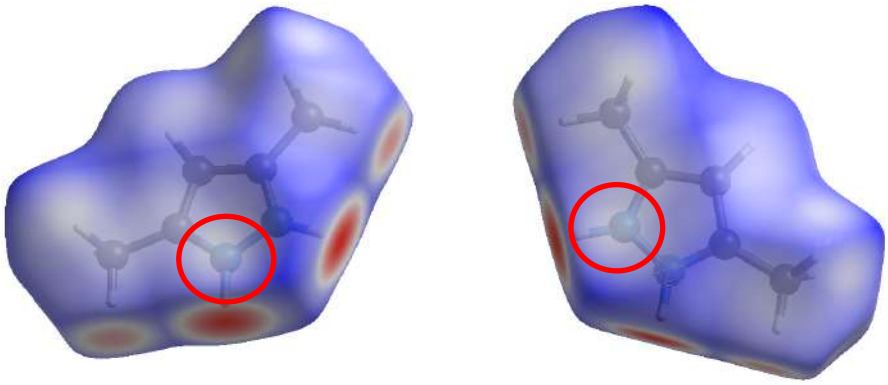

Figure 46. Representation of the zones where the weak hydrogen bond is established in the 3,5-dimethylpyrazole molecule. This zone is circled in red in the Hirshfeld surface.

III.8.2.2.3 3,4,5-trimethylpyrazole

The Hirshfeld surface of the 3,4,5-trimethylpyrazole is shown in Figure 47. The two red spots show the zone for possible hydrogen bond interactions.

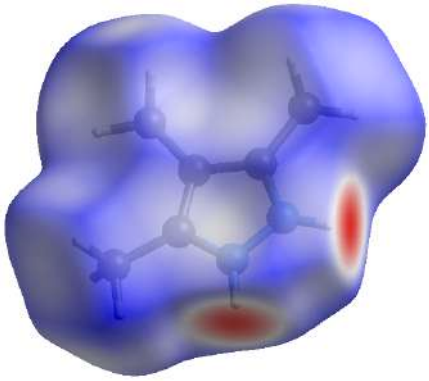

Figure 47. Hirshfeld surface of the 3,4,5-trimethylpyrazole compound.

An individual molecule of 3,4,5-trimethylpyrazole is surrounded by other seven different molecules, as shown in Figure 48.

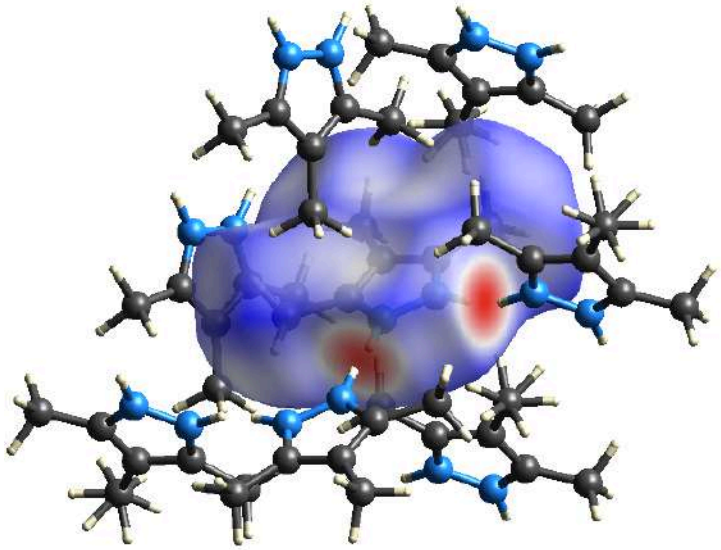

Figure 48. Representation of a molecule of 3,4,5-trimethylpyrazole and its surrounding molecules.

The crystal grows by a non-linear chain of molecules structured by units of six molecules. These units are promoted by the hydrogen bond interactions and the projection of the chain along the *c* axis, as shown in Figure 49.

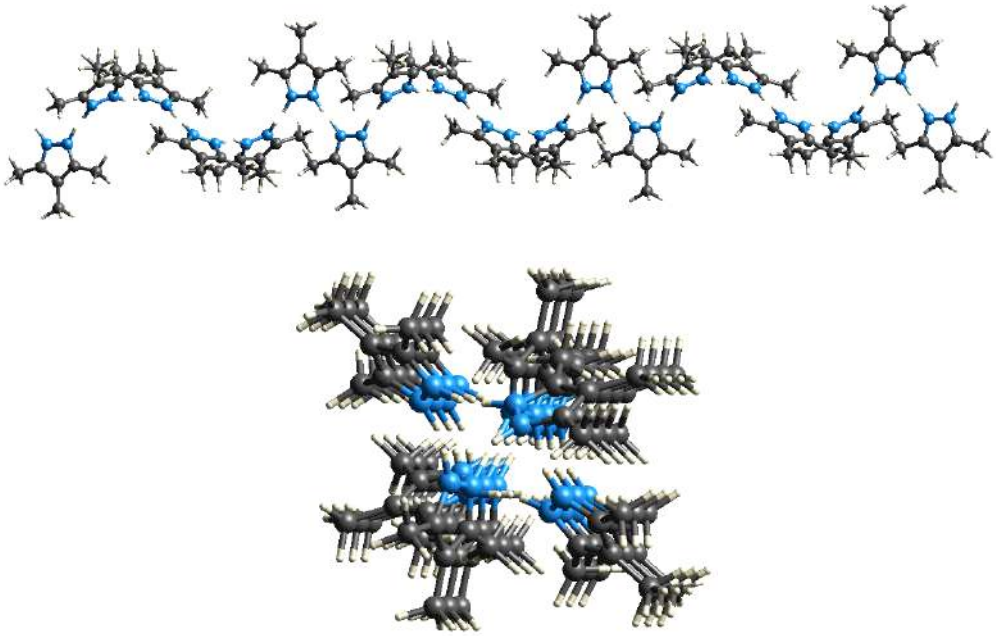

Figure 49. Illustration of the molecular chain formed in the crystal structure of the 3,4,5-trimethylpyrazole due to hydrogen bond interaction.

The steric effect of a third methyl group bonded to $C(4)$ atom, prevents the formation of trimers, as occurs in the case of the 3,5-dimethylpyrazole. Consequently, the formation of chains in this compound prevails.

The methyl groups in this molecule establish weak hydrogen bonds with the $N(1)/N(2)$ atoms of adjacent molecules, as reflected by the d_{norm} values of $0.0276, 0.0207$ and 0.0767 over the corresponding methyl groups $CH_3 - C(3)$, $CH_3 - C(4)$ and $CH_3 - C(5)$, as well as by the average distance and angle of a hydrogen atom of $CH_3 - N$ of $3{\cdot}10^{-10}$ m and 153.0º, measured between a methyl group to a nitrogen atom, as displayed in Figure 50.

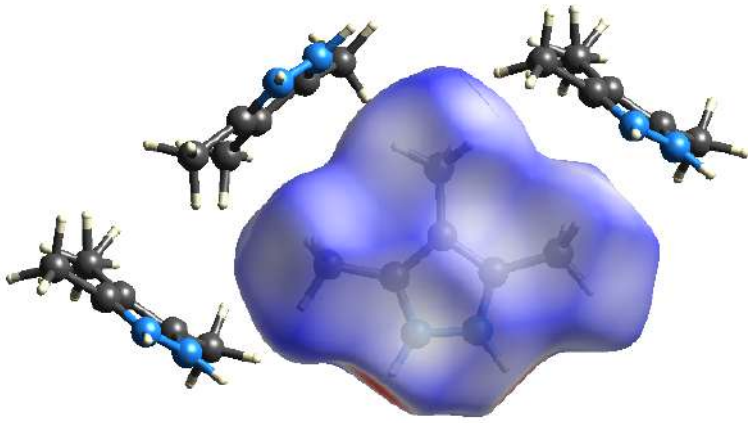

Figure 50. Ilustration of the $N - CH_3$ weak hydrogen bond interaction present between 3,4,5-trimethylpyrazole molecules. Each methyl group interacts with an N atom of an adjacent molecule.

Also, the group of $N(1) - N(2)$ interacts with two hydrogen atoms of two methyl groups, each hydrogen atom corresponds to two molecules located just in front of each face of the aromatic ring. This interaction is not considered as a $H \cdots \pi$ interaction because the hydrogen atoms do not point directly to the center of the aromatic ring, as it is shown in Figure 51. From the Hirshfeld surface, it is noticed that the white color is over a nitrogen atom and not over the ring center, as it would be expected in a pure $H \cdots \pi$ interaction.

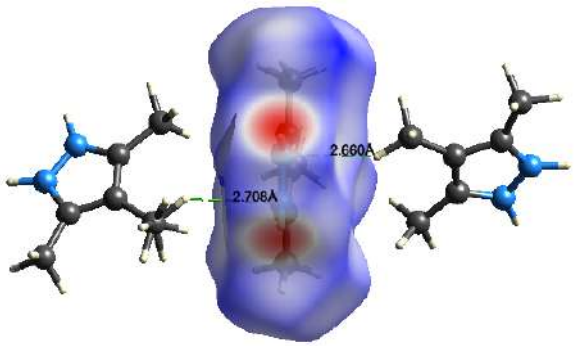

Figure 51. Each nitrogen atom over each face of the aromatic ring interacts with a hydrogen atom from an adjacent methyl group.

The methyl group bonded to the $C(4)$ atom establish dispersion interactions with the adjacent methyl groups, this is evidenced by the $d_{norm} = 0.0792$, as shown in Figure 52.

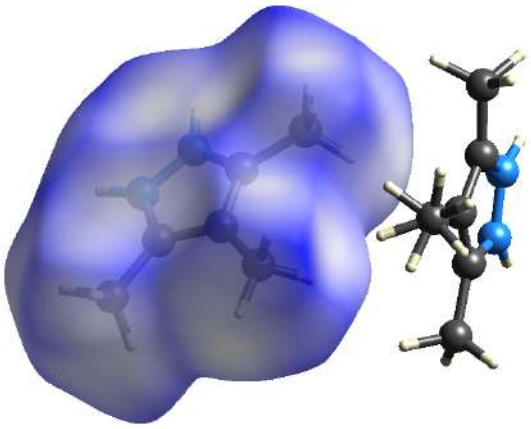

Figure 52. Illustration of the dispersion interactions established between 3,4,5-trimethylpyrazole molecules.

In Table 24. are summarized the intermolecular interactions present each of the pyrazole compounds crystal structures.

IV. Results

IV.1 Differential scanning calorimetry

The results for the differential scanning calorimetry for the purity determination, temperature and molar enthalpy of fusion are shown in tables 1 and 2.

Table 1. Results of differential scanning calorimetry analysis for the imidazole derivatives. The purity is in mole fraction percent, the temperature of melting T_{fus} is in K, and $\Delta_{fus}H$ is in kJ·mol^{-1}. The standard deviations are calculated as $\sigma = \sqrt{\frac{\sum_j (x_j - \bar{x})}{N-1}}$.

Compound	Purity	T_{fus}	$\Delta_{fus}H_{\mathrm{m}}$
Imidazole	99.95 ± 0.02 (5)*	362.3 ± 0.1	12.9 ± 0.4
2-methylimidazole	99.98 ± 0.01 (3)	417.6 ± 0.2	15.6 ± 0.1
2-ethylimidazole	99.89 ± 0.02 (5)	358.7 ± 0.1	8.9 ± 0.1
2-isopropylimidazole	99.82 ± 0.01 (3)	405.2 ± 0.2	14.8 ± 0.2

**Number of independent experiments*

Table 2. Results of the differential scanning calorimetry analysis, for the pyrazole derivatives. The purity is in mole fraction percent, the temperature of melting T_{fus} is in K, and $\Delta_{fus}H$ is in kJ·mol^{-1}. The standard deviations are calculated as $\sigma = \sqrt{\frac{\sum_j (x_j - \bar{x})}{N-1}}$.

Compound	Purity	T_{fus}	$\Delta_{fus}H_{\mathrm{m}}$
Pyrazole	99.94 ± 0.03 (4)*	340.44 ± 0.05	14.48 ± 0.18
3,5-dimethylpyrazole	99.96 ± 0.04 (4)	379.84 ± 0.19	17.38 ± 0.37
3,4,5-trimethylpyrazole	99.40 ± 0.06 (4)	408.74 ± 0.16	20.12 ± 0.24

**Number of independent experiments*

IV.2 Knudsen effusion results

The results of the molar enthalpy of sublimation values for the imidazole and pyrazole compounds are summarized in tables 3 and 4.

Table 3. Values for the molar enthalpy of sublimation in kJ·mol^{-1}, calculated from Knudsen effusion experiments. The temperature range is in K.

	$\Delta_{\mathrm{sub}}H_m$	$\Delta_{\mathrm{sub}}H_m$	T range
Compound	Literature	This work	This work
Imidazole	83.1 ± 0.2[119]	81.4 ± 1.4	286.11 - 309.51
2-methylimidazole	88.4 ± 0.7[120]	87.4 ± 4.5	286.11 - 306.69
2-ethylimidazole	89.6 ± 0.4[120]	85.8 ± 2.0	290.29 - 309.59
2-isopropylimidazole	*	92.2 ± 1.1	292.84 - 313.70

*no experimental value has been previously reported in the literature.

Table 4. Values for the molar enthalpy of sublimation in kJ·mol^{-1}, calculated from Knudsen effusion experiments. The temperature range is in K. *no experimental value has been previously reported in the literature.

	$\Delta_{\mathrm{sub}}H_m$	$\Delta_{\mathrm{sub}}H_m$	T range
Compound	Literature	This work	This work
Pyrazole	74.3 ± 0.4[119]	-	-
3,5-dimethylpyrazole	83.3 ± 0.2[121]	-	-
3,4,5-trimethylpyrazole	*	95.9 ± 2.0	288.112 – 303.229

All the experimental data for the Knudsen effusion measurements and results for the mass loss at each temperature and vapor pressure are supplied in the Appendix.

IV.3 Solution calorimetry

The enthalpy of solution values at infinite dilution $\Delta_{\mathrm{sol}}H_{\mathrm{m}}^{\infty}$, are summarized in tables 5 and 6. These were obtained from a quadratic fitting of the corresponding enthalpy of solution as a function of the molality. The intersection at zero molal concentration is the enthalpy of solution at infinite dilution. The standard deviation of $\Delta_{\mathrm{sol}}H_{\mathrm{m}}^{\infty}$ is taken as the standard deviation of the fitting for the extrapolated value Bevington[122].

Table 5. Values for the molar enthalpy of solution at infinite dilution, in kJ·mol^{-1}, at 298.15 K. calculated from solution calorimetry experiments, for the imidazole derivatives, in different solvents.

	$\Delta_{\mathrm{sol}}H_{\mathrm{m}}^{\infty}$		
Compound / Solvent	Water	Methanol	Acetonitrile
Imidazole	10.9 ± 0.3	13.1 ± 0.5	20.6 ± 0.1
2-methylimidazole	7.5 ± 0.3	12.5 ± 0.5	22.9 ± 0.3
2-ethlyimidazole	2.9 ± 0.2	11.2 ± 0.6	21.8 ± 0.2
2-isopropylimidazole	4.5 ± 0.4	12.6 ± 0.7	23.5 ± 0.3

Table 6. Values for the molar enthalpy of solution at infinite dilution, in kJ·mol^{-1}, at 298.15 K. calculated from solution calorimetry experiments, for the pyrazole derivatives in different solvents.

	$\Delta_{\mathrm{sol}}H_{\mathrm{m}}^{\infty}$		
Compound / Solvent	Water	Methanol	Acetonitrile
Pyrazole	12.4 ± 0.3	18.0 ± 0.9	18.2 ± 0.2
3,5-dimethylpyrazole	9.5 ± 0.5	18.0 ± 0.2	22.2 ± 0.4
3,4,5-trimethylpyrazole	8.6 ± 0.7	18.3 ± 0.5	23.6 ± 0.6

All the experimental data and results for each enthalpy of solution measurement are summarized in the Appendix.

IV.4 Enthalpy of solvation

The enthalpies of solvation were calculated from the equation $\Delta_{\mathrm{solv}}H^{\infty}_{\mathrm{m}} = \Delta_{\mathrm{sol}}H^{\infty}_{\mathrm{m}} - \Delta_{\mathrm{sub}}H_m$ using our own values of enthalpy of sublimation and the results are shown in tables 7 and 8.

Table 7. Values for the molar enthalpy of solvation, in kJ·mol^{-1}, for the imidazole derivatives in different solvents, at 298.15 K. The standard deviations are calculated as $\sigma = \sqrt{\sum_j(\sigma_j^2)}$.

	$\Delta_{\mathrm{solv}}H^{\infty}_{\mathrm{m}}$		
Compound / Solvent	Water	Methanol	Acetonitrile
Imidazole	-70.5 ± 1.4[a]	-68.3 ± 1.4	-60.8 ± 1.4
2-methylimidazole	-79.9 ± 4.5	-74.9 ± 4.5	-64.6 ± 4.5
2-ethylimidazole	-82.9 ± 2.0	-74.6 ± 2.1	-64.0 ± 2.0
2-isopropylimidazole	-87.7 ± 1.2	-79.6 ± 1.3	-68.8 ± 1.2

[a]*The uncertainty includes the corresponding uncertainties for the enthalpy of sublimation and enthalpy of solution.*

Table 8. Values for the molar enthalpy of solvation, in kJ·mol^{-1}, for the pyrazole derivatives in different solvents, at 298.15 K. The standard deviations are calculated as $\sigma = \sqrt{\sum_j(\sigma_j^2)}$.

	$\Delta_{\mathrm{solv}}H^{\infty}_{\mathrm{m}}$		
Compound / Solvent	Water	Methanol	Acetonitrile
Pyrazole	-61.9 ± 0.5	-56.3 ± 1.0	-56.0 ± 0.4
3,5-dimethylpyrazole	-73.6 ± 0.5	-65.1 ± 0.3	-60.9 ± 0.4
3,4,5-trimethylpyrazole	-87.6 ± 2.0	-77.6 ± 2.0	-72.3 ± 2.0

[a]*The uncertainty includes the corresponding uncertainties for the enthalpy of sublimation and enthalpy of solution.*

IV.5 Enthalpy of cavity formation

The results for the enthalpy of cavity formation values, calculated, with the Pierotti equation (equation (12)), are shown in tables 9 and 10.

Table 9. Values for the molar enthalpy of cavity formation, in kJ·mol^{-1}, at 298.15 K, for the imidazole derivatives.

Compound	$\Delta_{\mathrm{cav}}H$ (Water)	$\Delta_{\mathrm{cav}}H$ (Methanol)	$\Delta_{\mathrm{cav}}H$ (Acetonitrile)
Imidazole	4.7	20.2	26.6
2-methylimidazole	5.4	23.3	30.6
2-ethylimidazole	6.0	25.8	33.9
2-isopropoylimidazole	6.7	28.6	37.7

Table 10. Values for the molar enthalpy of cavity formation, in kJ·mol^{-1}, at 298.15 K, for the pyrazole compounds in different solvents.

Compound	$\Delta_{cav}H$ (Water)	$\Delta_{cav}H$ (Methanol)	$\Delta_{cav}H$ (Acetonitrile)
Pyrazole	4.7	20.2	26.6
3,5-dimethylpyrazole	6.1	26.2	34.5
3,4,5-trimethylpyrazole	6.7	28.4	38.1

IV.6 Molecular Volumes

The calculated molecular volumes from the electron density surfaces of the imidazole and pyrazole solutes are shown in tables 11 and 12; these values were obtained as described in the experimental section, Section III.5.

Table 11. Values for the estimated molecular volumes for the imidazole compounds, in m^3, obtained through the corresponding electron density surfaces.

Compound	10^{30} Molecular volume
Imidazole	44.8
2-methylimidazole	57.2
2-ethylimidazole	68.1
2-isopropylimidazole	81.5

Table 12. Values for the estimated molecular volumes for pyrazole compounds, in m^3, obtained through the corresponding electron density surfaces.

Compound	10^{30} Molecular volume
Pyrazole	44.8
3,5-dimethylpyrazole	70.1
3,4,5-trimethylpyrazole	83.0

IV.7 Enthalpy of interaction

Pierotti[19] also proposed the equation $\Delta_{solv}H_m^{\infty} = \Delta_{cav}H + \Delta_{int}H_m^{\infty} - RT + \alpha RT^2$ that relates the enthalpy of solvation with the enthalpy of cavity formation and a term that represents the enthalpy of interaction between solute and solvent. The values of enthalpy of interaction were calculated and the results are listed in tables 13 and 14. The used values of enthalpy of solvation are given in tables 7 and 8 and the enthalpy of cavity formation values given in tables 9 and 10. The used values of α are the given in Section III.5.

Table 13. Values for the molar enthalpy of interaction, in kJ·mol^{-1}, at 298.15 K, for the imidazole derivatives in the three used solvents. The standard deviations are calculated as $\sigma = \sqrt{\sum_j (\sigma_j^2)}$

	$\Delta_{int}H_m^{\infty}$ (Water)	$\Delta_{int}H_m^{\infty}$ (Methanol)	$\Delta_{int}H_m^{\infty}$ (Acetonitrile)
Imidazole	-72.9 ± 1.4	-86.9 ± 1.4	-85.9 ± 1.4
2-methylimidiazole	-83.0 ± 4.5	-96.6 ± 4.5	-93.8 ± 4.5
2-ethylimidazole	-86.6 ± 2.0	-98.8 ± 2.0	-96.4 ± 2.0
2-isopropylimidazole	-92.1 ± 1.2	-106.6 ± 1.3	-105.0 ± 1.2

Table 14. Values for the molar enthalpy of interaction, in kJ·mol^{-1}, at 298.15 K, for the pyrazole derivatives in the three used solvents. The standard deviations are calculated as $\sigma = \sqrt{\sum_j (\sigma_j^2)}$

	$\Delta_{int}H_m^{\infty}$ (Water)	$\Delta_{int}H_m^{\infty}$ (Methanol)	$\Delta_{int}H_m^{\infty}$ (Acetonitrile)
Pyrazole	-64.3 ± 0.5	-74.9 ± 1.0	-81.2 ± 0.4
3,5-dimethylpyrazole	-77.4 ± 0.5	-89.8 ± 0.3	-94.0 ± 0.4
3,4,5-trimethylpyrazole	-91.7 ± 2.1	-104.6 ± 2.0	-108.9 ± 2.0

IV.8 ^{1}H NMR chemical shift values

The ^{1}H NMR chemical shifts data of the imidazole derivatives in the different solvents are displayed in Table 15. In Figure 53 is shown the molecular structure of imidazole and their corresponding substituents that origins the studied solutes and the used atomic labels. All the NMR spectra are summarized in the Appendix.

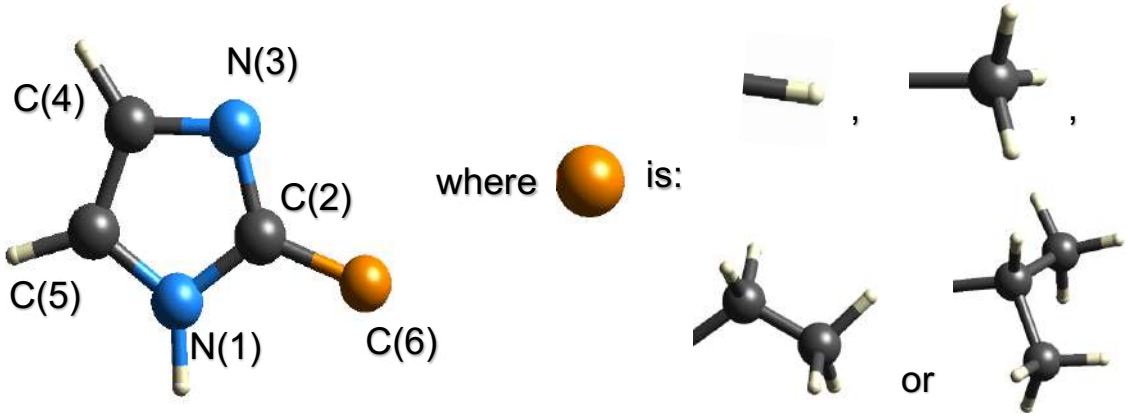

Figure 53. The molecular structure of the imidazole aromatic ring that shows the label of atoms, as described in Table 13 and in the discussion section.

The chemical shifts data of the imidazole and pyrazole derivatives, in deuterated water, methanol and acetonitrile are displayed in tables 15 and 16, respectively.

Table 15. ^{1}H NMR chemical shift, in ppm, of imidazole compounds in the three solvents. Tetramethylsilane has been used as internal reference.

Observed atom	δ (D_2O)	δ (CD_3OD)	δ (CD_3CN)
$H-C(2)$ Imidazole	7.67	7.70	7.62
$H-C(4), H-C(5)$Imidazole	7.03	7.07	7.06
$H-C(4), H-C(5)$ 2-methylimidazole	6.87	6.89	6.88
$H-C(4), H-C(5)$ 2-ethylimidazole	6.89	6.90	6.89
$H-C(4), H-C(5)$ 2-isopropylimidazole	6.89	6.90	6.89
$H-C(6)$ 2-methylimidazole	2.26	2.36	2.33
$H-C(6)$ 2-ethylimidazole	2.63	2.74	2.70
$H-C(6)$ 2-isopropylimidazole	2.97	3.05	3.02
$H-CH_3$ 2-ethylimidazole	1.15	1.29	1.26
$H-CH_3$ 2-isopropylimidazole	1.18	1.31	1.28
$H-N(1)$ Imidazole	not observed	not observed	10.67
$H-N(1)$ 2-methylimidazole			10.26
$H-N(1)$ 2-ethylimidazole			10.24
$H-N(1)$ 2-isopropylimidazole			10.12

In Figure 54 is shown the molecular structure of pyrazole and their corresponding substituents that origins the studied solutes and the atomic labels used.

Figure 54. The molecular structure of the pyrazole aromatic ring that shows the label of atoms, as described in Table 16 and in the discussion section.

Table 16. ^{1}H NMR chemical shift, in ppm, of pyrazole compounds in the three solvents. Tetramethylsilane has been used as internal reference.

Observed atom	δ (D_2O)	δ (CD_3OD)	δ (CD_3CN)
$H-C(4)$ Pyrazole	6.35	6.35	6.32
$H-C(4)$ 3,5-dimethylpyrazole	5.87	5.83	5.80
$H-C(3), H-C(5)$ Pyrazole	7.63	7.62	7.59
$H-CH_3$ 3,5-dimethylpyrazole	2.11	2.22	2.21
$H-CH_3$ 3,4,5-trimethylpyrazole	2.06	2.15	2.11
$H-N(1)$ Pyrazole			11.14
$H-N(1)$ 3,5-dimethylpyrazole	not observed	not observed	10.40
$H-N(1)$ 3,4,5-trimethylpyrazole			10.23

IV.9 Dipole moments

The calculated dipole moments of imidazole and pyrazole derivatives are shown in tables 17 and 18.

Table 17. Calculated dipole moment of the imidazole molecules, in Debye, obtained from quantum mechanics calculations.

Compound	μ
Imidazole	3.69
2-methylimidazole	3.57
2-ethylimidazole	3.48
2-isopropylimidazole	3.36

Table 18. Calculated dipole moment of the pyrazole molecules, in Debye, obtained from quantum mechanical calculations.

Compound	μ
Pyrazole	2.26
3,5-dimethylpyrazole	2.48
3,4,5-trimethylpyrazole	2.45

Illustrations of the dipole moments of the molecules are included in the Appendix.

IV.10 Crystal packing analysis of imidazole and pyrazole derivatives

IV.10.1 Imidazole derivatives

The labels of the imidazole derivatives atoms are shown in Figure 53. The hydrogen bond distances of the imidazole compounds in the crystal phase are listed in Table 19.

Table 19. Lengths in 10^{-10} m and angles in degrees for hydrogen bond in crystalline imidazole derivatives

Compound	Hydrogen bond length $(N-H), H\cdots N$	Hydrogen bond length $N-H\cdots N$	Hydrogen bond angle
Imidazole	(1.009), 1.885	2.842	157.31
2-methylimidazole	(1.009), 1.810	2.816	174.79
2-ethylimidazole	A (1.009), 1.829 B (1.009), 1.850	2.834 2.859	174.27 178.83
2-isopropylimidazole	A, C (1.009), 1.802 B (1.009), 1.941	2.708 2.976	142.35 167.01

One common characteristic between the imidazole derivatives in the crystal phase is that the aromatic ring includes two nitrogen atoms that can form hydrogen bond interactions, where the nitrogen $N(1)$ acts as a hydrogen bond donor and nitrogen $N(3)$ as an acceptor. This interaction is represented as $N(1)-H\cdots N(3)$. Also, the hydrogen bond interaction origins the formation of molecular lineal chains within the crystal structure and is the main responsible of the growth of the crystal along a defined axis. For imidazole and for the 2-methylimidazole the chain grows along the c axis, for the 2-ethylimidazole grows along the b axis and for the 2-isopropylimidazole the chain grows along an imaginary axis at 45º from the b axis.

The 2-ethylimidazole shows two different orientations of the ethyl group in the crystal phase, named A and B, and the 2-isopropylimidazole shows three different orientations of the isopropyl group, named A, B and C.

The values for d_{norm} of the Hirshfeld surface of the imidazole compounds over the $N(1)$ and $N(3)$ atoms are listed in Table 20.

Table 20. Values for d_{norm} of the Hirshfeld surface of the imidazole compounds over the $N(1)$ and $N(2)$ atoms.

Compound	$d_{norm}\ N-H\cdots N$	$d_{norm}\ N\cdots H-N$
Imidazole	-0.574	-0.575
2-methylimidazole	-0.633	-0.636
2-ethylimidazole	-0.618	-0.601
2-isopropylimidazole	-0.604	-0.495

The intermolecular interactions and some crystal parameters will be useful to understand the magnitude and trend of the thermochemical properties of these imidazole derivatives and an account of all the interactions extracted from the crystal structure analysis of them is summarized in Table 21.

Table 21. Summary of the intermolecular interactions, other than the hydrogen bond interaction, present in the crystal structures of the imidazole derivatives.

Compound	Interactions	Interaction distance d / 10^{-10} m, d_{norm} values
Imidazole	Weak hydrogen bond $C-H\cdots N$, acting in each imidazole molecule simultaneously, as a hydrogen bond donor and acceptor.	$d\ C(3)-H\cdots N=2.175$ $d_{norm}\ (Acceptor)=0.0864$ $d_{norm}\ (Donor)=0.0865$
	Dispersion interactions $C(4)-C(5)$, forming a molecular chain. The $C(4)$ always interacts with the $C(5)$ atom from an adjacent molecule and also the $C(5)$ atom only interacts with the $C(4)$ of an adjacent molecule.	$d\ C(4)-H\cdots H-C(5)=2.175$ $d_{norm}-C(4)=-0.0009$ $d_{norm}-C(5)=-0.0011$
2-methylimidazole	Interaction $C(5)-H\cdots\pi$ by donation of a hydrogen atom bonded to the $C(5)$ with the delocalized electron density of an adjacent molecule.	$d\ C(5)-H\cdots Hirshfeld\ surface=1.018$ $dC(5)-H\cdots\pi=2.687$ $d_{norm}\ \pi=-0.0825$ $d_{norm}\ C(5)=-0.0807$
	Interaction of the methyl group via dispersion interactions with $C(4), C(5)$ atoms of an adjacent molecule.	$d\ methyl\cdots C(4)-C(5)=2.845$ $d_{norm}\ methyl=0.0612$ $d_{norm}\ C(4)-C(5)=0.0555$
2-ethylimidazole	Dispersion interactions between ethyl groups of adjacent molecules with orientation A.	$d\ ethyl\cdots ethyl=3.286$ $d_{norm}=0.0973$

2-isopropylimidazole	Isopropyl group from an orientation B molecule interacts with the isopropyl group from an adjacent molecule and also with $C(4), C(5)$ atoms of an orientation A or C molecule.	$d\ isopropyl \cdots isopropyl = 1.468$ $d\ isopropyl \cdots H - C(4) = 2.097$ $d_{norm}/isopropyl = -0.6459$
	Molecular chains: first one formed by dispersion interactions between isopropyl group from an orientation A molecule with the $C(4)$ atom of an adjacent orientation B molecule.	$d_{norm}/C(4) = -0.2320$ $d\ C(4) - H \cdots isopropyl = 1.680$ $d_{norm}\ isopropyl = -0.4420$ $d_{norm}\ C(4) = -0.4433$
	Second chain formed by $H \cdots \pi$ interaction between the aromatic ring of an orientation B with the isopropyl group form an orientation A or C molecule and with the $C(4) - H$ of an adjacent orientation A or C molecule.	$d\ isopropyl \cdots \pi = 2.810$ $d\ C(4) \cdots \pi = 2.922$ $d_{norm}\ B\ molecule - isopropyl\ side = 0.0311$ $d_{norm}\ B\ molecule - H - C(4)\ side = 0.2191$
	The third type of molecular chain is formed via the dispersion interactions established between isopropyl groups from orientation A or C. The isopropyl groups favor an intricate dispersion web.	$d\ isopropyl \cdots isopropyl = 2.511$ $d_{norm}\ isopropyl = 0.0792$
	Dispersion interaction between isopropyl groups from orientation B.	$d\ isopropyl - isopropyl = 2.310$ $d_{norm}\ isopropyl = 0.1271$

IV.10.2 Pyrazole derivatives

The labels of the pyrazole derivatives atoms are shown in Figure 54. The hydrogen bond distances of the studied pyrazole derivatives in the crystal phase are listed in Table 22.

Table 22. Lengths in 10^{-10} m and angles in degrees for hydrogen bond in pyrazole derivatives.

Compound	Hydrogen bond length $(N-H), H \cdots N$	Hydrogen bond length $N-H \cdots N$	Hydrogen bond angle
Pyrazole	(1.009), 1.944	2.912	175.38, 159.93
3,5-dimethylpyrazole	(1.009), 1.970	2.971	171.53
3,4,5-trimethylpyrazole	(1.009), 1.914	2.912	176.13, 166.53. 162.91

As in the case of imidazole compounds, a common characteristic of these compounds is the formation of hydrogen bonds formed by two nitrogen atoms, where the nitrogen $N(1)$ acts as a hydrogen bond donor and nitrogen $N(2)$ as an acceptor. This interaction is represented as $N(1)-H \cdots N(2)$. Also, the hydrogen bond interaction origins the formation of molecular chains in the cases of pyrazole and 3,4,5-trimethylpyrazole. These chains are not as linear as in the case of the imidazole derivatives, due to the vicinity of the $N(1)-N(2)$ bond in the aromatic ring.

In the case of the crystal structures of 3,5-dimethyl and 3,4,5-trimethylpyrazole, apparently, they incorporate a molecular structure that does not correspond to the real one, because in both cases, the nitrogen atoms possess a hydrogen atom. This is a product of the structure refinement strategy. The reason for that is that tautomeric effect[123] between the hydrogen and nitrogen atoms in the pyrazole ring that provides extra symmetry to the molecules. However, this does not affect the spatial position of the hydrogen bond sequence in the crystal. In Figure 54, the extra hydrogen atoms have been removed.

In Table 22 can be observed that the shortest length and the closest angle to 180º correspond to the hydrogen bond in the crystal structure of 3,4,5-trimethylpyrazole, together with a similar dipole moment (See Table 18), suggest that is the strongest interaction among these compounds.

The values for d_{norm} of the Hirshfeld surface of the pyrazole compounds over the $N(1)$ and $N(2)$ atoms are listed in Table 23.

Table 23. Values for d_{norm} in the Hirshfeld surface over the nitrogen atoms in the pyrazole derivatives.

Compound	$d_{norm}\ N-H\cdots N$	$d_{norm}\ N\cdots H-N$
Pyrazole	-0.529	-0.568
3,5-dimethylpyrazole	-1.105	-1.105
3,4,5-trimethylpyrazole	-1.127	-1.152

It should be remarked that d_{norm} of 3,5-dimethyl and 3,4,5-trimethylpyrazole show a closer contact between the hydrogen bond atoms (see tables 20 and 23). These results suggest the higher thermochemical properties of the di- and tri- substituted pyrazoles.

The intermolecular interactions and some crystal parameters will be useful to understand the magnitude and trend of the thermochemical properties of these pyrazole derivatives and an account of all the interactions extracted from the crystal structure analysis of them is summarized in Table 24.

Table 24. Summary of interactions present in each crystal phase of pyrazole derivatives, other than hydrogen bond interaction.

Compound	Interactions	Interaction distance d/ 10^{-10} m, d_{norm} values
Pyrazole	Interaction $C(3)-H\cdots\pi$ and $C(5)-H\cdots\pi$ the donation of a hydrogen atom bonded to the $C(3)$ and $C(5)$ with the delocalized electron density from an adjacent molecule. Each molecule donates two hydrogen atoms and accepts two hydrogen atoms.	$dC(3)-H\cdots Hirshfeld\ surface = 1.078$ $dC(5)-H\cdots Hirshfeld\ surface = 1.145$ $dC(3)-H\cdots\pi = 2.874$ $dC(5)-H\cdots\pi = 2.831$ $d_{norm}\ \pi = -0.0152$ $d_{norm}\ C(3) = 0.0954$ $d_{norm}\ C(5) = -0.0174$
3,5-dimethylpyrazole	Weak hydrogen bond $C-H\cdots N$ between the methyl groups and the nitrogen atom from an adjacent molecule.	$d\ C-H\cdots N = 2.735$ $angle\ C(3)-H\cdots N = 132.50^{o}$ $d_{norm}\ N(1) = 0.0882$ $d_{norm}\ H-C = 0.0825$

	Dispersion interactions between methyl groups in the trimer structure, due the strong hydrogen bond interaction.	$d_{norm} - CH_3 = -0.4147$
3,4,5-trimethylpyrazole	Weak hydrogen bond between N and adjacent methyl group.	$d\ C - H \cdots N \approx 3.000$ $angle\ C(3) - H \cdots N = 153.0^o$
	Dispersion interactions between methyl group bonded to the $C(4)$ atom with adjacent methyl groups.	$d_{norm} - CH_3 = 0.0792$

V. Discussion

V.1 Enthalpy and temperature of fusion

V.1.1 Enthalpy and temperature of fusion of imidazole compounds

The temperatures and the enthalpy of fusion* of the imidazole compounds follow the trend: 2-ethylimidazole (358.7, 8.9) < Imidazole (362.3, 12.9) < 2-isopropylimidazole (405.2, 14.8) < 2-methylimidazole (417.6, 15.6), see Table 1.

It is important to take into account that in the melting process, in the initial and final states the molecular interactions that hold stable a condensed phase, still prevail. The enthalpy of fusion accounts the breaking of interactions in the solid phase and also the formation of new interactions in the liquid phase.

However, in this section, an effort to rationalize the values of the enthalpy and temperature of fusion from crystal packing analysis and intermolecular interactions present in each of the crystalline compounds is made.

In addition to the hydrogen bond that triggers the crystal growth along a linear axis, the tridimensional growth of the crystalline structure occurs through the dispersion or weak hydrogen bond interactions.

At this point, it is useful to remember that the molecule of 2-ethylimidazole has two orientations (A and B) in the crystal (see Table 21). However, as described in the Section V.1.2.1.3., the most significant intermolecular interaction present in the crystal structure of this compound is the hydrogen bond interaction and no other one. As a consequence, this compound melts at a lower temperature and has the lower value for the enthalpy of fusion (see Table 1), compared with the other imidazole derivatives, independently that, from the geometric parameters given in Table 19, the hydrogen bond is estimated to have a stronger magnitude, from its electrostatic characteristics.

As described in Table 21, the lowest values for the properties or the 2-ethylimidazole are justified by the absence of $H \cdots \pi$ and an assortment of dispersion interactions, present in the other imidazole derivatives in this series.

At comparing imidazole and 2-ethylimidazole, it is clear that the higher values corresponding to imidazole are justified by the presence of weak hydrogen bond interaction, represented by $C(2) - H \cdots N(2)$ and the dispersion interactions between $C(4)$ or $C(5)$ atoms with $C(5)$ or $C(4)$ of adjacent molecules. This compensates the fact that, among this series of compounds, the estimation of the magnitude of the imidazole hydrogen bond interaction is the lowest one compared with the other imidazole derivatives.

The compounds 2-methylimidazole and 2-isopropylimidazole have a solid-solid phase transition between ambient temperature and temperature of melting, as can be seen in the calorimetric register in Figure 55.

* Values in parentheses are in K for the temperature and in kJ·mol^{-1} for enthalpy values.

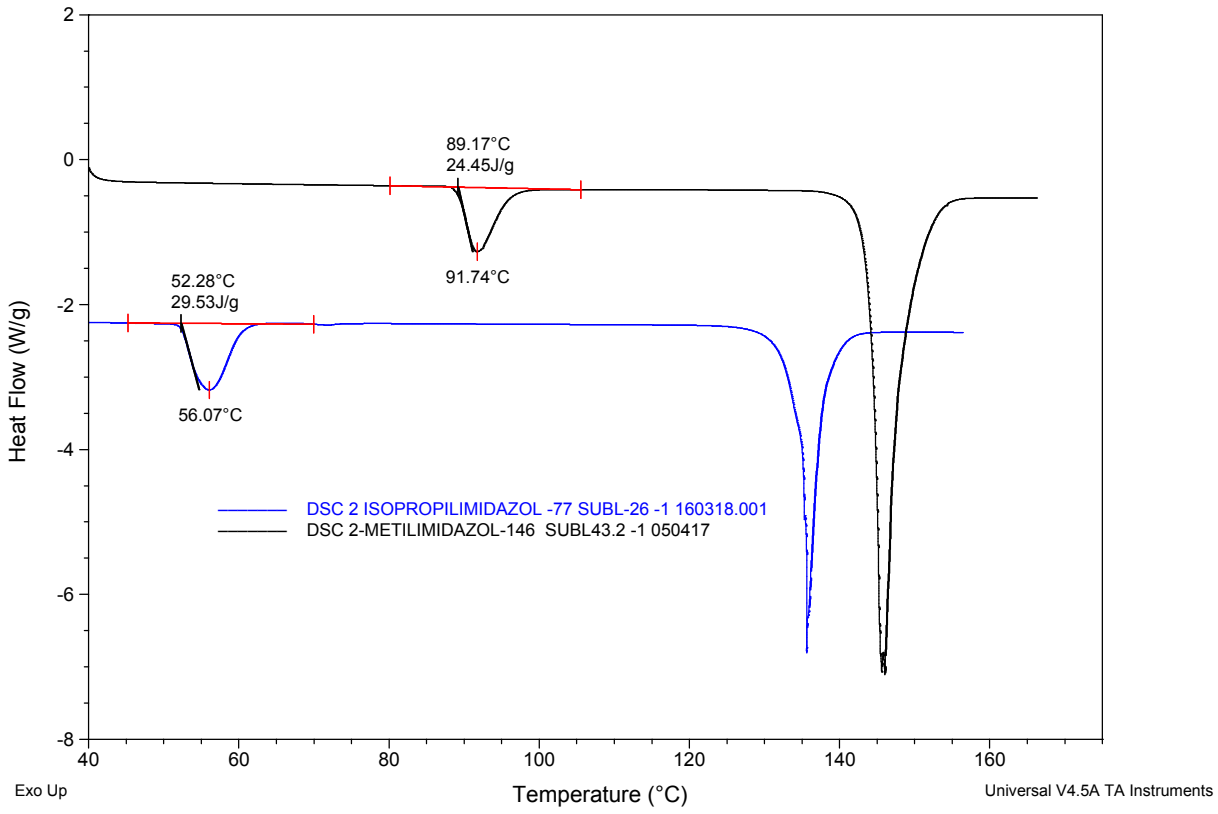

Figure 55. DSC thermal registers of 2-methylimidazole and 2-isopropylimidazole, showing the solid-solid transitions.

The X-ray diffraction studied confirmed the solid-solid transition of the crystalline system. In the 2-methylimidazole, the transition occurs at a temperature of 363.31 K with a molar enthalpy of 2.06 kJ·mol^{-1} and this transition is from an orthorhombic crystalline system $P2_12_12_1$ to a monoclinic $P2_1$. In the case of 2-isopropylimidazole, the transition occurs at a temperature of 325.4 K with a molar heat of 3.28 kJ·mol^{-1}, where the crystalline system, $P\bar{1}$, remains, but the cell dimensions change. This solid-solid transition means that the substances go to a more stable solid phase and then the fusion properties are improved, in the sense that the temperature and enthalpy of fusion are the highest for this series of compounds. Nevertheless, it is guaranteed that only one crystalline phase is present at room temperature.

In Table 19, when the hydrogen bond parameters for the compounds 2-methyl and 2-isopropylimidazole are compared, the magnitude of the interaction of 2-

methylimidazole could be estimated as the highest among the imidazole series. The hydrogen bond interaction is reflected in a stronger crystal structure and higher thermal stability, verified by the highest temperature of melting (see Table 1).

V.1.2 Enthalpy and temperature of fusion of pyrazole compounds

In the case of the pyrazole derivatives, the determined values for the temperature and enthalpy of fusion follow the trend: pyrazole (340.45, 14.5) < 3,5-dimethylpyrazole (379.8, 17.4) < 3,4,5-trimethylpyrazole (408.7, 201). This trend is explained in terms of the number and type of interactions present in their crystal phases. As reported in the work[124], in an electrostatic interaction, driven by a Coulombic potential, the distance between the interacting parts is one of the most relevant factors that affects the magnitude of such interaction. So, it is justifiable that the angle and length data, shown in Table 22, can be used to do a comparative scale of the hydrogen bond interaction. Therefore, weaker hydrogen bond interaction between pyrazole molecules, which in fact justifies the smaller temperature and enthalpy of fusion.

In a comparison of values given in Table 22 for 3,5-dimethylpyrazole and 3,4,5-trimethylpyrazole, the weak hydrogen bond that the methyl groups establish between adjacent molecules, the dispersion interactions between methyl groups bonded to the $C(4)$ atom in the 3,4,5-trimethylpyrazole with neighbor methyl groups and the stronger hydrogen bond interaction give support to the experimental values.

In this context, becomes interesting to study the process where the crystal phase interactions vanish in the final state. The enthalpy value of this process would include the whole summation of the magnitude of these interactions. A suitable experimental process that fulfills this requirement is the sublimation process.

V.2 Enthalpy of sublimation

As we have described in section V.1, the types of molecular interactions present in the crystal phase can explain the magnitude trend of thermochemical properties, such as the enthalpy of sublimation, a property that sums the whole summation of the magnitude of such interactions.

V.2.1 Enthalpy of sublimation of imidazole derivatives

At first instance, the hydrogen bond parameters give an initial approach to the enthalpy of sublimation values trend. In general, the hydrogen bond interaction present in the imidazole is estimated as the weakest one in the series of itself.

A comparison between the literature values with those obtained in this thesis for the enthalpy of sublimation of imidazole, 2-methylimidazole and 2-ethylimidazole, shows a discrepancy in the case of 2-ethylimidazole (see Table 3). The literature trend values

is: imidazole < 2-methylimidazole < 2-ethylimidazole; while the trend in this work is: imidazole < 2-ethylimidazole < 2-methylimidazol < 2-isopropylimidazole.

Concerning the trends described above and the value of the enthalpy of sublimation of 2-ethylimidazole, the crystal packing analysis reveals three important facts to consider for the crystal structure of 2-ethylimidazole: 1) The hydrogen bond interaction has the second shortest length and the closest angle to 180º; 2) There is no evidence of other types of interactions, such as $H \cdots \pi$, strong dispersion interactions or weak hydrogen bonds.

However, the hydrogen bond interaction compensates the lack of other types of interactions and leads to a higher enthalpy of sublimation, compared with imidazole. Also, the lack of other types of interaction could explain the fact that the enthalpy of sublimation of 2-ethylimidazole has a smaller value than of 2-methylimidazole.

The strong $H \cdots \pi$ interaction (see Table 21) present in the 2-methylimidazole, along with the stronger hydrogen bond interaction contributes to a higher enthalpy of sublimation compared with the corresponding for imidazole and 2-ethylimidazole.

In the case of the 2-isopropylimidazole, variety of molecular chains established in in the solid phase explain the highest enthalpy of sublimation value in the imidazole series.

V.2.2 Enthalpy of sublimation of pyrazole derivatives

The only experimental value for the enthalpy of sublimation determined in this work for this series of pyrazole derivatives was for the 3,4,5-trimethylpyrazole. The values for pyrazole and 3,5-dimethylpyrazole are taken from the literature (see Table 4).

From the hydrogen bond parameters (see Table 22), the weakest interaction is present in the pyrazole crystal structure. This is also explained from the d_{norm} values of the Hirshfeld surface over the nitrogen atoms of the aromatic ring.

Similarly, a trend was observed for the enthalpy of sublimation of the pyrazole derivatives, being the weakest interactions observed for pyrazole, compared with those of 3,5-dimethyl- and 3,4,5-trimethylpyrazole (see Table 23).

The 3,4,5-trimethylpyrazole shows the strongest hydrogen bond, as observed from the smallest $H \cdots N$ distance and the closest angle to 180º. Clearly, the greater number of interactions per molecule in the solid phase explains the fact that this compound has the highest enthalpy of sublimation among this series.

At comparing the values for the imidazole and pyrazole derivatives, a rationalization for the values of the enthalpy of sublimation can be made for the isomer compounds.

In the case of the imidazole and pyrazole, the difference between the experimental determined value for imidazole and the value for pyrazole (7 kJ·mol^{-1}, see tables 3 and 4) can be explained from the difference in the type of interactions in the solid phase. The hydrogen bond parameters of both compounds are practically the same. The weak hydrogen bond interaction in the imidazole crystal phase and the dispersion interactions established between aromatic carbons surpass the $H \cdots \pi$ interaction in pyrazole. The d_{norm} values for the imidazole Hirshfeld surface give evidence also of the contact of some atoms that could interact with each other (see Table 23).

For the other two cases, 2-ethylimidazole with 3,5-dimethylpyrazole and 2-isopropylimidazole with 3,4,5-trimethylpyrazole, there is no significative difference between the values for the enthalpy of sublimation, attributed only to difference in the experimental measurements.

V.3 Enthalpy of solution

The calorimetric values for the enthalpy of solution at infinite dilution are positive for all the studied compounds, indicating that the solution process is endothermic (see tables 5 and 6).

The enthalpy of solution at infinite dilution can be schematically represented by the equation $\Delta_{sol}H_m^{\infty} = \Delta_{solute-solvent}H + \Delta_{solute-solute}H + \Delta_{solvent-solvent}H$, in which the enthalpy of solution is accounted by the three terms of the right hand member, that represent the interactions present in the final and initial states of the solution process; the second and third terms of this equation are positive, because correspond to the breaking of interactions that maintain stable the solute solid and the liquid solvent phases. Then, these terms are proportional to the enthalpy of sublimation of the solute and the enthalpy of vaporization of the solvent, respectively. The enthalpy of vaporization values are: 43.9 ± 0.02, 37.4 ± 0.02, 32.9 ± 0.06 kJ·mol^{-1} for water, methanol and acetonitrile[125, 126], respectively.

The values of enthalpy of solution for the imidazole derivatives increase in the sequence: water, methanol and then acetonitrile. As expected for a given solute, the lower enthalpy of vaporization of the solvent, the greater enthalpy of solution. As also expected from the lack of strong solvent-solvent interactions, the enthalpy of solution values determined for the four imidazole derivatives in acetonitrile, closely follows the same pathway that the enthalpy of sublimation for the same compounds. This pathway is followed only approximately in methanol and is not followed at all in water. This behavior is shown in Figure 56.

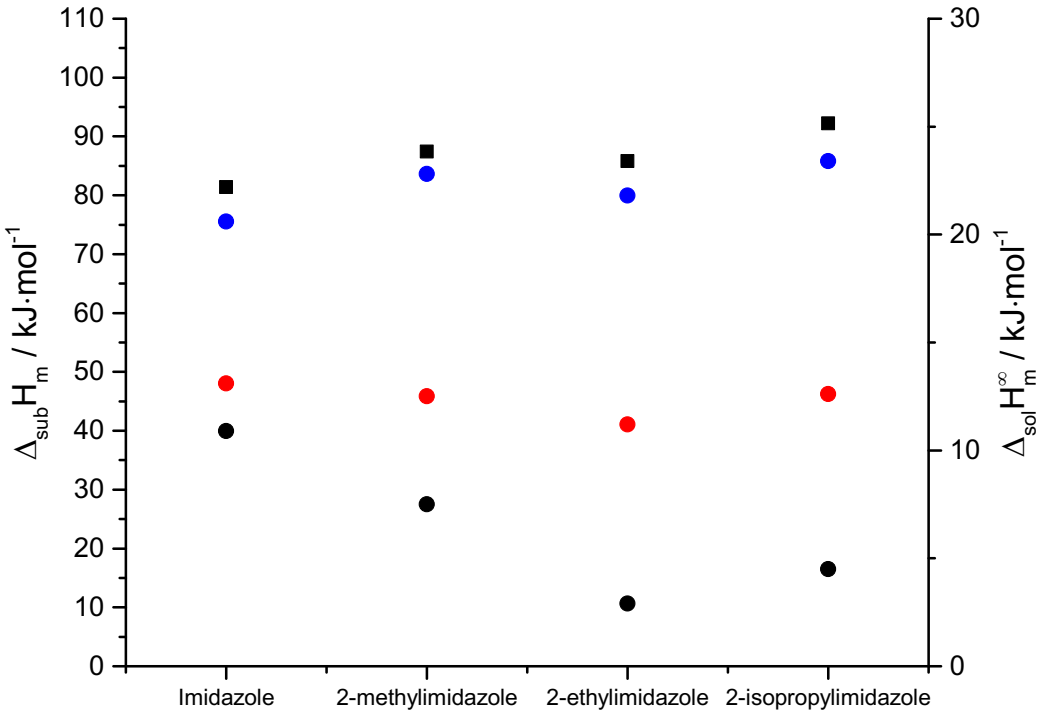

Figure 56. Values for the enthalpy of sublimation (■) for the imidazole solutes and the corresponding values for the enthalpy of solution in water (●), methanol (●) and acetonitrile (●).

The increment of the enthalpy of solution of the pyrazole derivatives in three different solvents follows the same trend as in the case of the imidazole compounds: water, methanol and acetonitrile. It is worth to notice that the enthalpies of solution at infinite dilution of the pyrazole derivatives are the same (18 kJ·mol^{-1}) in methanol (see Table 6). This similarity is only apparent, due to the enthalpy terms shown in the schematization of $\Delta_{sol}H_m^{\infty}$ compensate with each other, giving the same enthalpy value. The precise discussion of the magnitude of the solute-solvent interactions will be given in terms of the values of the enthalpy of interaction in Section V.6.

The enthalpy of solution of pyrazole derivatives in acetonitrile, closely follows the behavior of the corresponding enthalpy of sublimation, while the corresponding behavior of the enthalpy of solution values in methanol and in water is deviated in a more important way. This is represented in Figure 57.

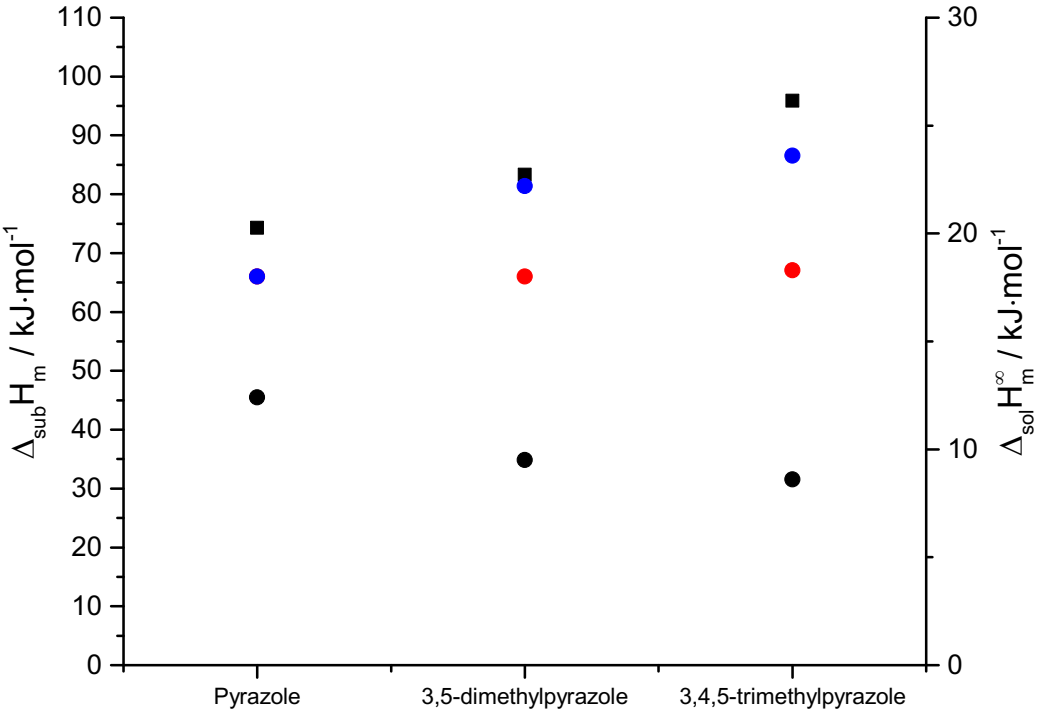

Figure 57. Values for the enthalpy of sublimation (■) for the pyrazole solutes and the corresponding values for the enthalpy of solution in water (●), methanol (●) and acetonitrile (●).

For both series of compounds, the enthalpy of solution values determined in the solvent acetonitrile, at the concentration range (10^{-2} to 10^{-3} m), do not change significantly. This indicates that the formed solutions are at the condition of the infinite dilution limit. This can be explained from the fact that, given the chemical nature of the solutes and acetonitrile, a more favorable solution process is present in a “like-like” chemical environment[2]. Also, the molecular interactions present between the imidazole and pyrazole derivatives with this solvent, such as hydrogen bond or dipole-dipole interactions, are stronger compared to similar types of interaction in solvents, such as water and methanol, mainly due to the greater dipole moment of the acetonitrile (see Section V.7).

In these systems, the hydrophobic plays[127] also an important role. In acetonitrile, the hydrophobicity of the solutes is practically absent and the phenomenon of self-aggregation is practically non-existent. This explains the independence of the enthalpy of solution in acetonitrile with the solute concentration. In contrast, the enthalpy of solution in water and methanol is strongly dependent on the concentration. Subsequently, it is concluded that, in the case of acetonitrile, the infinite dilution condition is reached in this concentration range (10^{-2} to 10^{-3} m).

The solution process is spontaneous at the experimental conditions (temperature and pressure) and with a positive enthalpy of solution. Thus, the entropy term in the

equation $\Delta G = \Delta H - T\Delta S < 0$, must be positive. This indicates that the solution process promotes disorganization from the initial to the final state. Nevertheless, because the solution process is endothermic and is carried out in *quasi*-adiabatic conditions, the whole heat of solution is transferred from the solvent. The solvent reorganizes itself and it loses degrees of freedom due to the new interactions with the solute molecules. The solute molecules in the initial state exist in a stable and "ordered" condensed phase, while in the final state are equally distributed in the solution phase (ideal solution), where the solid phase order has vanished. The degrees of freedom from solute molecules rise due to the new interactions established with the solvent molecules.

From a statistical mechanical point of view, the solution process increases the available microstates of the system, derived from the breaking of solute and solvent structure and the formation of new interactions formed between solute and solvent, such as hydrogen bond interactions. Some equivalent arguments have been given to explain values for the enthalpy of solution and the increasing of entropy and disorder in several systems[72, 73].

V.4 Enthalpy of solvation

As expected, the enthalpies of solvation are negative for all the solutes in all the solvents, due to the establishment of new solute-solvent interactions, which is an exothermic process (see tables 7 and 8).

In both, imidazole and pyrazole derivatives, the enthalpy of solvation closely follows, in all cases, the trend of the enthalpy of sublimation values for the corresponding solutes. This gives a good support of the reliability of the experimental results reported in this work.

In the initial state of the solvation process, the solute is in the ideal gas phase, where no interactions are present. By this reason, the solvation process is used in the study of solute-solvent interactions. In figures 58 and 59 are displayed the enthalpy of desolvation values (the negative values for the enthalpy of solvation) of all compounds under study, as well as the values for the enthalpies of sublimation of the corresponding solutes.

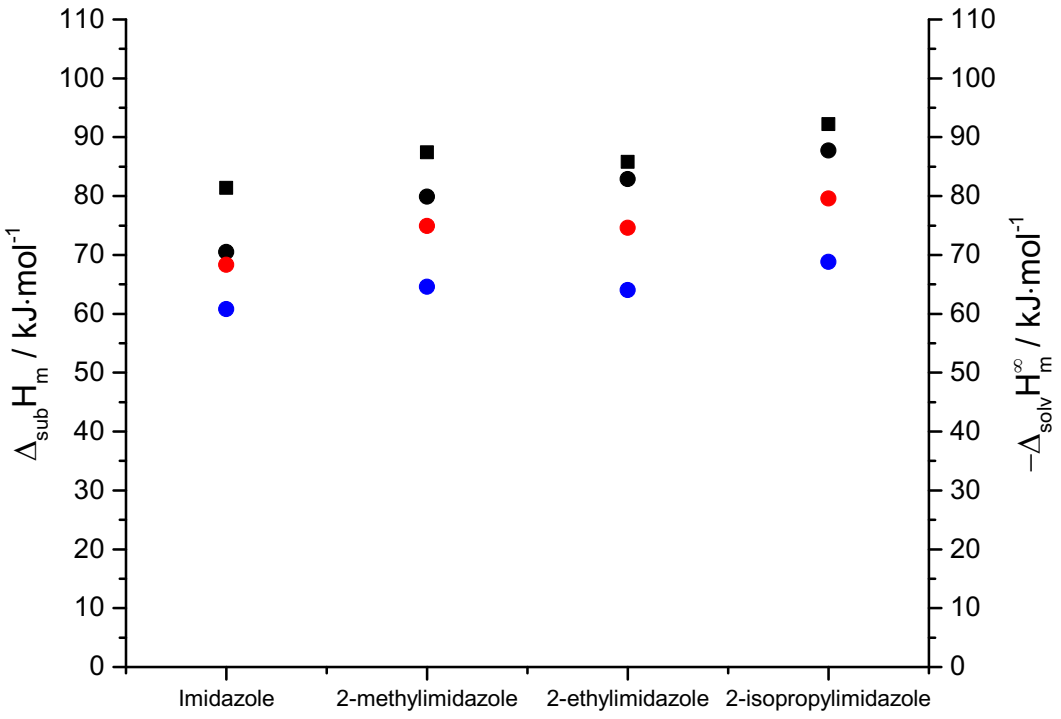

Figure 58. Values for enthalpy of sublimation (■) for the imidazole solutes and the corresponding values for the enthalpy of solvation in water (●), methanol (●) and acetonitrile (●).

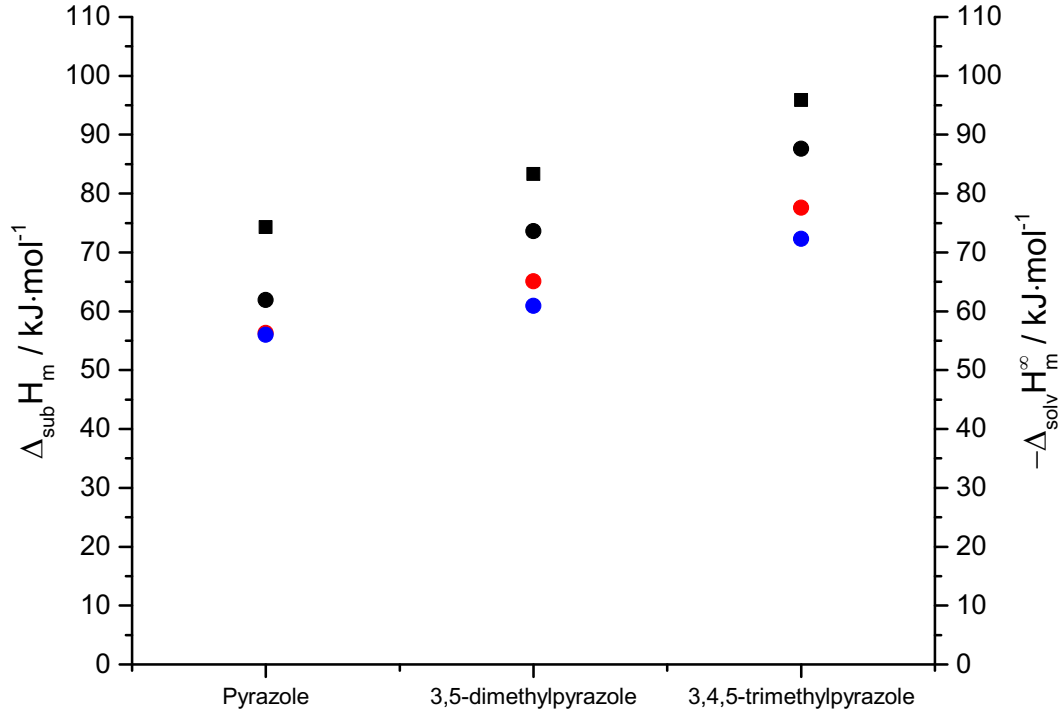

Figure 59. Values for enthalpy of sublimation (■) for the pyrazole solutes and the corresponding values for the enthalpy of solvation in water (●), methanol (●) and acetonitrile (●).

In addition, as the solute volume increases, the enthalpy of solvation increases. The establishment of new interactions between the alkyl group in imidazole derivatives and the methyl groups bonded to the aromatic ring in the pyrazole derivatives with the solvents through dipole-induced dipole and dispersion interactions improve the solvation process.

The enthalpy of solvation for the pyrazole compounds increases as the molecular volume increases, as in the case of the imidazole series, but for different reasons. In the case of the series of pyrazoles, it is clear that the methyl groups enhance the capacity of interaction with the solvents. Other than the dispersion interactions that can be established between the methyl groups and the solvents, the inductive effect generated by the methyl groups enhances the dipole-dipole interaction because it increases the dipole moment of the pyrazole derivatives (see Table 18). In this case, the increase of the enthalpy of solvation is promoted by a volume and by an electronic effect.

The enthalpy of solvation values trend is correct, but according to the organic nature of the imidazole and pyrazole solutes[2], a higher magnitude of the enthalpy of interaction in acetonitrile and methanol than in water, is foreseen and a more precise molecular approach to the results is necessary. The influence of the molecular nature of each solvent must be incorporated to complete the analysis of these results and this will be provided in Section V.7.

V.5 Enthalpy of cavity formation

The calculated values of enthalpy of cavity formation of each solute in the different solvents show that the solutes have the smallest value in water, followed by methanol and the highest in acetonitrile (see tables 9 and 10). From these results, it can be concluded that even that the solvent-solvent interactions in water have a higher magnitude than in acetonitrile, the smaller size of the water molecule decreases the enthalpy necessary to open a suitable cavity for a solute molecule inside the solvent. As suggested by Pohorille[128], the energetics of the cavity formation inside a solvent is more dependent on the molecular volume rather than on the intermolecular interactions inside the solvents.

V.6 Enthalpy of interaction

The specific interactions established between the imidazole and pyrazole derivatives with water and methanol, are of the same type and number. In both solvents the main interactions can be described as follows: a) the hydrogen bonds represented as: $N-H\cdots O$ and $O-H\cdots N$; b) the electric quadrupole and electric dipole present in the imidazole ring, coupled with the solvent molecules which also behave as an electric dipole, leads to electrostatic interactions that stabilize a solvent cloud around the solute molecule; c) the proton bonded to the oxygen atom in water or methanol that interacts

with a delocalized electronic density over each face of the aromatic imidazole ring, currently described as $H \cdots \pi$ interaction.

The only difference on the enthalpy of interaction values can correspond to the fact that the methyl group of methanol leads to other type of non-specific interactions, which are not present in water. These dispersion interactions exist between the methyl group of methanol and the aromatic ring fragment of $C(4) - C(5)$ in the case of imidazole and the fragment of $C(3) - C(4) - C(5)$ in pyrazole. The methyl group contributes to an increment, in average, of 12 kJ·mol^{-1} to the enthalpy of interaction from dispersion forces.

In this way, the dispersion forces are responsible for a stronger interaction in methanol than in water, as revealed by the increase of the enthalpy of interaction. Because the dipole moment and the angle of the substituents over the oxygen atom for water and methanol are similar, apparently these properties have no influence over the magnitude of the specific interactions. These differences are shown in Table 25.

Table 25. Differences between the values of the enthalpy of interaction for each compound in methanol and water. These values are marked in **bold**.

Compound/Solvent	$-\Delta_{int}H_m^{\infty}$ (Water)	$-\Delta_{int}H_m^{\infty}$ (Methanol)	$-\Delta_{int}H_m^{\infty}$ (Methanol) – ($-\Delta_{int}H_m^{\infty}$ (Water))
Imidazole	72.9	86.9	**14.0**
2-methylimidazole	83.0	96.6	**13.6**
2-ethylimidazole	86.6	98.8	**12.2**
2-isopropyimidazole	92.1	106.6	**14.6**
Pyrazole	64.3	74.9	**10.6**
3,5-dimethylpyrazole	77.4	89.9	**12.5**
3,4,5-trimethylpyrazole	91.7	104.9	**13.2**
Average			**13.0**

The specific interactions established between the both series of solutes and the acetonitrile, can be described as follows: a) the hydrogen bond represented as $N - H \cdots N$, being this interaction the only present of this type, due to the aprotic nature of the solvent; b) the dipole-dipole interaction that arises from the coupling of the dipole and quadrupole moment of the imidazole/pyrazole ring with the dipole moment of the solvent acetonitrile. In this case, no $H \cdots \pi$ interactions can be established because acetonitrile is not capable to donate hydrogen atoms. In contrast, acetonitrile has the highest dipole moment compared with water and methanol (3.45, 1.82 and 1.7 D[129], respectively). Consider equation (36) for the dipole-dipole interaction[4], the highest dipole moment of 3.45 D makes possible stronger specific interactions with the solute molecules. In particular, the hydrogen bond (which is a special case of a dipole-dipole interaction) $N - H \cdots N$ between acetonitrile and the imidazole/pyrazole ring is stronger than hydrogen bond $N - H \cdots O$ in water and in methanol.

$$u_{d.d.}(r) = -\frac{2\mu_1^2\mu_2^2}{(4\pi\epsilon_0)^2(3k_BT)}\frac{1}{r^6} \quad (36)$$

Considering just one solute, the dipole-dipole interaction between the solute and water/methanol and acetonitrile, the interaction potential of the last one is close to four times higher than the same interaction in water or methanol. Also, being the hydrogen bond interaction electrostatic in nature, it is expected that a difference in the dipole moments of the solvents would have a direct effect in the magnitude of the established hydrogen bond interaction. The dipole moment of acetonitrile is practically double than the value for water and methanol and this property can be considered the responsible for an electrostatic solvent effect.

As can be observed in Figure 60, three parallel lines corresponding to the three solvents are displayed and those for methanol and acetonitrile are practically superposed. From this superposition of the values of the enthalpy of interaction as a function of the molecular volume of the imidazole solutes in methanol and acetonitrile, is understood as that just one hydrogen bond of type $N-H\cdots N$ and the solvent effect produced by the double value of the dipole moment of acetonitrile, compensate the two hydrogen bonds of type $N-H\cdots O$ and $O-H\cdots N$ and two $H\cdots\pi$ interactions present in methanol. This can be considered as an important "solvent-interaction compensation".

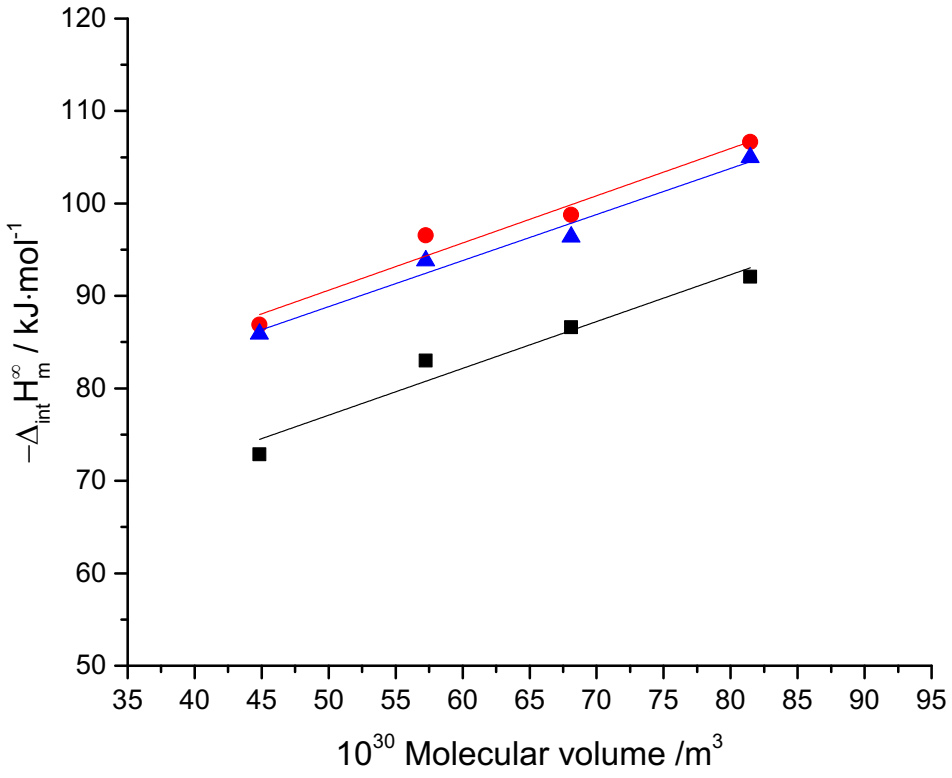

Figure 60. Enthalpy of interaction for the imidazole solutes in water (■), methanol (●) and acetonitrile (▲) as a function of the estimated molecular volume of the solutes.

These results reveal that for the imidazole solutes and solvents studied in this work, the specific interactions are concentrated just on the aromatic ring. According to that, the enthalpy of interaction increases just from non-specific interactions in terms of the available surface on the substituent. This is consistent with the observation of Savage and Wood[130], that found that a reference solute interacting with solutes increasing their size of alkyl groups present the regularity: the larger the hydrocarbon group, the more positive the interaction.

The least squares analysis of the data shown in Figure 60 leads to an increase of the enthalpy of interaction of $(0.50\pm0.060)\cdot10^{-30}$ kJ·mol^{-1}·m^{-3}. From the same analysis, the difference of the molar enthalpy of interaction between all the solutes with acetonitrile or methanol and with water is evaluated as $-(12.7\pm0.5)$ kJ·mol^{-1}.

In the case of the pyrazole derivatives, the magnitude of the enthalpy of interaction in acetonitrile is the highest for all compounds. This magnitude decreases successively to methanol and then in water. This trend is explained from the fact that, although the solvents water and methanol establish two hydrogen bond interactions with a solute molecule, the position of the atoms $N(1)$ and $N(2)$ in the pyrazole ring are just at one bond close. It can be assumed that there is a steric effect between solvent molecules when they interact with each nitrogen atom. Thus, the hydrogen bond geometry is not as appropriate as in the case of the imidazole ring. This effect is not present in the solvent acetonitrile, due to its aprotic nature, where just one nitrogen atom establishes the hydrogen bond interaction. Also, due to the dipole moment of the solvent acetonitrile is the highest among the solvents, the dipole-dipole interaction is stronger with acetonitrile than with water or methanol.

The dependence of the enthalpy of interaction of the pyrazole compounds with the molecular volume exhibits a quadratic behavior, as shown in Figure 61.

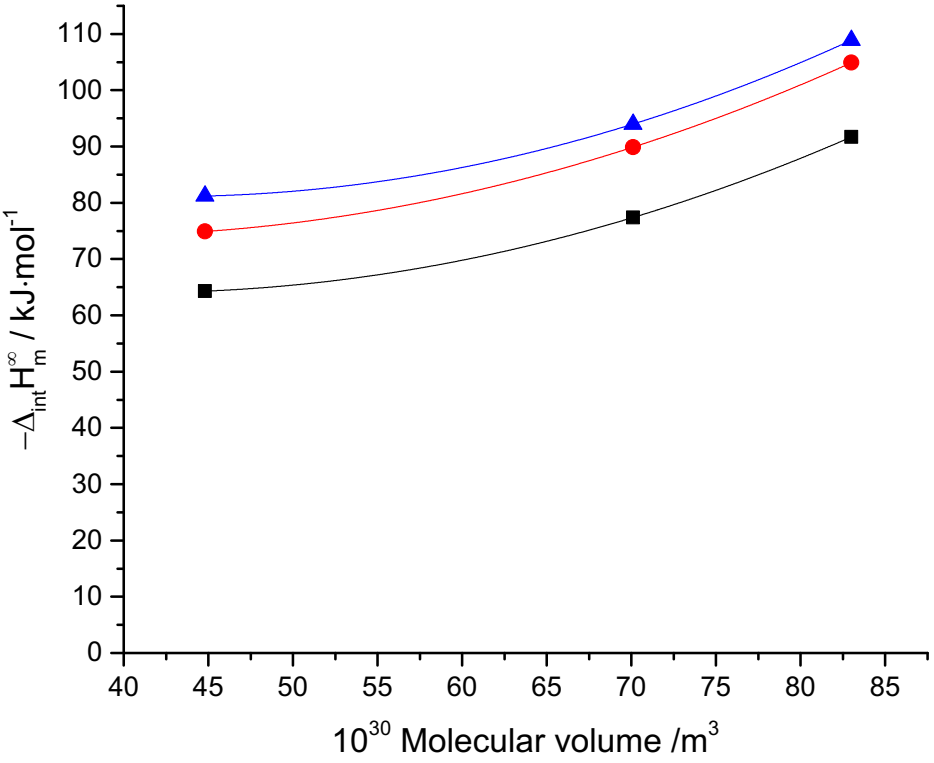

Figure 61. Enthalpy of interaction for the pyrazole solutes in water (■), methanol (●) and acetonitrile (▲) as a function of the estimated molecular volume of the solutes.

This behavior is explained from the fact that, in contrast to the case of the imidazole series, the volume of the pyrazole compounds increases with the successive bonding of methyl groups over the aromatic ring and not with the increment in the size of an alkyl radical over just one position in the aromatic ring. The inductive effect of the methyl groups increases the electronic density in the aromatic ring, which is easier polarizable by the solvent. The quadratic behavior of the dependence of the enthalpy of interaction with the molecular volume gives evidence that the increment of the enthalpy of interaction values is due to both a volume and an electronic effect; this is a different behavior in the imidazole series, where the electronic density of the aromatic ring is not changed as the molecular volume increases, from the compounds 2-methylimidazole to 2-isopropylimidazole.

From tables 13 and 14, the differences of the enthalpies of interaction between solute molecules in each solvent can be calculated. The difference between the values for the root heterocycle, imidazole or pyrazole, and the corresponding more substituted derivatives, 2-isopropylimidazole [19.2 (water), 19.7 (methanol) and 19.1 (acetonitrile) kJ·mol^{-1}] or 3,4,5-trimethylpyrazole [27.4 (water), 29.7 (methanol) and 27.7 (acetonitrile) kJ·mol^{-1}]. In the case of imidazole derivatives, the difference is very close to the average 19.3 kJ·mol^{-1} in the three solvents and in the case of pyrazole, the difference is close to the average 28.4 kJ·mol^{-1}, in the three solvents.

These values (19.3 and 28.4 kJ·mol^{-1}) indicate that this increment does not depend on the chemical nature of the solvent and this effect is expected for other polar solvents. This increment is only due to the alkyl radical size and the heterocyclic ring nature. These differences are shown in Table 26.

Table 26. Difference between the enthalpy of interaction of 2-isopropylimidazole and imidazole in each solvent. These values are marked in **bold**.

Compound/Solvent	$-\Delta_{int}H_m^{\infty}$ (Water)	$-\Delta_{int}H_m^{\infty}$ (Methanol)	$-\Delta_{int}H_m^{\infty}$ (Acetonitrile)
Imidazole	72.9	86.9	85.9
2-isopropyimidazole	92.1	106.6	105.0
$-\Delta_{int}H_m^{\infty}$ (2-isopropylimidazole) – ($-\Delta_{int}H_m^{\infty}$(imidazole))	**19.2**	**19.7**	**19.1**
Pyrazole	64.3	74.9	81.2
3,4,5-trimethylpyrazole	91.7	104.9	108.9
$-\Delta_{int}H_m^{\infty}$ (3,4,5-trimethylpyrazole) – ($-\Delta_{int}H_m^{\infty}$(pyrazole))	**27.4**	**29.7**	**27.7**

In relation of enthalpy of interaction relative to isomers, the difference in this property is more significant between imidazole and pyrazole. This could be explained form the difference in the dipole moments of both molecules, due to the position of the nitrogen atoms in the aromatic ring. In the case of the pyrazole molecule, the electrostatic effect of the partial charges of the nitrogen atoms diminishes the magnitude of the dipole moment of the molecule and this is reflected in a decrement in the dipole-dipole interaction, present between all solutes with all solvents. Also, the position of the nitrogen atoms in the pyrazole aromatic ring creates a steric effect that affects the geometry of the hydrogen bond formed with water and methanol. The difference decreases in the solvent acetonitrile because of the formation of just one hydrogen bond between solute and solvent.

In a similar way, the difference in the dipole moment between 2-ethylimidazole and 3,5-dimethylpyrazole explain the difference in the the enthalpy of interaction. The imidazole derivative has a higher dipole moment and the position of the nitrogen atoms in the aromatic cycle affect the geometry (and therefore the magnitude) of the hydrogen bond interaction established with water and methanol. In relation to the difference of 9 kJ·mol^{-1} in the solvent methanol, the establishment of dipole-induced dipole interactions between the solvent and the alkyl substituents are taken into account. Probably, the ethyl group has a higher polarizability than summation of the polarization of two methyl groups.

A limit case is reached in the 2-isopropylimidazole and 3,4,5-trimethylpyrazole derivatives. The difference of the enthalpy of interaction between these molecules and the solvents is not as significant as in the other isomer cases.

V.7 ^{1}H NMR of the studied compounds

The chemical shift is dependent on the electronic environment of the nuclei in a molecule[4]. Hence, the solvation process in different solvents involves different kind of molecular interactions, all of these from electrostatic nature. Thus, these interactions must affect the electronic behavior of the molecule and their atoms in particular. Consequently, the ^{1}H NMR spectra would be sensible to the solvation features in the three different solvents used in this research. This premise is verified from the chemical shift values displayed in the tables 15 and 16.

V.7.1 ^{1}H NMR of imidazole derivatives

V.7.1.1 Aromatic protons

V.7.1.1.1 $\mathbf{H-N(1)}$

The chemical shift (δ) corresponding to the proton $H-N(1)$ in acetonitrile, decreases with the following trend: Imidazole > 2-methylimidazole > 2-ethylimidazole > 2-isopropylimidazole. From the values of the dipole moment included in Table 17, is observed that the lower the dipole moment of the solute molecule, the lower the value of the chemical shift. The magnitude range of the chemical shifts (going from 10.67 to 10.12, from imidazole to 2-isopropylimidazole) suggests that the hydrogen bond interaction declines in magnitude, as the dipole moment of the solute decreases. However, the individual interaction between a solute molecule and acetonitrile is stronger compared to water or methanol. In a previous work[131] has been studied the dependence of the magnitude of the hydrogen bond with the electronegativity of the donor and acceptor atoms. The fact that more interactions are possible in a bulkier alkyl group, such as the isopropyl substituent, compensates the fact of this decreasing magnitude in the hydrogen bond interaction.

V.7.1.1.2 $\mathbf{H-C(2)}$ atom

The chemical shift value for $H-C(2)$ is higher than those of $H-C(4), H-C(5)$ protons. This proton is deshielded by the near presence of two nitrogen atoms. Then, it is expected that the corresponding chemical shift does not change significantly with different solvents. This fact could indicate that no specific interaction at $H-C(2)$ will be relevant in the imidazole molecule.

V.7.1.1.3 $\mathbf{H-C(4)}$ and $\mathbf{H-C(5)}$ atoms

The chemical shifts values for $H-C(4)$ and $H-C(5)$ atoms are close to the values for the aromatic hydrogen atoms in benzene (7.3 ppm). They do not change significantly from one solvent to another. This indicates that the specific interactions established between the aromatic ring and the solvents do not change from one solvent to another. The change in the enthalpy of interaction is due only to the alkyl substituent size.

In particular, the higher frequency value of the chemical shift, the greater the electronic interaction of the solvent with the solute. This result is consistent with the values established for the enthalpies of interaction.

V.7.1.2 Alkyl protons

These protons denoted as $H-C(6)$, correspond to methyl protons in the case of 2-methyl imidazole, to methylene protons in the case of 2-ethylimidazole or to only one proton over $C(6)$ in the case of 2-isopropylimidazole. In any solvent, the resonance frequency of the $H-C(6)$ increases as the volume of the alkyl group increases. Then, a similar trend of the enthalpy of interaction due to the establishment of more interactions with a bulkier alkyl substituent is verified.

The dependence of $\Delta_{\mathrm{int}}H_m^{\infty}$ with δ of $H-C(6)$ is shown in Figure 62. This dependence gives an insight in how the increment in size in the alkyl substituent affects the chemical environment of this atom.

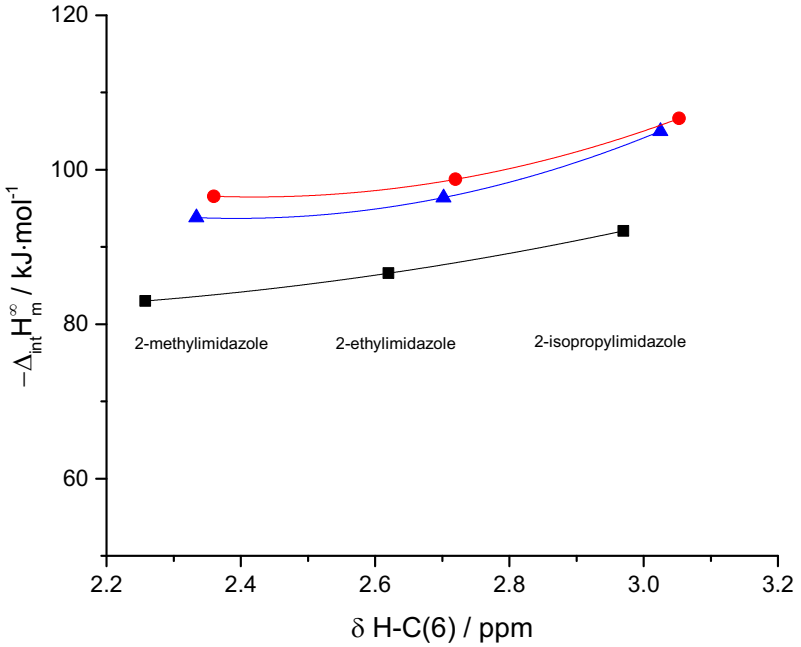

Figure 62. Enthalpy of interaction of 2-methylimidazole, 2-ethylimidazole and 2-isopropylimidazol in correlated with the chemical shifts values of the $H-C(6)$ in water water (■), methanol (●) and acetonitrile (▲).

This figure shows that the solvent effects of methanol or acetonitrile are more alike between them and different form the solvent effects of water in this atom. The substitution of the imidazole ring with an alkyl group of increasing size, as methyl, ethyl and isopropyl, enhances the deshielding effect in the $H-C(6)$. This effect leads to an increment in the enthalpy of interaction, whose quadratic dependence with the chemical shift is indicative that this deshielding effect reaches a limit and does not increase for a larger size of the substituent. The results for the least square fitting of this dependence, is provided as supplementary information in Appendix.

The most important difference in chemical shifts of the hydrogen atoms at $C(4)$ and $C(5)$ occurs in the imidazole and 2-methylimidazole molecules, as a result of the inductive effect promoted by the methyl group. This difference is not so relevant when the 2-methyl, 2-ethyl or 2-isopropyl groups are substituted in the molecule of imidazole.

V.7.1.3 Alkyl radical hydrogen atoms

The different chemical shifts of the hydrogen atoms in the alkyl groups give clear evidence that an increase in the enthalpies of solvation and interaction is strongly influenced by the size of the aliphatic chain, due to the increasing in the number of the possible interactions that can be established between the solute and the solvent. The size of the alkyl radical improves the solvation process and increases the magnitude of the enthalpy of interaction.

The chemical shift values of the hydrogen atoms in the alkyl group that are substituted in the aromatic ring increase as the volume of this group increases. A higher increment of the chemical shift is observed at the hydrogen atoms of the methyl groups of each alkyl substituent. This fact supports that the terminal hydrogen atoms are the most important to establish interactions with the solvent.

V.7.2 ^{1}H NMR of pyrazole derivatives

V.7.2.1 Aromatic protons

V.7.2.1.1 $\mathbf{H-N(1)}$

In the pyrazole series, the chemical shift (δ) corresponding to the proton $H-N(1)$ in acetonitrile, decreases with the following trend: Pyrazole > 3,5-dimethylpyrazole > 3,4,5-trimethylpyrazole (see Table 16).

The decrease in the chemical shift value of the $H-N(1)$ proton in acetonitrile is due to the increase of electron density in the aromatic ring. The inductive effect promoted by the substitution with a methyl group affects the electronic environment, causing a shielding effect in the hydrogen atom. This effect is higher in 3,4,5-trimethylpyrazole

than in 3,5-dimethylpyrazole because of the inclusion of a third methyl group. The great difference in the chemical shift in pyrazole (11.14) with the value in 3,4,5-trimethylpyrazole (10.23) supports this proposition (see Table 18).

From the values of $H-N(1)$ chemical shift for the imidazole and pyrazole derivatives, the hydrogen bond interaction established between $N(1)-H$ and the solvents has a higher deshielding effect, giving evidence that this interaction is stronger between the pyrazole compounds and the solvents.

V.7.2.1.2 $\mathbf{H-C(4)}$ atom

The chemical shift $H-C(4)$ atom is only present in pyrazole and 3,5-dimethylpyrazole and does not have significant change between solvents, although the values are quite different between these two compounds. This can be explained from the inductive effect triggered by two methyl groups that are substituting the aromatic ring in the 3,5-dimethylpyrazole, which donates electronic density to the π system. This effect enhances the electronic density and has a shielding effect in the whole aromatic ring.

V.7.2.1.3 $\mathbf{H-C(3)}, \mathbf{H-C(5)}$ atoms

These atoms are only present in the pyrazole and are chemically equivalent. The difference between the chemical shift values in the three solvents is not significant, giving hint that these part of the aromatic ring does not participate in establishing specific interaction with the solvents.

V.7.2.2 Methyl hydrogen atoms

The chemical shift values for the hydrogen atoms in the methyl groups are not significantly different among the solvents, although the values are slightly higher in methanol. As in the case of the imidazole compounds, these values indicate that terminal methyl groups play an important role in favoring the solvation process.

In the case of the pyrazole series, the ^{1}H NMR spectroscopy is not sensible enough to give chemical shift values that result in significant differences in order to correlate them with the enthalpy of interaction, as in the case of the imidazole compounds.

The ^{13}C and ^{15}N NMR spectroscopy seemed as a suitable tool to study the solvent effect in the pyrazole molecules, but at this time, technical problems in the NMR devices would not allow to collect spectroscopic data that could be related with the enthalpy of interaction values.

VI. Conclusions

As proposed in the introduction section and verified through the obtained thermochemical results in this work, and the corresponding analysis and discussion on the base of their chemical and crystal structure, the imidazole and pyrazole derivatives are relatively small molecules with several and special structural characteristics that promote molecular interactions in the solid phase and in solution with different solvents. Each of these compounds present unique individual features concerning the interactions in the solid phase that explain the magnitudes of solid phase thermochemical stability and properties. The chemical structure of the heterocycle ring, which contains two nitrogen atoms, causes that each compound presents different types and strength of interactions, that lead to specific thermochemical behavior in solid and solution phase.

In general, the hydrogen bond interaction $N - H \cdots N$ between successive molecules is the main responsible for the growing of the crystal structure of the studied compounds. In the case of the imidazole compounds, this interaction causes the molecules to form straight molecular chains along a specific axis.

The $N - N$ bond in the pyrazole compounds causes that these molecular chains in the solid phase are not as linear as in the imidazole derivatives. The extreme case occurs in the crystal structure of the 3,5-dimethylpyrazole that exhibits a singular behavior. The crystal growth occurs not due to the interactions between individual molecules, but from trimer structures. Then, this arrangement promotes the hydrogen bond and dispersion interactions among neighbor molecules and in addition these trimer structures form well-defined layers. This is a singular feature of this crystalline structure compared to the other studied compounds.

The dispersion forces and in some cases the $H \cdots \pi$ interaction, promote the tridimensional growth of the crystal structure of the solutes and play an important role in the fusion and sublimation parameters.

The values for the enthalpy and temperature of fusion can correctly be rationalized with the crystal structure features. The thermal stability of the studied compounds is mainly correlated to the hydrogen bond distances and molecular interactions. Nevertheless, it has been evidenced that the fusion parameters are not the most suitable properties that give insight about the magnitude of the intermolecular interactions present in the solid phase, but the enthalpy of sublimation values do it correctly.

It has been shown that the enthalpy of sublimation values trend for the studied compounds can be explained and rationalized from the crystal packing analysis of the studied compounds, because this thermodynamic property accounts for the whole magnitude of the solid-state interactions. The analysis of the interactions that are present in the solid phase, through the CrystalExplorer 17 software, of the studied compounds supports the experimental values obtained in this work.

The schematic representation of the enthalpy of solution in contributions from the enthalpy of sublimation of the solutes and the enthalpy of vaporization of the solvents makes possible the explanation of the trend of values founded. Also, concerning about the endothermic and spontaneity nature in all cases, it is clear that the solution process carries a disorganization of the solute understood as an increase in its degrees of freedom, but also an organization in the solvent structure, due to the new interactions established with the solutes and the restrictions that this implies.

The enthalpy of sublimation of a family of organic compounds can be estimated if this value is known for one of the elements and the enthalpies of solution are experimentally determined in a solvent with low enthalpy of vaporization.

The determined enthalpies of solvation are exothermic in all the studied compounds in this work. The absence of solute-solute interactions in the final state is reflected by the similar pathway followed by the enthalpy of solvation and the corresponding enthalpy of sublimation, for all the studied compounds.

From the obtained enthalpy values, it is clear that the solvation process has a greater magnitude in the solvent water, supported by the enthalpy of cavity formation values. Nevertheless, the chemical nature of solutes and solvents gives insight that a term that accounts only the magnitude of solute-solvent interactions is needed, the enthalpy of interaction.

The Pierotti equation provides the correct values for the enthalpy of interaction between solute and solvent. In the case of the imidazole series, this property increases linearly with the molecular volume. This is evidence that the interactions established between the solvent and the aromatic ring contribute similarly to the magnitude of this property and that the increment is a volume effect only, caused by the dispersion interactions due to the alkyl group.

In this study has been substantiated that the magnitude of the obtained thermochemical properties accounts correctly for all the energy of non-covalent interactions present in the stable pure or solution phases involved in these series of chemical compounds. The thermochemical experimental procedures lead to know the magnitude range of enthalpies of solvation (-56 to -88 $kJ \cdot mol^{-1}$) or interaction (-73 to -109 $kJ \cdot mol^{-1}$) and also the trend of these properties when the chemical structure is slightly modified, ranging from 2 to 30 $kJ \cdot mol^{-1}$. Moreover, the differences of these enthalpy values for the imidazole or pyrazole derivatives are also explained in terms of the chemical structure.

It is worth to notice that the enthalpy of interaction in the case of imidazole derivatives has a linear correlation with the estimated molecular volume and in the case of pyrazole derivatives this correlation is a quadratic one. This fact is probably associated to a combination of a volume and an electronic effect.

The fact of a good correlation between macroscopic and microscopic properties, supports that the experimental results obtained for the enthalpy of solution and sublimation are reliable.

The chemical shift values obtained from ^{1}H NMR spectroscopy support the trend of the enthalpy of interaction values for the imidazole series and give a molecular insight of which sites of the solute molecules participate in the interaction of the solutes with the solvents. The magnitude of the molecular interactions between solute and solvent, derived from the experimental measurements based on thermodynamics, account correctly the intermolecular interactions. Additionally, the trend of these properties is supported by the shielding/deshielding effects observed from ^{1}H NMR molecular spectroscopy.

In the case of the pyrazole series, the ^{1}H NMR chemical shift values do not correlate with the enthalpy of interaction values.

The real trend of the quantitative strength interaction between an organic solute with different solvents must be absolutely based on the knowledge of the derived thermochemical enthalpy of interaction, and not just on the enthalpy of solvation.

The magnitude of the thermodynamic quantities depends directly on the molecular properties and interactions present in the phase under study. In this work, the thermochemical study of these interactions in the solvation process and their rationalization with the established molecular interactions has been supported by molecular or spectroscopic properties. These two different approaches converge in the understanding of solute-solvent interactions in the solvation process.

Appendix

In this appendix is shown the experimental data for the differential scanning calorimetry, Knudsen effusion and the solution calorimetry experiments, together with the polynomial fitting of the data. There are also included the NMR spectra of all the solutes in the deuterated solvents, the mass spectrometry experiments, used to discard the formation of dimers in the gas phase and the crystal data for the 2-ethylimidazole and 2-isopropylimidazole compounds and illustration of the calculated normalized dipole moment vector for each compound.

A.1 Differential scanning calorimetry experiments. Purity, temperature and enthalpy of fusion

In tables A1 to A7 are displayed the mass of the sample (*m*), used in each experiment; the purity obtained from the DSC individual register; the melting temperature obtained for each experiment and the corresponding enthalpy of fusion.

10^6 *m*/(kg)	Purity/mol %	T/K	$\Delta_{fus}H_m$ /(kJ·mol^{-1})
8.54	99.97	362.30	12.76
9.02	99.99	362.21	13.23
6.68	99.94	362.30	12.77
6.53	99.96	362.19	12.92
9.55	99.92	362.40	12.63

Table A1. Purity, temperature and enthalpy of fusion of imidazole.

10^6 *m*/(kg)	Purity/mol %	T/K	$\Delta_{fus}H_m$ /(kJ·mol^{-1})
9.33	99.98	417.01	15.50
9.50	99.99	417.07	15.67
10.91	99.98	416.77	15.64

Table A2. Purity, temperature and enthalpy of fusion of 2-methylimidazole.

10^6 *m*/(kg)	Purity/mol %	T/K	$\Delta_{fus}H_m$ /(kJ·mol^{-1})
6.12	99.92	359.77	8.94
5.54	99.88	358.68	8.87
5.91	99.89	358.67	8.89
5.62	99.88	358.55	8.94
7.01	99.90	358.66	8.99
10.26	99.93	358.77	8.77

Table A3. Purity, temperature and enthalpy of fusion of 2-ethylimidazole.

10^6 *m*/(kg)	Purity/mol %	T/K	$\Delta_{fus}H_m$ /(kJ·mol^{-1})
8.91	99.82	405.42	14.70
9.32	99.83	405.04	14.88
8.03	99.81	405.22	14.62

Table A4. Purity, temperature and enthalpy of fusion of 2-isopropylimidazole.

10^6 *m*/(kg)	Purity/mol %	T/K	$\Delta_{fus}H_m$ /(kJ·mol^{-1})
8.78	99.97	340.43	14.67
6.53	99.92	340.38	14.51
9.54	99.96	340.48	14.51
7.28	99.93	340.49	14.24

Table A5. Purity, temperature and enthalpy of fusion of pyrazole.

10^6 *m*/(kg)	Purity/mol %	T/K	$\Delta_{fus}H_m$ /(kJ·mol^{-1})
2.92	99.98	379.76	16.97
2.58	99.98	379.62	17.18
2.38	99.90	380.01	17.56
3.45	99.98	379.99	17.80

Table A6. Purity, temperature and enthalpy of fusion of 3,5-dimethylpyrazole.

10^6 *m*/(kg)	Purity/mol %	T/K	$\Delta_{fus}H_m$ /(kJ·mol^{-1})
5.62	99.39	408.79	19.89
5.85	99.37	408.68	20.11
5.58	99.35	408.59	20.01
11.63	99.49	409.93	20.25

Table A7. Purity, temperature and enthalpy of fusion of 3,4,5-trimethylpyrazole.

A.2 Results for the Knudsen Effusion Measurements

In Tables A8 to A12 are summarized the experimental data and results for the Knudsen effusion experiments. In the first row are given the geometrical features of the effusion hole. The first column displays the temperature at which experiment was performed. The second to fourth column contains the effusion data: the mass loss Δm, the elapsed time under high vacuum and the calculated effusion rate. The last column shows the determined vapor pressure.

A.2.1 Imidazole series

$10^8 A$ = 4.908 m^2, Φ = 250 μm				
T/K	$-10^6\ \Delta m$/(kg)	t/s	$-10^{11}\ \mathrm{d}m/\mathrm{d}t$ /(kg·s^{-1})	P/Pa
286.114	1.058	140641	0.752	0.072
287.801	1.315	145199	0.906	0.087
289.477	0.872	93120	0.936	0.090
291.570	1.822	149460	1.219	0.117
293.592	2.164	144720	1.496	0.139
295.622	2.794	153300	1.823	0.177
298.987	4.035	145860	2.766	0.270
301.923	4.416	99612	4.433	0.435
303.311	6.430	135468	4.747	0.466
304.819	5.087	91019	5.589	0.551
306.288	8.312	128999	6.443	0.636
307.786	7.295	91080	8.009	0.793
309.508	9.003	96540	9.326	0.926

Table A8. Experimental results for the Knudsen effusion experiments for imidazole.

$10^8 A$ = 4.908 m^2, Φ = 250 μm				
T/K	$-10^6\ \Delta m$/(kg)	t/s	$-10^{11}\ \mathrm{d}m/\mathrm{d}t$ /(kg·s^{-1})	P/Pa
292.840	0.501	158400	0.316	0.028
294.753	0.849	158400	0.536	0.047
296.688	0.858	144000	0.596	0.053
301.075	1.011	97200	1.040	0.093
302.554	1.436	126342	1.137	0.102
304.604	2.521	145620	1.731	0.155
306.690	2.778	133380	2.083	0.187
308.550	3.454	141120	2.447	0.221
311.069	4.412	144240	3.059	0.277
313.700	5.636	142200	3.963	0.361

Table A9. Experimental results for the Knudsen effusion experiments for 2-methylimidazole.

10^7A = 7.853 m^2, Φ =1000 μm				
T/K	-10^6 Δm/(kg)	*t*/s	-10^{11} d*m*/d*t* /(kg·s^{-1})	P/Pa
290.295	7.8727	154800	5.086	0.026
295.742	16.371	153000	10.700	0.055
298.422	20.492	144000	14.230	0.073
300.914	28.130	144300	19.490	0.100
303.378	37.365	144000	25.950	0.134
309.594	74.082	144000	51.450	0.231
10^6A = 1.484 m^2, Φ =1375 μm				
T/K	-10^6 Δm/(kg)	*t*/s	-10^{11} d*m*/d*t* /(kg·s^{-1})	P/Pa
290.295	22.191	154800	14.010	0.027
295.742	29.117	153000	19.030	0.051
298.422	35.689	144000	24.780	0.067
300.914	49.471	144300	34.280	0.093
303.378	66.130	144000	45.920	0.125
309.594	133.063	144000	92.400	0.177

Table A10. Experimental results for the Knudsen effusion experiments for 2-ethylimidazole.

10^6A = 1.484 m^2, Φ =1375 μm				
T/K	-10^6 Δm/(kg)	*t*/s	-10^{11} d*m*/d*t* /(kg·s^{-1})	P/Pa
286.114	5.822	140641	4.139	0.010
287.801	7.375	145199	5.079	0.013
289.477	5.773	93120	6.199	0.015
291.570	11.73	149460	7.849	0.017
293.592	14.48	144720	10.001	0.025
295.622	21.01	153300	13.703	0.035
298.987	28.96	145860	19.856	0.050
301.075	26.68	97200	27.447	0.070
302.554	41.82	126342	33.099	0.084
304.604	58.90	145620	40.448	0.104
306.690	68.53	133380	51.383	0.132

Table A11. Experimental results for the Knudsen effusion experiments for 2-isopropylimidazole.

A.2.2 Pyrazole series

10^8A = 4.908 m^2, Φ = 250 μm				
T/K	$-10^6\ \Delta m$/(kg)	*t*/s	-10^{11} d*m*/d*t* /(kg·s)	P/Pa
288.112	0.494	86400	0.572	0.043
288.221	0.913	152300	0.599	0.045
291.436	1.321	140220	0.942	0.071
296.829	2.941	170580	1.724	0.132
298.900	2.780	161880	1.717	0.194
298.975	2.410	95460	2.523	0.193
300.154	2.757	91800	3.000	0.231
300.210	4.858	170100	2.866	0.219
302.193	5.410	144300	3.750	0.289
303.229	6.248	157380	3.970	0.307

Table A12. Experimental results for the Knudsen effusion experiments for 3,4,5-trimethylpyrazole.

A.3 Results for the Enthalpy of Solution Experiments

All experiments were carried out in a solution calorimetry equipment, that consists of a thermostated bath TAM III at a fixed temperature of 298.15 K ± 0.0001K and a calorimetric cell Thermometric 2225 at 300 rpm, as described in section III.3. The data reported in tables A14-A34 is the mass, in kg, the corresponding molality, m in $mol \cdot kg^{-1}$, the heat of calibration of each experiment, Q_{cal} in J, the experimental heat of reaction calculated by the SolCal software, Q_{reac} in J, the real heat of solution, calculated at subtracting the experimental heat of an empty glass ampule breaking in each solvent, Q_{break}, shown in Table A13, from the experimental heat of reaction, Q_{real} in J, the average of the cell heat capacity, $\bar{C}$ in $J \cdot K^{-1}$, the corrected temperature rise, ΔT_{corr} in K and the obtained heat of solution, $\Delta_{sol}H_m$, in $kJ \cdot mol^{-1}$, obtained at dividing the real heat of solution by the number of moles of each solute. After each table of data and results for the solution calorimetry experiments, the results for the molar enthalpy of solution for each experiment are graphically displayed in order to show the behavior of this property with respect to the molality. The polynomial or linear fitting results were obtained from the use of OriginPro 2015 (64-bit) Sr1 b9.2.257 software.

Solvent	$10^3\ Q_{break}$ / J
Water	94.943
Methanol	93.235
Acetonitrile	180.291

Table A13. Experimental heat of an empty glass breaking in each solvent.

10^6 mass	10^3 m	Q_{cal}	Q_{reac}	Q_{real}	$\bar{C}$	$10^3\ \Delta T_{corr}$	$\Delta_{sol}H_m$
4.156	2.45	0.77	0.828	0.733	114.001	-7.266	12.013
4.161	2.45	0.77	0.817	0.722	112.445	-7.272	11.814
4.577	2.70	0.90	0.846	0.751	114.621	-7.378	11.166
4.932	2.91	0.98	0.969	0.874	113.906	-8.506	12.064
5.285	3.11	1.02	0.996	0.901	112.849	-8.823	11.602
5.579	3.29	1.10	1.077	0.982	113.306	-9.508	11.984
5.861	3.45	1.10	1.143	1.048	112.125	-10.196	12.174
6.051	3.57	1.18	1.123	1.028	112.572	-9.976	11.567
6.106	3.60	1.17	1.181	1.086	114.778	-10.290	12.109
6.628	3.91	1.33	1.277	1.182	113.853	-11.216	12.141
6.734	3.97	1.40	1.254	1.159	112.867	-11.100	11.718
7.113	4.19	1.40	1.356	1.261	111.796	-12.133	12.070
7.164	4.22	1.40	1.385	1.290	112.412	-12.319	12.259
7.752	4.57	1.50	1.425	1.330	111.402	-12.790	11.681
7.848	4.62	1.57	1.503	1.408	111.916	-13.430	12.214
8.067	4.75	1.60	1.548	1.453	111.579	-13.875	12.263
8.165	4.81	1.65	1.552	1.457	111.904	-13.865	12.149
8.546	5.04	1.67	1.629	1.534	111.074	-14.668	12.221
8.840	5.21	1.80	1.723	1.628	114.341	-15.070	12.538
9.367	5.52	1.78	1.782	1.687	111.454	-15.989	12.262
9.545	5.63	1.86	1.877	1.782	115.229	-16.287	12.711
10.047	5.92	1.96	1.985	1.890	115.001	-17.365	12.807
10.159	5.99	1.95	1.970	1.875	115.032	-17.128	12.566
10.620	6.26	2.07	2.067	1.972	115.152	-17.946	12.642
10.736	6.33	2.18	2.044	1.949	110.214	-18.547	12.359
11.302	6.66	2.30	2.210	2.115	115.259	-19.176	12.740
11.883	7.00	2.30	2.270	2.175	115.020	-19.737	12.461
11.937	7.03	2.44	2.249	2.154	109.795	-20.480	12.285
11.939	7.04	2.50	2.238	2.143	114.918	-19.474	12.220
12.040	7.10	2.36	2.367	2.272	115.046	-20.576	12.847
12.742	7.51	2.70	2.464	2.369	114.965	-21.436	12.658
13.017	7.67	2.54	2.586	2.491	115.318	-22.423	13.028
13.415	7.91	2.70	2.543	2.448	114.171	-22.275	12.424
14.084	8.30	2.72	2.784	2.689	115.086	-24.190	12.999
15.988	9.42	3.20	2.998	2.903	114.105	-26.275	12.362
18.736	11.04	3.78	3.663	3.568	115.334	-31.764	12.965

Table A14. Experimental results for the solution calorimetry experiments of imidazole in water at 298.15 K.

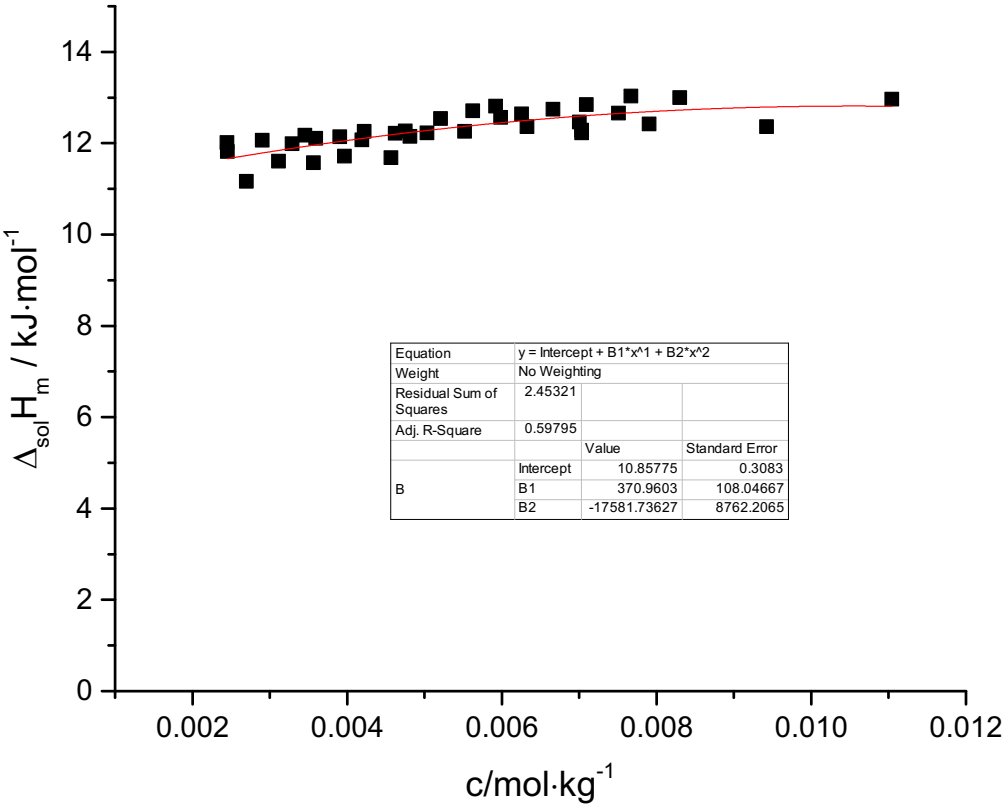

Figure A1. Graphical representation of the experimental enthalpies of solution as a function of the molality of the final solution for imidazole in water at 298.15 K. The polynomial fitting is shown in the box in the middle of the figure. The intercept value and its corresponding standard deviation are taken as the enthalpy of solution at infinite dilution.

10^6 mass	10^3 m	Q_{cal}	Q_{reac}	Q_{real}	$\bar{C}$	$10^3\ \Delta T_{corr}$	$\Delta_{sol}H_m$
6.113	2.99	0.68	0.711	0.616	114.367	-6.219	8.278
6.890	3.37	0.84	0.806	0.711	113.159	-7.119	8.468
7.355	3.59	0.85	0.842	0.747	113.173	-7.438	8.336
7.897	3.86	0.94	0.913	0.818	112.666	-8.099	8.500
8.215	4.01	0.94	0.954	0.859	115.997	-8.228	8.585
9.134	4.46	1.06	1.097	1.002	118.810	-9.232	9.007
9.284	4.54	1.10	1.052	0.957	113.942	-9.234	8.463
9.434	4.61	1.08	1.086	0.991	111.706	-9.719	8.625
10.379	5.07	1.21	1.184	1.089	114.007	-10.388	8.615
11.248	5.50	1.29	1.309	1.214	114.753	-11.410	8.861
12.552	6.13	1.46	1.425	1.330	113.864	-12.518	8.700
12.852	6.28	1.55	1.474	1.379	112.062	-13.149	8.810
13.971	6.83	1.62	1.637	1.542	115.040	-14.228	9.062
14.809	7.24	1.78	1.706	1.611	110.977	-15.375	8.932
16.039	7.84	1.88	1.884	1.789	115.465	-16.320	9.158
18.566	9.07	2.15	2.105	2.010	113.679	-18.521	8.889
20.720	10.12	2.40	2.404	2.309	114.830	-20.935	9.149

Table A15. Experimental results for the solution calorimetry experiments of 2-methylimidazole in water at 298.15 K.

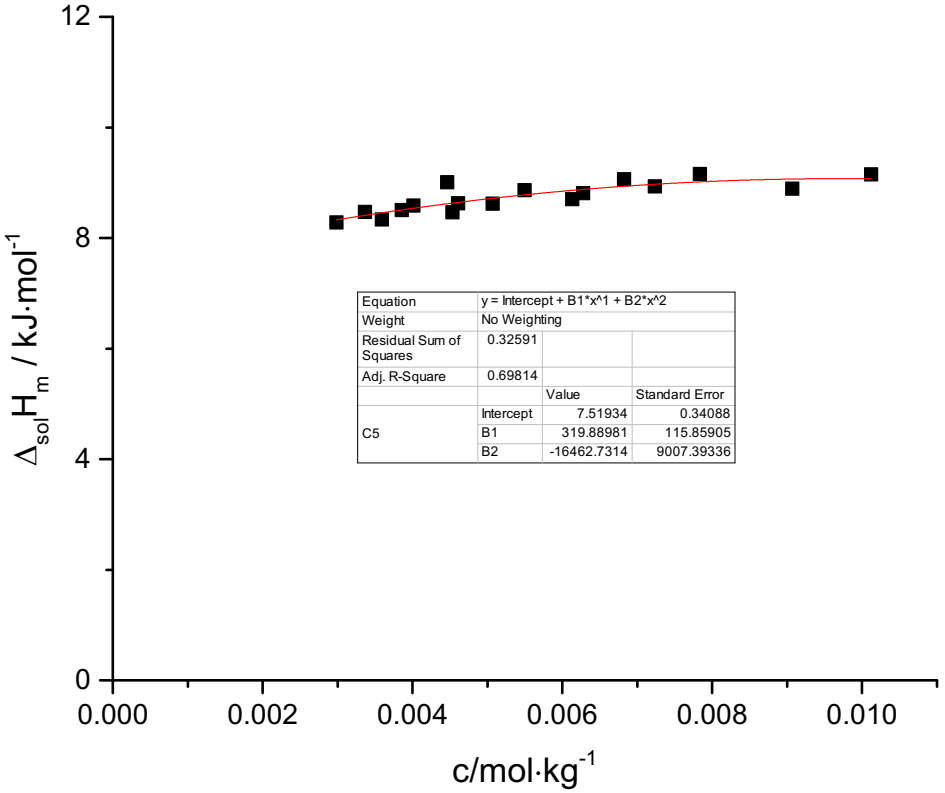

Figure A2. Graphical representation of the experimental enthalpies of solution as a function of the molality of the final solution for 2-methylimidazole in water at 298.15 K. The polynomial fitting is shown in the box in the middle of the figure. The intercept value and its corresponding standard deviation are taken as the enthalpy of solution at infinite dilution.

10^6 mass	10^3 m	Q_{cal}	Q_{reac}	Q_{real}	$\bar{C}$	$10^3\ \Delta T_{corr}$	$\Delta_{sol}H_m$
6.427	2.682	0.30	0.363	0.268	113.683	-3.190	4.005
7.656	3.195	0.43	0.435	0.340	113.155	-3.848	4.275
8.230	3.435	1.00	0.450	0.355	117.544	-3.826	4.144
9.370	3.911	0.52	0.501	0.406	112.846	-4.443	4.170
10.106	4.218	0.55	0.564	0.469	114.787	-4.912	4.460
10.294	4.296	0.60	0.574	0.479	113.409	-5.060	4.472
11.332	4.729	0.63	0.649	0.554	113.834	-5.704	4.703
12.161	5.075	0.68	0.669	0.574	114.535	-5.841	4.538
12.678	5.291	0.71	0.721	0.626	115.702	-6.228	4.744
13.533	5.648	0.81	0.768	0.673	112.876	-6.805	4.782
14.398	6.009	0.83	0.805	0.710	112.339	-7.163	4.739
15.758	6.577	0.90	0.884	0.789	115.783	-7.632	4.811
15.932	6.649	0.93	0.905	0.810	113.340	-7.982	4.886
16.956	7.077	1.00	0.965	0.870	112.553	-8.579	4.935
17.884	7.464	1.03	1.020	0.925	112.465	-9.069	4.973
18.920	7.896	1.11	1.070	0.975	114.412	-9.356	4.954
20.844	8.699	1.20	1.143	1.048	112.705	-10.145	4.834
22.891	9.554	1.31	1.285	1.190	115.801	-11.096	4.998
24.551	10.246	1.55	1.349	1.254	113.247	-11.909	4.910

Table A16. Experimental results for the solution calorimetry experiments of 2-ethylimidazole in water at 298.15 K.

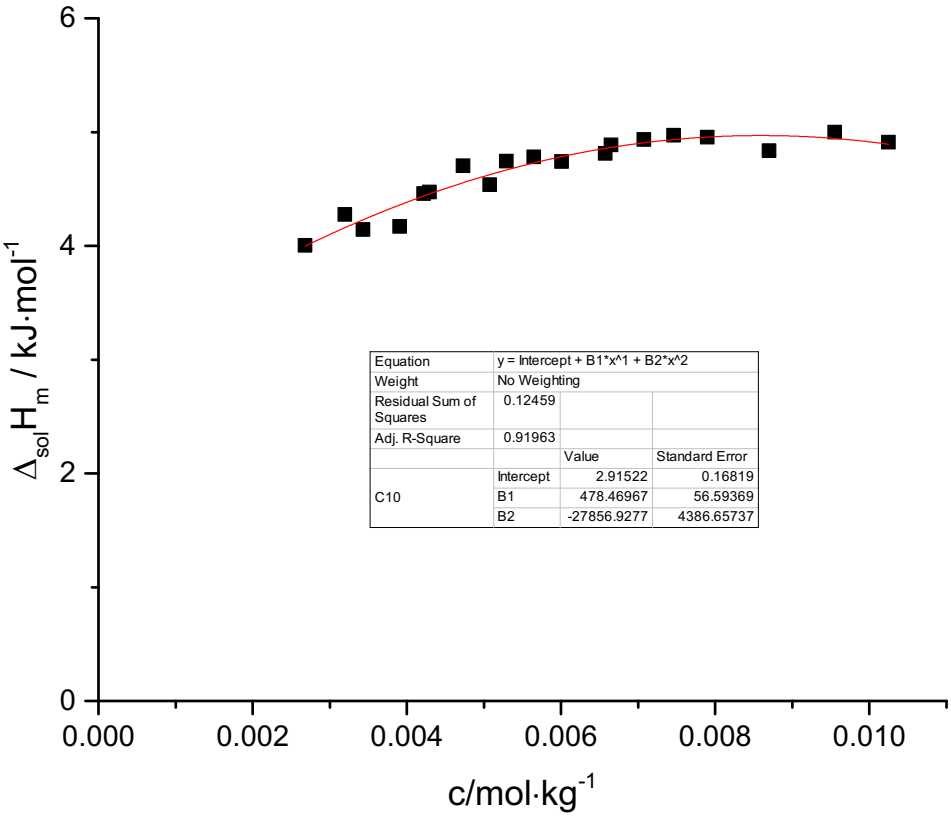

Figure A3. Graphical representation of the experimental enthalpies of solution as a function of the molality of the final solution for 2-ethylimidazole in water at 298.15 K. The polynomial fitting is shown in the box in the middle of the figure. The intercept value and its corresponding standard deviation are taken as the enthalpy of solution at infinite dilution.

10^6 mass	10^3 m	Q_{cal}	Q_{reac}	Q_{real}	$\bar{C}$	$10^3\ \Delta T_{corr}$	$\Delta_{sol}H_m$
8.196	2.985	0.47	0.472	0.377	113.966	-4.138	5.062
9.512	3.464	0.49	0.512	0.417	115.577	-4.428	4.827
9.587	3.492	0.50	0.522	0.427	116.139	-4.496	4.909
10.412	3.792	0.60	0.570	0.476	115.948	-4.920	5.031
10.705	3.899	0.55	0.545	0.450	115.526	-4.718	4.632
11.364	4.139	0.60	0.570	0.475	115.912	-4.915	4.602
12.459	4.538	0.67	0.683	0.588	113.759	-6.001	5.197
14.687	5.349	3.60	0.721	0.627	115.890	-6.225	4.699
15.644	5.698	0.84	0.859	0.764	114.473	-7.503	5.379
17.336	6.314	2.10	0.876	0.781	115.885	-7.560	4.964
18.392	6.698	0.92	0.942	0.847	114.820	-8.201	5.071
18.566	6.762	0.98	0.984	0.890	115.851	-8.498	5.278
20.290	7.390	1.10	1.056	0.961	113.176	-9.328	5.218
21.928	7.986	1.20	1.140	1.045	111.161	-10.253	5.250
25.003	9.106	1.35	1.297	1.202	111.527	-11.629	5.296
28.205	10.272	1.50	1.423	1.328	111.176	-12.799	5.187

Table A17. Experimental results for the solution calorimetry experiments of 2-isopropylimidazole in water at 298.15 K.

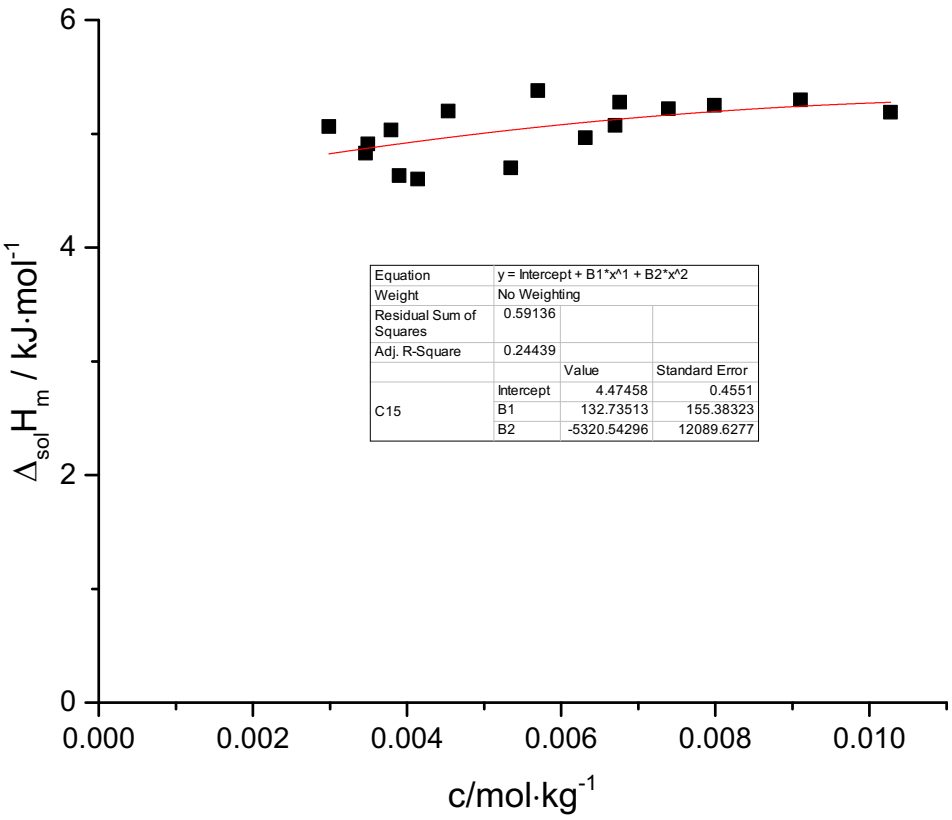

Figure A4. Graphical representation of the experimental enthalpies of solution as a function of the molality of the final solution for 2-isopropylimidazole in water at 298.15 K. The polynomial fitting is shown in the box in the middle of the figure. The intercept value and its corresponding standard deviation are taken as the enthalpy of solution at infinite dilution.

10^6 mass	10^3 m	Q_{cal}	Q_{reac}	Q_{real}	$\bar{C}$	$10^3\ \Delta T_{corr}$	$\Delta_{sol}H_m$
3.887	2.291	0.97	0.887	0.792	112.658	-7.880	13.873
4.136	2.437	1.04	0.920	0.825	113.778	-8.084	13.577
4.789	2.822	1.20	1.107	1.012	113.283	-9.776	14.387
5.229	3.082	1.23	1.210	1.115	112.920	-10.757	14.518
5.581	3.289	1.34	1.325	1.230	114.315	-11.593	15.005
6.381	3.760	1.57	1.482	1.387	111.370	-13.311	14.799
6.837	4.029	1.70	1.591	1.496	112.298	-14.080	14.897
7.346	4.329	1.80	1.737	1.642	113.776	-15.271	15.218
7.809	4.602	1.85	1.820	1.725	109.817	-16.573	15.039
8.322	4.904	2.03	1.931	1.836	111.506	-17.320	15.020
8.689	5.121	2.10	2.048	1.953	114.206	-17.935	15.303
8.828	5.202	2.09	2.117	2.022	115.113	-18.390	15.594
9.381	5.528	2.16	2.241	2.146	115.265	-19.440	15.574
10.109	5.957	2.40	2.383	2.288	115.044	-20.711	15.409
10.347	6.098	2.45	2.464	2.369	115.457	-21.338	15.588
10.554	6.220	2.46	2.476	2.381	115.125	-21.507	15.359
10.671	6.289	2.52	2.506	2.411	114.815	-21.830	15.382
10.971	6.465	3.15	2.626	2.531	115.258	-22.782	15.706
11.072	6.525	2.67	2.687	2.592	114.769	-23.412	15.938
11.834	6.974	2.83	2.804	2.709	114.948	-24.396	15.585
11.914	7.021	2.90	2.851	2.756	115.311	-24.725	15.749
12.603	7.427	3.10	2.919	2.824	113.633	-25.692	15.255
13.125	7.735	3.20	3.087	2.992	115.503	-26.832	15.520
14.089	8.303	3.35	3.349	3.254	115.061	-29.109	15.724
15.175	8.943	3.64	3.603	3.508	115.569	-31.179	15.738
16.034	9.449	3.80	3.847	3.752	115.700	-33.248	15.931
17.207	10.140	4.15	4.061	3.966	115.562	-35.141	15.692

Table A18. Experimental results for the solution calorimetry experiments of pyrazole in water at 298.15 K.

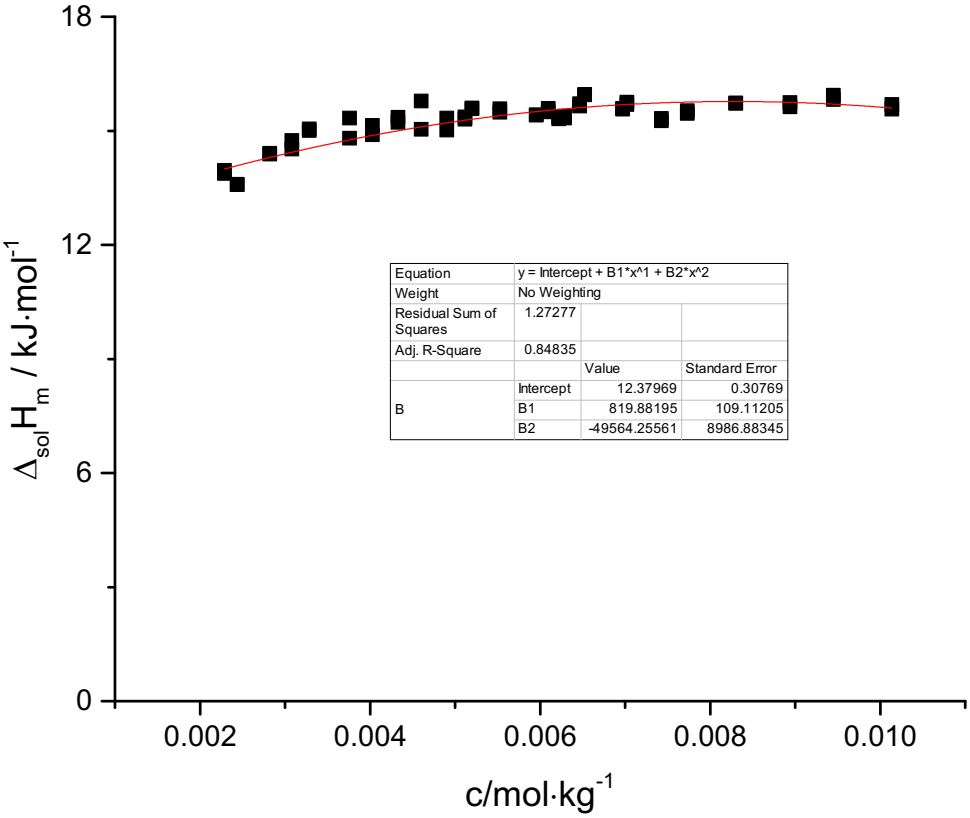

Figure A5. Graphical representation of the experimental enthalpies of solution as a function of the molality of the final solution for pyrazole in water at 298.15 K. The polynomial fitting is shown in the box in the middle of the figure. The intercept value and its corresponding standard deviation are taken as the enthalpy of solution at infinite dilution.

10^6 mass	10^3 m	Q_{cal}	Q_{reac}	Q_{real}	$\bar{C}$	$10^3\ \Delta T_{corr}$	$\Delta_{sol}H_m$
7.235	3.019	0.83	0.86	0.766	112.853	-7.631	10.181
9.580	3.998	1.15	1.10	1.007	110.024	-10.021	10.106
10.565	4.409	1.25	1.20	1.108	110.922	-10.842	10.082
11.791	4.921	1.42	1.38	1.283	114.146	-12.071	10.461
12.505	5.219	1.46	1.45	1.350	110.929	-13.027	10.379
13.150	5.488	1.55	1.50	1.403	111.309	-13.456	10.257
15.452	6.449	1.69	1.81	1.716	114.629	-15.799	10.676
17.005	7.097	1.97	2.02	1.923	114.270	-17.660	10.871
19.008	7.933	2.25	2.16	2.069	109.400	-19.781	10.464
20.296	8.470	2.40	2.36	2.262	113.577	-20.748	10.714
21.719	9.064	2.56	2.50	2.401	114.845	-21.736	10.628
24.371	10.171	2.80	2.85	2.759	115.612	-24.682	10.883

Table A19. Experimental results for the solution calorimetry experiments of 3,5-dimethylpyrazole in water at 298.15 K.

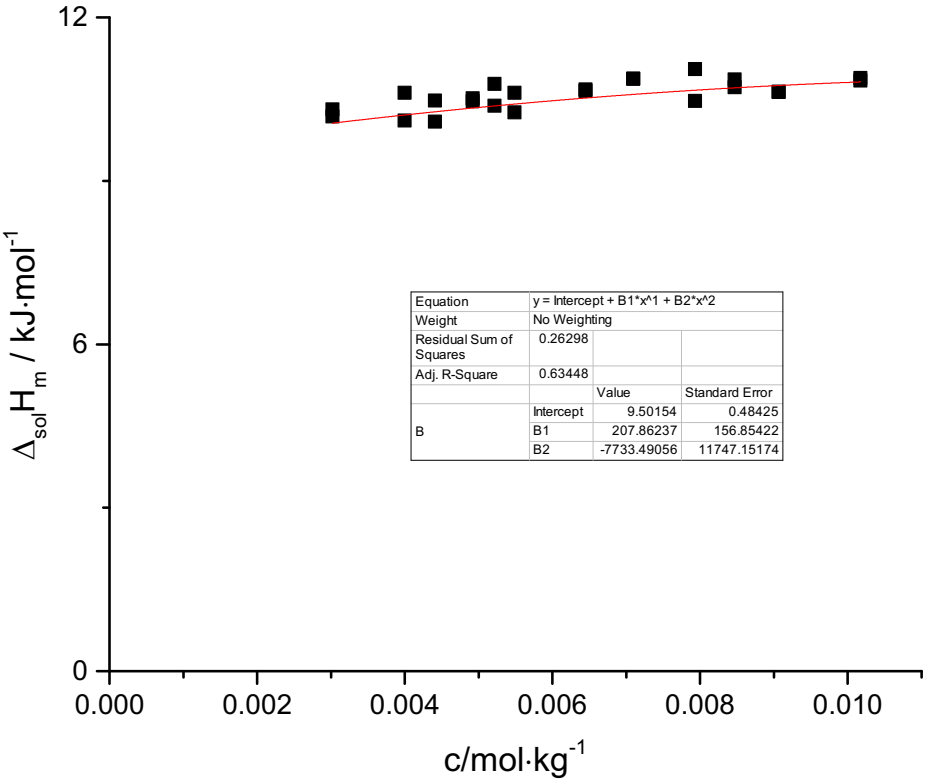

Figure A6. Graphical representation of the experimental enthalpies of solution as a function of the molality of the final solution for 3,5-dimethylpyrazole in water at 298.15 K. The polynomial fitting is shown in the box in the middle of the figure. The intercept value and its corresponding standard deviation are taken as the enthalpy of solution at infinite dilution.

10^6 mass	10^3 m	Q_{cal}	Q_{reac}	Q_{real}	$\bar{C}$	$10^3\ \Delta T_{corr}$	$\Delta_{sol}H_m$
5.436	1.98	0.62	0.554	0.459	116.529	-4.759	9.303
7.268	2.65	0.79	0.739	0.645	113.880	-6.494	9.769
8.727	3.18	0.81	0.924	0.829	115.628	-7.993	10.465
11.099	4.04	1.15	1.150	1.055	113.593	-10.122	10.472
13.074	4.76	1.30	1.269	1.174	111.432	-11.387	9.892
15.516	5.65	1.55	1.510	1.415	113.672	-13.284	10.047
22.883	8.34	2.13	2.220	2.125	115.132	-19.286	10.230
27.571	10.04	2.54	2.440	2.345	109.544	-22.274	9.370

Table A20. Experimental results for the solution calorimetry experiments of 3,4,5-trimethylpyrazole in water at 298.15 K.

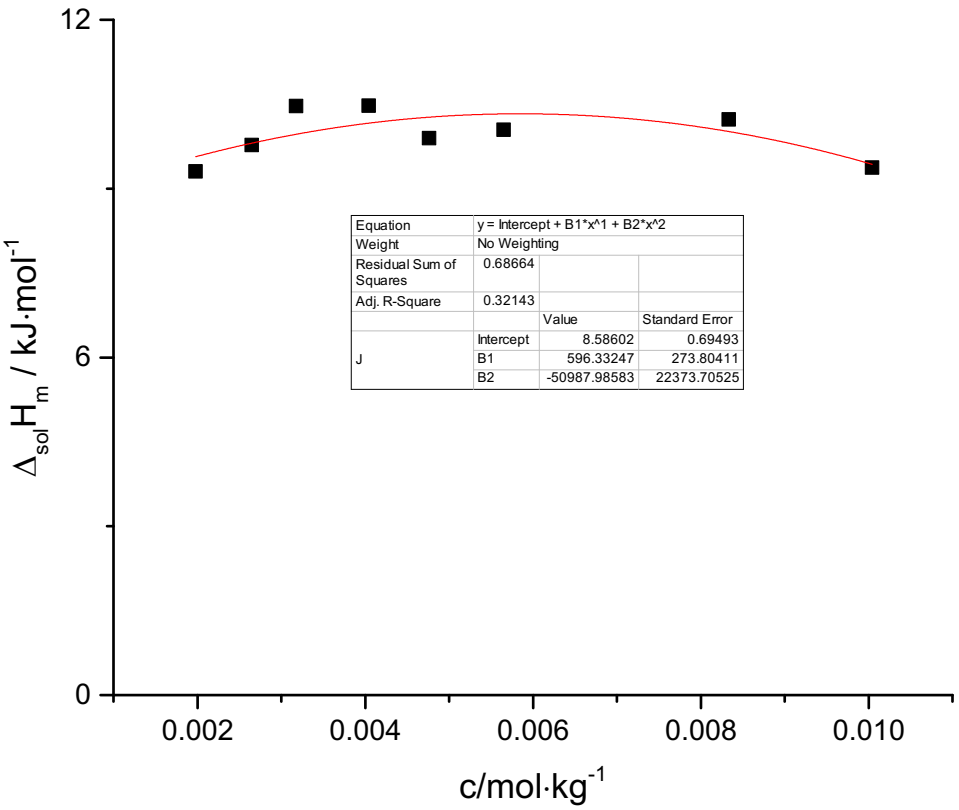

Figure A7. Graphical representation of the experimental enthalpies of solution as a function of the molality of the final solution for 3,4,5-trimethylpyrazole in water at 298.15 K. The polynomial fitting is shown in the box in the middle of the figure. The intercept value and its corresponding standard deviation are taken as the enthalpy of solution at infinite dilution.

10^6 mass	10^3 m	Q_{cal}	Q_{reac}	Q_{real}	$\bar{C}$	$10^3\ \Delta T_{corr}$	$\Delta_{sol}H_m$
4.153	3.103	0.89	0.779	0.686	60.382	-12.901	11.241
4.523	3.380	0.51	0.808	0.715	60.528	-13.353	10.762
6.851	5.119	0.94	1.071	0.978	61.522	-17.402	9.716
8.330	6.224	1.15	1.251	1.158	60.938	-20.534	9.462
8.751	6.539	1.15	1.301	1.208	60.722	-21.421	9.396
10.334	7.722	1.43	1.445	1.352	59.792	-24.168	8.905
10.567	7.896	1.50	1.502	1.409	59.089	-25.417	9.076
11.846	8.851	1.66	1.609	1.516	59.691	-26.961	8.711
13.313	9.948	1.82	1.778	1.685	58.417	-30.428	8.615
15.376	11.489	2.12	1.913	1.820	60.602	-31.564	8.057

Table A21. Experimental results for the solution calorimetry experiments of imidazole in methanol at 298.15 K.

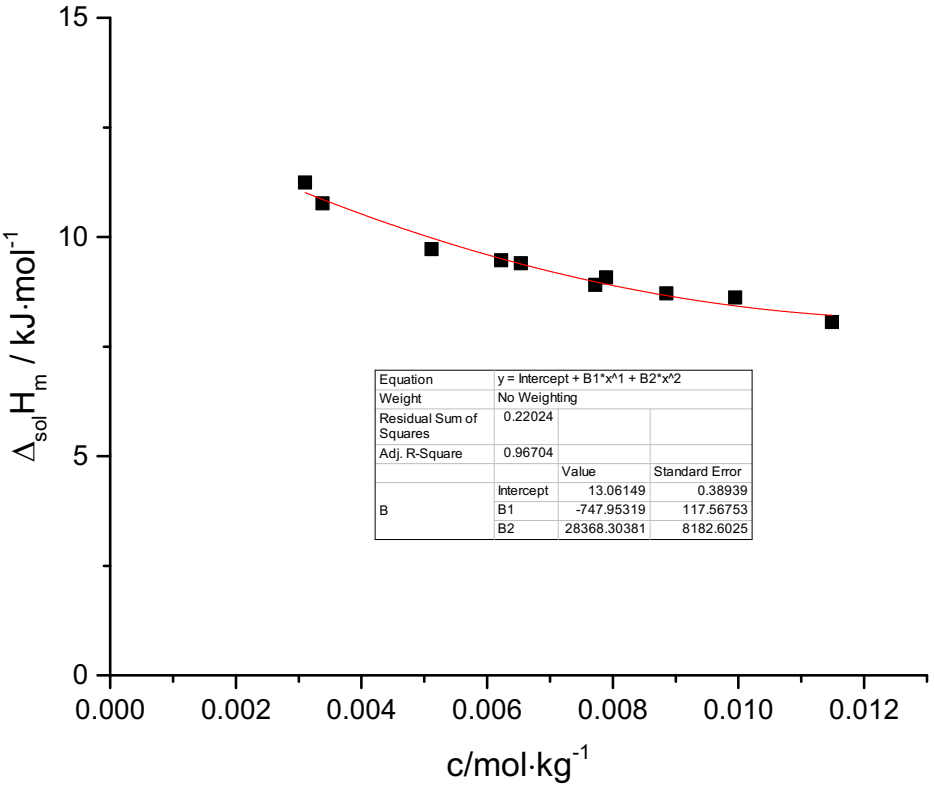

Figure A8. Graphical representation of the experimental enthalpies of solution as a function of the molality of the final solution for imidazole in methanol at 298.15 K. The polynomial fitting is shown in the box in the middle of the figure. The intercept value and its corresponding standard deviation are taken as the enthalpy of solution at infinite dilution.

10^6 mass	10^3 m	Q_{cal}	Q_{reac}	Q_{real}	$\bar{C}$	$10^3\ \Delta T_{corr}$	$\Delta_{sol}H_m$
5.086	3.151	0.73	0.751	0.657	60.573	-12.392	10.612
6.337	3.926	0.86	0.869	0.776	60.004	-14.489	10.056
7.033	4.357	0.83	0.928	0.835	60.604	-15.317	9.748
7.519	4.658	0.98	1.008	0.915	61.310	-16.414	9.988
8.273	5.126	1.03	1.080	0.987	61.439	-17.585	9.793
8.483	5.256	1.06	1.058	0.965	61.299	-17.285	9.337
9.092	5.633	2.29	1.126	1.033	60.285	-18.672	9.326
9.756	6.044	1.30	1.176	1.083	58.926	-19.959	9.112
10.346	6.410	1.34	1.242	1.149	61.054	-20.350	9.116
11.412	7.070	1.35	1.367	1.274	59.739	-22.884	9.164
13.293	8.236	1.47	1.501	1.408	59.245	-25.337	8.695
14.584	9.036	1.80	1.563	1.470	57.629	-27.130	8.274
16.634	10.306	2.10	1.788	1.695	59.324	-30.137	8.365

Table A22. Experimental results for the solution calorimetry experiments of 2-methylimidazole in methanol at 298.15 K.

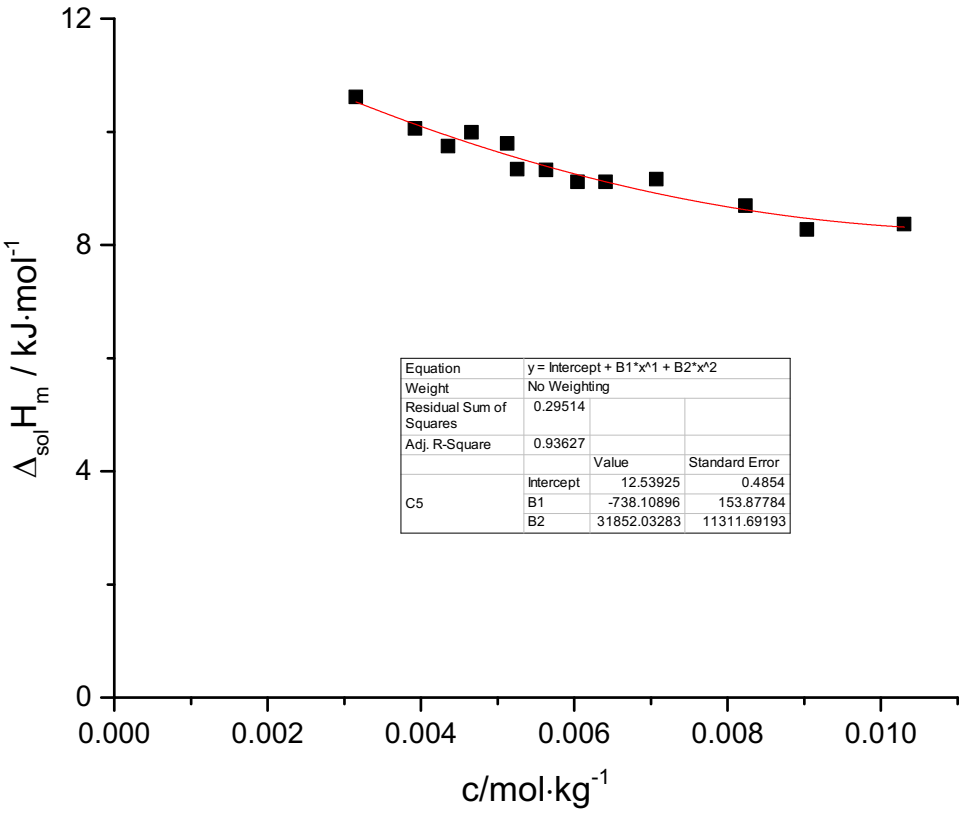

Figure A9. Graphical representation of the experimental enthalpies of solution as a function of the molality of the final solution for 2-methylimidazole in methanol at 298.15 K. The polynomial fitting is shown in the box in the middle of the figure. The intercept value and its corresponding standard deviation are taken as the enthalpy of solution at infinite dilution.

10^6 mass	10^3 m	Q_{cal}	Q_{reac}	Q_{real}	$\bar{C}$	$10^3\ \Delta T_{corr}$	$\Delta_{sol}H_m$
6.398	3.39	0.66	0.650	0.557	59.700	-10.891	8.368
6.698	3.54	0.64	0.644	0.551	59.588	-10.811	7.907
8.449	4.47	0.72	0.717	0.624	60.199	-11.913	7.099
9.101	4.82	0.76	0.761	0.668	60.375	-12.612	7.058
10.008	5.30	0.85	0.826	0.733	60.198	-13.721	7.038
10.845	5.74	0.92	0.842	0.749	60.701	-13.878	6.641
11.030	5.84	0.93	0.855	0.762	60.089	-14.230	6.640
12.860	6.80	0.90	0.967	0.874	59.441	-16.276	6.535
14.842	7.85	1.26	0.980	0.887	61.067	-16.052	5.745
16.712	8.84	1.10	1.174	1.081	58.961	-19.918	6.217
20.324	10.75	1.50	1.328	1.235	59.239	-22.292	5.840

Table A23. Experimental results for the solution calorimetry experiments of 2-ethylimidazole in methanol at 298.15 K.

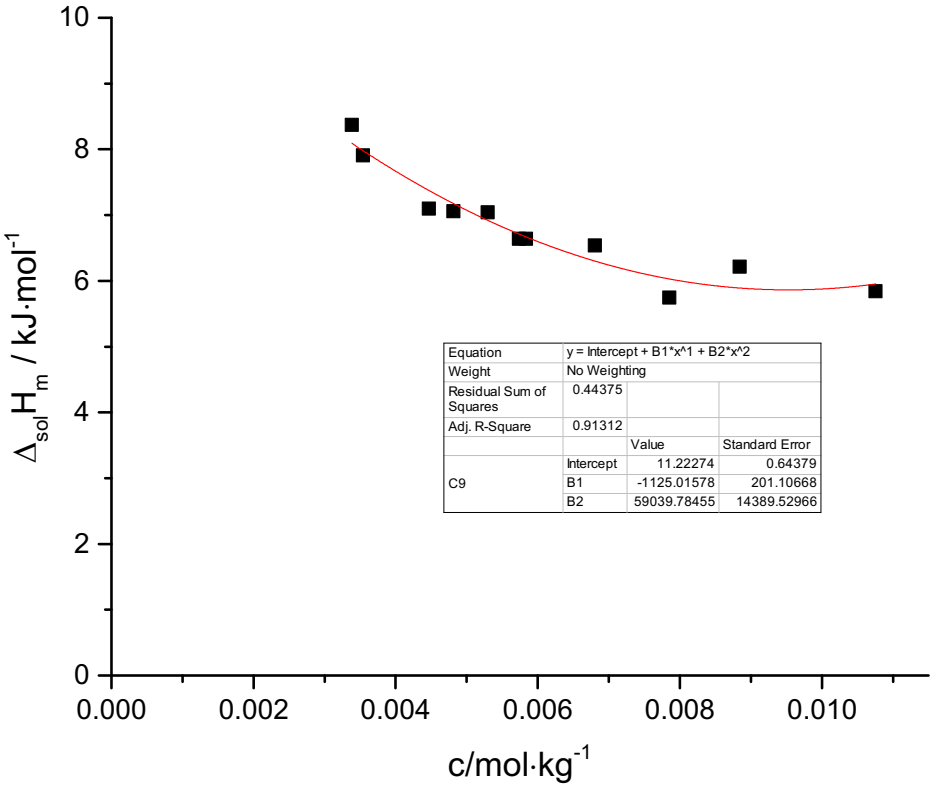

Figure A10. Graphical representation of the experimental enthalpies of solution as a function of the molality of the final solution for 2-ethylimidazole in methanol at 298.15 K. The polynomial fitting is shown in the box in the middle of the figure. The intercept value and its corresponding standard deviation are taken as the enthalpy of solution at infinite dilution.

10^6 mass	10^3 m	Q_{cal}	Q_{reac}	Q_{real}	$\bar{C}$	$10^3\ \Delta T_{corr}$	$\Delta_{sol}H_m$
7.747	3.580	0.770	0.751	0.658	60.715	-12.371	9.354
9.654	4.460	0.720	0.854	0.761	60.410	-14.144	8.686
11.647	5.380	1.000	0.977	0.884	60.795	-16.070	8.359
13.116	6.060	1.100	1.043	0.950	61.267	-17.016	7.977
15.932	7.360	1.300	1.157	1.064	58.245	-19.869	7.355
18.137	8.380	1.350	1.340	1.247	60.750	-22.051	7.573
20.210	9.330	1.700	1.420	1.327	59.354	-23.918	7.232

Table A24. Experimental results for the solution calorimetry experiments of 2-isopropylimidazole in methanol at 298.15 K.

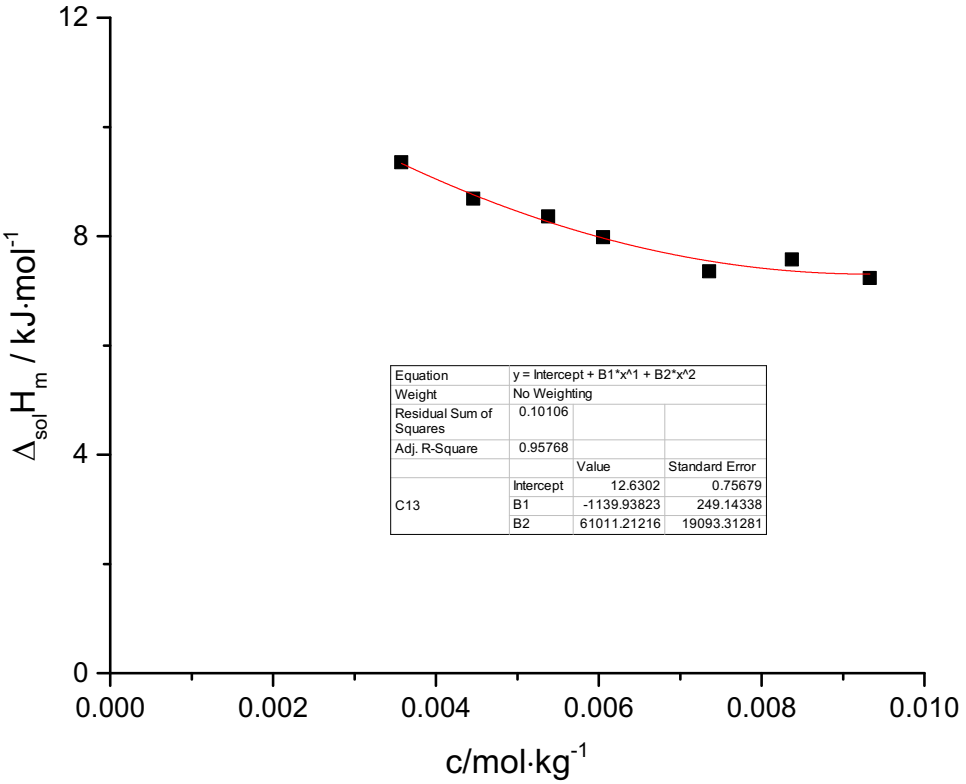

Figure A11. Graphical representation of the experimental enthalpies of solution as a function of the molality of the final solution for 2-isopropylimidazole in methanol at 298.15 K. The polynomial fitting is shown in the box in the middle of the figure. The intercept value and its corresponding standard deviation are taken as the enthalpy of solution at infinite dilution.

10^6 mass	10^3 m	Q_{cal}	Q_{reac}	Q_{real}	$\bar{C}$	$10^3\ \Delta T_{corr}$	$\Delta_{sol}H_m$
3.321	2.481	0.800	0.790	0.697	61.493	-12.859	14.287
4.009	2.996	0.900	0.945	0.852	59.545	-15.872	14.464
4.595	3.433	1.080	0.994	0.901	60.199	-16.508	13.343
5.633	4.209	1.180	1.106	1.013	60.522	-18.269	12.240
6.520	4.872	1.170	1.221	1.128	61.137	-19.977	11.776
7.381	5.515	1.330	1.344	1.251	60.554	-22.199	11.537
8.557	6.394	1.540	1.621	1.528	60.006	-27.016	12.155
9.929	7.419	1.830	1.758	1.665	59.101	-29.752	11.415
10.519	7.860	1.890	1.858	1.765	59.026	-31.477	11.422
11.987	8.957	2.120	2.094	2.001	58.862	-35.570	11.363
13.411	10.021	2.340	2.402	2.309	60.559	-39.659	11.720

Table A25. Experimental results for the solution calorimetry experiments of pyrazole in methanol at 298.15 K.

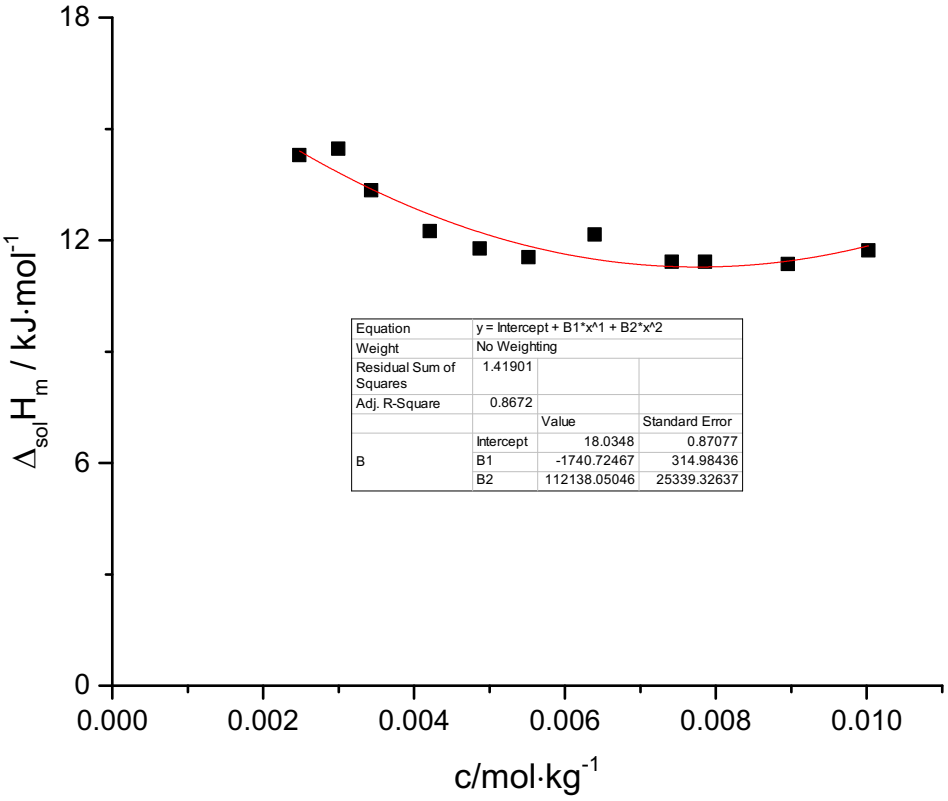

Figure A12. Graphical representation of the experimental enthalpies of solution as a function of the molality of the final solution for pyrazole in methanol at 298.15 K. The polynomial fitting is shown in the box in the middle of the figure. The intercept value and its corresponding standard deviation are taken as the enthalpy of solution at infinite dilution.

10^6 mass	10^3 m	Q_{cal}	Q_{reac}	Q_{real}	$\bar{C}$	$10^3\ \Delta T_{corr}$	$\Delta_{sol}H_m$
3.502	1.853	0.920	0.665	0.572	61.306	-10.849	15.697
4.023	2.129	1.070	0.741	0.648	61.876	-11.977	15.481
4.515	2.389	1.200	0.820	0.727	60.726	-13.505	15.476
5.704	3.018	0.970	0.983	0.890	61.165	-15.908	14.995
6.625	3.506	1.000	1.083	0.990	60.802	-17.802	14.362
8.228	4.354	1.210	1.242	1.149	61.357	-20.246	13.421
9.417	4.983	1.390	1.386	1.293	60.130	-23.057	13.197
10.301	5.451	1.533	1.508	1.415	60.476	-24.939	13.203
11.229	5.942	1.630	1.581	1.488	61.038	-25.896	12.737
11.733	6.209	1.600	1.657	1.564	60.775	-27.268	12.812
13.718	7.259	1.860	1.875	1.782	58.789	-31.888	12.486
15.041	7.959	2.040	2.017	1.924	58.808	-34.291	12.295
17.440	9.228	2.350	2.327	2.234	60.230	-38.636	12.313
19.169	10.143	2.580	2.525	2.432	59.729	-42.268	12.195

Table A26. Experimental results for the solution calorimetry experiments of 3,5-dimethylpyrazole in methanol at 298.15 K

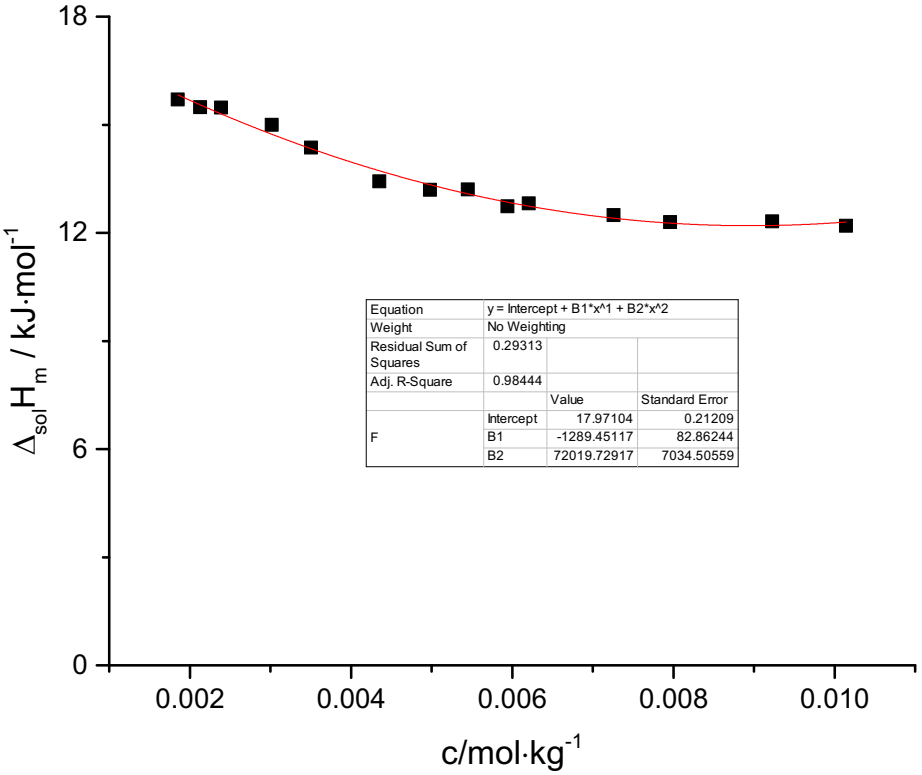

Figure A13. Graphical representation of the experimental enthalpies of solution as a function of the molality of the final solution for 3,5-dimethylpyrazole in methanol at 298.15 K. The polynomial fitting is shown in the box in the middle of the figure. The intercept value and its corresponding standard deviation are taken as the enthalpy of solution at infinite dilution.

10^6 mass	10^3 m	Q_{cal}	Q_{reac}	Q_{real}	$\bar{C}$	$10^3\ \Delta T_{corr}$	$\Delta_{sol}H_m$
6.783	3.130	0.980	1.016	0.923	60.674	-16.751	14.986
10.349	4.780	1.300	1.371	1.278	59.785	-22.934	13.601
14.287	6.600	2.000	1.731	1.638	59.761	-28.970	12.628
17.949	8.290	2.050	2.101	2.008	60.137	-34.931	12.322
21.687	10.020	2.500	2.445	2.352	60.331	-40.519	11.946

Table A27. Experimental results for the solution calorimetry experiments of 3,4,5-trimethylpyrazole in methanol at 298.15 K

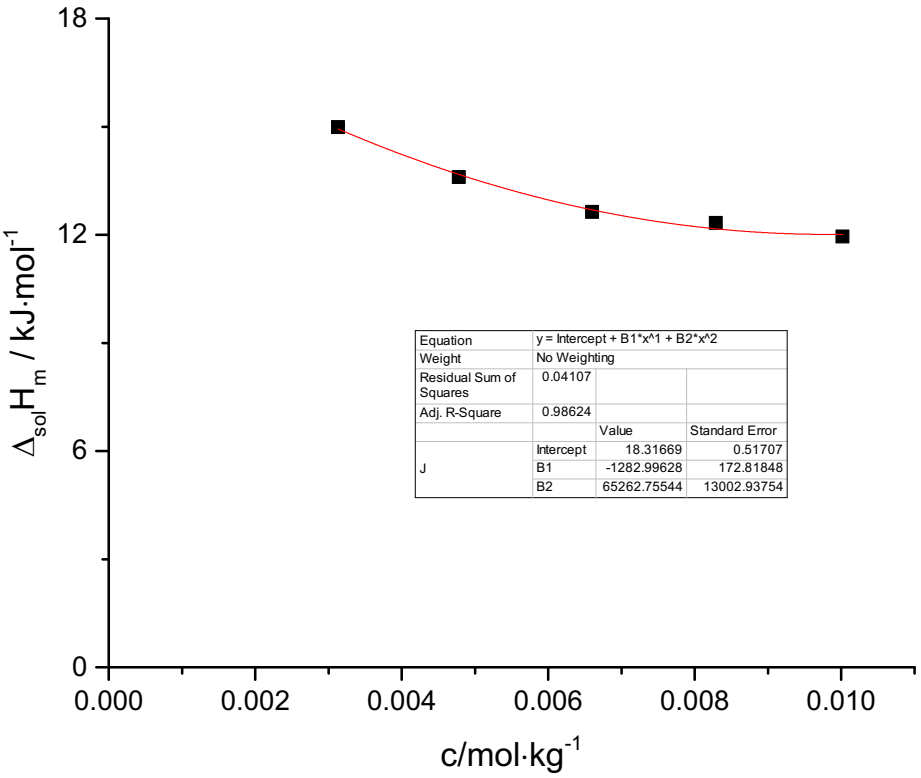

Figure A14. Graphical representation of the experimental enthalpies of solution as a function of the molality of the final solution for 3,4,5-trimethylpyrazole in methanol at 298.15 K. The polynomial fitting is shown in the box in the middle of the figure. The intercept value and its corresponding standard deviation are taken as the enthalpy of solution at infinite dilution.

10^6 mass	10^3 m	Q_{cal}	Q_{reac}	Q_{real}	$\bar{C}$	$10^3\ \Delta T_{corr}$	$\Delta_{sol}H_m$
2.993	2.236	1.060	1.093	0.913	52.233	-20.925	20.761
3.499	2.614	1.230	1.228	1.048	52.950	-23.192	20.385
4.104	3.067	1.370	1.416	1.236	52.752	-26.843	20.499
8.957	6.693	2.800	2.877	2.697	52.649	-54.647	20.497
9.760	7.293	2.000	3.112	2.932	53.488	-58.185	20.450
10.743	8.027	3.500	3.469	3.289	53.865	-64.405	20.841
12.808	9.570	4.039	4.057	3.877	54.044	-75.065	20.606
13.585	10.151	4.350	4.301	4.121	53.230	-80.805	20.650
14.213	10.620	4.480	4.505	4.325	53.341	-84.450	20.715

Table A28. Experimental results for the solution calorimetry experiments of imidazole in acetonitrile at 298.15 K

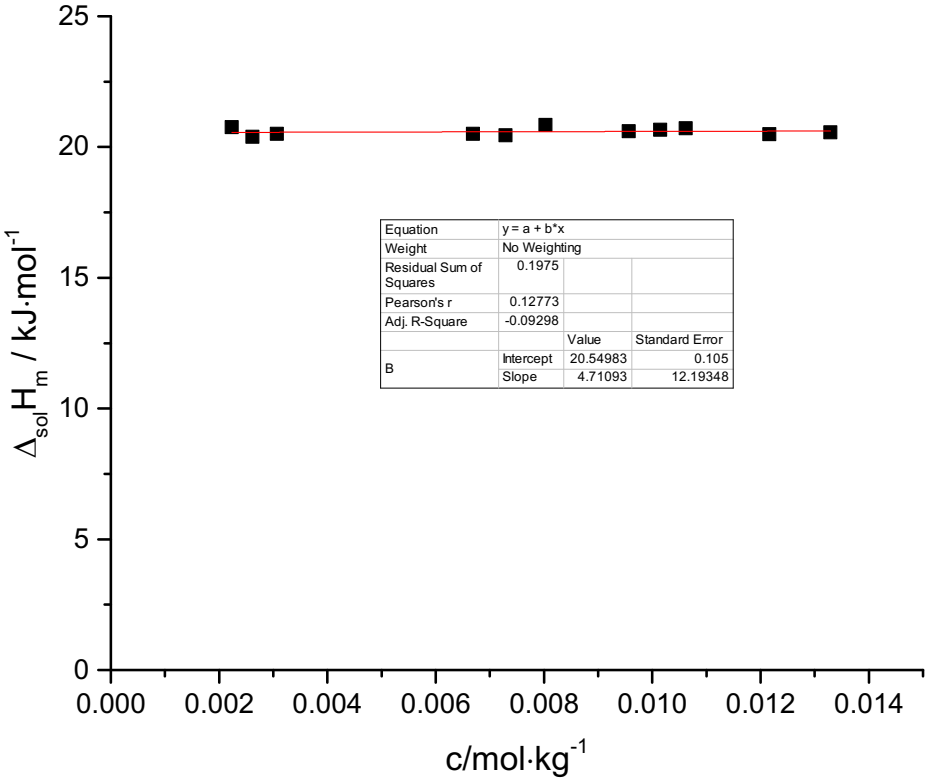

Figure A15. Graphical representation of the experimental enthalpies of solution as a function of the molality of the final solution for imidazole in acetonitrile at 298.15 K. The polynomial fitting is shown in the box in the middle of the figure. The intercept value and its corresponding standard deviation are taken as the enthalpy of solution at infinite dilution.

10^6 mass	10^3 m	Q_{cal}	Q_{reac}	Q_{real}	$\bar{C}$	$10^3\ \Delta T_{corr}$	$\Delta_{sol}H_m$
4.787	2.966	1.500	1.513	1.333	52.420	-28.864	22.857
6.548	4.057	2.000	1.942	1.762	53.247	-36.472	22.089
7.705	4.774	2.400	2.297	2.117	52.598	-43.679	22.554
9.012	5.584	2.700	2.708	2.528	53.261	-50.849	23.028
10.476	6.491	3.000	3.064	2.884	52.971	-57.850	22.600
11.230	6.958	3.300	3.169	2.989	52.878	-59.938	21.850
13.321	8.254	3.880	3.813	3.633	53.686	-71.028	22.389
14.883	9.222	4.300	4.249	4.069	53.648	-79.199	22.444
16.158	10.012	4.650	4.428	4.248	52.477	-84.376	21.583

Table A29. Experimental results for the solution calorimetry experiments of 2-methylimidazole in acetonitrile at 298.15 K

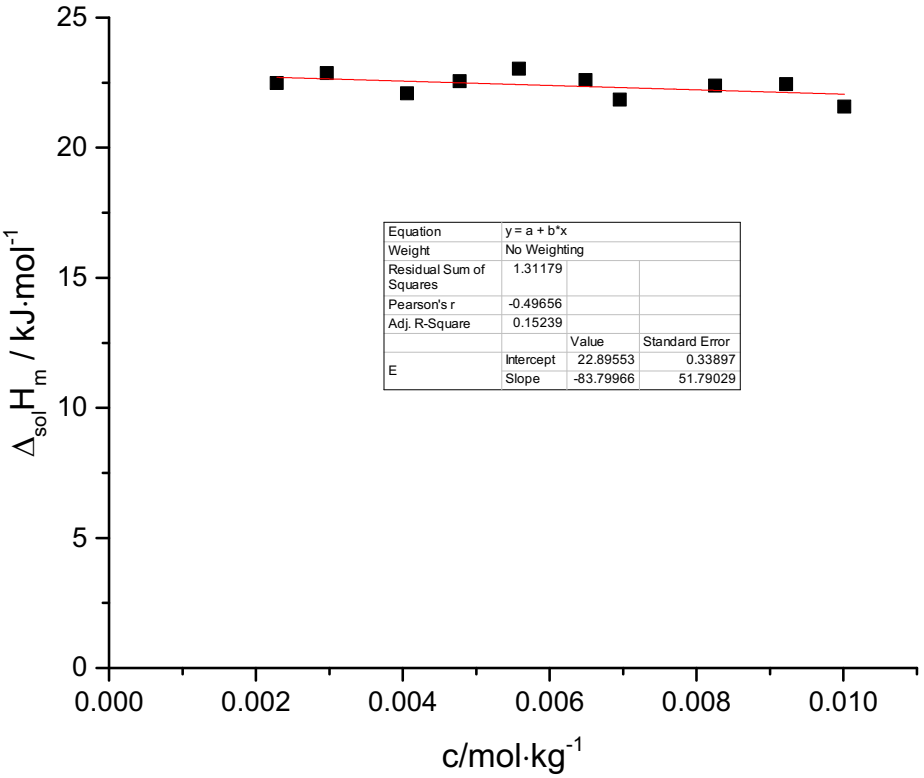

Figure A16. Graphical representation of the experimental enthalpies of solution as a function of the molality of the final solution for 2-methylimidazole in acetonitrile at 298.15 K. The polynomial fitting is shown in the box in the middle of the figure. The intercept value and its corresponding standard deviation are taken as the enthalpy of solution at infinite dilution.

10^6 mass	10^3 m	Q_{cal}	Q_{reac}	Q_{real}	$\bar{C}$	$10^3\ \Delta T_{corr}$	$\Delta_{sol}H_m$
7.064	3.738	1.800	1.789	1.609	53.217	-33.608	21.892
8.559	4.529	2.200	2.118	1.938	52.870	-40.066	21.763
9.479	5.016	3.330	2.275	2.095	52.872	-43.022	21.243
11.542	6.108	2.850	2.755	2.575	52.665	-52.307	21.444
13.741	7.271	3.500	3.285	3.105	52.867	-62.140	21.720
20.949	11.086	4.900	4.819	4.639	53.349	-90.327	21.286

Table A30. Experimental results for the solution calorimetry experiments of 2-ethylimidazole in acetonitrile at 298.15 K

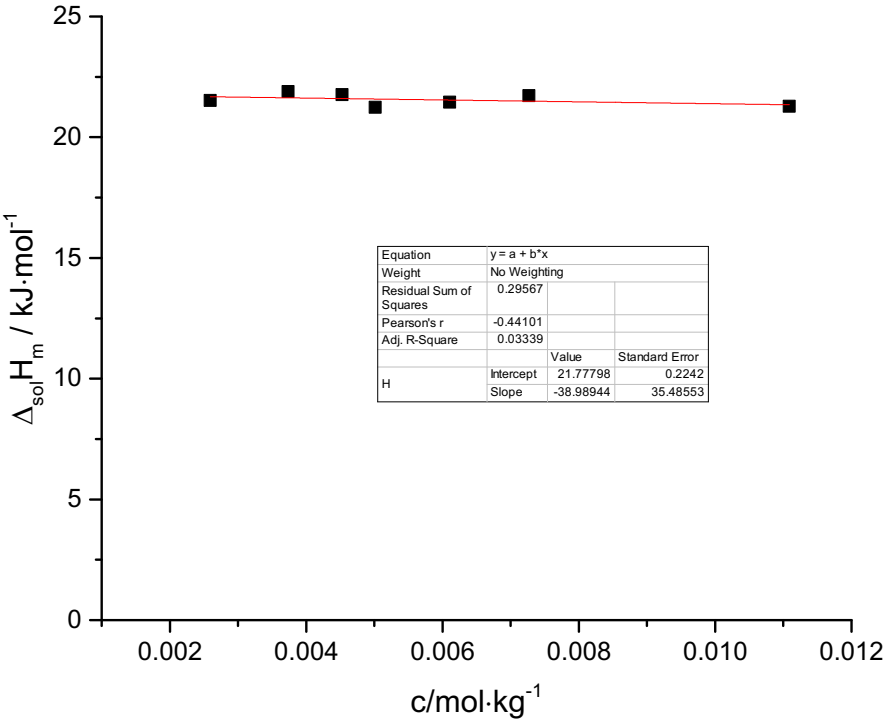

Figure A17. Graphical representation of the experimental enthalpies of solution as a function of the molality of the final solution for 2-ethylimidazole in acetonitrile at 298.15 K. The polynomial fitting is shown in the box in the middle of the figure. The intercept value and its corresponding standard deviation are taken as the enthalpy of solution at infinite dilution.

10^6 mass	10^3 m	Q_{cal}	Q_{reac}	Q_{real}	$\bar{C}$	$10^3\ \Delta T_{corr}$	$\Delta_{sol}H_m$
7.844	3.622	2.100	1.859	1.679	51.944	-34.786	23.576
8.568	3.956	2.100	1.978	1.798	51.436	-38.463	23.113
10.541	4.868	2.580	2.429	2.249	51.845	-46.855	23.500
12.470	5.758	3.200	2.866	2.686	52.251	-54.851	23.726
13.518	6.242	3.300	3.103	2.923	52.229	-59.405	23.818
17.565	8.111	4.000	3.967	3.787	53.288	-74.454	23.749
20.972	9.684	4.740	4.700	4.520	53.200	-88.347	23.741
23.511	10.857	5.300	5.117	4.937	53.239	-96.121	23.131

Table A31. Experimental results for the solution calorimetry experiments of 2-isopropylimidazole in acetonitrile at 298.15 K

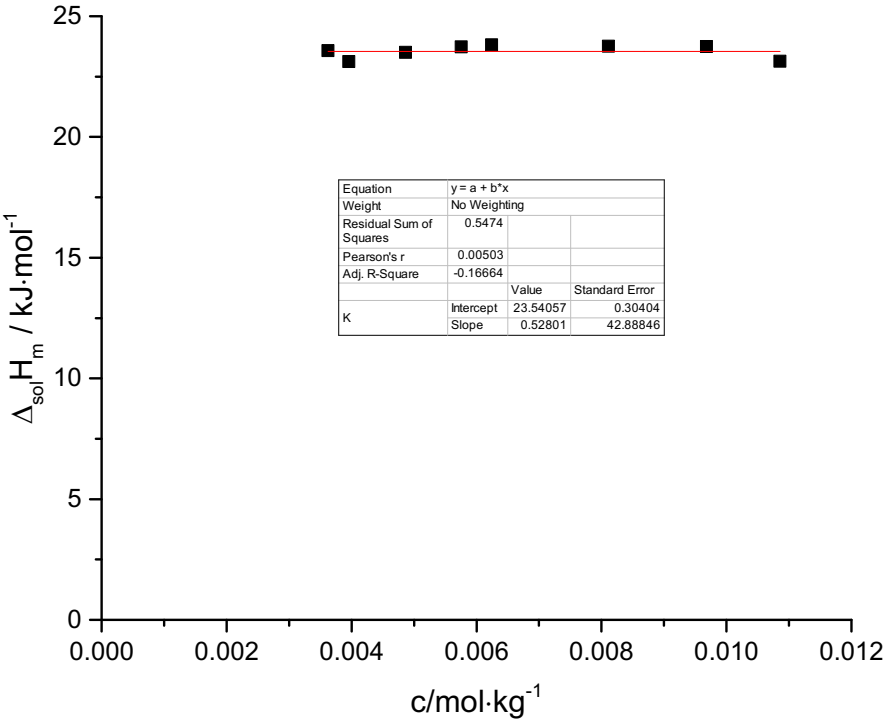

Figure A18. Graphical representation of the experimental enthalpies of solution as a function of the molality of the final solution for 2-isopropylimidazole in acetonitrile at 298.15 K. The polynomial fitting is shown in the box in the middle of the figure. The intercept value and its corresponding standard deviation are taken as the enthalpy of solution at infinite dilution.

10^6 mass	10^3 m	Q_{cal}	Q_{reac}	Q_{real}	$\bar{C}$	$10^3\ \Delta T_{corr}$	$\Delta_{sol}H_m$
2.768	2.096	0.930	0.962	0.782	52.881	-18.192	19.226
4.329	3.278	1.370	1.299	1.119	52.075	-24.929	17.593
5.707	4.322	1.750	1.660	1.480	52.102	-31.852	17.652
6.984	5.289	2.100	2.041	1.861	52.890	-38.594	18.138
8.439	6.390	2.450	2.551	2.371	52.813	-48.296	19.125
9.551	7.232	2.720	2.745	2.565	52.511	-52.281	18.281
10.567	8.002	1.620	3.020	2.840	52.493	-57.523	18.295
12.015	9.098	4.630	3.440	3.260	52.931	-64.993	18.470
13.126	9.940	3.700	3.725	3.545	53.344	-69.824	18.385
13.456	10.189	3.800	3.850	3.670	52.758	-72.968	18.566
13.784	10.438	3.900	3.931	3.751	53.001	-74.170	18.525
16.707	12.651	4.740	4.765	4.585	52.050	-91.550	18.682
24.092	18.243	6.850	6.757	6.577	52.392	-128.979	18.584

Table A32. Experimental results for the solution calorimetry experiments of pyrazole in acetonitrile at 298.15 K.

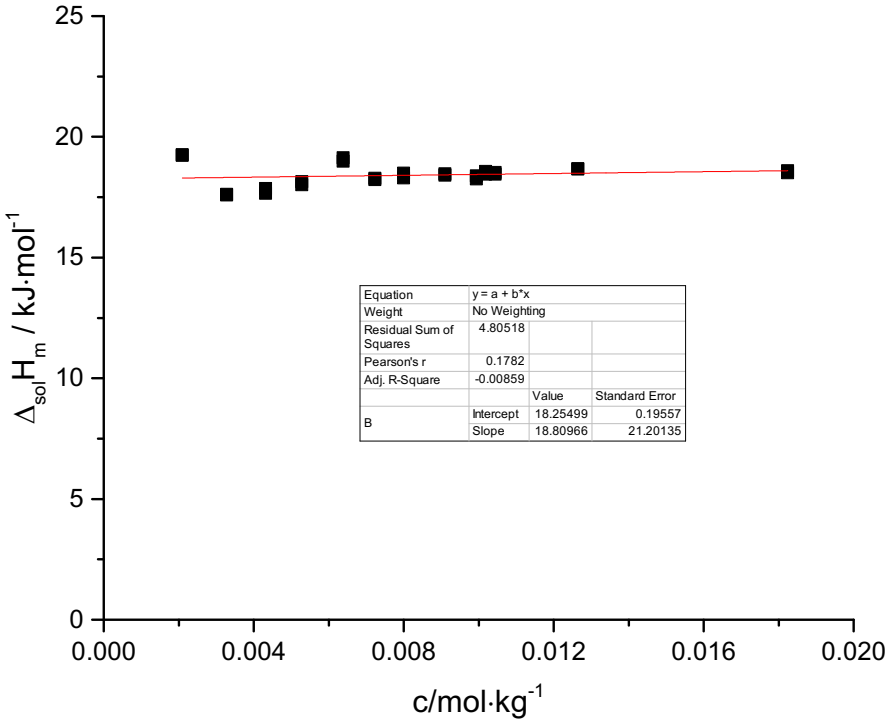

Figure A19. Graphical representation of the experimental enthalpies of solution as a function of the molality of the final solution for pyrazole in acetonitrile at 298.15 K. The polynomial fitting is shown in the box in the middle of the figure. The intercept value and its corresponding standard deviation are taken as the enthalpy of solution at infinite dilution.

10^6 mass	10^3 m	Q_{cal}	Q_{reac}	Q_{real}	$\bar{C}$	$10^3\ \Delta T_{corr}$	$\Delta_{sol}H_m$
6.618	3.549	1.850	1.801	1.621	51.303	-36.099	23.542
8.222	4.409	2.050	2.107	1.927	52.421	-40.197	22.527
9.327	5.002	2.330	2.381	2.201	52.887	-45.018	22.682
10.116	5.425	2.580	2.530	2.350	52.881	-47.842	22.329
11.219	6.017	2.950	2.919	2.739	53.048	-55.032	23.467
11.316	6.069	2.770	2.894	2.714	53.805	-53.796	23.053
12.398	6.649	3.100	3.087	2.907	52.868	-58.385	22.538
12.424	6.663	3.170	3.114	2.934	52.615	-59.178	22.699
12.734	6.829	3.200	3.122	2.942	53.411	-58.446	22.207
13.528	7.255	3.480	3.376	3.196	52.431	-64.385	22.709
13.588	7.287	3.460	3.413	3.233	53.041	-64.339	22.870
15.816	8.482	4.100	3.890	3.710	52.806	-73.664	22.548
16.335	8.760	4.100	4.197	4.017	52.854	-79.415	23.638
17.648	9.464	4.450	4.489	4.309	53.102	-84.542	23.470
18.950	10.163	4.750	4.827	4.647	53.656	-89.954	23.572

Table A33. Experimental results for the solution calorimetry experiments of 3,5-dimethylpyrazole in acetonitrile at 298.15 K

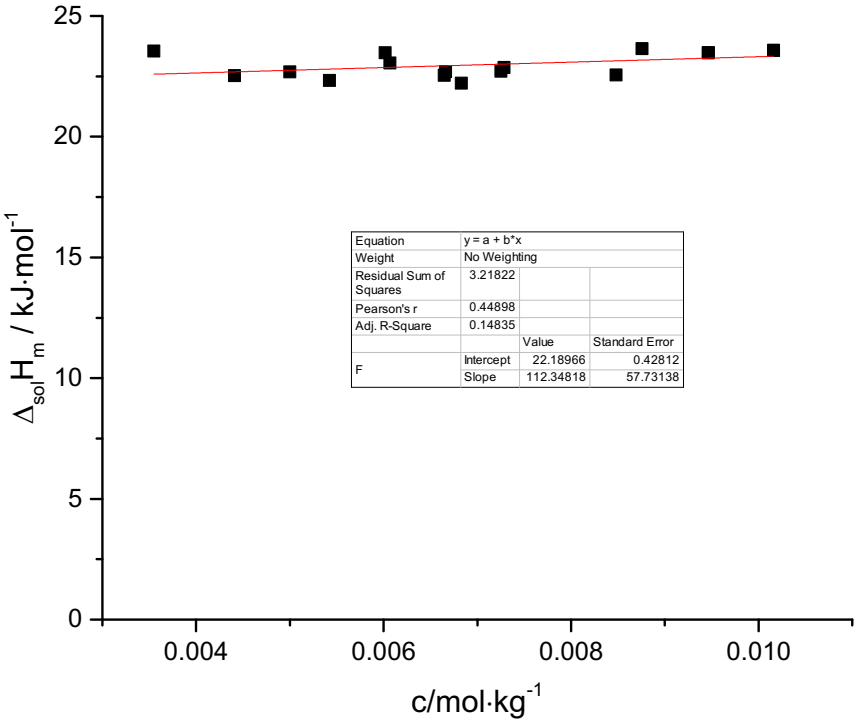

Figure A20. Graphical representation of the experimental enthalpies of solution as a function of the molality of the final solution for 3,5-dimethylpyrazole in acetonitrile at 298.15 K. The polynomial fitting is shown in the box in the middle of the figure. The intercept value and its corresponding standard deviation are taken as the enthalpy of solution at infinite dilution.

10^6 mass	10^3 m	Q_{cal}	Q_{reac}	Q_{real}	$\bar{C}$	$10^3\ \Delta T_{corr}$	$\Delta_{sol}H_m$
6.683	3.580	1.570	1.618	1.438	53.585	-30.186	23.699
10.428	5.590	2.350	2.367	2.187	52.594	-45.006	23.100
13.891	7.450	3.060	3.183	3.003	53.609	-59.368	23.812
17.598	9.440	4.520	3.818	3.638	53.104	-71.894	22.771
22.093	11.850	5.000	4.901	4.721	53.302	-91.956	23.538

Table A34. Experimental results for the solution calorimetry experiments of 3,4,5-trimethylpyrazole in acetonitrile at 298.15 K

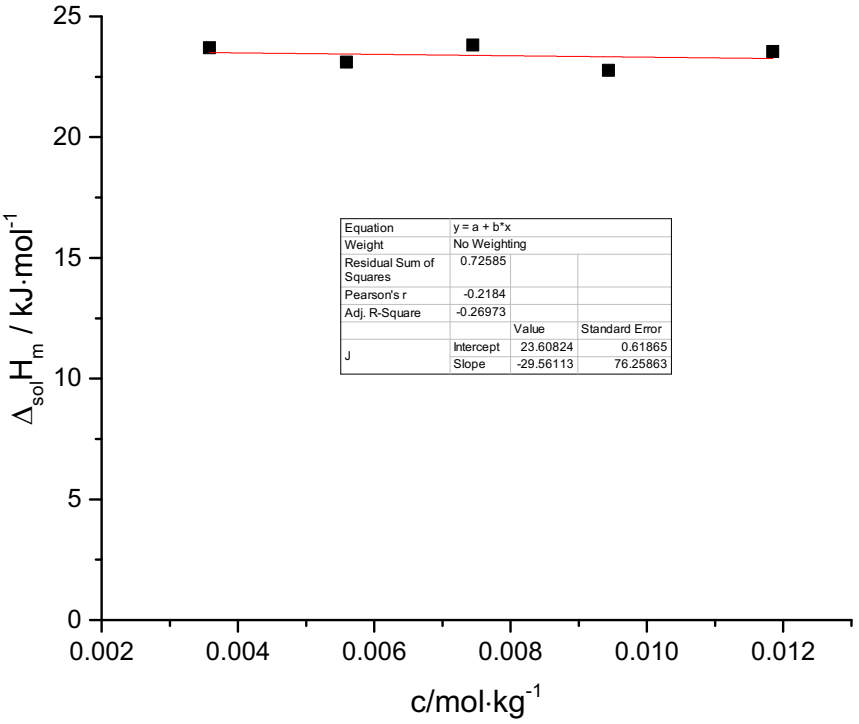

Figure A21. Graphical representation of the experimental enthalpies of solution as a function of the molality of the final solution for 3,4,5-trimethylpyrazole in acetonitrile at 298.15 K. The polynomial fitting is shown in the box in the middle of the figure. The intercept value and its corresponding standard deviation are taken as the enthalpy of solution at infinite dilution.

A.4 NMR spectra for the studied compounds

The NMR spectra were obtained in a Bruker 400 MHz spectrometer. In the following images are shown the spectra for each of the studied compounds in the corresponding deuterated solvents. Each image is labeled to indicate the solute and solvent, corresponding to each spectra.

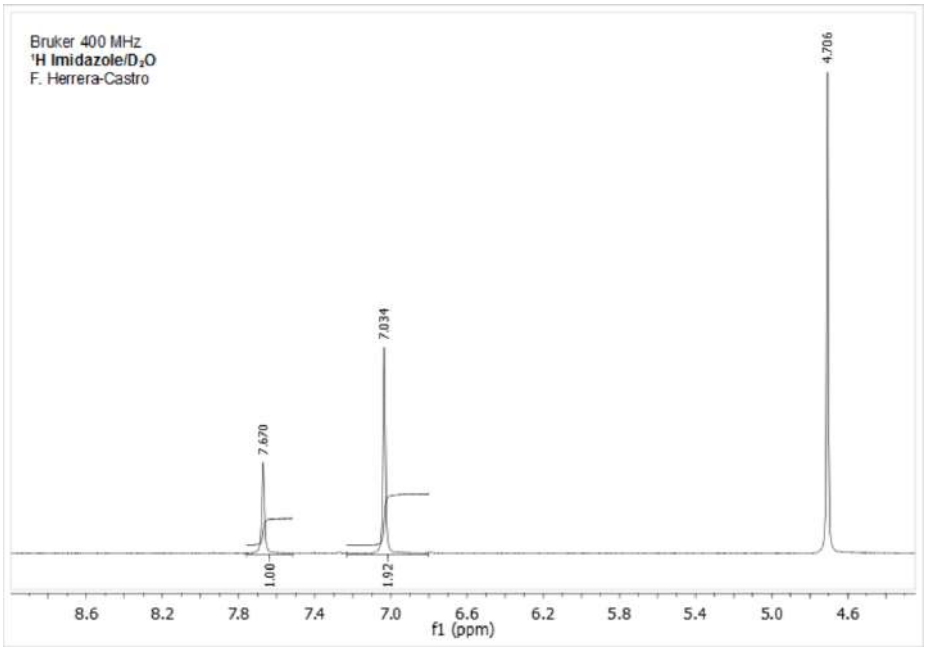

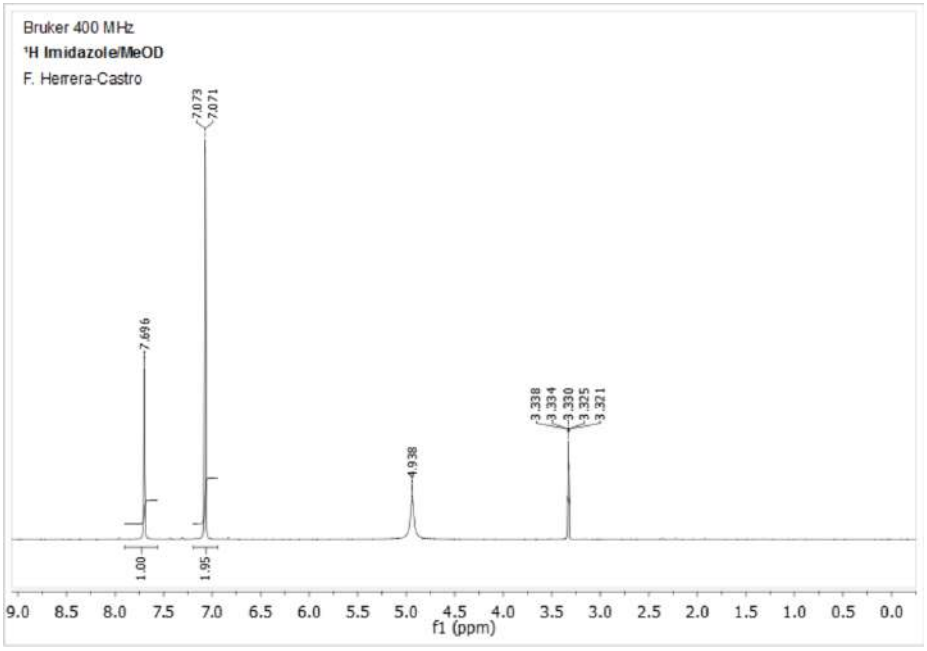

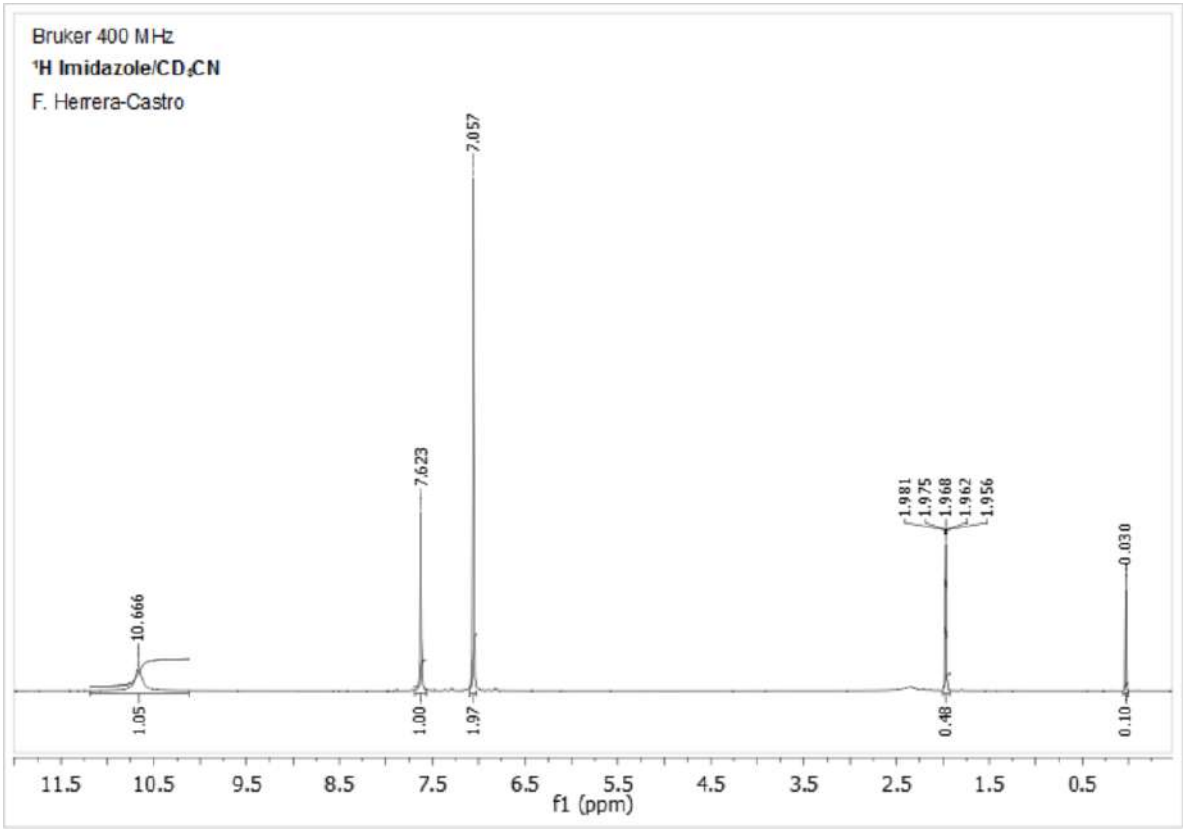
Bruker 400 MHz
¹H Imidazole/CD₃CN
F. Herrera-Castro
7.057
7.623
1.981
1.975
1.968
1.962
1.956
0.030
10.666
1.05
1.00
1.97
0.48
0.10
11.5
10.5
9.5
8.5
7.5
6.5
5.5
4.5
3.5
2.5
1.5
0.5
f1 (ppm)

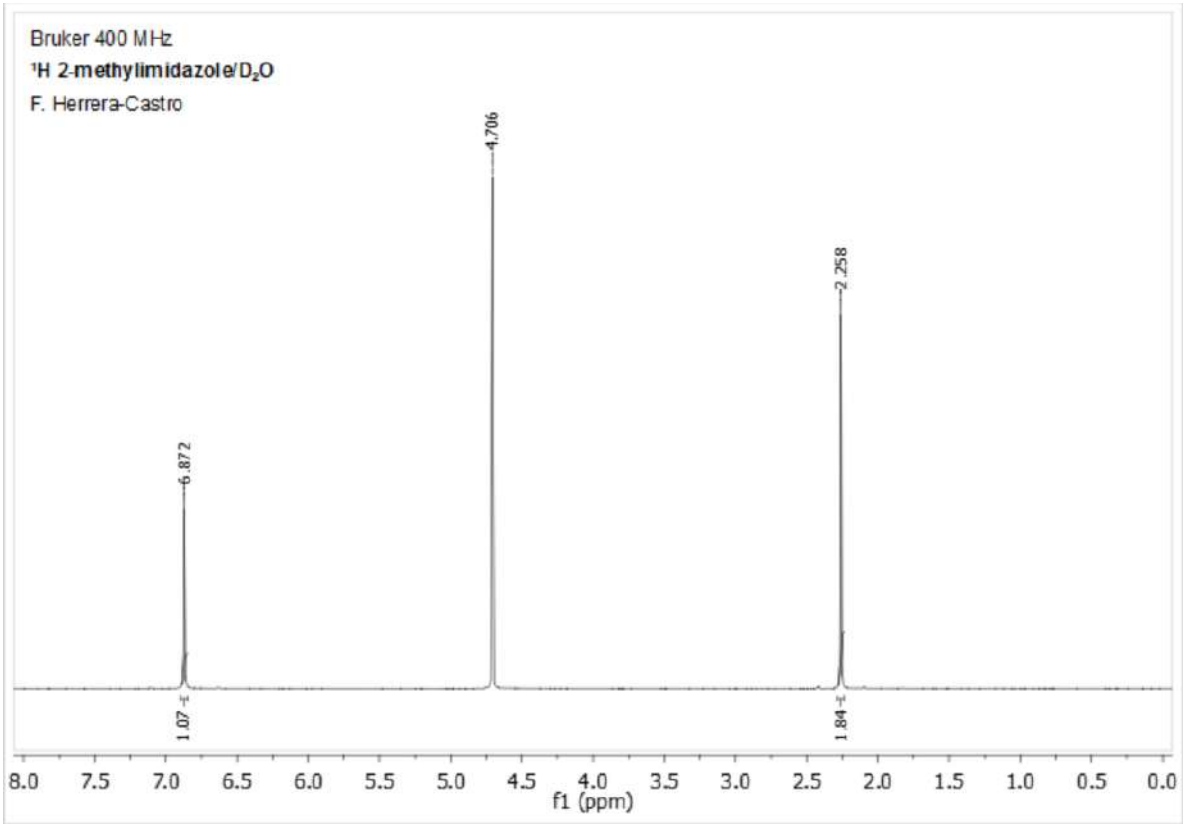
Bruker 400 MHz
¹H 2-methylimidazole/D₂O
F. Herrera-Castro
4.706
2.258
6.872
1.07
1.84
8.0
7.5
7.0
6.5
6.0
5.5
5.0
4.5
4.0
3.5
3.0
2.5
2.0
1.5
1.0
0.5
0.0
f1 (ppm)

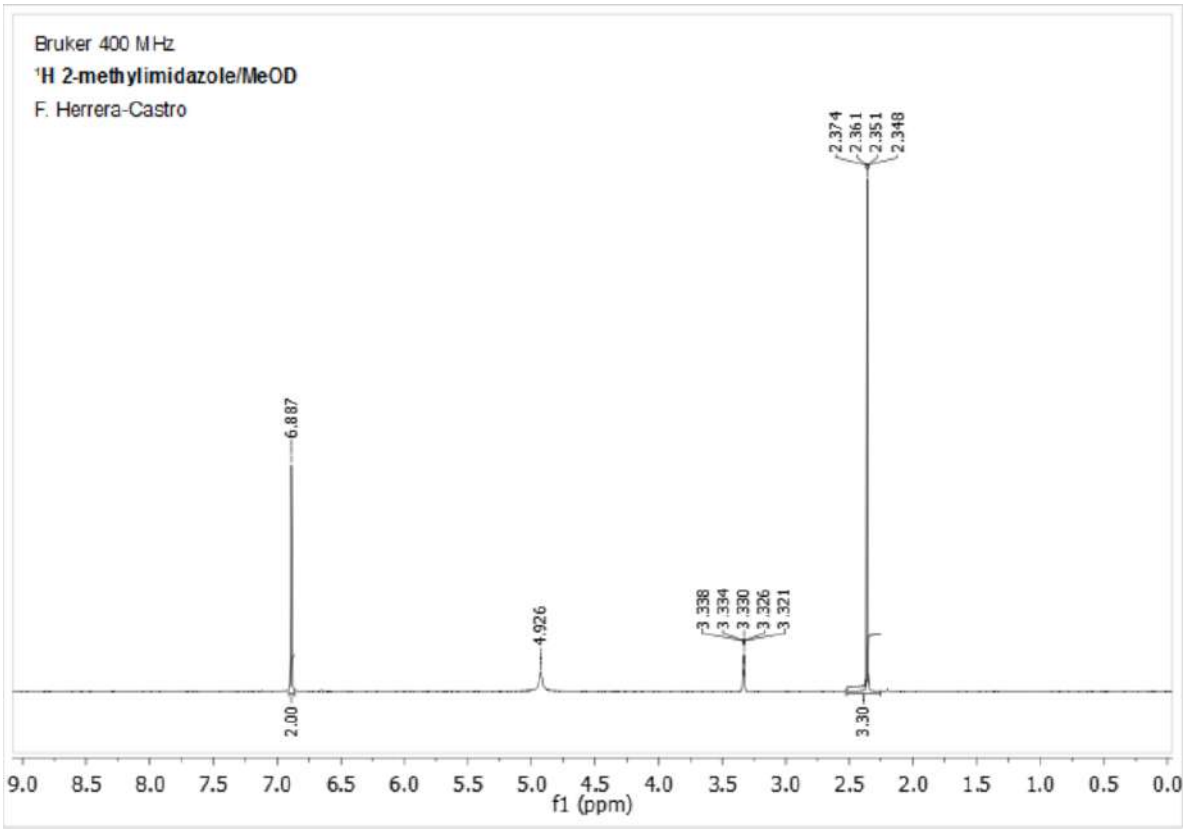
Bruker 400 MHz
¹H 2-methylimidazole/MeOD
F. Herrera-Castro
2.374
2.361
2.351
2.348
6.887
4.926
3.338
3.334
3.330
3.326
3.321
2.00
3.30
9.0 8.5 8.0 7.5 7.0 6.5 6.0 5.5 5.0 4.5 4.0 3.5 3.0 2.5 2.0 1.5 1.0 0.5 0.0
f1 (ppm)

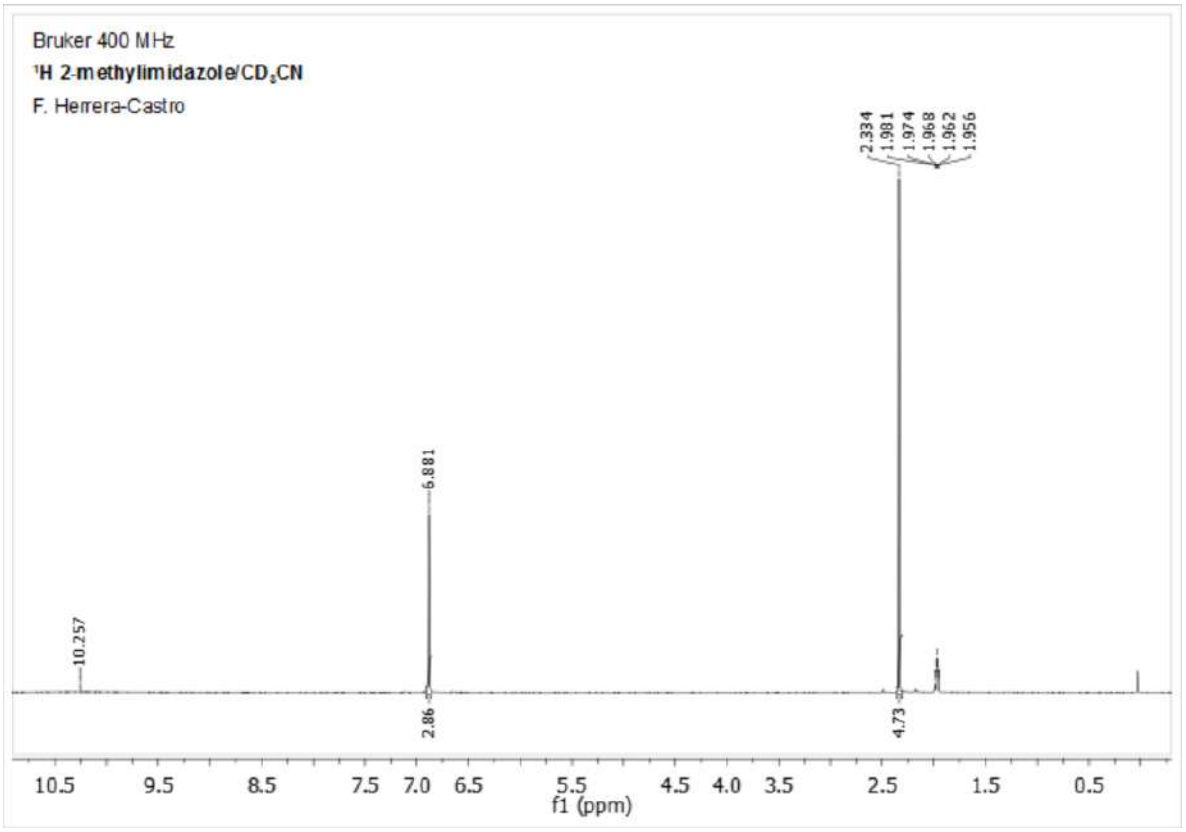
Bruker 400 MHz
¹H 2-methylimidazole/CD₃CN
F. Herrera-Castro
2.334
1.981
1.974
1.968
1.962
1.956
6.881
10.257
2.86
4.73
10.5 9.5 8.5 7.5 7.0 6.5 5.5 4.5 4.0 3.5 2.5 1.5 0.5
f1 (ppm)

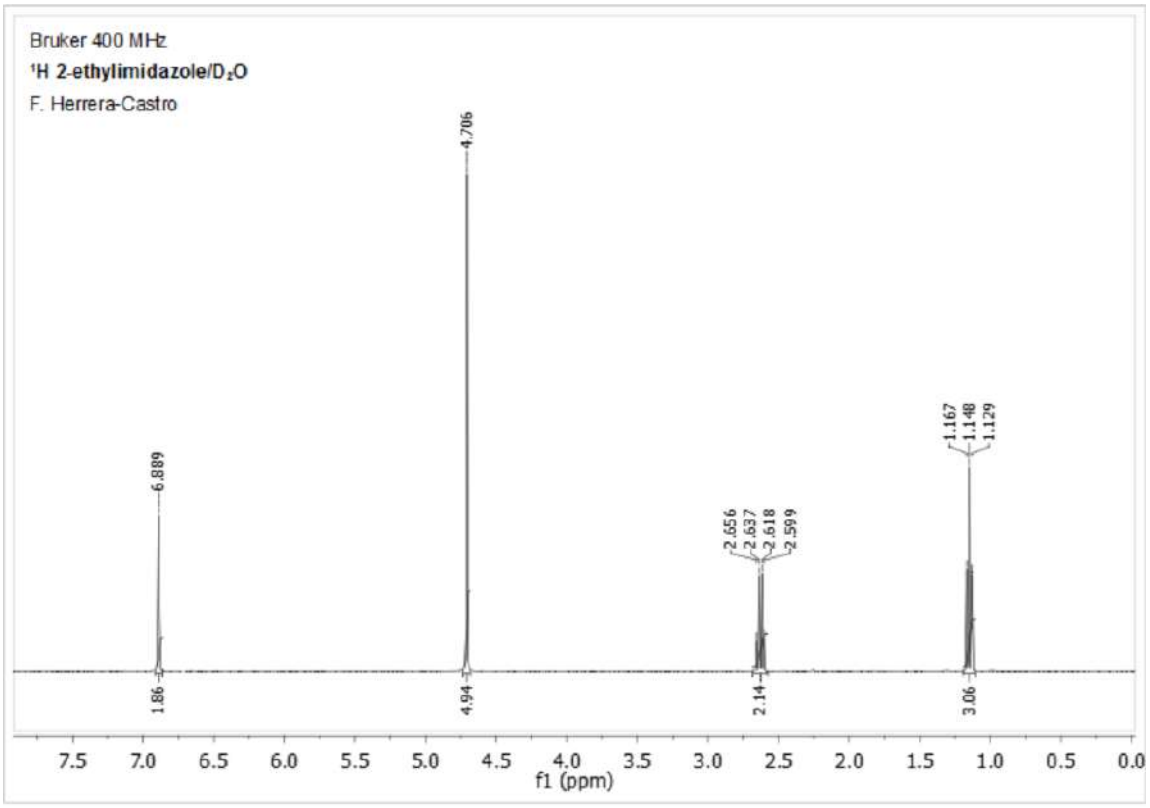
Bruker 400 MHz
¹H 2-ethylimidazole/D₂O
F. Herrera-Castro
4.706
6.889
2.656
2.637
2.618
2.599
1.167
1.148
1.129
1.86
4.94
2.14
3.06
f1 (ppm)

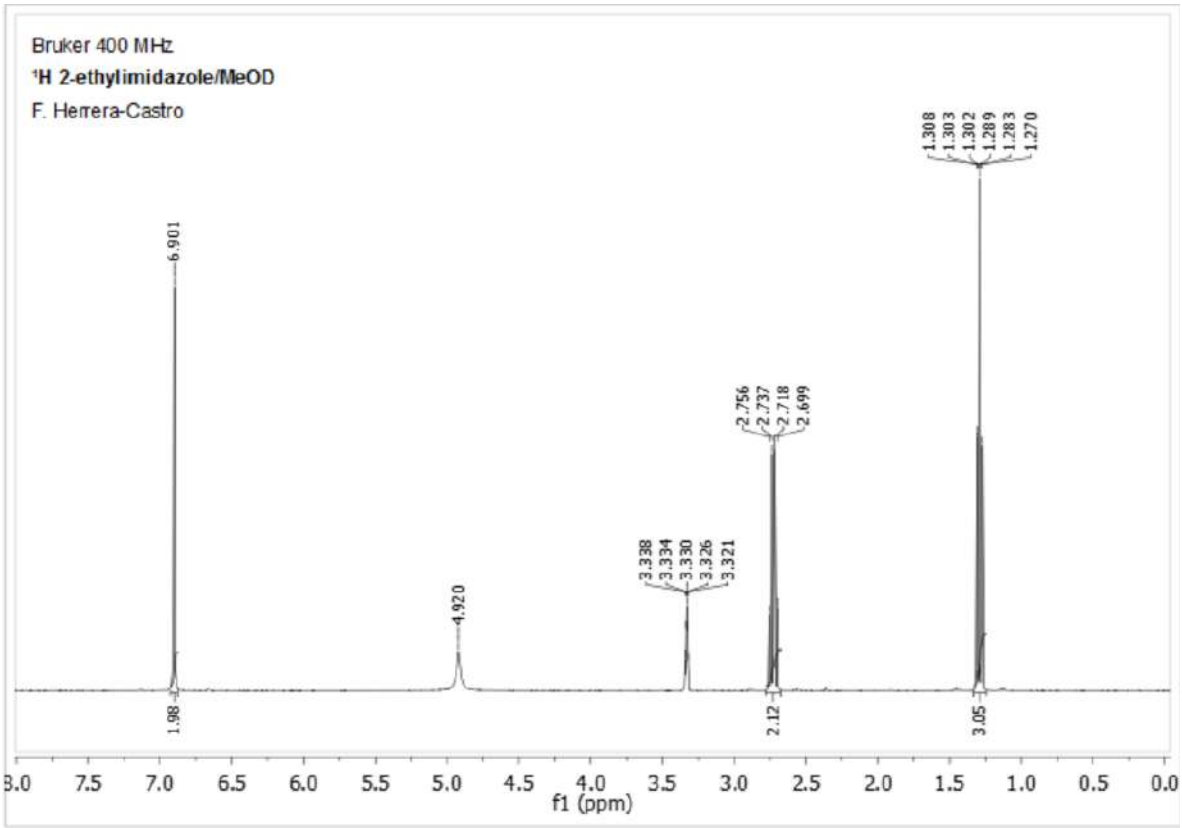
Bruker 400 MHz
¹H 2-ethylimidazole/MeOD
F. Herrera-Castro
6.901
4.920
3.338
3.334
3.330
3.326
3.321
2.756
2.737
2.718
2.699
1.308
1.303
1.302
1.289
1.283
1.270
1.98
2.12
3.05
f1 (ppm)

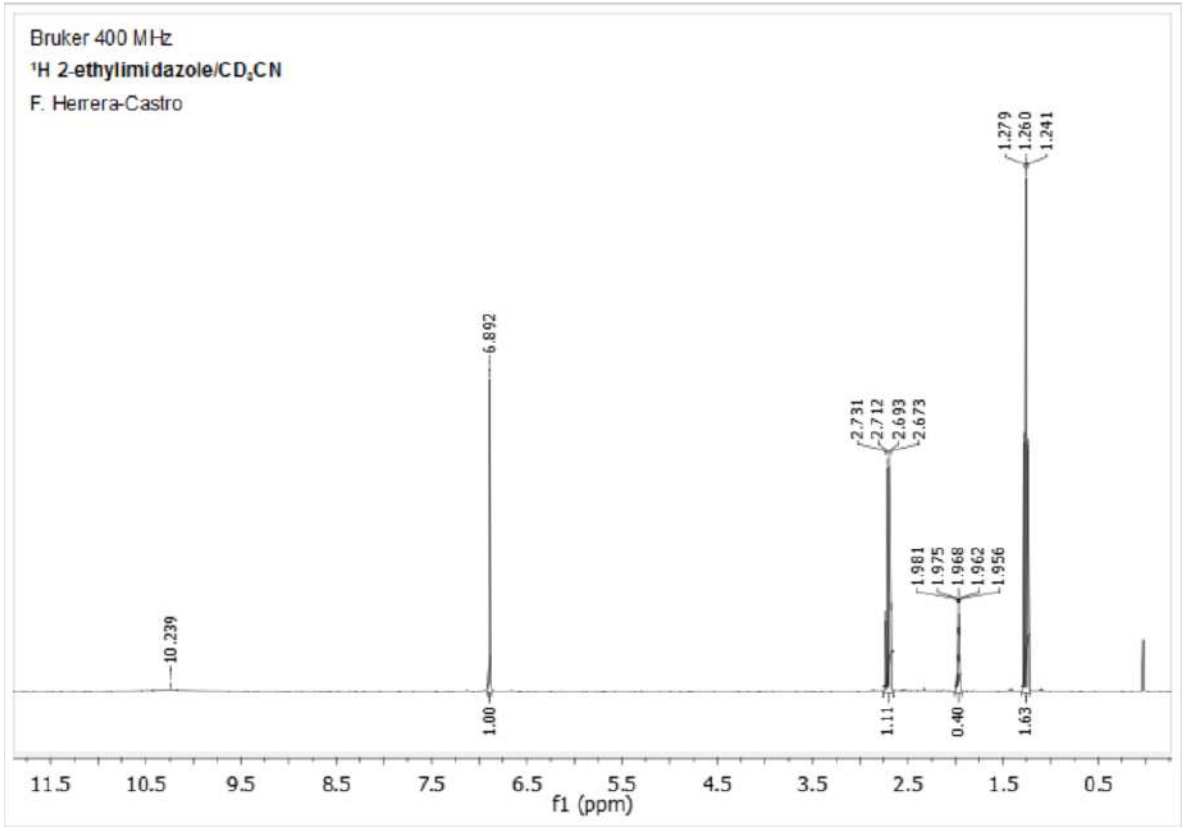
Bruker 400 MHz
¹H 2-ethylimidazole/CD₃CN
F. Herrera-Castro
10.239
6.892
2.731
2.712
2.693
2.673
1.981
1.975
1.968
1.962
1.956
1.279
1.260
1.241
1.00
1.11
0.40
1.63
11.5
10.5
9.5
8.5
7.5
6.5
5.5
4.5
3.5
2.5
1.5
0.5
f1 (ppm)

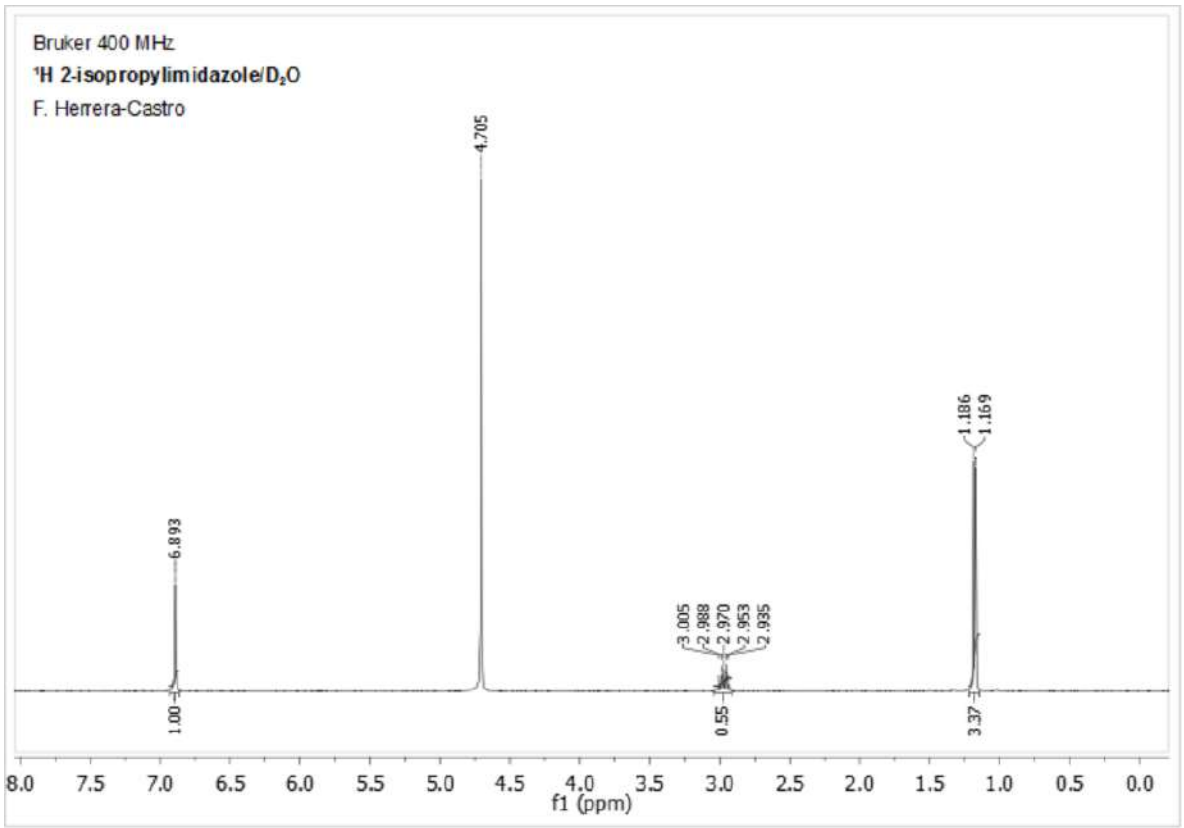
Bruker 400 MHz
¹H 2-isopropylimidazole/D₂O
F. Herrera-Castro
6.893
4.705
3.005
2.988
2.970
2.953
2.935
1.186
1.169
1.00
0.55
3.37
8.0
7.5
7.0
6.5
6.0
5.5
5.0
4.5
4.0
3.5
3.0
2.5
2.0
1.5
1.0
0.5
0.0
f1 (ppm)

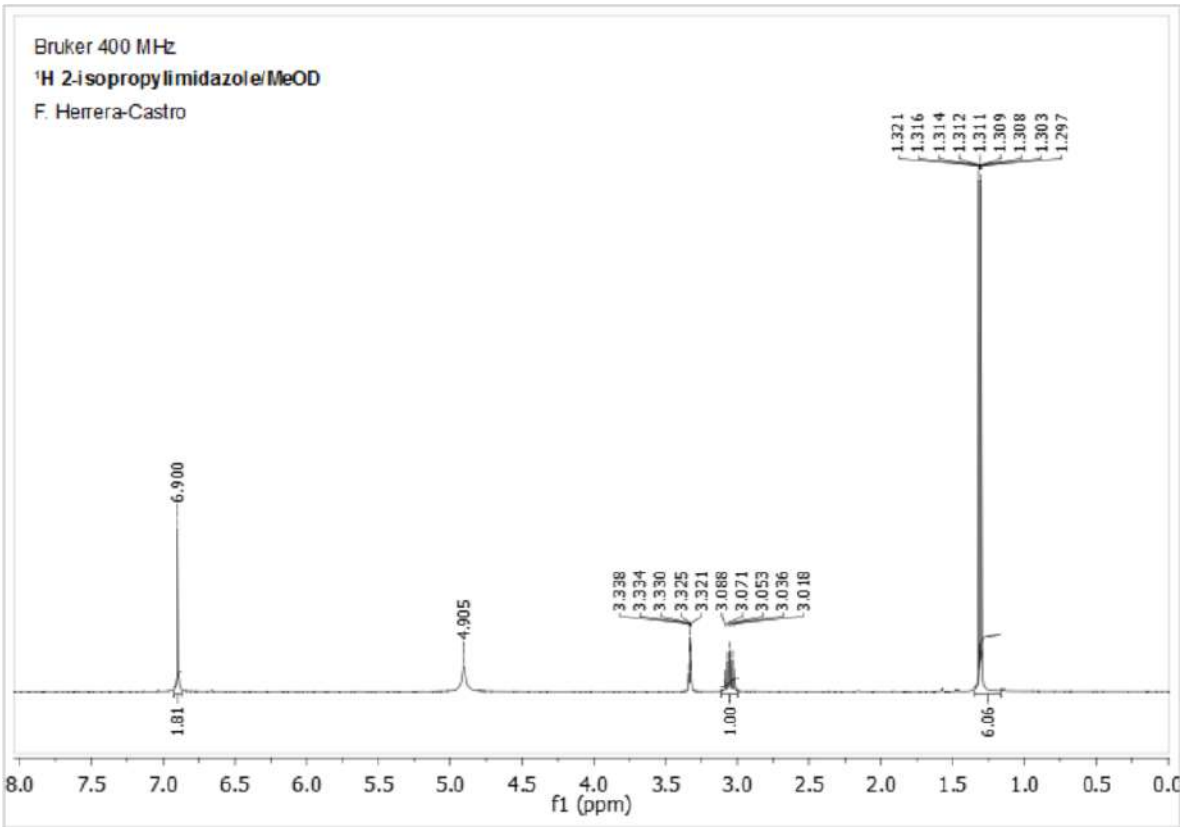
Bruker 400 MHz
¹H 2-isopropylimidazole/MeOD
F. Herrera-Castro
1.321
1.316
1.314
1.312
1.311
1.309
1.308
1.303
1.297
6.900
4.905
3.338
3.334
3.330
3.325
3.321
3.088
3.071
3.053
3.036
3.018
1.81
1.00
6.06
f1 (ppm)

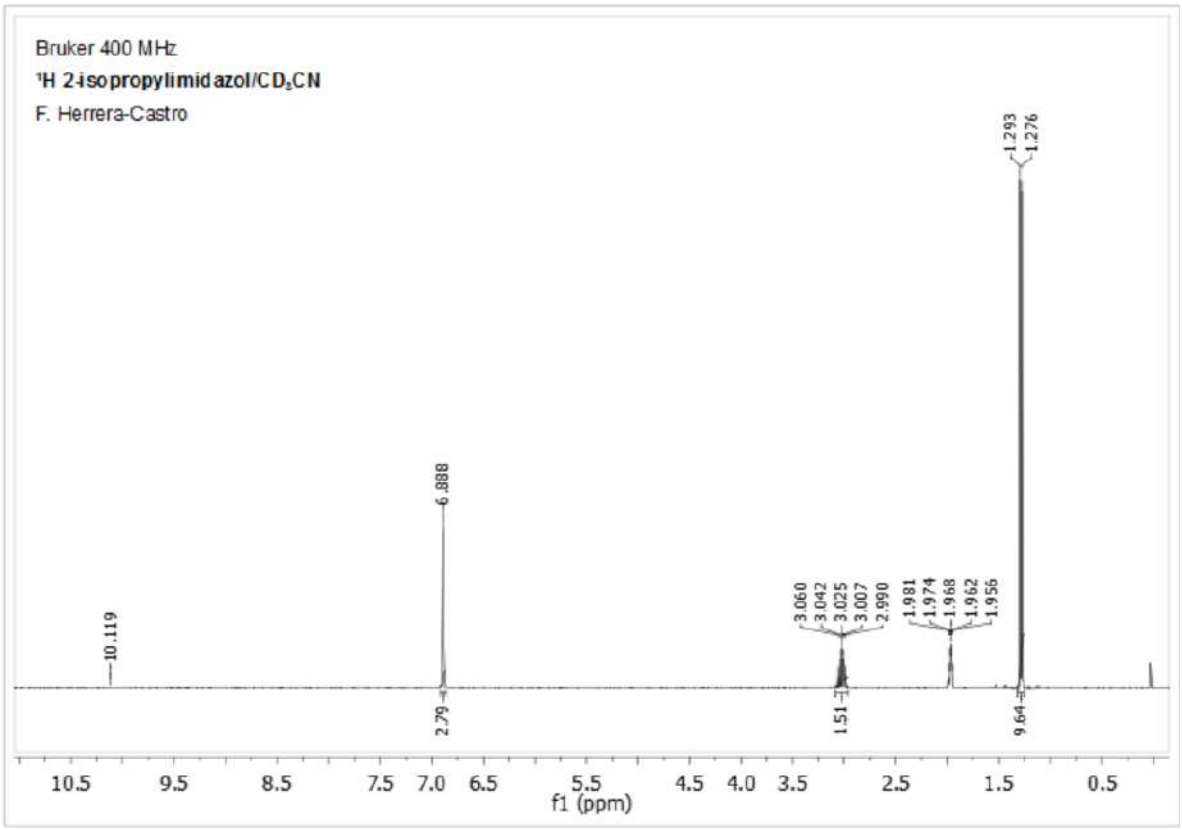
Bruker 400 MHz
¹H 2-isopropylimidazol/CD₃CN
F. Herrera-Castro
1.293
1.276
6.888
10.119
3.060
3.042
3.025
3.007
2.990
1.981
1.974
1.968
1.962
1.956
2.79
1.51
9.64
f1 (ppm)

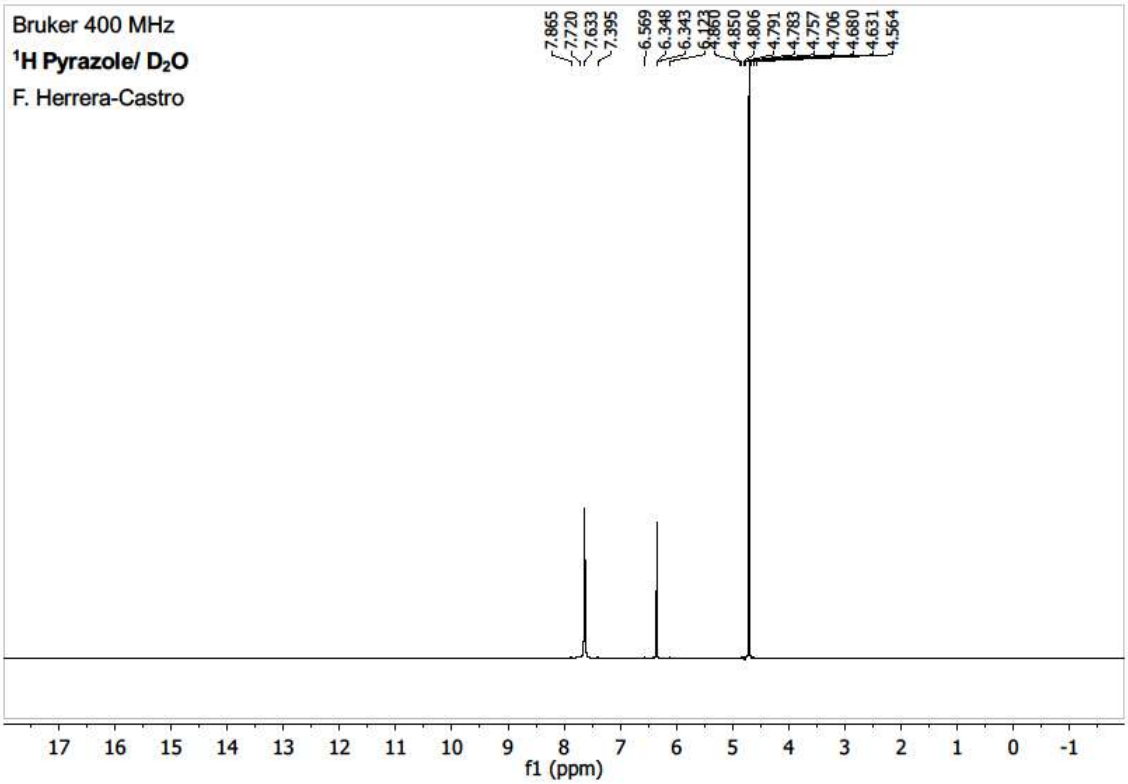
Bruker 400 MHz
¹H Pyrazole/ D₂O
F. Herrera-Castro
7.865
7.720
7.633
7.395
6.569
6.348
6.343
4.850
4.806
4.791
4.783
4.757
4.706
4.680
4.631
4.564
17 16 15 14 13 12 11 10 9 8 7 6 5 4 3 2 1 0 -1
f1 (ppm)

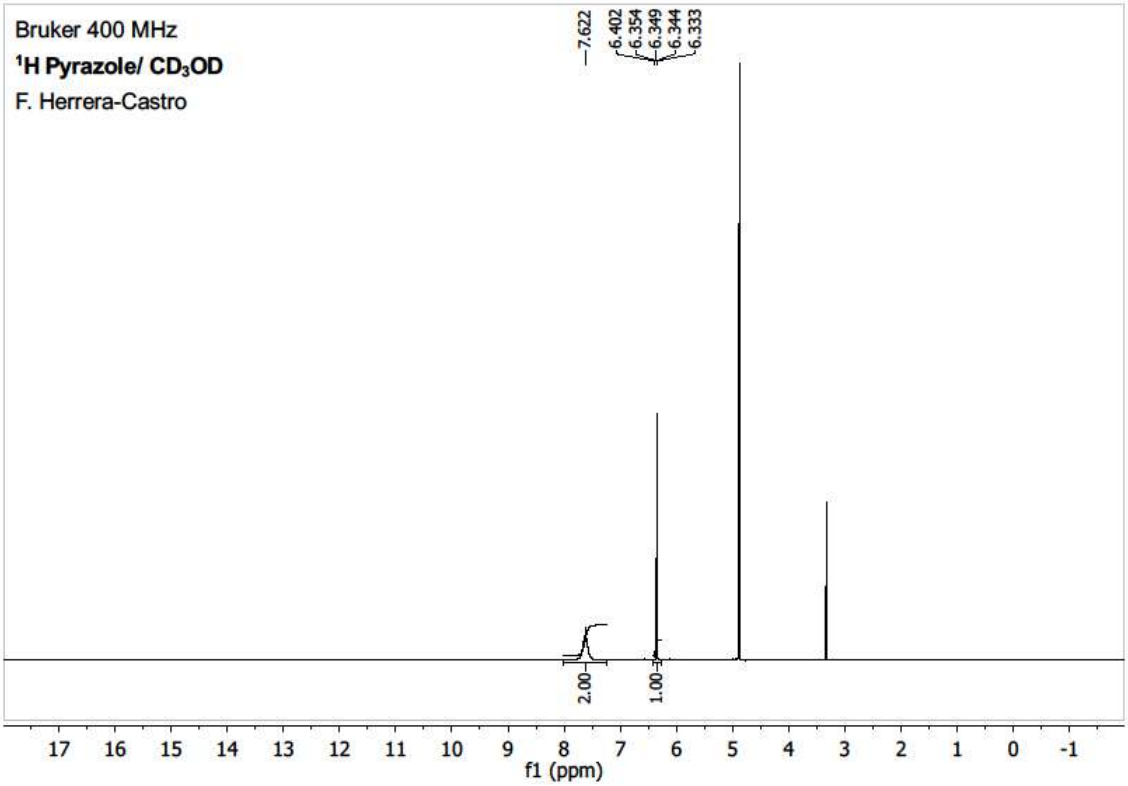
Bruker 400 MHz
¹H Pyrazole/ CD₃OD
F. Herrera-Castro
7.622
6.402
6.354
6.349
6.344
6.333
2.00
1.00
17 16 15 14 13 12 11 10 9 8 7 6 5 4 3 2 1 0 -1
f1 (ppm)

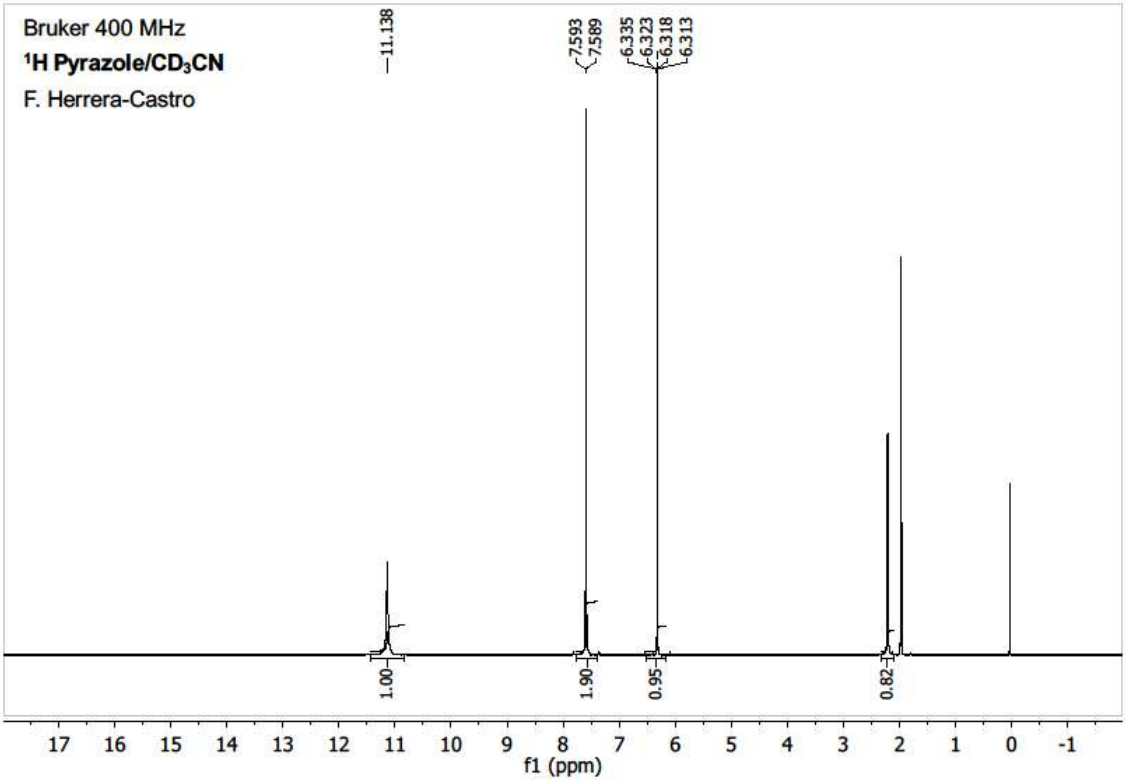
Bruker 400 MHz
¹H Pyrazole/CD₃CN
F. Herrera-Castro
11.138
7.593
7.589
6.335
6.323
6.318
6.313
1.00
1.90
0.95
0.82
17 16 15 14 13 12 11 10 9 8 7 6 5 4 3 2 1 0 -1
f1 (ppm)

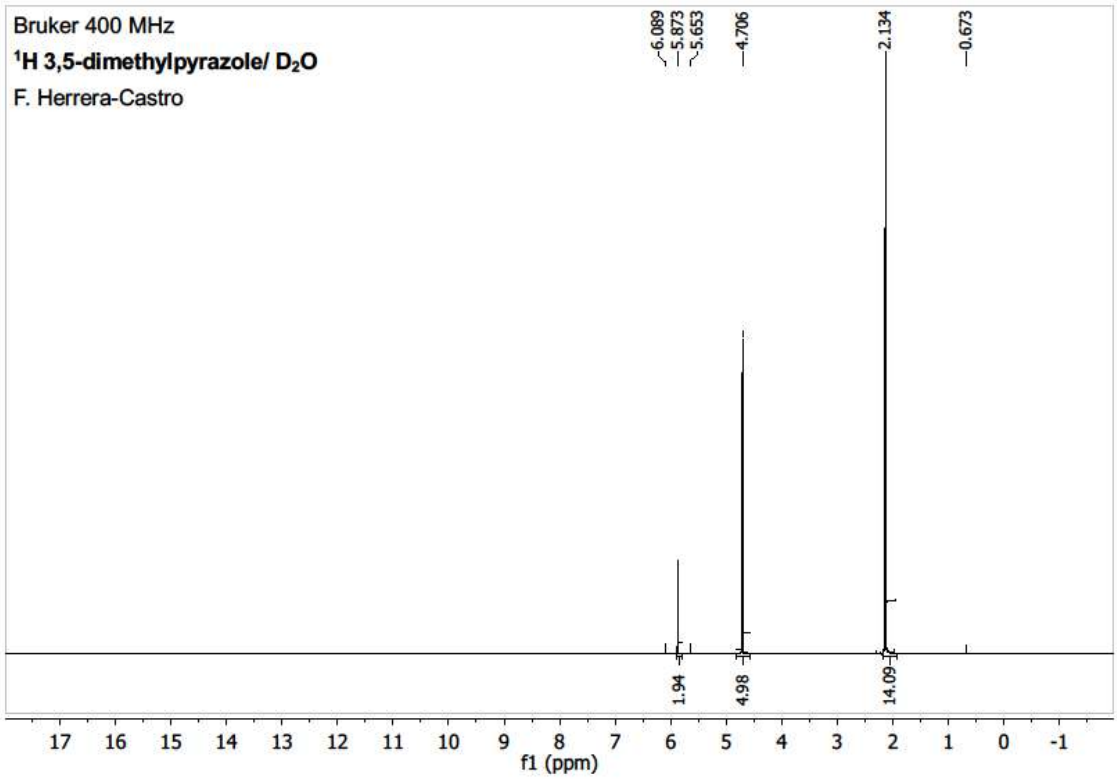
Bruker 400 MHz
¹H 3,5-dimethylpyrazole/ D₂O
F. Herrera-Castro
6.089
5.873
5.653
4.706
2.134
0.673
1.94
4.98
14.09
17 16 15 14 13 12 11 10 9 8 7 6 5 4 3 2 1 0 -1
f1 (ppm)

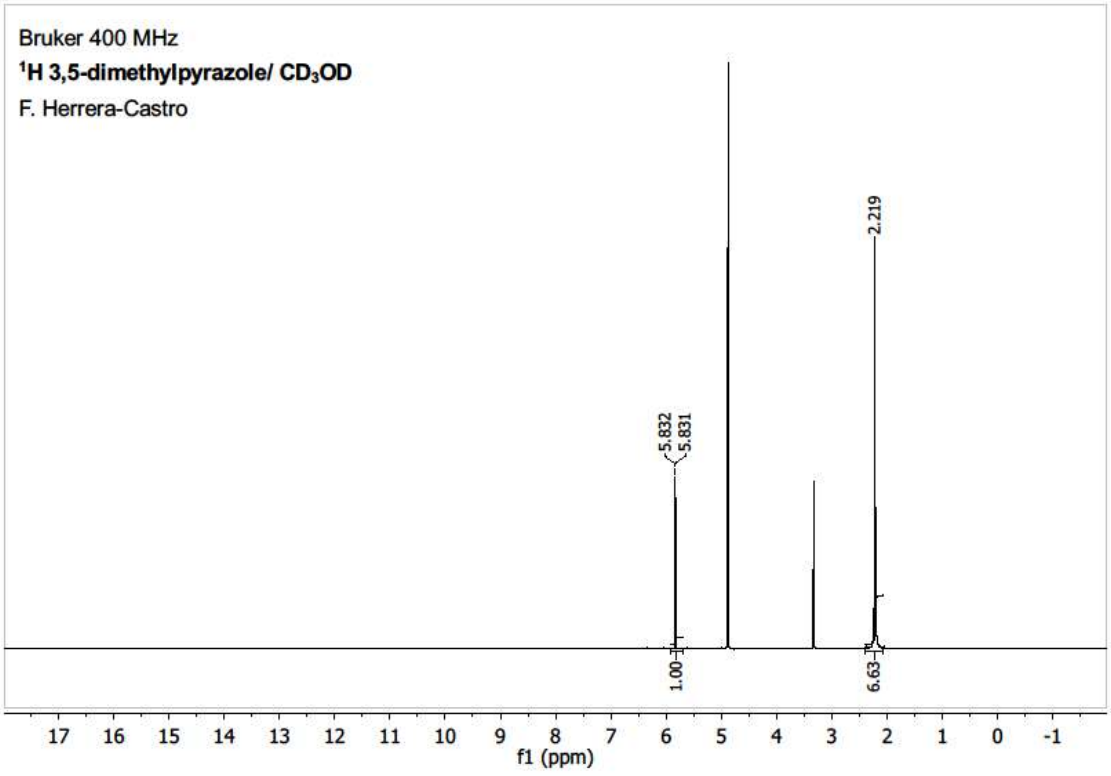
Bruker 400 MHz
¹H 3,5-dimethylpyrazole/ CD3OD
F. Herrera-Castro
2.219
5.832
5.831
1.00
6.63
17 16 15 14 13 12 11 10 9 8 7 6 5 4 3 2 1 0 -1
f1 (ppm)

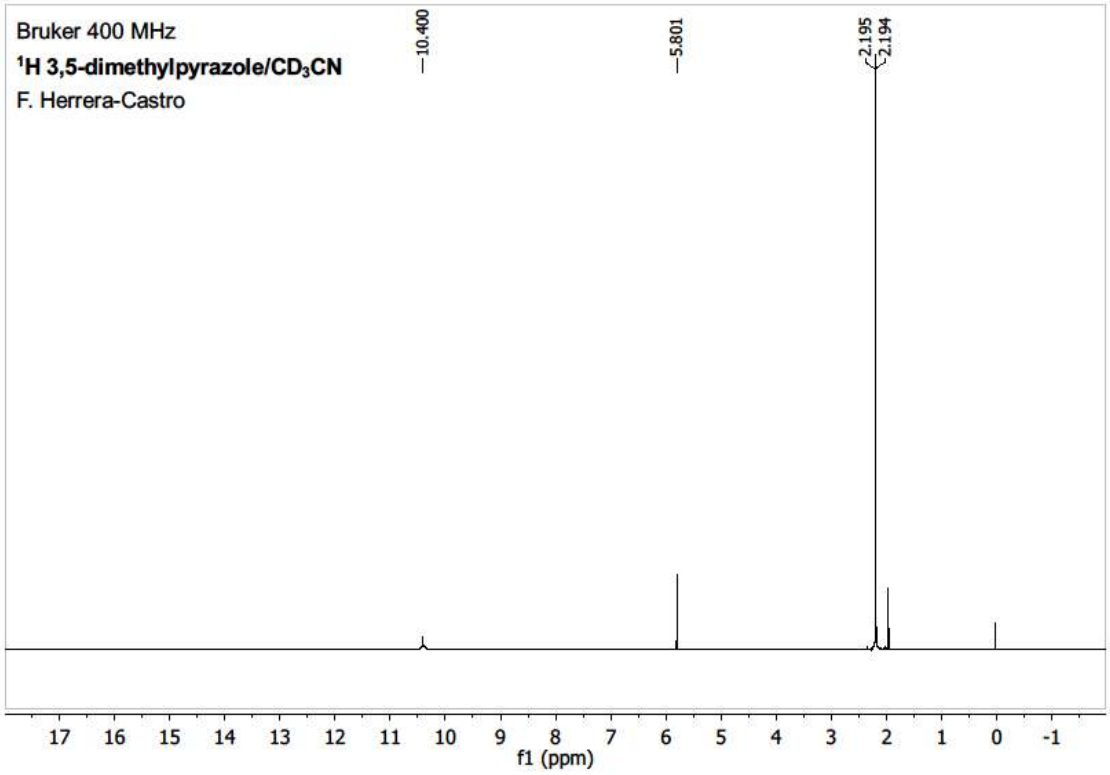
Bruker 400 MHz
¹H 3,5-dimethylpyrazole/CD3CN
F. Herrera-Castro
10.400
5.801
2.195
2.194
17 16 15 14 13 12 11 10 9 8 7 6 5 4 3 2 1 0 -1
f1 (ppm)

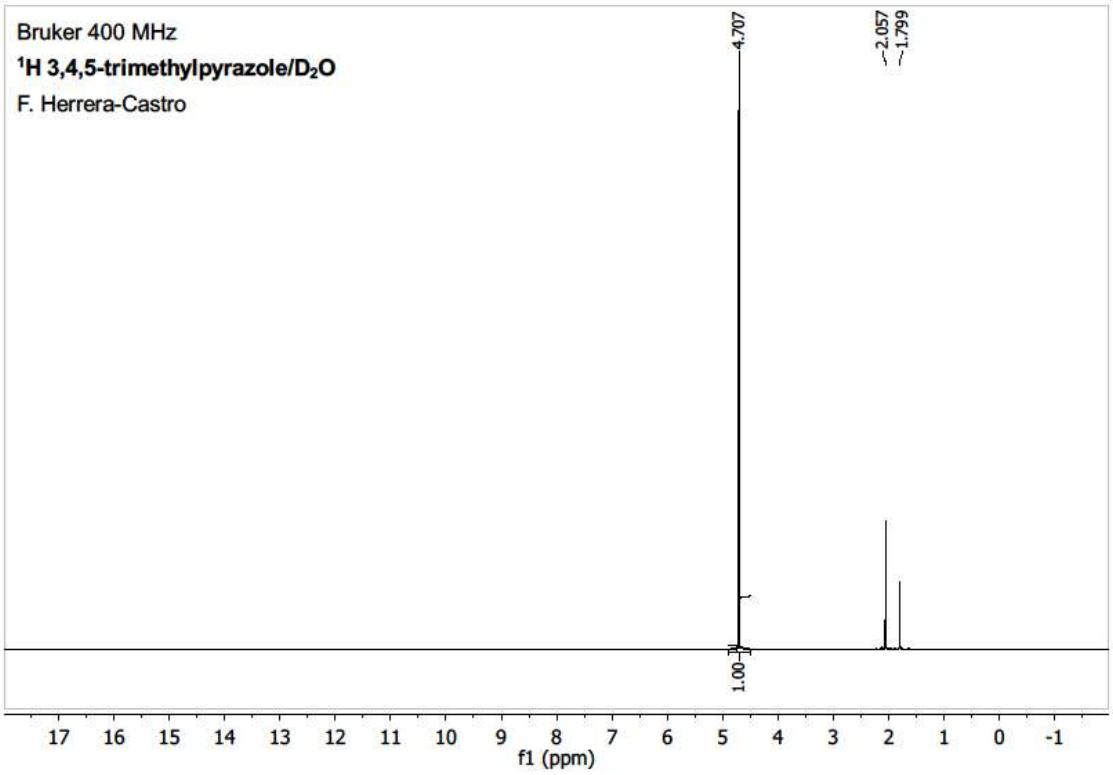
Bruker 400 MHz
¹H 3,4,5-trimethylpyrazole/D₂O
F. Herrera-Castro
4.707
2.057
1.799
1.00
17 16 15 14 13 12 11 10 9 8 7 6 5 4 3 2 1 0 -1
f1 (ppm)

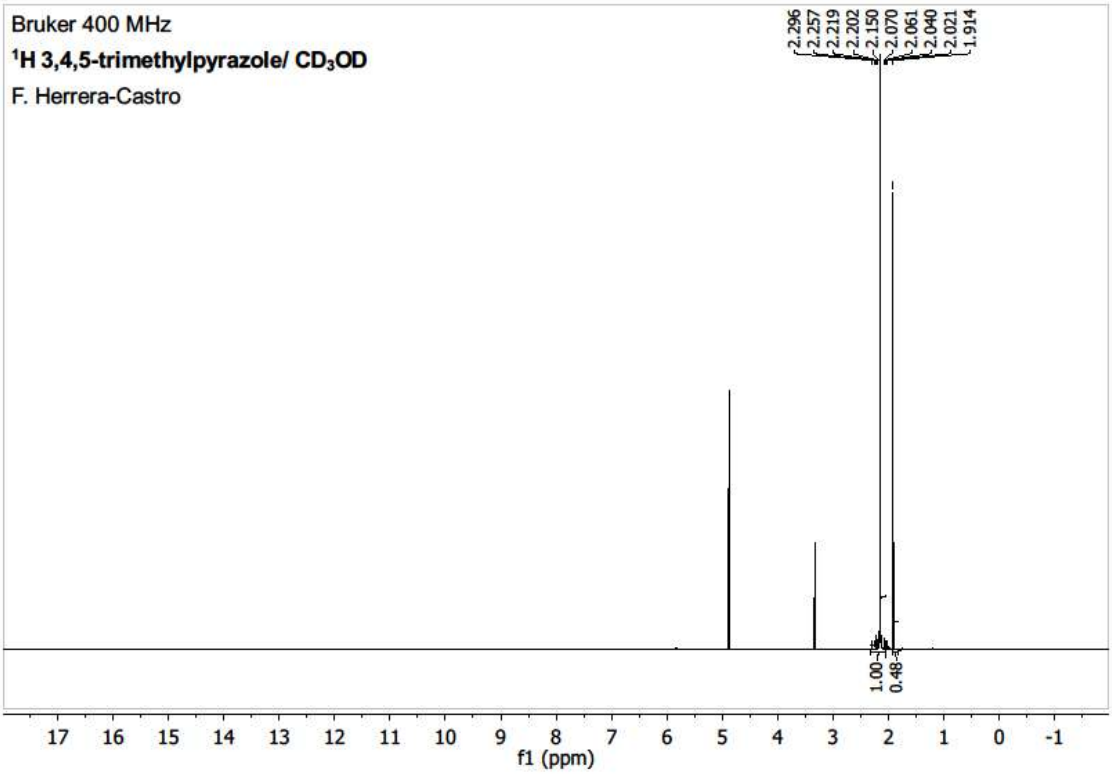
Bruker 400 MHz
¹H 3,4,5-trimethylpyrazole/ CD₃OD
F. Herrera-Castro
2.296
2.257
2.219
2.202
2.150
2.070
2.061
2.040
2.021
1.914
1.00
0.48
17 16 15 14 13 12 11 10 9 8 7 6 5 4 3 2 1 0 -1
f1 (ppm)

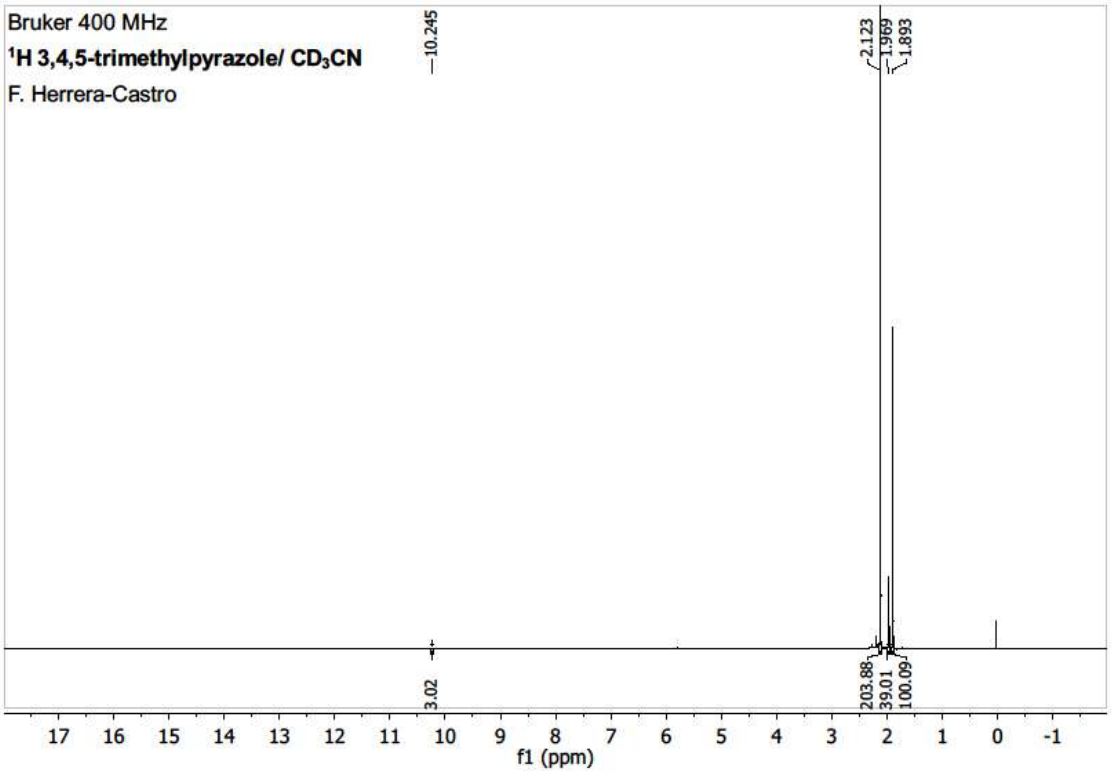
Bruker 400 MHz
¹H 3,4,5-trimethylpyrazole/ CD₃CN
F. Herrera-Castro
10.245
2.123
1.969
1.893
3.02
203.88
39.01
100.09
17 16 15 14 13 12 11 10 9 8 7 6 5 4 3 2 1 0 -1
f1 (ppm)

A.5 Mass spectrometry experiments

The mass spectrometry experiments were performed in an Agilent single quad 6120 spectrometer at room temperature under a potential of 70 eV. The pressure is reduced until $2x10^{-4}$ Pa. The experiments were carried out in acetonitrile. From these spectra, the presence of dimers in the gas phase is discarded. The labels used for description of studied solute are: IM for imidazole, 2M-IM for 2-methylimidazole, 2ETIM for 2-ethylimidazole, 2ISIM for 2-isopropylimidazole, PIR for pyrazole, DIMPIR for 3,5-dimethylpyrazole and TRIM for 3,4,5-trimethylpyrazole.

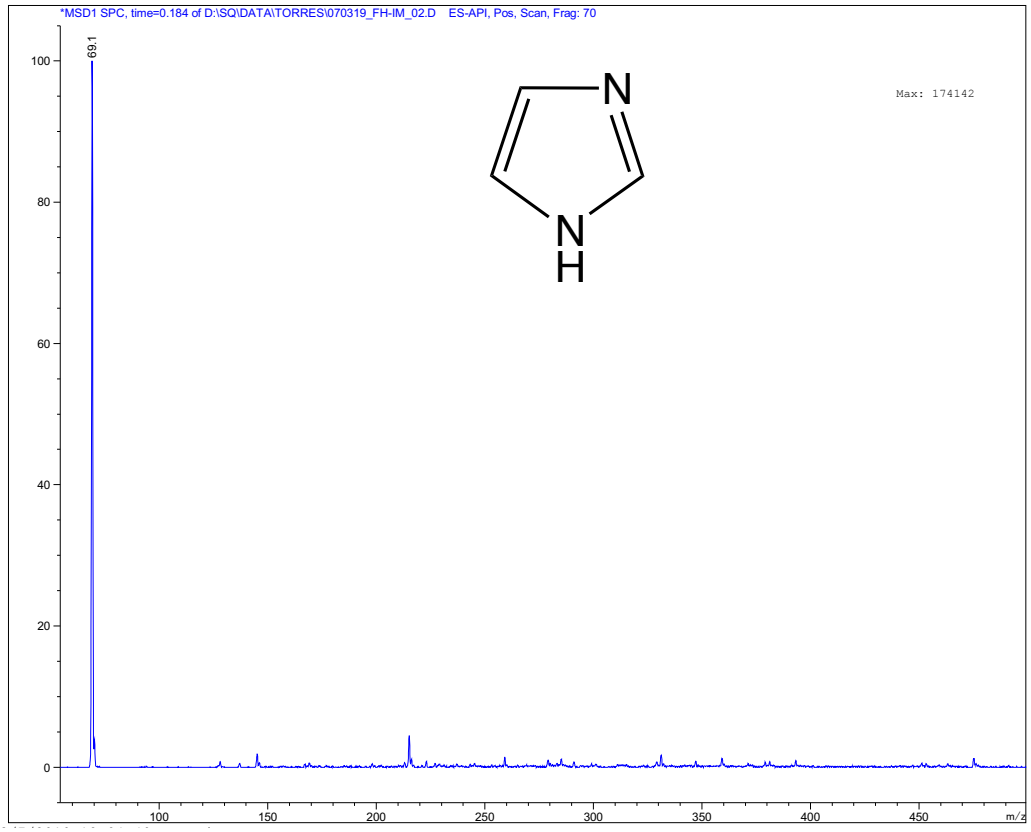

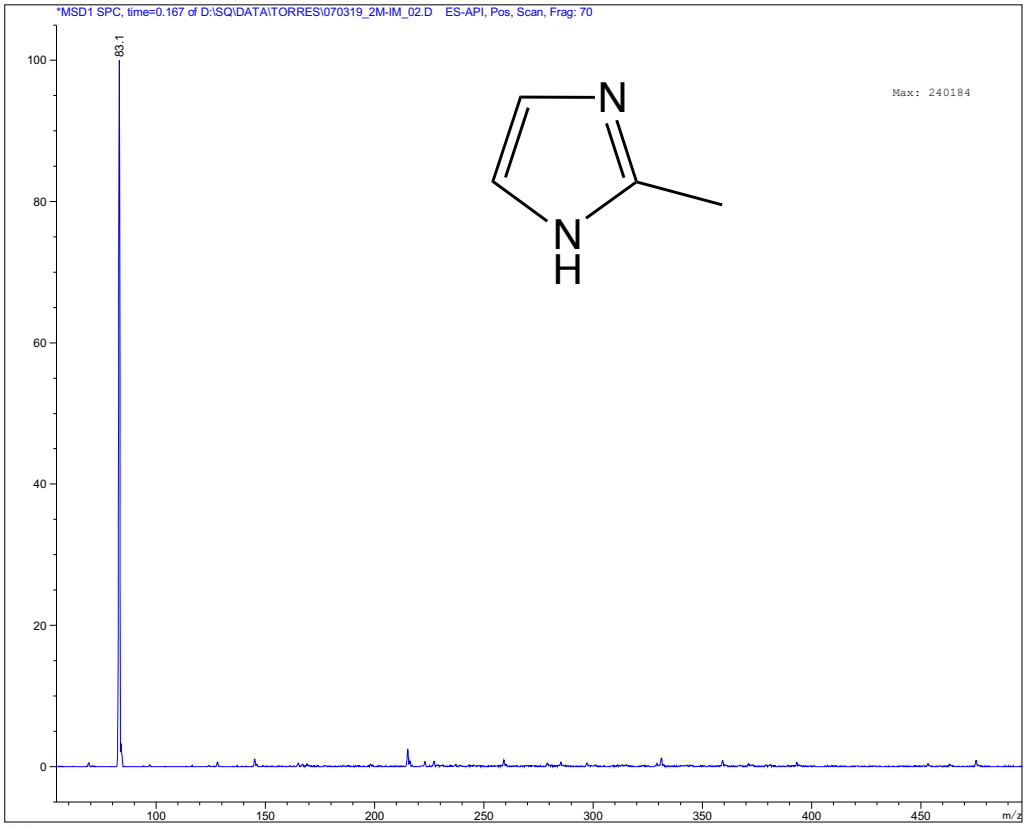
*MSD1 SPC, time=0.167 of D:\SQ\DATA\TORRES\070319_2M-IM_02.D ES-API, Pos, Scan, Frag: 70
Max: 240184
83.1
N
N
H
100
80
60
40
20
0
100
150
200
250
300
350
400
450
m/z

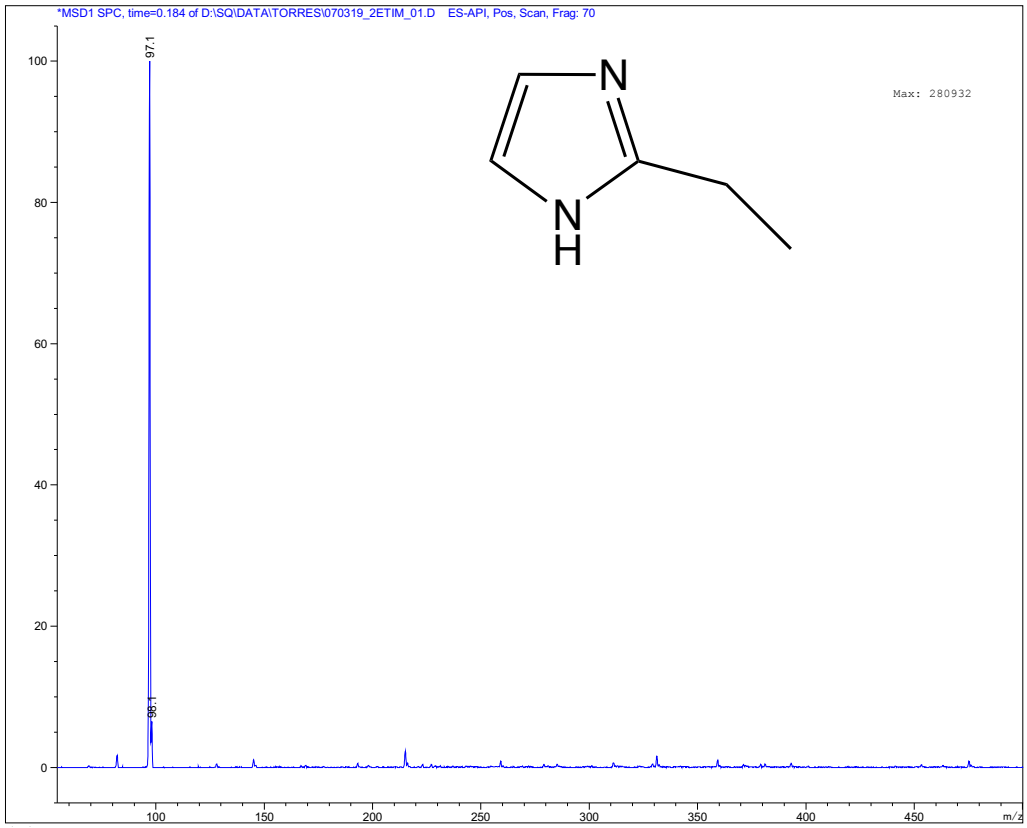
*MSD1 SPC, time=0.184 of D:\SQ\DATA\TORRES\070319_2ETIM_01.D ES-API, Pos, Scan, Frag: 70
Max: 280932
97.1
98.1
N
N
H
100
80
60
40
20
0
100
150
200
250
300
350
400
450
m/z

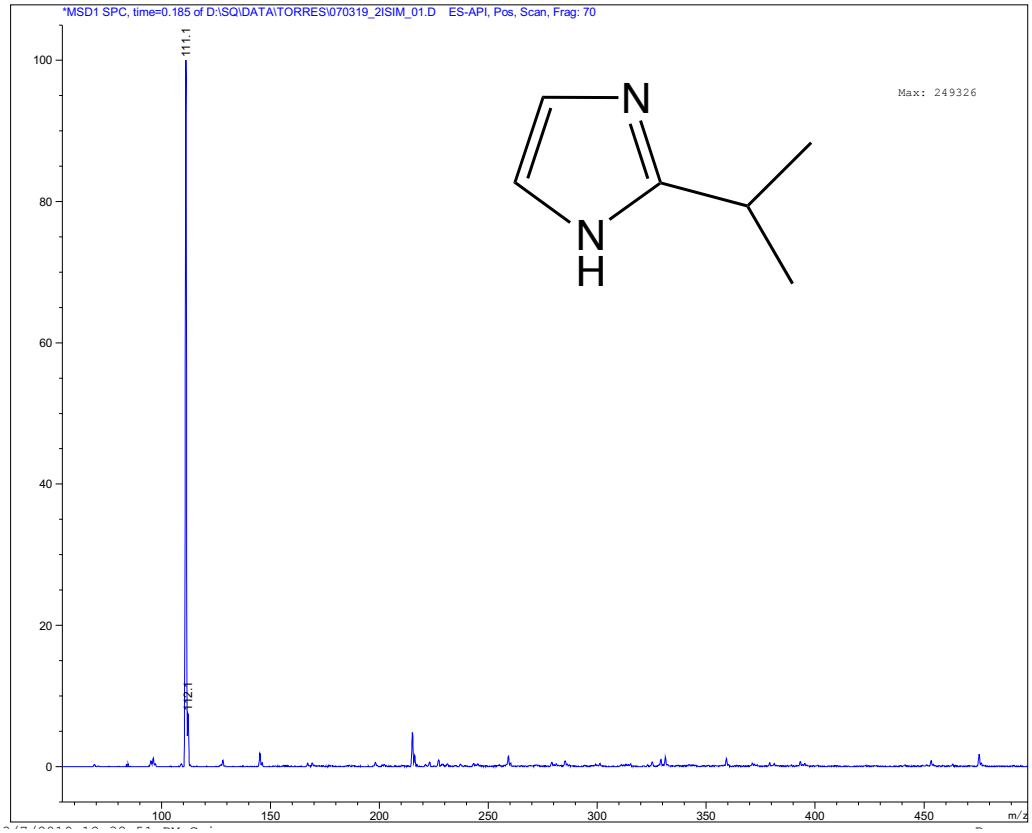
*MSD1 SPC, time=0.185 of D:\SQ\DATA\TORRES\070319_2ISIM_01.D ES-API, Pos, Scan, Frag: 70
111.1
112.1
Max: 249326
N
N
H
100
80
60
40
20
0
100
150
200
250
300
350
400
450
m/z

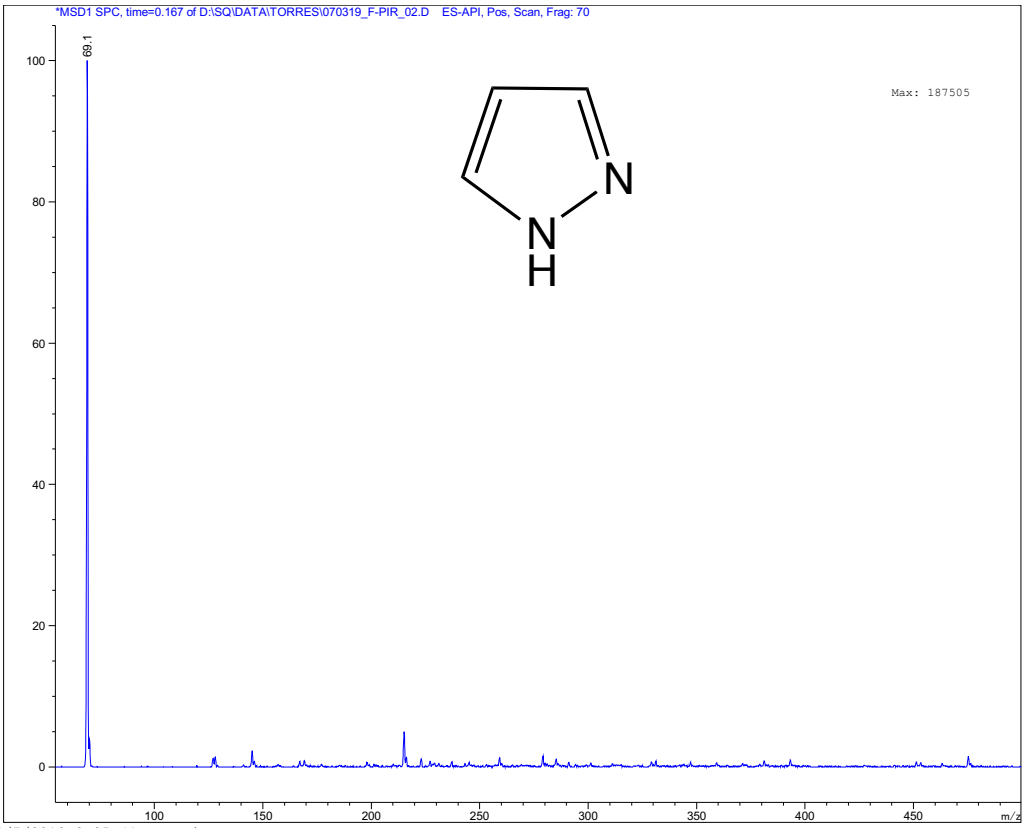
*MSD1 SPC, time=0.167 of D:\SQ\DATA\TORRES\070319_F-PIR_02.D ES-API, Pos, Scan, Frag: 70
69.1
Max: 187505
N
N
H
100
80
60
40
20
0
100
150
200
250
300
350
400
450
m/z

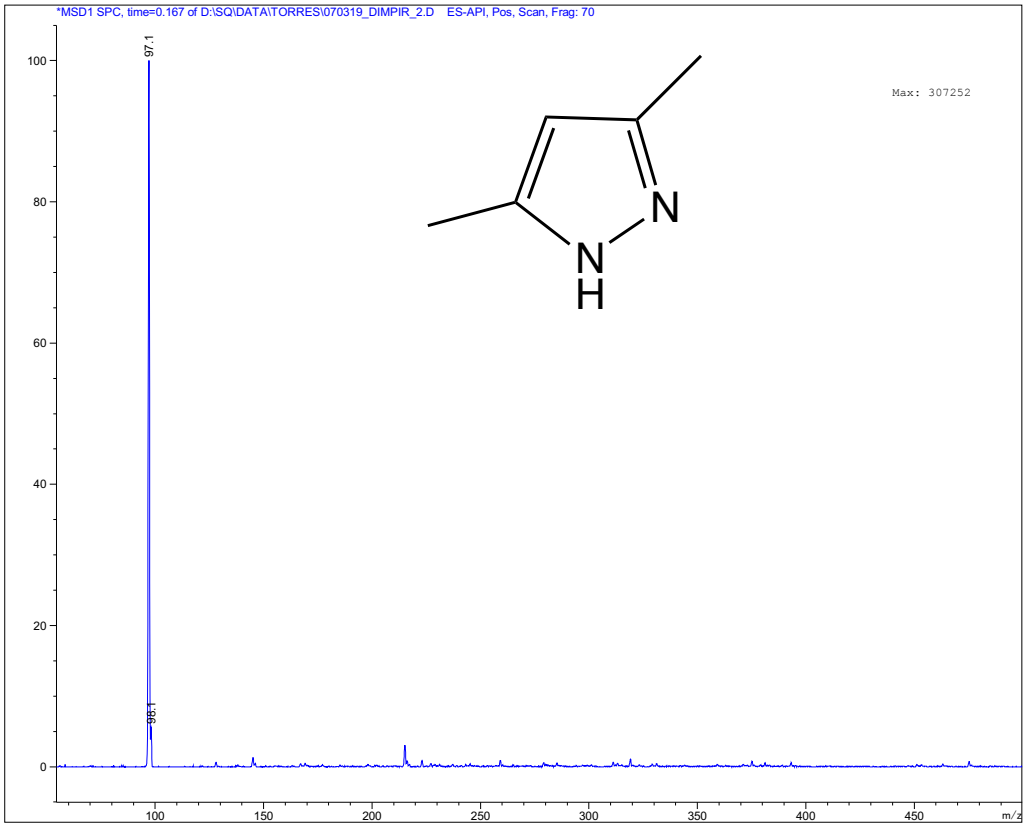
*MSD1 SPC, time=0.167 of D:\SQ\DATA\TORRES\070319_DIMPIR_2.D ES-API, Pos, Scan, Frag: 70
Max: 307252
97.1
98.1
N
N
H
100
80
60
40
20
0
100
150
200
250
300
350
400
450
m/z

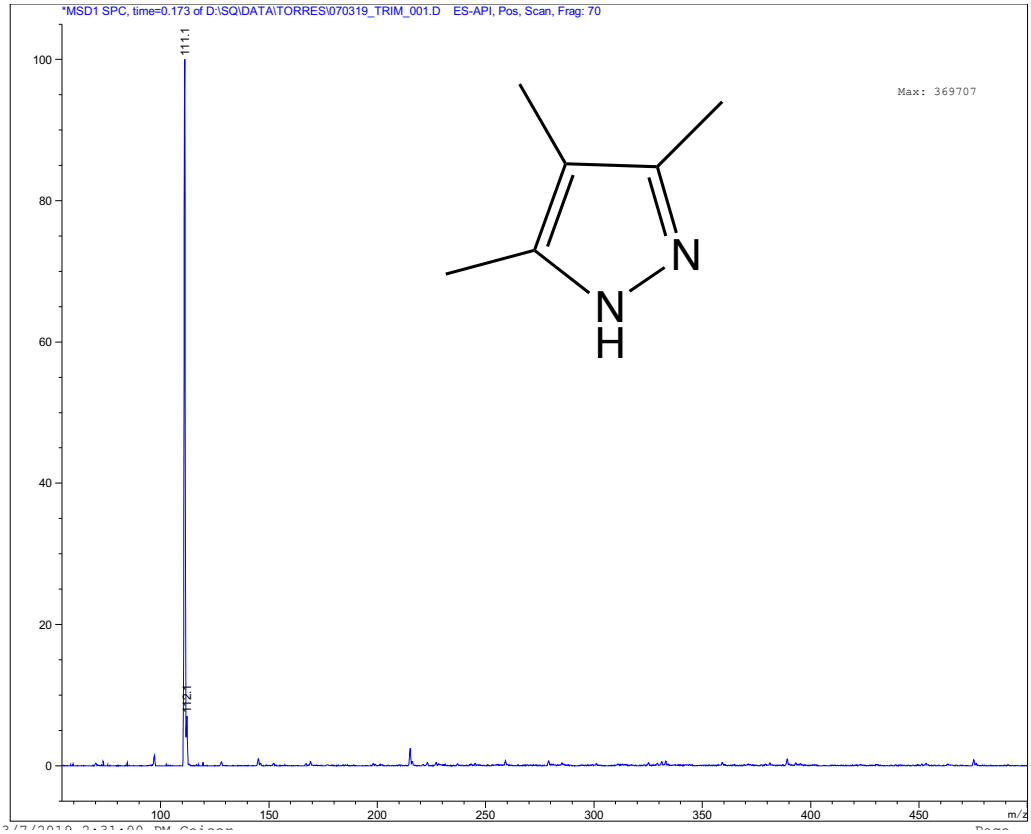
*MSD1 SPC, time=0.173 of D:\SQ\DATA\TORRES\070319_TRIM_001.D ES-API, Pos, Scan, Frag: 70
Max: 369707
111.1
112.1
N
N
H
100
80
60
40
20
0
100
150
200
250
300
350
400
450
m/z

A.6 X-ray data

In Table A35 is shown the essential crystallographic data for the compounds 2-ethylimidazole, obtained from monocrystal x-ray diffraction experiments in a Bruker D8 VENTURE device and 2-isopropylimidazole, obtained from x-ray powder diffraction experiments in a Bruker D8 ADVANCE ECO device.

Compound	2-ethylimidazole	2-isopropylimidazole
Empirical formula	C_5 H_8 N_2	C_6 H_{10} N_2
Formula weight	96.13	110.16
Crystal system	Triclinic	Triclinic
Space Group	$P\bar{1}$	$P\bar{1}$
Unit cell dimensions a, b, c, (Å); α, β, γ (deg)	a= 7.0731(8) b= 9.7973(9) c= 10.1963(11) α= 113.896(5) β= 106.836(4) γ= 96.496(4)	a= 7.62209 b= 7.96594 c= 11.86393 α= 84.441 β= 84.274 γ= 101.764
Volume (Å^3)	596.483	696.596
Z	2	2

Table A35. Crystallographic data for the x-ray structures determined in Cinvestav. The data for 2-ethylimidazole and 2-isopropylimidazole is shown.

A.7 Dipole moments

The normalized dipole moment vectors for each solute molecule are illustrated in Figure A22 as a red arrow. From the quantum mechanical calculations, as described in Section III.7, the components of each vector were obtained. The normalized vector is calculated at dividing each component by the norm of the dipole moment vector. The illustrations were made in the Avogadro Software v1.2.0.

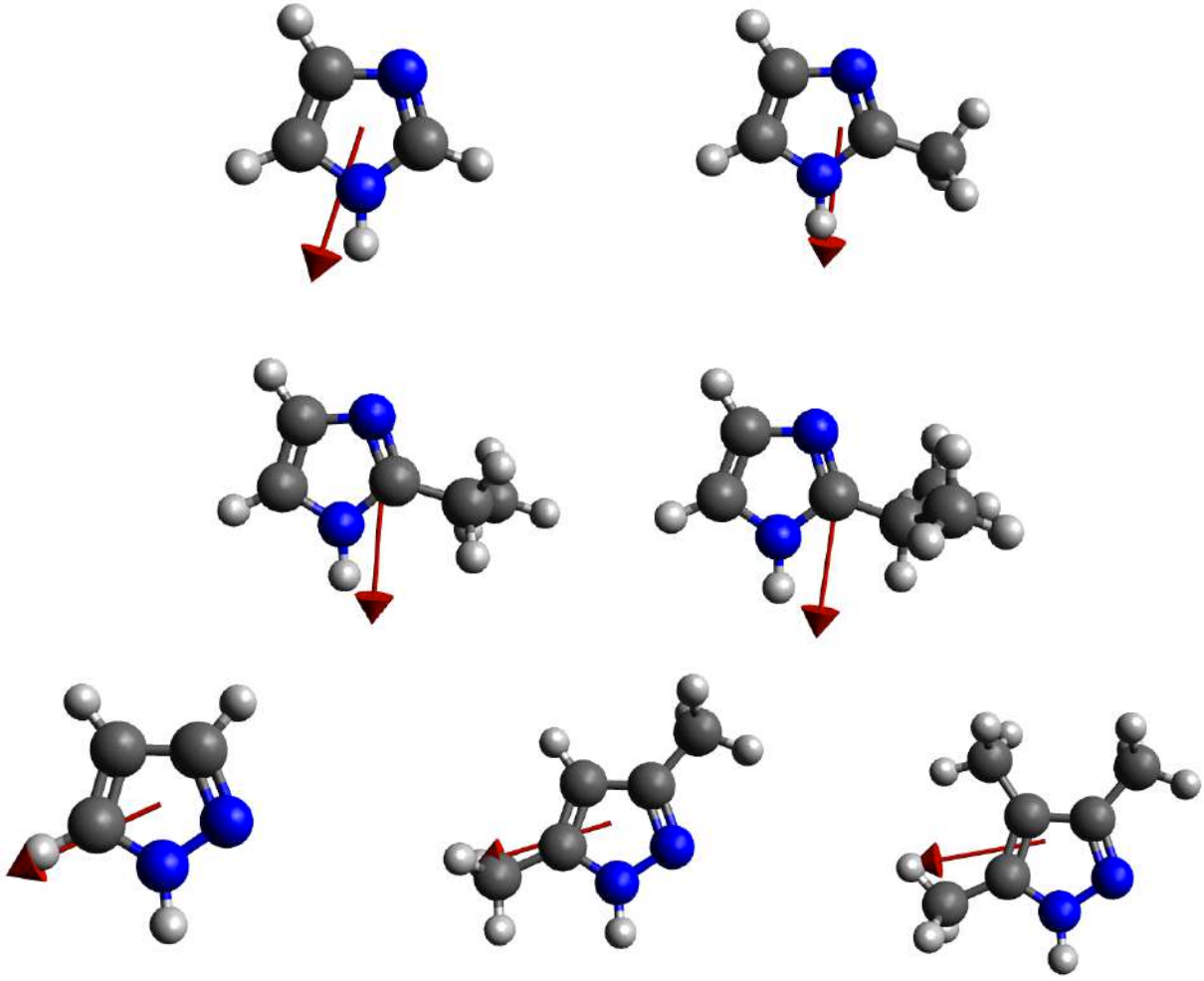

Figure A22. Illustration of the normalized dipole moment vector in each of the compounds. The vector is represented as a red arrow.

References

1. Supramolecular chemistry. Steed J. W., Atwood, J. L. 2nd edition. John Wiley and Sons, Ltd. Chippenham, Wiltshire (2009).
2. Solvents and solvent effects in organic chemistry. Reichardt, C., Welton, T. 4th ed. Wiley-VCH Verlag GmbH & Co. KGaA. Weinheim (2011).
3. What is solvatochromism? Marini, A., Muñoz-Losa, A., Biancardi, A., Mennuci, B., J. Phys. Chem. B (2010) 114, 17128-17135.
4. Physical Chemistry. A Molecular Approach. McQuarrie, D., Simon, J. University Science Books. USA (1997).
5. Organic Crystal Engineering. Ed. By Tieknik, E. R., Vittal, J., Zaworotko, M. J., John Wiley and Sons, Chippenham, Wiltshire (2010).
6. The influence of the extrapolation method on enthalpies of solution at infinite dilution. Sanahuja, A., Gómez-Estévez, J. L., Thermochim. Acta (1985) 94, 223-229.
7. Unified description of infinite-dilution thermodynamics properties for aqueous solutes. Harvey, A. H., Levelt Sengers, J. M. H., Tanger IV, J. C., J. Phys. Chem. (1991) 95, 932-937.
8. Standard thermodynamics of transfer. Uses and misuses. Ben-Naim, A., J. Phys. Chem. (1978) 82, 792-803.
9. Solvation thermodynamics. Ben-Naim, A., Springer Science+Business Media LLC. New York (1987).
10. Solvation Thermodynamics: Theory and applications. Ben-Amotz, D., Raineri, F. O., Stell, G., J. Phys. Chem. B (2005) 109, 6866-6878.
11. Solvent scaling scheme for studying solvent restructuring thermodynamics in solvation processes. Raineri, F. O., Wiseb, P., Ben-Amotz, D., J. Mol. Liq. (2018) 270, 114–127.
12. Inhomogeneous fluid approach to solvation thermodynamics. 1. Theory. Lazaridis, T., J. Phys. Chem. B (1998) 102, 3531-3541.
13. Inhomogeneous fluid approach to solvation thermodynamics. 2. Applications to simple fluids. Lazaridis, T., J. Phys. Chem. B (1998) 102, 3542-3550.
14. A new method for the extraction of specific interaction enthalpy from the enthalpy of solvation. Solomonov B. N., J. Phys. Org. Chem. (2005) 18, 49–61.
15. Non-additivity in the solvation enthalpies of substituted phenols and estimation of their enthalpies of vaporization/sublimation at 298.15 K. Nagrimanov, R. N., Samatov, A. A., Solomonov, B. N., J. Mol. Liq. (2016) 221, 914–918.
16. Enthalpies of solvation of hydroxyl cyclohexane derivatives in different solvents Costa, E., Eusebio, M. E., Redinha, J. S., Leitão, M. L. P., J. Chem. Thermodyn. (1999) 31, 895–903.
17. On the interpretation of the enthalpy of solvation of hydroxyl cyclohexane derivatives in different solvents. Costa, E., Eusebio, M. E., Redinha J.S., Leitão, M.L.P., J. Chem. Thermodyn. (2000) 32, 311-317.
18. Use of quantitative structure–property relationships to study the solvation process of 18-crown-6. Reis, M., Nunes, N., Elvas-Leitão, R., Martins, F., Thermochim. Acta (2015) 604, 140–144.

19. Scaled particle theory of aqueous and non-aqueous solutions. Pierotti, R. A. Chem. Rev., (1976) 76, 717-726.
20. Physical Chemistry, Berry, R., Rice, S., Ross, J., John Wiley and Sons, Ltd. USA (1980).
21. Stone, A. The theory of intermolecular forces. Second Edition. Oxford University Press. Croydon (2013).
22. Core Concepts in Supramolecular Chemistry. Steed, J., Turner, D. R., Wallace, K. J., John Wiley and Sons, Ltd. Chippenham, Wiltshire (2007).
23. Ariga, K., Kunitake, T., Supramolecular Chemistry-Fundamentals and Applications. Springer-Verlag, Heidelberg (2006).
24. The Lock and Key Principle. The state of the art-100 years on. Ed by Jean-Paul Behr. John Wiley and Sons Ltd. Guilford, Surrey (1994).
25. http://chemistry.elmhurst.edu/vchembook/571lockkey.html visited 18/June/2019.
26. Lock-and-Key Principle on a Microscopic Scale: The case of the propylene oxide···ethanol complex. Borho, N., Xu, Y., Angew. Chem. Int. Ed., (2007) 46, 2276-2279.
27. Self-Assembly at all scales. Whitesides, G. M., Grzymbowski, B., Science (2002), 295 (5564), 2418-2421.
28. Self-Assembled monolayers of thiolates of metals as a form of nanotechnology. Love, J. C., Estroff, L. A., Kriebel, J. K., Nuzzo, R. G., Whitesides, G. M., Chem. Rev. (2005) 105, 1103-1169.
29. Water-mediated ion pairing: occurrence and relevance. van der Vegt, N. F. A., Haldrup, K., Roke, S., Zheng, J., Lund, M., Bakker, H. J. Chem. Rev. (2016) 116, 7626-7641.
30. The solvent dimethyl sulfoxide. Martin, D., Weise, A., Niclas, H. J., Angew. Chem. Int. Ed. (1967), vol. 6, 4, 318-334.
31. Dimerization of merocyanine dyes. Structural and energetic characterization of dipolar dye aggregartes and implications for nonlinear optical materials. Würthner, F., Yao, S., Debaerdemaeker, T., Wortmann, R., J. Am. Chem. Soc. (2002), 124, 9431-9447.
32. Thermodynamic analysis of the mutual solubilities of normal alkanes and water. Tsonopoulos, C. Fluid Ph. Equilibria (1999), 156, 21-33.
33. The Cation-π interaction. Ma., J. C., Dougherty, D. A., Chem. Rev. (1997), 97, 1303-1324.
34. The Cation-π interaction. Dougherty, D. A. Acc. Chem. Res. (2013), 46(4), 885-893.
35. Cation-π interactions in chemistry and biology: a new view of benzene, phe, tyr and trp. Science (1996), 271, 163-168.
36. The interaction of Gold(I) cations with 1,3-Dienes. Sanguramath, R., Hooper, T. N., Butts, C. P., Green, M., McGrady, J. E., Russel, C. A., Angew. Chem. Int. Ed. (2011), 50, 7592-7595.
37. Cation-Alkene interaction. Premkumar, J. R., Sastry, G. N., J. Phys. Chem. A (2014) 118, 11388-11398.
38. Anion-π interactions: Do they exist? Quiñonero, D., Garau C., Rotger C., Frontera, A., Ballester, P., Costa, A., Deyà P. M., Angew. Chem. Int. Ed. (2002), 41, 3389-3392.

39. Putting Anion-π interactions into perspective. Frontera, A., Gamez, P., Mascal, M., Mooibroek, T., Reedijk, J., Angew. Chem. Int. Ed. (2011), 50, 9564-9583.
40. Aromatic interactions. Hunter, C. A., Lawson, K. R., Perkins, J., Urch, C. J., J. Chem. Soc., Perkin Trans. 2, (2001), 651-669.
41. Attractive intermolecular edge-to-face aromatic interactions in flexible organic molecules. Jennings, W. B., Farrell, B. M., Malone, J. F. Acc. Chem. Res. (2001), 34, 885-894.
42. The nature of $\pi - \pi$ interactions. Hunter, C. A., Sanders, J. K. M. J. Am. Chem. Soc. (1990), 112, 5525-5534.
43. The importance of pi-interactions in crystal engineering. Ed. by Tiekink, E. R. T., Zukerman-Schpector, J. John Wiley & Sons, Ltd. United Kingdom (2012).
44. Rethinking the terms “pi-stacking”. Martinez, C. R., Iverson, B. L. Chem. Sci. (2012), 3, 2191-2201.
45. What is the covalency of hydrogen bonding? Grabowski, S. J. (2011) 111, 2597-2625.
46. The nature of the chemical bond. Pauling, L. 3rd ed. Cornell University Press. USA(1960).
47. The Weak Hydrogen Bond, Desiraju, G., Thomas, S. Oxford University Press. Online. (2001).
48. Unraveling the hydrogen bond network in a theophylline-pyridoxine salt cocrystal by a combined X-ray diffraction, solid-state NMR and computational approach. Rossi, F., Vioglio, P. C., Bordigon, S., Giorgio, V., Nervi, C., Priola, E., Gobetto, R., Yazawa, K., Chierotti, M. R. Cryst. Growth Des. (2018), 18, 2225-2233.
49. Cocrystals of 3,5-dimethylpyrazole and salicylic acid: controlled formation of trimers via O-H···N hydrogen bonds. López, C., Claramunt, R. M., García, M A., Pinilla, E., Torres, R., Alkorta, I., Elguero, J. Cryst. Growth Des. (2007), 7, 6, 1176-1184.
50. Design of supramolecular layers via self-assembly of imidazole and carboxylic acids. MacDonald, J. C., Dorrestein, P. C., Pilley, M. M. Cryst. Growth Des. (2001), 1, 29-38.
51. Surveying macrocyclic chemistry: from flexible crown ethers to rigid cyclophanes. Liu, Z., Mohan Nalluri, S. K., Stoddart, J. F. Chem. Soc. Rev. (2017), 46, 2459-2478.
52. Facile fabrication of polyaniline nanotubes using the self-assembly behavior based on the hydrogen bonding: a mechanistic study and application in high-performance electrochemical supercapacitor electrode. Wu, W., Pan, D., Li, Y., Zhao, G., Jing, L., Chen, S. Electrochimica Acta (2015) 152, 126-134.
53. Supramolecular construction of multifluorescent gels: interfacial assembly of discrete fluorescent gels through multiple hydrogen bonding. Ji, X., Shi, B., Wang, H., Xia, D., Jie, K., Wu, L., Huang, F., Adv. Mater. (2015), 27, 8062-8066.
54. Non-classical hydrogen bond triggered strand displacement for analytical applications and DNA nanostructure assembly. Han, M., Fan, Q., Zhang, Y., Xu, L., Yu, C., Su, X. New J. Chem, (2018), 42, 6636-6639.
55. Hydrogen bridges in crystal engineering: Interactions without borders. Desiraju, G. Acc. Chem. Res. (2002), 35, 565-573.
56. Dispersion Forces I. Buhmann, S. Y. Springer Verlag. Heidelberg. (2012).

57. Molecular quantum electrodynamics. Salam, A. Jonh Wiley & Sons, Inc. USA (2010).
58. Intermolecular and surfaces forces. Israelachvili, J.. Academic Press 3rd ed. (2011) USA.
59. How well does the Lennard-Jones potential represents the thermodynamic properties of noble gases? Rutkai, G., Thol, M., Span, R., Vrabec, J. Molecular Physics, (2017), 115, 1104-1121.
60. Vapor pressures and vaporization enthalpies of the n-alkanes from C_{21} to C_{30} at T=298.15 K by correlation gas chromatography. Chickos, J. S., Hansha, W. J. Chem. Eng. Data (2004), 49, 77-85.
61. The crystal as a supramolecular entity. Ed. by Desiraju, G. John Wiley and Sons Ltd. United Kingdom (1996).
62. Crystal packing, hydrogen bonding, and the effect of crystal forces on molecular conformation. Dauber, P., Hagler, A. T. Acc. Chem. Res. (1980), 13, 105-112.
63. New trends in crystal engineering. Braga, D., Brammer, L., Champness, N. R. CrystEngComm (2005), 7(1), 1-19.
64. Supramolecular synthons in crystal engineering- a new organic synthesis. Desiraju, G. Angew. Chem. Int. Ed. Engl. (1995), 34, 2311-2327.
65. Measuring enthalpy of sublimation for active pharmaceutical ingredients: validate crystal energy and predict crystal habit. Taulelle, P., Sitja, G., Pépe, G., Garcia, E., Hoff, C., Veesler, S. Cryst. Growth Des. (2009) 9, 4706-4709.
66. Sulfonamide molecular crystals: structure, sublimation thermodynamic characteristics, molecular packing, hydrogen bonds network. Perlovich, G. L., Ryzhakov, A. M., Tkachev, V. V., Hansen, L. Kr., Raevsky, O. A. Cryst. Growth Des. (2013), 13, 4002-4016.
67. Probing the accuracy of first-principles modeling of molecular crystals: calculation of sublimation pressures. Cervinka, C., Fulem, M. Cryst. Growth Des. (2019), 19, 808-820.
68. Chemical thermodynamics. Rock, P. A. University Science Books. USA (1983).
69. Experimental thermodynamics Volume II, chapter 13. Ambrose, D. Springer Science+Business Media, LLC. USA (1975).
70. Kinetic theory of gases. Kauzmann, W. W. A. Benjamin. USA (1966).
71. The kinetic theory of gases. Some modern aspects. Knudsen, M. 2nd ed. Methuen & Co. Ltd. London (1946).
72. Thermodynamics of nickel and cobalt removal from aqueous solution by layered crystalline organofunctionalized barium phosphate. Lazarini, A. M., Airoldi, C. J., Chem. Thermodyn. (2009), 41, 21–25.
73. Adsorption of mercury cation on chemically modified clay. Guerra, D. L., Ribeiro-Viana, R., Airoldi, C., Mater. Res. Bull. (2009), 44, 485-491.
74. A thermodynamic analysis of solvation. Yu, H., Karplus, M. J. Chem. Phys. (1988), 89, 2366-2379.
75. Potential distribution theory and the statistical mechanics of fluids. Widom, B. J. Phys. Chem. (1982), 86, 869-872.
76. The statistical mechanical theory of solutions I. Kirkwood, J. G., Buff, F. P. J. Chem. Phys. (1951), 19, 774-777.
77. The statistical thermodynamics of multicomponent systems. McMillan, W. G., Mayer, J. E. J. Chem. Phys. (1945) 13, 276-305.

78. Statistical mechanics of rigid spheres. Reiss, H., Frisch, H. L., Lebowitz, J. L. J. Chem. Phys. (1959) 31, 369.
79. Linear solvation energy relationships. 46. An improved equation for correlation and prediction of octanol/water partition coeffcients of organic nonelectrolytes (including strong hydrogen bond donor solutes). Kamlet, M. J., Doherty, R. M., Abraham, M. H., Marcus, Y., Taft, R. J. Phys. Chem. (1988) 92, 5244-5255.
80. Solvation thermodynamics and the physical-chemical meaning of the constant in Abraham solvation model. van Noort, P. C. M. Chemosphere (2012) 87, 125-131.
81. The solvatochromic comparison method I. The β-scale of solvent hydrogen bond acceptor (HBA) basicities. Kamlet, M., Taft, R. W. J. Am. Chem. Soc. (1976), 98, 377-383.
82. The solvatochromic comparison method 2. The α-scale of solvent hydrogen bond donor (HBD) acidities. Taft, R. W., Kamlet, M. J. Am. Chem. Soc. (1976), 98, 2886-2894.
83. The solvatochromic comparison method 6. The π^*-scale of solvent polarities. Kamlet, M. J., Abboud, J. L., Taft, R. W. J. Am. Chem. Soc. (1977) 99, 6027-6038.
84. Linear free energy relationships. Local empirical rules-or fundamental laws of chemistry?. Sjöström, M., Wold, S. Acta. Chem. Scand. (1981) 35, 537-554.
85. Enthalpies of hydrogen bond formation of 1-octanol with aprotic organic solvents. A comparison of the solvation enthalpy, pure base, and non-hydrogen-bonding baseline methods. Stepehenson, W. K., Fuchs, R. Can. J. Chem. (1985) 85, 342-348.
86. Studies of hydrogen-bonded complex formation III. Thermodynamics of complexing by infrared spectroscopy and calorimetry. Arnett, E. M., Joris, L., Mitchell, E., Murty, T. S. S. R., Gorrie, T. M., Schleyer, P. v. R. J. Am. Chem. Soc. (1970) 92, 2365-2377.
87. Toward a solvent basicity scale: the calorimetry of the pyrrole probe. Catalán, J., Gómez, J., Couto, A., Laynez, J. J. Am. Chem. Soc. (1990) 112, 1678-1681.
88. Towards a solvent acidity scale: the calorimetry of the N-methyl imidazole probe. Catalán, J., Couto, A., Gómez, J., Laynez, J. J. J Chem. Soc. Perkin Trans. 2 (1992) 1181-1185.
89. Thermodynamic study of (perfluoroalkane + alkane) mixtures: Excess and solvation enthalpies. Duce, C., Tiné, M. R., Lepori, L., Matteoli, E. J. Chem. Thermodynam. (2007) 39, 1346-1353.
90. van der Waals volumes and Radii. Bondi, A. J. Phys. Chem. (1964), 68, 441-451.
91. Enthalpies of solvation of ethylene oxide oligomers $CH_3O(CH_2CH_2O)_m\ CH_3$ (n=1 to 4) in different H-bonding solvents: methanol, chloroform and water. Group contribution method as applied to the polar oligomers. Barannikov, V. P., Guseynov, S. S., Vyugin, A. I. J. Chem. Thermodynam. (2011) 43, 1928-1935.
92. An equation for describing the enthalpy of nonspecific solvation of nonelectrolytes. Solomonov, B. N., Novikov, V. B., Solomonov, A. B. Russ. J. Phys. Chem. (2000) 74, 1102-1108.
93. A new method for the extraction of specific interaction enthalpy from the enthalpy of solvation. Solomonov, B. N., Novikov, V. B., Varfolomeev, M. A., Mileshko, N. M. J. Phys. Org. Chem. (2005) 18, 49-61.
94. Properties of hydrophobic free energy found by gas-liquid transfer. Baldwin, R. L. Proc. Natl. Acad. Sci. U.S.A. (2013) 110, 1670-1673.

95. Origin of the change in solvation enthalpy of the peptide group when neighboring peptide groups are added. Avbelj, F., Baldwin, R. L. Proc. Natl. Acad. Sci. U.S.A. (2009) 106, 3137-3141.
96. Differential scanning calorimetry. Höhne, G. W. H., Hemminger, W. F., Flammersheim, H. J. 2nd ed. Springer-Verlag Berlin Heidelberg (2003).
97. Calculation methods in reaction calorimetry. Wadsö, I. Science tools. (1966), 13, 33-39.
98. The design, construction, and testing of a new Knudsen effusion apparatus. Ribeiro da Silva, M. A. V., Monte, M. J. S., Santos, L. M. N. B. F., J. Chem. Thermodyn. (2006) 38, 778-787.
99. Aqueous solutions of nonpolar gases. Pierotti, R. A., J. Phys. Chem. (1965) 69, 281-288.
100. Derivation of Stockmayer potential parameters for polar fluids. van Leeuwen, M.E., Fluid Phase Equilib., (1994) 99, 1-18.
101. Thermal pressure and energy volume coefficients for the acetonitrile + water systems. Grant-Taylor, D., Macdonald, D. D., Can. J. Chem. (1976) 54, 2813-2819.
102. Transport properties of the binary mixtures of the three organic liquids toluene, methanol, and cyclohexane. Lapeira, E., Gebhardt, M., Triller, T., Mialdun, A., Köhler, W., Shevtsova, V., Bou-Ali, M. M., J. Chem. Phys. (2017) 146, 094507.
103. Turner, M. J., McKinnon, J. J., Wolff, S. K., Grimwood, D. J., Spackman, P. R., Jayatilaka, D., Spackman, M. A., CrystalExplorer17 (2017). University of Western Australia.
104. Jayatilaka, D., Grimwood, D. J. (2003) Tonto: A Fortran Based Object-Oriented System for Quantum Chemistry and Crystallography. In: Sloot, P. M. A., Abramson D., Bogdanov A. V., Gorbachev Y. E., Dongarra J. J., Zomaya A. Y. (eds) Computational Science – ICCS 2003. Lecture Notes in Computer Science, Vol. 2660. Springer, Berlin, Heidelberg.
105. Köster, A. M., Geudtner, G., Alvarez-Ibarra, A., Calaminici, P., Casida, M. E., Carmona-Espindola, J., Dominguez, V. D., Flores-Moreno, R., Gamboa, G. U., Goursot, A., Heine, T., Ipatov, A., de la Lande, A., Janetzko, F., del Campo, J. M., Mejia-Rodriguez, D., Reveles, J. U., Vasquez-Perez, J. U., Vela, A., Zuniga-Gutierrez, B., Salahub, D. R., *deMon2k, Version 5. The deMon Developers* (Cinvestav, Mexico City, 2018) see: http://www.demon-software.com.
106. Generalized gradient approximation made simple. Perdew, J. P., Burke, K., Ernzerhof, M., Phys. Rev. Lett. (1996) 77, 3865-3868.
107. Köster, A. M., Geudtner, G., Gamboa, G.U., Alvarez-Ibarra, A., Calaminici, P., Flores-Moreno, R., Goursot, A., Mejia-Rodriguez, D., Pettersson, L. M., Vasquez-Perez, J., Zuniga-Gutierrez, B., The deMon2k User's Guide, Version 5.0, edited by Trickey, S. B. and D. R. Salahub (Cinvestav, Mexico City, 2018).
108. The Cambridge Structural Database. Groom, C. R., Bruno, I. J., Lightfoot M. P., Ward, S. C. Acta. Cryst. B. (2016) 872, 171-179.
109. Bonded-atom fragments for describing molecular charge densities. Hirshfeld, F. L. Theoret. Chim. Acta (Berl.) (1977) 44, 129-138.
110. A novel definition of a molecule in a crystal. Spackman, M. A., Byrom, P. G. Chem. Phys. Lett. (1997) 267, 215-220.

111. Hirshfeld surface analysis. Spackman, M. A., Jayatilaka, D. Cryst. Eng. Comm. (2009) 11, 19-32.
112. Molecular surfaces from the promolecule: a comparison with Hertree-Fock *Ab Initio* electron density surfaces. Mitchel, A. S., Spackman, M. A. J. Comput. Chem. (2000) 21, 933-942.
113. Strong intermolecular interactions shaping small piano-stool complex. Hey, J, Andrada, D. M, Michel, R., Mata, R. A., Stalke, D., Angew. Chem. Int. Ed. (2013) 52, 10365-10369.
114. Porous molecular crystals by macrocyclic coordination supramolecules. Bassanetti, I., Comotti, A., Sozzani, P., Bracco, S., Calestani, G., Mezzadri, F., Marchiò, L. J. Am. Chem. Soc (2014) 136, 14883-14895.
115. Bridging crystal engineering and drug discovery by utilizing intermolecular interactions and molecular shapes in crystals. Spackman, P. R., Yu, L., Morton, C J., Parker, M. W., Bond, C. S., Spackman, M. A., Jayatilaka, D., Thomas, S. P., Angew. Chem. Int. Ed (2019) 58, 1-6.
116. SSZ-87: A borosilicate zeolite with unusually flexible 10-ring pore openings. Smeets, S., McCusker, L. B., Baerlocher, C., Xie, D., Chen, C-Y., Zones, S. I. J. Am. Chem. Soc. (2015) 137, 2015-2020.
117. Energetic salts with π-stacking and hydrogen bond interactions lead the way to future energetic materials. Zhang, J., Zhang, Q., Vo, T. T., Parrish, D. A., Shreeve, J. M. J. Am. Chem. Soc. (2015) 137, 1697-1704.
118. Formamidinium nitroformate: an insensitive RDX alternative. Baster, A. F., Martin I., Christe K. O., Haiges, R. J. Am. Chem. Soc. (2018) 140, 15089-15098.
119. Thermochemical properties of N-heterocyclic compounds I. Enthalpies of combustion, vapour pressures and enthalpies of sublimation, and enthalpies of formation of pyrazole, imidazole, indazole, and benzimidazole. Jiménez, P, Roux, M.V., Turrión, C., Gomis, F., J. Chem. Thermodyn. (1987) 19, 985-992.
120. Thermochemical properties of N-heterocyclic compounds IV. Enthalpies of combustion, vapour pressures and enthalpies of sublimation, and enthalpies of formation of 2-methylimidazole and 2-ethylimidazole. Jiménez, P, Roux, M.V., Turrión, C., J. Chem. Thermodyn., (1992) 24, 1145-1149.
121. Effect of the replacement of a methyl by trifluoromethyl group on the acid-base properties of pyrazoles. Elguero, J., Yranzo, G. I., Catalán, J., G. de Paz, J. L., Anvia, F., Taft, R. W. J. Org.. Chem. (1991) 56, 3942-3947.
122. Bevington, P., Data reduction and error analysis for the physical sciences, McGraw Hill, USA, (1969).
123. A study on the pyrazoles: tautomerism, conformation, acidity, and basicity by means of AM1 semiempirical methods in the gas and aqueous solution. Güven, A., Kaniskan, N. J. Mol. Struct. (1999), 488, 125-134.
124. Calculation of intermolecular interaction energies by direct numerical integration over electron densities. 2. An improvement polarization model and the evaluation of dispersion and repulsion energies. Gavezzotti, A. J. Phys. Chem. (2003) 107, 2344-2353.
125. Enthalpies of vaporization of some aliphatic alcohols. Polák, J., Benson, G. C., J. Chem. Thermodyn. (1971) 3, 235-242.
126. Enthalpies of vaporization of organic compounds IV Alkyl Nitriles. Howard, P. B., Wadsö, I., Acta Chem. Scand. (1970) 24, 145-149.

127. The hydrophobic effect. Kronberg, B. Curr. Opin. Colloid Interface Sci.(2016) 22, 14-22.
128. Cavities in molecular liquids and the theory of hydrophobic solubilities. Pohorille, A., Pratt, L. R. J. Am. Chem. Soc. (1990) 112, 5066-5074.
129. Selected values of electric dipole moments for molecules in the gas phase. Nelson, R. D. Jr., Lide, D. R. Jr., Maryott, A. A., National Standard Reference Data Series. National Bureau of Standards 10. Category 3- Atomic and Molecular Properties (1967).
130. Enthalpy of dilution of aqueous mixtures of amides, sugars, urea, ethylene glycol and penterythirol at 25 ºC: enthalpy of interaction of the hydrocarbon, amide and hydroxul functional groups in dilute aqueous solutions. Savage, J. J., Wood, R. H., J. Solution Chem. (1975) 5, 733-750.
131. Covalent nature of the strong homonuclear hydrogen bond. Study of the O-H···O system by crystal structure correlation methods. Gilli, P., Bertolasi, V., Gilli, G., J. Am. Chem. Soc. (1994) 116, 909-915.

Annex

First publication of this work :

Understanding the solvation process and solute-solvent interactions of imidazole compounds in three different solvents through solution calorimetry and ^{1}H NMR spectroscopy. Herrera-Castro, F., Torres, L. A. J. Mol. Liq. (2019) 284, 232-240.

This work has been presented in the next events:

1. Filiberto Herrera Castro, Luis Alfonso Torres Gómez and Myriam Campos. “Aproximación experimental de la solvatación de algunos heterociclos de cinco miembros, en diferentes solventes” in Primer Coloquio Nacional de Calorimetría, Análisis Térmico y Termoquímica. Guadalajara, Jalisco, México (2014).

2. Filiberto Herrera Castro and Luis Alfonso Torres Gómez. “Determinación de entalpías de solución de compuestos de la familia del imidazol, en diferentes solvents” in Segundo Coloquio Nacional de Calorimetría, Análisis Térmico y Termoquímica. Puebla, Puebla, México (2016).

3. Filiberto Herrera Castro and Luis Alfonso Torres Gómez. “Enthalpies of solvation through experimental determination of enthalpies of sublimation and solution of imidazole-derivatives compounds in various solvents. An effort to quantify the molecular interactions in solution” in 13th Mediterranean Conference on Calorimetry and Thermal Analysis, Loano, Italy (2017).